

**Charakterisierung Patienten-stämmiger  
Glioblastomstammzellkulturen zur Prognose von  
Patientenüberleben und zur Stratifizierung einer  
K<sub>Ca</sub>-gerichteten Radiotherapie**

**Dissertation**

der Mathematisch-Naturwissenschaftlichen Fakultät  
der Eberhard Karls Universität Tübingen  
zur Erlangung des Grades eines  
Doktors der Naturwissenschaften  
(Dr. rer. nat.)

vorgelegt von  
Katrín Mareike Ganser  
aus Sigmaringen

Tübingen  
2023

Gedruckt mit Genehmigung der Mathematisch-Naturwissenschaftlichen Fakultät der  
Eberhard Karls Universität Tübingen.

Tag der mündlichen Qualifikation:

23.01.2024

Dekan:

Prof. Dr. Thilo Stehle

1. Berichterstatter:

Prof. Dr. Peter Ruth

2. Berichterstatter:

Prof. Dr. Stephan Huber

3. Berichterstatter:

Prof. Dr. Matthias Schwab

# Inhaltsverzeichnis

Abkürzungsverzeichnis .....	1
Zusammenfassung .....	2
Summary .....	3
Erklärung zum Eigenanteil der Dissertation.....	6
1. Einleitung.....	8
1.1 Glioblastoma multiforme.....	8
1.1.1 Definition und Therapie .....	8
1.1.2 Diagnose und Abgrenzung.....	8
1.1.3 Molekulare Subtypen des Glioblastoms .....	9
1.1.4 Glioblastom Stammzellen (GSC).....	10
1.1.5 Glioblastom-Stammzellmarker.....	11
1.2 Kaliumkanäle.....	12
1.2.1 Ca <sup>2+</sup> - aktivierbare Kaliumkanäle .....	12
1.2.2 Bisherige Erkenntnisse der Rolle von IK <sub>Ca</sub> und BK <sub>Ca</sub> Kanälen in der Krebspathophysiologie.....	13
2. Zielsetzung .....	16
3. Ergebnisse.....	17
3.1. Identifizierung einer molekularen proneuralen zu mesenchymalen mRNA-Signatur in GSC Primärkulturen .....	17
3.2. Funktionelle Bedeutung der molekularen mRNA-Signatur .....	19
3.2.1 Assoziation mit Radiosensitivität und Invasionsverhalten <i>in vitro</i> .....	19
3.2.2 Assoziation mit klinischen Daten der Tübinger Kohorte .....	20
3.2.3 Assoziation mit klinischen Daten von Glioblastom-Datenbanken .....	21
3.3 Expression von IK <sub>Ca</sub> -, BK <sub>Ca</sub> - und Stammzellmarkern in Primärkulturen von Glioblastom-Stammzellen aus Patientenresektaten .....	22
3.4 Effekte einer IK <sub>Ca</sub> bzw. BK <sub>Ca</sub> Blockade auf GSC-Kulturen <i>in vitro</i> .....	24
3.4.1 Funktionelle Bedeutung der IK <sub>Ca</sub> und BK <sub>Ca</sub> Kanäle für die DNA-Reparatur .....	24
3.4.2 Funktionelle Bedeutung der IK <sub>Ca</sub> und BK <sub>Ca</sub> Kanäle für das klonogene Überleben und den Zellzyklus .....	25
3.4.3 Funktionelle Bedeutung von IK <sub>Ca</sub> und BK <sub>Ca</sub> für die Gel-Invasion .....	26
3.5 Orthotope <i>Xenotransplantation</i> von aus Patienten stammenden GSCs in immunkompromittierte Mäuse und Überwachung der Glioblastombildung .....	27
3.5.1 Häufigkeit von ALDH1A3-exprimierenden GSCs <i>in vivo</i> .....	28
3.6. Effekte einer <i>in vivo</i> IK <sub>Ca</sub> bzw. BK <sub>Ca</sub> Blockade auf <i>Xenotransplantate</i> von aus Patienten stammenden GSC Kulturen .....	29

3.6.1 Abhängigkeit der Glioblastom-Hirninfiltration und der DNA-Doppelstrangbruch-Reparatur von $IK_{Ca}$ und $BK_{Ca}$ Kanälen <i>in vivo</i> .....	29
3.6.2 Auswirkungen einer $IK_{Ca}$ -Kanalblockade auf das Tumorwachstum (des LK7- <i>Xenotransplantats</i> ) und das Überleben der Mäuse.....	31
3.7 Potentielle Aussagekraft von prä-operativen MRT-Aufnahmen auf die molekulare mRNA-Signatur .....	32
4. Diskussion .....	33
5. Schlussfolgerung .....	39
Literaturverzeichnis .....	41
Danksagung .....	52
Anhang - Publikationen .....	53

## Abkürzungsverzeichnis

ACTB	Beta actin
ALDH1A3	Aldehyde Dehydrogenase 1 Family Member A3
BK <sub>Ca</sub> / KCa1.1	Big conductance calcium-activated potassium channel
CXCR4	CXC chemokine receptor type 4
EGFRvIII	Epidermal growth factor receptor variant III
GBM	Glioblastoma multiforme
GFAP	Glial fibrillary acidic protein
(p)GSC	(patient derived) glioblastoma stem cell
Iba1	Ionized calcium-binding adapter molecule 1
IDH	Isocitrate dehydrogenase
IK <sub>Ca</sub> / KCa3.1	Intermediate conductance calcium-activated potassium channel
IF	Immunofluorescence
IR	Irradiation
Ivy GAP	Ivy Glioblastoma Atlas Project database
<i>KCNN4</i>	gene, encoding the IK <sub>Ca</sub> channel
<i>KCNMA1</i>	gene, encoding the BK <sub>Ca</sub> channel
KPS	Karnofsky Performance Scale
MGMT	O-6-methylguanine-DNA methyltransferase
OS	overall survival (Gesamtüberleben)
Pax	Paxilline
P <sub>cc</sub>	Pearson correlation coefficient
PE	plating efficiency
REMBRANDT	Repository for Molecular Brain Neoplasia Data
SOX2	sex determining region Y (SRY)- box 2
SF	survival fraction
TCGA	The Cancer Genome Atlas
TMZ	Temozolomide
γH2AX	Phosphor-histone H2AX

## Zusammenfassung

Das Glioblastom multiforme stellt den aggressivsten, hirneigenen Tumor bei Erwachsenen dar, dessen mittlere Überlebensrate trotz multimodaler Therapie nach Diagnose unter zwei Jahren liegt. Gründe für die schlechte Prognose sind das typischerweise stark infiltrierende Wachstum und die Therapieresistenz, die wahrscheinlich auf stammzellähnliche Glioblastomzellen (GSC), insbesondere vom mesenchymalen Typ, zurückzuführen sind. Die Identifikation molekularer Glioblastomsubtypen durch definierte Markermoleküle könnte eine Strategie zur Stratifizierung der Patient:innen für neue personalisierte Therapieoptionen sein. Aus diesem Grund wurde im ersten Teil der Arbeit aus primären Glioblastom-Stammzellkulturen die mRNA-Expression von zehn Stammzell-, Resistenz- und Invasionsmarkern analysiert. Aus deren Expressionsprofil wurde darauffolgend eine mRNA-Signatur abgeleitet, welche die GSC-Kulturen in proneurale/mesenchymale Subtypen klassifizierte. Die mRNA-Signatur korrelierte dabei mit der Radioresistenz und Invasivität der Kulturen *in vitro*. Außerdem konnte beobachtet werden, dass vor allem bei Patient:innen mit mesenchymalen GSC Kulturen multifokale Rezidive auftraten. Hierbei war das Gesamtüberleben kürzer/reduziert gegenüber Patient:innen mit einem proneuralen Subtyp, welche überwiegend unifokale Rezidive aufzeigten.

Zusammengenommen konnte beobachtet werden, dass ein mesenchymaler GSC-Subtyp mit einer erhöhten Malignität einherging. Da zwei mesenchymale Marker der mRNA-Signatur für die beiden Calcium-aktivierbaren Kaliumkanäle  $IK_{Ca}$  und  $BK_{Ca}$  kodieren, wurden im zweiten Teil der Arbeit mögliche Effekte einer  $IK_{Ca}$ - bzw.  $BK_{Ca}$ -Blockade begleitend zur Bestrahlung in den GSC-Kulturen *in vitro* und in orthotopen *Xenotransplantaten in vivo* untersucht. Eine  $IK_{Ca}$ - bzw.  $BK_{Ca}$ -Blockade schien dabei in einigen aber nicht allen Zelllinien die Doppelstrangbruchreparatur *in vitro* und *in vivo* zu hemmen und teilweise auch die Invasivität der Zellen zu reduzieren. Das Ansprechen auf eine Blockade dieser Kanäle war dabei nicht wie erwartet von ihrer mRNA-Expression abhängig, daher müssen andere prädiktive Marker zur Patientenstratifizierung gefunden werden.

Zusammenfassend konnte gezeigt werden, dass die aus Glioblastom-Resektionsmaterial angezüchteten und GSC-angereicherten Kulturen wahrscheinlich die Zellsubpopulation des Glioblastoms darstellen, die für den Krankheitsverlauf und Therapieansprechen ausschlaggebend sind. Die identifizierte molekulare mRNA-Signatur aus diesen Kulturen könnte ein prognostischer Parameter für das Rezidivmuster und das Überleben der jeweiligen Patient:innen darstellen. Zudem zeigen die Ergebnisse des zweiten Teils der Arbeit, dass eine begleitende  $K_{Ca}$ -Blockade zur Strahlentherapie eine mögliche neue Strategie in der Glioblastomtherapie sein könnte.

## Summary

Glioblastoma multiforme represents the most aggressive brain-derived tumor in adults with a median survival rate of less than two years after diagnosis despite multimodal therapy. Reasons for the poor prognosis include highly infiltrative growth and therapy resistance, probably of stem cell-like glioblastoma (GSC) cells, particularly of the mesenchymal subtype of GSCs. Identification of molecular glioblastoma subtypes by defined marker molecules of the tumor might be a strategy to stratify patients for new personalized therapy options. Therefore, in the first part of this work, mRNA expression of ten stem cell-, resistance- and invasion markers was analyzed in patient-derived glioblastoma stem cell cultures. Their expression profiles were subsequently used to derive a proneural-to-mesenchymal mRNA signature that classifies the GSC phenotype. The mRNA signature correlated with the radio resistance and invasiveness of the cultures *in vitro*. In addition, patients with mesenchymal GSC cultures exhibited mainly multifocal recurrence and shorter overall survival than patients with proneural GSC cultures. The latter patients predominantly showed unifocal tumor recurrences. We concluded that a mesenchymal GSC-subtype is associated with increased malignancy. Since two mesenchymal markers of the mRNA signature encode the calcium-activated potassium channels  $IK_{Ca}$  and  $BK_{Ca}$ , the second part of the work investigated possible effects of  $IK_{Ca}$  or  $BK_{Ca}$  blockade concomitant to irradiation. Here, pharmacological  $IK_{Ca}$  or  $BK_{Ca}$  blockade appeared in some but not all GSCs to interfere with double-strand break repair *in vitro* and in orthotopic *xenograft* mouse models *in vivo*. In addition,  $IK_{Ca}$  or  $BK_{Ca}$  blockade inhibited in some but not all GSCs gel invasion *in vitro* and brain infiltration *in vivo*. Unexpectedly, the effects of channel targeting did not correlate with the channel mRNA abundances in the GSC cultures, suggesting that further predictive markers must be identified for patient stratification to  $IK_{Ca}$ - or  $BK_{Ca}$ -targeting therapies.

In conclusion, GSC-enriched cultures derived from resection specimens likely represent the cell subpopulation of glioblastoma that is critical for disease progression and treatment response. The identified molecular mRNA signature of these cultures is probably prognostic for the recurrence pattern and survival of the patients. In addition, the results of the second part of the work show that concomitant  $K_{Ca}$  blockade to radiotherapy might be a promising new strategy in glioblastoma therapy in the future.

## Anteil an gemeinschaftlichen Veröffentlichungen

Erklärung nach § 5 Abs. 2 Nr. 7 der Promotionsordnung der Mat.- Nat. Fakultät

Name: Katrin Mareike Ganser

### Liste der Publikationen

1. Neuhaus E, Zirjacks L, **Ganser K**, Klumpp L, Schüler U, Zips D, Eckert F, Huber SM. Alternating Electric Fields (TFields) Activate Cav1.2 Channels in Human Glioblastoma Cells. *Cancers (Basel)*;11(1):110. doi: 10.3390/cancers11010110.
2. Palme D, Misovic M, **Ganser K**, Klumpp L, Salih HR, Zips D, Huber SM. hERG K<sup>+</sup> Channels Promote Survival of Irradiated Leukemia Cells. *Front Pharmacol.* 2020;11:489. doi: 10.3389/fphar.2020.00489.
3. Vatter T, Klumpp L, **Ganser K**, Stransky N, Zips D, Eckert F, Huber SM. Against Repurposing Methadone for Glioblastoma Therapy. *Biomolecules.* 2020;10(6):917. doi: 10.3390/biom10060917. PMID: 32560384; PMCID: PMC7356722.
4. Zirjacks L, Stransky N, Klumpp L, Prause L, Eckert F, Zips D, Schleicher S, Handgretinger R, Huber SM, **Ganser K**. Repurposing Disulfiram for Targeting of Glioblastoma Stem Cells: An In Vitro Study. *Biomolecules.* 2021;11(11):1561. doi: 10.3390/biom11111561
5. **Ganser K**, Eckert F, Riedel A, Stransky N, Paulsen F, Noell S, Krueger M, Schittenhelm J, Beck-Wödl S, Zips D, Ruth P, Huber SM, Klumpp L. Patient-individual phenotypes of glioblastoma stem cells are conserved in culture and associate with radioresistance, brain infiltration and patient prognosis. *Int J Cancer.* 2022;150(10):1722-1733. doi: 10.1002/ijc.33950.
6. Stransky N, **Ganser K**, Naumann U, Huber SM, Ruth P. Tumoricidal, Temozolomide- and Radiation-Sensitizing Effects of K<sub>Ca</sub>3.1 K<sup>+</sup> Channel Targeting In Vitro Are Dependent on Glioma Cell Line and Stem Cell Fraction. *Cancers (Basel).* 2022;14(24):6199. doi: 10.3390/cancers14246199.
7. Eckert F, **Ganser K**, Bender B, et al. Potential of pre-operative MRI features in glioblastoma to predict for molecular stem cell subtype and patient overall survival [published online ahead of print, 2023 Aug 22]. *Radiother Oncol.* 2023;109865. doi:10.1016/j.radonc.2023.109865
8. **Ganser K**, Stransky N, Abed T, Quintanilla-Martinez L, Gonzalez-Menendez I, Naumann U, Koch P, Krueger M, Ruth P, Huber SM, and Eckert F. K<sub>Ca</sub> channel targeting impairs DNA repair and invasion capability of patient-derived glioblastoma stem cells in culture and orthotopic mouse xenografts, 2023, *submitted*



9. Groß L, Abed T, Huber SM, **Ganser K**. Oncogenic Ca<sup>2+</sup> signaling-mediated radioresistance of cancer cells, 2023, *submitted*
10. Stransky N, **Ganser K**, Quintanilla-Martinez L, Gonzalez-Menendez I, Naumann U, Eckert F, Koch P, Huber SM, Ruth P. Efficacy of Combined Tumor Irradiation and KCa3.1-Targeting with TRAM-34 in a Syngeneic Glioma Mouse Model, 2023, *in revision*

Liste der Übersichtsartikel

1. **Ganser K**, Klumpp L, Bischof H, Lukowski R, Eckert F, Huber SM. Potassium Channels in Cancer. *Handb Exp Pharmacol.* 2021;267:253-275. doi: 10.1007/164\_2021\_465.
2. Abed T, **Ganser K**, Eckert F, Stransky N, Huber SM. Ion channels as molecular targets of glioblastoma electrotherapy *Front Cell Neurosci.* 2023;17:1133984. doi: 10.3389/fncel.2023.1133984.

Der Inhalt dieser kumulative Promotionsschrift umfasst die Studien Ganser et al. 2022, Ganser et al. 2023 und Eckert et al 2023 (in der Liste **blau** markiert).

Publikationen							
Nr.	Accepted for publication (yes/no)	Number of all authors	Position of the candidate in the list of authors	Scientific ideas of candidate (%)	Data generation by candidate (%)	Analysis and interpretation by candidate (%)	Paper writing by candidate (%)
5.	yes	13	1	40	70	70	60
7.	yes	10	2	20	40	40	10
8.	no	11	1	70	90	90	60

I certify that the above statement is correct.

Tübingen, 25.09.2023

\_\_\_\_\_  
[Katrin Mareike Ganser] (candidate)

I / We certify that the above statement is correct.

Tübingen, 25.09.2023

\_\_\_\_\_  
[apl. Prof. Dr. Stephan Huber] (Supervisor)

## Erklärung zum Eigenanteil der Dissertation

Alle Versuche wurden mit den unten beschriebenen Ausnahmen am Universitätsklinikum Tübingen, Abteilung Experimentelle Radioonkologie unter der Betreuung von apl. Prof. Dr. Stephan Huber und Prof. Dr. Peter Ruth und zeitweiser Assistenz durch Heidrun Faltin von mir selbständig durchgeführt.

Die Studie Ganser et al. 2022 wurde im Rahmen des Promotionsprojekts von MSc. Lukas Klumpp begonnen. Herr Klumpp zog (später auch zusammen mit Dr. Andreas Riedel) aus Tumorsektaten einer Kohorte von 23 Tübinger Glioblastom-Patient:innen Glioblastom-Stammzell (GSC)-anreichernde Kulturen an. Er etablierte und optimierte dabei die Glioblastomzell-Isolierung und die Kulturbedingungen, vermehrte und kryo-asservierte frühe Passagen der GSC-Kulturen, definierte die Stammzell-mRNA-Marker zur molekularen Charakterisierung der Stammzell-Subpopulationen, identifizierte insbesondere den  $\text{Ca}^{2+}$ -aktivierten  $\text{IK}_{\text{Ca}}$   $\text{K}^{+}$ -Kanal und den C-X-C Chemokin-Rezeptor CXCR4 als mesenchymalen Stammzellmarker, etablierte den Gel-Invasions- und Limited-Dilution-Assay (LDA) zur funktionellen Charakterisierung der Stammzell-Subpopulationen und charakterisierte die *in vitro* Spheroid-zu-Monolayer Wachstumsmorphologie der GSC-Kulturen. Zusätzlich wies mich Herr Klumpp in die stereotaktische Transplantation von den GSCs in das rechte Striatum der Maus ein und Herr Klumpp errichtete (und pflegte zunächst) zusammen mit Frau PD Dr. Franziska Eckert und Herrn Dr. Paulsen die klinische und *in vitro*-Datenbanken der Tübinger Glioblastom-Kohorte. Zudem lud er Transkriptom- und klinische Daten aus öffentlich zugänglichen Glioblastom-Datenbanken herunter, filterte und bereitete diese statistisch auf. Herr apl. Prof Stephan Huber führte die Patch-Clamp-Experimente durch.

In Anschluss an diese Vorarbeiten, bestimmte ich für diese Studie in den GSC-Kulturen die mRNA Abundanzen der Stammzellmarker, definierte zusammen mit Herrn Klumpp eine proneural zu mesenchymale mRNA-Signatur und charakterisierte den molekularen Stammzellphänotyp über diese mRNA-Signatur. Ich analysierte die Radiosensitivität und Invasionsneigung der einzelnen Kulturen mittels LDA bzw. Gel-Invasionsassay, assoziierte die molekularen mit den funktionellen *in vitro*-Eigenschaften der GSC-Kulturen und testete schlussendlich auf Korrelationen zwischen Rezidivierungsmuster bzw. progressionsfreiem und Gesamtüberleben der

Glioblastompatient:innen mit der proneural zu mesenchymalen mRNA-Signatur ihrer GSC-Kulturen, führte den Großteil der statistischen Tests durch, bereitete die Daten graphisch auf und schrieb zusammen mit apl. Prof. Dr. Stephan Huber den ersten Entwurf dieser Veröffentlichung.

Für die Studie Ganser et al, 2023 (submitted) wurde ein Teil der immunhistochemischen Färbung in der Mauspathologie-Facility der Universität Tübingen durch Frau Prof. Leticia Quintanilla-Martinez und Frau Dr. Irene Gonzalez-Menendez durchgeführt, sowie die Patch-Clamp-Experimente durch apl. Prof. Stephan Huber.

Für die Studie Eckert et al. 2023 habe ich die funktionellen *in vitro*-Daten beigetragen.

Ich versichere, das Manuskript selbstständig unter Mithilfe von apl. Prof. Dr. Stephan Huber verfasst und keine weiteren als die von mir angegebenen Quellen verwendet zu haben.

---

Ort, Datum

---

[Katrín Mareike Ganser]

# 1. Einleitung

## 1.1 Glioblastoma multiforme

### 1.1.1 Definition und Therapie

Das Glioblastoma multiforme (GBM), definiert als WHO-Grad 4, IDH-Wildtyp (Rushing (2021)) stellt den häufigsten, aggressivsten, hirneigenen Tumor bei Erwachsenen dar. Die Standardtherapie bei neu diagnostiziertem GBM besteht aus der größtmöglichen Tumorresektion, gefolgt von einer Strahlentherapie (60 Gy in 30 Fraktionen) mit konkomitanter und adjuvanter Chemotherapie mit dem Alkylans Temozolomid (TMZ) (Stupp et al. 2009). Trotz dieser multimodalen Therapie liegt das mittlere Gesamtüberleben von Glioblastompatient:innen nach Diagnose bei unter zwei Jahren. (Kudulaiti et al. 2021) Aktuelle klinische Studien, in denen neue Therapiestrategien einschließlich Immuntherapien getestet wurden, ergaben bislang keinen Überlebensvorteil (Bagley et al. 2022). Die einzige innovative neue Therapie, die im letzten Jahrzehnt eingeführt wurde, besteht aus einer Elektrotherapie mit lokal applizierten niederenergetischen Wechselstromfeldern (Tumor Treating Fields, TTF), die optional begleitend zur adjuvanten Temozolomid-Erhalttherapie, bei Patient:innen mit gutem klinischen Zustand (KPS  $\geq$  70%) eingesetzt werden kann (Stupp et al. 2015, Stupp and Ram 2017, Kudulaiti et al. 2021). Die Identifikation neuer Therapieoptionen des GBM bleibt somit eine herausfordernde Aufgabe der (prä)klinischen Forschung.

### 1.1.2 Diagnose und Abgrenzung

Eine erste Verdachtsdiagnose des GBM kann bereits in einer T1-gewichteten Magnetresonanztomographie (MRT) mit Kontrastmittelgabe getroffen werden, welche zur weiteren Abklärung meist neurologischer Symptome (Kopfschmerzen, Schwindel, Krampfanfälle, Lähmungen und Wesensveränderungen) durchgeführt wird. Hierbei ist typischerweise das diffus wachsende, kontrastmittelanreichernde vitale Tumorgewebe, welches meist große zentrale Nekrosen und Einblutungen beinhaltet, von einem tumor-assoziierten Ödem umgeben (Hammoud et al. 1996). Histologisch gesichert wird das GBM durch Analyse der Biopsie / des resezierten Tumorgewebes, welches mehrkernige Riesenzellen, palisadenartige polymorphe Zellen und Nekrosen aufweist (Mikkelsen et al. 2021). Vom ähnlich aussehenden niedergradigen Astrozytom oder Oligodendrogliom wird das GBM Grad 4 durch Nachweis der

fehlenden Isocitrat-Dehydrogenase 1/2 (IDH1/2) Mutationen abgegrenzt (Rushing 2021). Des Weiteren wurden in der Vergangenheit molekulare Subgruppen des GBM identifiziert, die im nächsten Abschnitt beschrieben werden.

### 1.1.3 Molekulare Subtypen des Glioblastoms

(Epi-)Genom- und Transkriptomanalysen von Glioblastom-Biopsien oder Resektionsgewebe zeigten eine große intertumorale Heterogenität und ermöglichten die Identifizierung verschiedener molekularer Glioblastom-Untergruppen (Ma et al. 2020). Diese wurden als klassische, proneurale, mesenchymale und zunächst auch neurale Subtypen beschrieben (Verhaak et al. 2010, Wang et al. 2017), wobei auch mehrere molekulare Subtypen in einem Tumor vorkommen können (Patel et al. 2014). Später wurde gezeigt, dass der neurale Subtyp wahrscheinlich nur das Resultat eines hohen Anteils von Normalgewebe im analysierten Tumorgewebe war. Die definierten Subgruppen unterscheiden sich zudem in ihrem immunologischen Mikromilieu (Mikroenvironment) (Wang et al. 2017). Bei geringer intratumoraler Heterogenität kann die Identifizierung des Subtyps zudem als prognostischer Faktor herangezogen werden (Yoon et al. 2016, Li et al. 2018, Zhang et al. 2021). Auch eine stark ausgeprägte intratumorale Heterogenität allein wurde bereits als Marker für eine schlechtere Prognose identifiziert (Liesche-Starnecker et al. 2020). Neben diesen Subtypen wurden auch weitere prognostische bzw. prädiktive Marker für den Krankheitsverlauf bzw. das Therapieansprechen beim Glioblastom gefunden. Zu diesen gehört die Methylierung des Promotors des Temozolomid-Resistenzgens MGMT (O6-Methylguanin-DNA-Methyltransferase), die mit einer besseren Prognose verbunden ist (Alnahhas et al. 2020). Die Analyse von Genom-, Transkriptom- und Methylom-Daten bei Glioblastompatient:innen trug zum Verständnis der Tumorgenese, zur Subklassifizierung des Tumors und zur Abgrenzung zu anderen Hirntumor-Entitäten bei (Karimi et al. 2019). Sie kann aber mit Ausnahme des IDH-Mutations- und MGMT-Promotor-Methylierungsstatus bis dato nicht zur Prognose des Krankheitsverlaufs oder zur Therapiestratifizierung verwendet werden. (Herrlinger et al. 2019). Gründe dafür könnte der zeitliche Aufwand (im Mittel 25 Tage) (Karimi et al. 2019) und die begrenzte Verfügbarkeit der Analysemethoden in den Zentren sein (Villani et al. 2023).

Es wird vermutet, dass die schlechte Prognose und das hohe Therapieversagen zudem stark vom immunsuppressiven Tumormilieu, dem infiltrativen Wachstum und der Therapieresistenz von Glioblastomzellen abhängt. Letzteres ist vor allem auf die Eigenschaften der stammzellähnlichen Glioblastomzellen zurückzuführen (Wang et al. 2017).

#### 1.1.4 Glioblastom Stammzellen (GSC)

Laut der Krebsstammzelltheorie (Reya et al. 2001) weist die überwiegende Mehrheit der Glioblastomzellen einen "differenzierten" Phänotyp auf, während nur ein kleiner Anteil der Tumorzellen einen stammzellartigen (oder tumorinitiierenden) Phänotyp zeigt. Neben diesen transformierten Zellen rekrutiert das Glioblastom verschiedene andere Zellarten wie Astrozyten, Mikroglia, myeloische Zellen, Neuronen, normale Stammzellen etc., die zusammen einen großen Anteil der Gesamttumormasse ausmachen (Hambardzumyan et al. 2016). Glioblastom Stammzellen (GSCs) gelten als die therapieresistenteste Subpopulation eines Tumors, da sie (im Vergleich zu Bulk-Zellen) langsamer proliferieren, die apoptotischen Signalwege herunterregulieren, die DNA-Reparatur und die oxidative Abwehr hochregulieren und sich besser an Stressoren des Tumormikromilieus anpassen, die durch Entzündungen, Hypoxie, niedrige pH-Werte und Nährstoffmangel entstehen (Lathia et al. 2015). Außerdem können GSCs bei Anwesenheit von Stressoren (z.B. Radiochemotherapie) in den Zellzyklusarrest übergehen und sich nach der Therapie beschleunigt repopulieren. (Batlle and Clevers 2017).

Wegen des kleinen Anteils der GSCs an der Gesamttumormasse, sind GSC-spezifische Marker mit potenziell prognostischem oder prädiktivem Wert für den Krankheitsverlauf in den Transkriptomdaten von Glioblastom-Biopsie- und Resektionsproben unterrepräsentiert. Die mRNA-Einzelzellsequenzierung identifizierter Glioblastomzellen ist ein aufwändiger Ansatz zur Gewinnung von GSC-spezifischen Transkriptomdaten (Wang et al. 2017). Alternativ kann in Primärkulturen, kultiviert in serumfreien Medium, das für die Selektion oder Induktion neuraler Stamm-/Progenitorzellen entwickelt wurde, der Anteil an GSCs enorm vergrößert werden (Bhat et al. 2013, Riedel et al. 2021). Ein Nachteil von GSC angereicherten Primärkulturen stellen die potentielle kulturbedingten Veränderungen der Genexpressionsmuster dar, da eine hohe Plastizität innerhalb der verschiedenen GSC und "differenzierten" (d.h. herunterregulierte Expression von Stammzellmarkern)

Phänotypen vermutet werden (Bhat et al. 2020). Darüber hinaus fehlt in Primärkulturen die wechselseitige Interaktion zwischen den GSCs und der Mikroumgebung des Tumors. Innerhalb der perivaskulären Stammzellnischen tragen z.B. Interaktionen zwischen Endothel- und Tumorzellen zur Induktion und/oder Aufrechterhaltung des GSC-Phänotyps bei (Yan et al. 2014). Es liegen nur wenige Daten (Barnes et al. 2018) über den Grad der De- oder Transdifferenzierung von GSC-Subtypen während der isolierten Primärkultur vor. Ein wichtiger Vorteil der Verwendung von primären GSC-Kulturen ist jedoch, dass angereicherte GSCs die funktionelle Charakterisierung von GSC-Subpopulationen *in vitro* ermöglichen.

Es wurden zwei verschiedene Subpopulationen von GSCs - mesenchymale und proneurale - beschrieben, die sich im Expressionsmuster von Stammzellmarkern unterscheiden (Mesrati et al. 2020, Tang et al. 2021). Interaktionen innerhalb des Glioblastom-Mikromilieus ermöglichen aufgrund hoher phänotypischer Plastizität den Übergang zwischen "differenzierten", proneuralen und mesenchymalen GSC-Phänotypen (Eckerdt and Plataniias 2023). In Analogie zu den Eigenschaften der epithelial- zu mesenchymalen Transition (EMT) als postulierte Voraussetzung für die Metastasierung von Krebszellen (Puram et al. 2017), wird vermutet, dass eine proneural- zu mesenchymale Transition (PMT) das Auswandern von Glioblastomzellen und die Infiltration des Gehirns fördert (Yusuf et al. 2022). In Primärkulturen ist ein mesenchymaler GSC-Phänotyp über sein Transkriptionsprofil hinaus durch eine adhäsive Wachstumsmorphologie und eine höhere Strahlenresistenz (Batlle and Clevers 2017) sowie durch schnellere Zell-Migration und Gel-Invasion (Kahlert et al. 2012, Binda et al. 2017) gekennzeichnet als der proneurale GSC-Phänotyp, der durch die Bildung von 3D Kulturen - sogenannten Spheroïden - gekennzeichnet ist.

#### 1.1.5 Glioblastom-Stammzellmarker

Für die Definition der Subpopulationen der GSCs wurden in der Literatur viele verschiedene Stammzellmarker beschrieben (Tang et al. 2021) wobei in dieser Dissertation nur auf einige verwendete Marker eingegangen wird.

Ein weit verbreiteter Marker für den mesenchymalen Subtyp ist die Aldehyd-Dehydrogenase-1A3 (ALDH1A3) (Mao et al. 2013, Cheng et al. 2016, Du et al. 2016, Li et al. 2018, Chen et al. 2019), welche Retinal zu Retinsäure oxidiert (Ying et al. 2011). Retinsäure wiederum hemmt nachweislich den Notch1-Signalweg (Fan et al.

2010) und die Expression der proneuralen Stammzellmarker Prominin-1 (CD133), Musashi1 (MSI1), Nestin und Sox2 in Glioblastomzellen (Ying et al. 2011). Die Variante III des epidermalen Wachstumsfaktor-Rezeptors (EGFRvIII) hingegen induziert Berichten zufolge die proneuralen Stammzellmarker Notch1, Sox2, Nestin und Prominin-1 (CD133) in Glioblastomzellen und unterdrückt die Expression des astrozytären Differenzierungsmarkers GFAP (glial fibrillary acidic protein) (Emlet et al. 2014, Yin et al. 2015, Kim et al. 2021). Zudem trägt der Chemokinrezeptor CXCR4, welcher auch mesenchymale hämatopoetische Stammzellen in Nischen des Knochenmarks hält (Levesque and Winkler 2008), zur Selbsterneuerung, Migration, Infiltration und Strahlenresistenz von Glioblastomzellen bei und wird daher als Stammzellmarker in Glioblastomen angesehen (Fareh et al. 2012).

Neben den erwähnten Stammzellmarkern wurde auch eine erhöhte Expression von Calcium aktivierbaren Kalium Kanälen hoher ( $BK_{Ca}$ ) und mittlerer ( $IK_{Ca}$ ) Leitfähigkeit in stammzellangereicherten (Primär)kulturen gefunden (Rosa et al. 2017, Klumpp et al. 2018), wobei die mRNA-Expressionslevel von  $IK_{Ca}$  und ALDH1A3 stark miteinander korrelierten (Klumpp et al. 2018). Darüber hinaus wurden diese Kaliumkanäle bereits in vielen Tumorentitäten mit einer erhöhten Malignität in Verbindung gebracht, wodurch sie als potentielle Zielstrukturen für neue Behandlungsstrategien in der aktuellen Forschung untersucht werden.

## 1.2 Kaliumkanäle

Die Familie der Kaliumkanäle lässt sich in verschiedene Untergruppen einteilen, die sich von ihrer Struktur, ihrer Aktivierbarkeit und ihrer Funktion voneinander unterscheiden. (Kaczmarek et al. 2017) Strukturell bestehen Kaliumkanäle aus vier  $\alpha$ -Untereinheiten, welche als Tetramer die membranintegrierte Pore formen sowie aus  $\beta$ -Untereinheiten, die durch Zusammenlagerung mit  $\alpha$ -Untereinheiten ein Heterotetramer bilden können (Christie et al. 1990).

### 1.2.1 $Ca^{2+}$ - aktivierbare Kaliumkanäle

Die Vertreter der  $Ca^{2+}$  - aktivierten Kaliumkanäle können nochmals nach ihrer Einzelkanal-Leitfähigkeit in drei Gruppen unterteilt werden, die sich z.T. in ihrer Struktur aber v.a. in ihren biophysikalischen Eigenschaften unterscheiden. Sie werden als SK1-3 - (small conductance, 2-20 pS;  $K_{Ca2.1-3}$ ),  $IK_{Ca}$  - (intermediate conductance,



20-60 pS; KCa3.1, KCNN4) und BK<sub>Ca</sub>- (large conductance, 150-300 pS; KCa1.1, Slo1, KCNMA1) Kanäle mit jeweils niedriger, mittlerer oder hoher Leitfähigkeit bezeichnet (Stocker 2004). Obwohl die fast ubiquitär exprimierten BK<sub>Ca</sub>-Kanäle auch spannungsabhängig sind, würden sie für die Öffnung eine zu hohe Depolarisation des Membranpotenzials benötigen, die unter physiologischen Bedingungen nicht erreicht werden kann. Durch den Anstieg intrazellulären Ca<sup>2+</sup> wird die Spannungs-Aktivierungsschwelle weiter in negative, physiologische Spannungsbereiche verschoben, wodurch sich die Kanalpore öffnet (Carrasquel-Ursulaez et al. 2022). Im Gegensatz dazu öffnen SK und IK<sub>Ca</sub>-Kanäle spannungsunabhängig über die Bindung von freiem Ca<sup>2+</sup> an Calmodulin (Ca<sup>2+</sup>-Sensor), welches fest am C-Terminus der Kanäle bindet (Nam et al. 2021). IK<sub>Ca</sub>-Kanäle werden physiologisch im Gefäßsystem, im lymphatischen Gewebe, im Knochenmark und in verschiedenen Blutzellen sowie im Magen-Darm-Trakt exprimiert. Neben den im letzten Abschnitt erwähnten physiologischen Funktionen wird im Speziellen für IK<sub>Ca</sub> und BK<sub>Ca</sub> eine Assoziation mit der Malignität verschiedener Tumorentitäten angenommen, deren heutige Erkenntnisse im nächsten Absatz zusammengefasst werden.

### 1.2.2 Bisherige Erkenntnisse der Rolle von IK<sub>Ca</sub> und BK<sub>Ca</sub> Kanälen in der Krebspathophysiologie

Zahlreiche Publikationen deuten darauf hin, dass verschiedene Tumorentitäten mesenchymalen (Sarkom, Leukämie), epithelialen (z. B. Prostatakarzinom) oder glialen Ursprungs IK<sub>Ca</sub> - Kanäle stark überexprimieren (Überblick s.(Mohr et al. 2019). Auch wurde eine veränderte Expression des BK<sub>Ca</sub>-Kanals in mehrere Krebsarten einschließlich Brustkrebs (Mohr et al. 2020) sowie Glioblastom (Liu et al. 2002) nachgewiesen. Diese Hochregulation in verschiedenen Tumorentitäten klassifiziert sie als "Onkokanäle". (Überblick s. (Ganser et al. 2021)). In Krebszellen spielen diese Kanäle bei der Zellzykluskontrolle (Parihar et al. 2003, Du et al. 2019), der malignen Progression (Song et al. 2017), der Gewebeinvasion (Edalat et al. 2016, Rosa et al. 2017, Catacuzzeno and Franciolini 2018, Stransky et al. 2023), Fernmetastasierung (Khaitan et al. 2009, Rabjerg et al. 2015), Chemo- (D'Alessandro et al. 2016, Pillozzi et al. 2018) und Radioresistenz (Stegen et al. 2015, Mohr et al. 2019, Stransky et al. 2022) nachweislich eine entscheidende Rolle.

Letztere Funktion der Kanäle wird durch frühere Publikationen untermauert. Diese zeigen, dass eine  $IK_{Ca}$ -Hemmung durch TRAM-34 oder eine  $BK_{Ca}$ -Blockade durch Paxilline die Strahlenresistenz oder die Tumorstreuung in den Glioblastom-Zelllinien T98G (Edalat et al. 2016), U87MG, (Steinle et al. 2011), U521 (Turner et al. 2014, Stegen et al. 2016), GL261 (Ruggieri et al. 2012), GL-15 (Fioretti et al. 2006) *in vitro* oder in präklinischen ektopischen oder orthotopen Gliom *in vivo*-Modellen (D'Alessandro et al. 2013, Stegen et al. 2015, Edalat et al. 2016, Stransky et al. 2023) hemmen. In Brusttumorproben wurde außerdem durch Expressionsprofile eine Hochregulation der  $IK_{Ca}$  Expression in der Krebsstammzellpopulation beobachtet (Bai et al. 2007, Panaccione et al. 2017). Wie  $IK_{Ca}$  wurden auch  $BK_{Ca}$  (Bai et al. 2007) und CXCR4 (Ji et al. 2020) mit normalen, aus Fettgewebe stammenden mesenchymalen Stammzellen in Verbindung gebracht, was auf eine spezifische Funktion von  $IK_{Ca}$ ,  $BK_{Ca}$  und CXCR4 in mesenchymalen GSCs hindeuten könnte. Daher könnte eine pharmakologische  $IK_{Ca}$ - oder  $BK_{Ca}$ -Blockade eine vielversprechende neue Strategie in der Krebs- und insbesondere in der Glioblastomtherapie sein (Ohya et al. 2009, Todesca et al. 2021).

Neben den in der Grundlagenforschung verwendeten Inhibitoren TRAM-34 bzw. Paxilline sind bereits Wirkstoffe für andere Indikationen zugelassen, für die (zusätzlich) eine inhibitorische Wirkung auf  $IK_{Ca}$  bzw.  $BK_{Ca}$  Kanäle nachgewiesen wurde. Das topisch angewendete Breitbandantimykotikum Clotrimazol weist eine ähnliche Struktur wie TRAM-34 auf und blockiert den  $IK_{Ca}$  Kanal mit einer  $IC_{50}$  von 0.92  $\mu$ M (Palchadhuri et al. 2008). Außerdem wurde der selektive  $IK_{Ca}$ -Blocker Senicapoc (ICA-17043,  $IC_{50}$ =11 nM) (Stocker et al. 2003) bereits in einer klinischen Phase III Studien zur Behandlung von Sichelzellanämie getestet und gut vertragen (Ataga et al. 2011, Ataga et al. 2021). Weitere Phase II Studien zur Behandlung von Alzheimer (ClinicalTrials.gov-Identifikationsnummer NCT04804241) oder Asthma (ClinicalTrials.gov-Identifikationsnummern: NCT00861211, NCT00861185) sind noch nicht abgeschlossen.

Auch  $BK_{Ca}$  scheint durch zwei zugelassene Wirkstoffe (Haloperidol und Chlorpromazin;  $IC_{50}$  (1,1-3,6 bzw. 2,3-8,1  $\mu$ M) (Lee et al. 1997) aus der Gruppe der typischen Neuroleptika inhibiert zu werden. Haloperidol und Chlorpromazin werden zur Behandlung von (akuten) Psychosen, Schizophrenie und bipolaren Störungen

eingesetzt. Da sie im Gehirn angereichert werden (Huang and Ruskin 1964, Korpi et al. 1984) könnte die benötigte Konzentration zur Blockade von BK<sub>Ca</sub> Kanälen erreicht werden. In einer Phase-I-Dosiseskalationsstudie wird derzeit die Verabreichung von Chlorpromazin als Zusatztherapie zur Radiochemotherapie mit Temozolomid zur Behandlung neu diagnostizierter Glioblastome untersucht (klinische ClinicalTrials.gov-Identifikationsnummer NCT05190315), um zu klären, ob eine Chlorpromazin-Therapie bei vermeintlich BK<sub>Ca</sub>-hemmenden Konzentrationen im Gehirn bei Glioblastom-Patient:innen grundsätzlich möglich ist.

## 2. Zielsetzung

Wie in der Einleitung bereits beschrieben, handelt es sich beim Glioblastoma Multiforme (GBM) um einen bösartigen, sehr aggressiven Hirntumor für den seit Jahren keine innovativen Behandlungsmöglichkeiten entwickelt werden konnten, die zu einer deutlichen Verlängerung des Überlebens (Median < 2 Jahren) beitragen. Die schlechte Krankheitsprognose resultiert sehr wahrscheinlich aus dem hoch infiltrativen Wachstum von proliferativen, im Gehirn stark verteilten Glioblastom-Zellen, welche eine Tumor-Komplettresektion erschweren, sowie aus der hohen Resistenz der Glioblastomzellen gegenüber Strahlen- und Chemotherapie. Man nimmt an, dass insbesondere die Tumorstammzell-Subpopulation zur Therapieresistenz und Therapieversagen beiträgt.

Der erste Teil des Projekts hat das Ziel, Subpopulationen von Glioblastomstammzellen (GSC) aus Primärkulturen, die in Tübingen aus Glioblastomresektaten von 23 Glioblastompatient:innen gewonnen wurden, mit Hilfe einer molekularen mRNA-Signatur zu identifizieren. Anschließend sollen die Phänotypen dieser Stammzell-Subpopulationen funktionell charakterisiert und ihre intrinsische Radioresistenz und Invasivität mit der molekularen mRNA-Signatur assoziiert werden. Als letztes soll überprüft werden, ob zwischen der molekularen mRNA-Signatur bzw. dem funktionellen Phänotyp in den jeweiligen GSC-Kulturen und den Rezidivierungsmustern bzw. Gesamtüberleben der dazugehörigen Glioblastompatient:innen eine Korrelation vorliegt. Eine derartige Korrelation würde auf den prognostischen Wert des *in vitro* GSC-Phänotyps für den Krankheitsverlauf hinweisen und könnte möglicherweise zukünftig zur Stratifizierung der Patienten bei neuen Therapieansätzen verwendet werden.

Die beiden als „Onkokanäle“ eingestuften  $\text{Ca}^{2+}$ -aktivierten Kaliumkanäle  $\text{IK}_{\text{Ca}}$  und  $\text{BK}_{\text{Ca}}$  werden in den hoch-malignen und invasiven mesenchymalen Glioblastom-Stammzellen stark exprimiert. Die „Druggability“ dieser Kanäle eröffnet die Möglichkeit, sie als potentielle neue Zielstrukturen für neue Therapiestrategien von Glioblastompatient:innen zu nutzen. Aus diesem Grund soll im zweiten Teil des Projekts die Durchführbarkeit sowie die antiinvasive und radiosensibilisierende Wirksamkeit einer pharmakologischen  $\text{K}_{\text{Ca}}$ -Kanal Blockade in primären GSC-anreichernden Kulturen *in vitro* und nach deren orthotopen *Xenotransplantation* im Gliom-Mausmodell *in vivo* untersucht werden.

### 3. Ergebnisse

*Studie 1. Ganser K, Eckert F, Riedel A, Stransky N, Paulsen F, Noell S, Krueger M, Schittenhelm J, Beck-Wödl S, Zips D, Ruth P, Huber SM, Klumpp L. Patient-individual phenotypes of glioblastoma stem cells are conserved in culture and associate with radioresistance, brain infiltration and patient prognosis. Int J Cancer. 2022;150(10):1722-1733. doi: 10.1002/ijc.33950.*

#### 3.1. Identifizierung einer molekularen proneuralen zu mesenchymalen mRNA-Signatur in GSC Primärkulturen

Wegen der geringen Größe der Tübinger Kohorte, bestehend aus 23 Glioblastompatient:innen (Ganser et al. 2022, Suppl. Tabelle S1), wäre die statistische Wahrscheinlichkeit extrem gering, mittels Transkriptomanalyse mRNA-Marker oder eine abgeleitete molekulare Signatur zu identifizieren, die mit klinischen Daten der Patient:innen korreliert und prognostische Aussagen machen zu können. Daher wurde eine andere Strategie gewählt, die in diesem Abschnitt näher erläutert wird.

Zunächst wurde die mRNA-Abundanz von etablierten Stammzell- und Resistenzmarkern (Stegen et al. 2015, Stegen et al. 2016, Klumpp et al. 2018) in jeder der 24 GSC Primärkulturen mittels PCR bestimmt. Diese waren im Speziellen Nanog (Transkriptionsfaktor), CD133 (Prominin-1, Glykoprotein), Nestin (Intermediärfilament), Notch1 (Membranrezeptor), Sox2 (Transkriptionsfaktor), Oct4 (POU5F1, Transkriptionsfaktor), MSI1 (Musashi-1, RNA-bindendes Protein) und ALDH1A3 (Aldehyddehydrogenase-1A3), des neuralen Stammzell-/Glia-Vorläufermarkers FABP7 (zytoplasmatisches Fettsäure-bindendes Protein-7), des Astrozyten-Differenzierungsmarkers GFAP (glial fibrillary acidic protein, intermediate filament) bzw. der Invasionsmarker CXCR4 (Chemokinrezeptor), SDF1 (stromal cell derived factor-1, CXCL12, Chemokin) (Edalat et al. 2016), MMP2, -9, (Matrix Metalloproteinase-2 und -9) und der pro-migratorischen Ionenkanäle  $IK_{Ca}$  (*KCNN4*) (Ruggieri et al. 2012),  $BK_{Ca}$  (*KCNMA1*) (Steinle et al. 2011, Edalat et al. 2016) und TRPM8 (Melastatin-Familienmitglied-8 der nichtselektiven Transient-Rezeptor-Potential-Kationenkanäle) (Klumpp et al. 2017). Die Abundanzen dieser mRNAs zwischen den einzelnen GSC-Primärkulturen variierten zwar stark, jedoch konnten positive und negative Korrelationen zwischen den mRNA-Expressionsleveln verschiedener Marker festgestellt werden (Ganser et al. 2022, Abb. 1A). Nestin als

proneuraler Marker korrelierte dabei positiv ( $P_{cc} = 0,47 - 0,65$ ) mit FABP7, Notch1, Sox2 und MSI1, während der mesenchymale Marker ALDH1A3 (schwach) positiv ( $P_{cc} = 0,30 - 0,43$ ) mit  $IK_{Ca}$ ,  $BK_{Ca}$ , CXCR4 und OCT4 assoziierte. (Ganser et al. 2022, Abb. 1A). Außerdem zeigten die GSC-Primärkulturen unterschiedliche Wachstumsphänotypen, die von frei-schwimmenden Neurosphären (Wachstumsscore 1) bis hin zu adhärennten Zellmonolayern reichten (Wachstumsscore 4) (Ganser et al. 2022, Abb. 1B). Angesichts der bereits berichteten unterschiedlichen morphologischen Wachstumsphänotypen von mesenchymalen und proneuralen GSC-Subpopulationen in Primärkultur (Mao et al. 2013) wurde diese Einstufung zur Identifizierung einer molekularen proneuralen zu mesenchymalen mRNA-Signatur genutzt. Über den Wachstumsscore und insbesondere die oben genannten Korrelationen der mRNA-Abundanzen wurden zwei Gruppen mesenchymaler bzw. proneuraler Marker definiert und eine molekulare Signatur berechnet, die am besten mit dem Wachstumsphänotyp korrelierte (Ganser et al. 2022, Abb. 1C,  $P_{cc} = 0,82$ ). Dabei wurde jeweils das Verhältnis zwischen ihren mittleren Häufigkeiten gebildet, wobei die "mesenchymale" im Zähler (ALDH1A3,  $IK_{Ca}$ ,  $BK_{Ca}$ , CXCR4, OCT4) und die "proneurale" Markergruppe (Nestin, Notch1, Sox2, MSI1, FABP7) im Nenner gesetzt wurde. Die Heatmap (Ganser et al. 2022, Abb. 1D) veranschaulicht die Abhängigkeit zwischen den mRNA-Abundanzen und der definierten molekularen mRNA-Signatur der zehn Marker.

Schließlich konnte eine Abhängigkeit der molekularen Signatur vom Kontakt zur Kunststoffoberfläche der Kultivierungsgefäße (Ganser et al. 2022, Abb. 1E) und eine Veränderung dieser während der Kultivierungsdauer (>50 Passagen, Abb. 1F) ausgeschlossen werden. Im Anhang der referierten Publikation (Ganser et al. 2022, Suppl. Material, Teil C, Suppl Abb. S1-S4) konnte außerdem eine positive Korrelation einiger gemessener mRNA Expressionslevel mit zugehöriger (funktioneller) Proteinexpression mittels Durchflusszytometrie (ALDH1A3, CXCR4), Western Blot (ALDH1A3, Nestin) und (stichprobenartig) über Patch Clamp (LK7, LK19,  $IK_{Ca}$ ) Analyse beobachtet werden, was darauf hinweist, dass auch das Protein funktionell exprimiert wird.

## 3.2. Funktionelle Bedeutung der molekularen mRNA-Signatur

### 3.2.1 Assoziation mit Radiosensitivität und Invasionsverhalten *in vitro*

Um die funktionelle Bedeutung der berechneten mRNA-Signatur mit der intrinsischen Radiosensitivität zu bestimmen wurde das klonogene Überleben bestrahlter GSC Primärkulturen analysiert. Dabei wurden deutliche Unterschiede der Überlebenskurven zwischen den Kulturen (Ganser et al. 2022, Abb. 2A) und eine Korrelation ( $P_{cc} = 0,62$ ) zwischen den Überlebensraten nach Bestrahlung mit einer Dosis von 4 Gy ( $SF_{4Gy}$ ) und der molekularen mRNA-Signatur (Ganser et. al 2022, Abb. 2B) festgestellt. Einer Einteilung der  $SF_{4Gy}$  Werte über den Median der molekularen mRNA-Signatur ergab eine tendenziell ( $p = 0,063$ , n.s.) höhere intrinsische Radioresistenz von mesenchymalen GSC-Primärkulturen verglichen mit proneuralen Kulturen (Ganser et. al 2022, Abb. 2C). Zusammengefasst, deutet dies auf eine funktionelle Bedeutung der molekularen proneuralen zu mesenchymalen mRNA-Signatur auf die intrinsische Radiosensitivität der GSC-Primärkulturen hin.

Um die Auswirkung der Strahlentherapie auf die molekulare proneurale zu mesenchymale mRNA-Signatur abzuschätzen, wurde eine fraktionierte Bestrahlung von 5x 8 Gy an 5 aufeinanderfolgenden Tagen angewendet, die als dosisäquivalent zur standardmäßigen normofraktionierten Strahlentherapie von 60 Gy in 30 Fraktionen über 6 Wochen angesehen wurde. (s. Abschnitt: „Hypo-fractionated radiation protocol“ im Anhang von Ganser et. al 2022). In proneuralen GSCs (< mediane Signatur) führte die fraktionierte Bestrahlung zu einer Erhöhung des Wachstumsscores (Ganser et. al 2022, Abb. 2D) und proneuraler zu mesenchymaler Signatur, während in mesenchymalen GSCs (> mediane Signatur) kein solcher Anstieg nachweisbar war (Abb. 2E). Dies deutet auf eine mesenchymale Progression von proneuralen und intermediären, aber nicht von mesenchymalen GSC Primärkulturen hin.

Um die Bedeutung der molekularen mRNA-Signatur auf das Invasionsverhalten zu untersuchen, wurden Sphäroide der GSC Primärkulturen in ein Fibrinigel eingebettet. Mesenchymale, adhärent wachsende Kulturen wurden hierfür im Vorfeld durch speziell beschichtete Kulturflaschen mit geringer Anheftung als Sphäroide kultiviert. Schließlich wurden an den Tagen 0, 7, 14 und 21 nach der Einbettung die Invasionsflächen sowie die maximalen Invasionsdistanzen der matrixinfiltrierenden Zellen analysiert (Abb. 2F). Die 2D-projizierte Invasionsfläche pro Tag (Ganser et. al 2022, Abb. 2G) und die maximale Invasionsdistanz pro Tag (Ganser et. al 2022, Abb. 2H) korrelierten hierbei

positiv mit der molekularen mRNA-Signatur ( $P_{cc} = 0,81$  bzw.  $0,72$ ). Dies weist auf eine zusätzliche funktionelle Bedeutung der molekularen mRNA-Signatur für die Invasivität der GSC Primärkulturen hin.

Als nächster Schritt wurde die molekulare mRNA-Signatur mit den klinischen Daten der Tübinger Kohorte von Glioblastom-Patienten in Verbindung gebracht, von denen die GSC-Primärkulturen stammten.

### 3.2.2 Assoziation mit klinischen Daten der Tübinger Kohorte

Um die prognostische oder prädiktive Bedeutung der molekularen mRNA-Signatur für die Klinik zu identifizieren, wurden das Auftreten des neu diagnostizierten Glioblastoms und des Rezidivs (unifokal vs. multifokal) sowie das krankheitsfreie und Gesamtüberleben der Tübinger Glioblastom Patient:innen mit der molekularen mRNA-Signatur in Verbindung gebracht. Eine Patientin entwickelte zwei Glioblastome, einen MGMT-Promotor-unmethylierten Frontaltumor mit einer mesenchymalen mRNA-Signatur und einen MGMT-Promotor-methylierten temporo-okzipitalen Tumor mit einer proneuralen mRNA-Signatur, sodass 24 GSC Primärkulturen isoliert wurden (Ganser et al. 2022, Suppl. Tabelle S1).

Im ersten Punkt muss berücksichtigt werden, dass die GSC Primärkulturen ausschließlich aus Resektionsmaterial und nicht aus Biopsien generiert wurden (Etablierung, Isolation, Kultivierung, siehe Klumpp et al. 2018). Aus diesem Grund sind multifokale Primärtumore in dieser Kohorte wahrscheinlich unterrepräsentiert, da sie oft nicht chirurgisch reseziert werden. Konkret stammen nur drei der 24 herangezögten GSC Primärkulturen aus Resektionsmaterial von neudiagnostizierten multifokal Glioblastomen, welche mesenchymale (Rang 7/24 und 9/24) und intermediäre (Rang 13/24) molekulare mRNA-Signaturen aufwiesen. Durch die geringe Anzahl der GSC aus multifokalen GBM Resektaten, konnte keine Schlussfolgerung einer Korrelation zwischen den primären Tumorherden (uni- vs. multifokal) und molekularer mRNA-Signatur gezogen werden (Daten nicht gezeigt). Bei Betrachtung der Rezidivmuster konnte jedoch eine signifikant höhere mRNA-Signatur von multifokal ( $n = 11$ ) gegenüber unifokal ( $n = 7$ ) rezidivierenden Glioblastomen festgestellt werden (Ganser et. al 2022, Abb. 3A, B). Dies könnte auf eine Tumorausbreitung hindeuten, die mit mesenchymalen Glioblastomstammzellen assoziiert ist.



Für die Analyse des krankheitsfreien und Gesamtüberlebens, waren für 17 der 23 Patient:innen klinische Nachbeobachtungsdaten von  $\geq 10$  Monate verfügbar. Insgesamt erhielten 19 der 23 Patient:innen eine fraktionierte Strahlentherapie in verschiedenen Schemata und 14 begleitende Temozolomidtherapie. Außerdem wurden 4 Patient:innen im Rahmen einer klinischen Studie mit Nivolumab behandelt (siehe Ganser et. al 2022, Tab. S1). Trotz dieses sehr heterogenen Patientenkollektivs zeigte die Analyse des krankheitsfreien Überlebens eine schwache Tendenz ( $p = 0,22$ ) einer negativen ( $P_{\text{cc}} = -0,30$ ; Ganser et. al 2022, Abb. 3C) Korrelation und das Gesamtüberleben eine stark negative ( $P_{\text{cc}} = -0,81$ ; Ganser et. al 2022, Abb. 3D) Korrelation mit der molekularen mRNA-Signatur. Dies zeigten auch die Kaplan-Meier-Überlebenskurven (Abb. 3E, links), bei denen sich das krankheitsfreie Überleben zwischen Patient:innen mit proneuralen ( $\leq$  Median der molekularen mRNA-Signatur) GSCs und solchen mit mesenchymalen GSCs ( $>$  Median) nicht signifikant unterscheidet. Im Gegensatz dazu übertraf das Gesamtüberleben von Patient:innen mit proneuralen ( $\leq$  medianer molekularer mRNA-Signatur) GSCs in univariaten Tests signifikant ( $p \leq 0,001$ , Log-Rank-Test) das von Patient:innen mit mesenchymalen ( $>$  Median) GSCs (Ganser et. al 2022, Abb. 3E, rechts). Bemerkenswerterweise korreliert die molekulare mRNA-Signatur nicht mit etablierten prognostischen / prädiktiven Markern wie dem Patientenalter oder dem MGMT-Promotor Methylierungsstatus (Daten nicht gezeigt), was darauf schließen lässt, dass die molekulare mRNA-Signatur als unabhängiger prognostischer Marker gesehen werden kann.

### 3.2.3 Assoziation mit klinischen Daten von Glioblastom-Datenbanken

Als letztes wurde untersucht, ob sich die Assoziation zwischen Gesamtüberleben und der molekularen proneural zu mesenchymaler Signatur auch in öffentlich-zugänglichen Daten der Glioblastom-Datenbanken widerspiegelt. Hierzu wurde erneut die molekulare Signatur aus den mRNA-Expressionsdaten der zehn (Stammzell)-Marker aus den Datenbanken "The Cancer Genome Atlas" (TCGA), "Ivy Glioblastoma Atlas Project database" (Ivy GAP) und "Repository for Molecular Brain Neoplasia Data" (REMBRANDT) berechnet und Kaplan-Meier Kurven erstellt. In univariaten Tests der TCGA- und der Ivy-GAP-Datenbank zeigte sich eine bessere Überlebensrate von Patient:innen mit "proneuralen" Glioblastomen gegenüber Patient:innen mit "mesenchymalen" Tumoren nur, wenn die Stratifizierung anhand des besten Schwellenwerts durchgeführt wurde (Ganser et al. 2022, Abb. 3F, G). In der

REMBRANDT-Datenbank hingegen war kein Unterschied zwischen Patient:innen mit "proneuralen" und "mesenchymalen" Glioblastomen erkennbar (Abb. 3H). Wenn die Analyse der REMBRANDT-Datenbank jedoch für eine geringerer Heterogenität auf eine Untergruppe jener Patient:innen beschränkt wurde, die für eine Bestrahlung plus Temozolomid-Chemotherapie vorgesehen waren (REMBRANDT\*), so wiesen die Überlebenskurven erneut auf eine bessere Prognose für Patient:innen mit "proneuralen" im Vergleich zu denen mit "mesenchymalen" Tumoren hin (Ganser et al. 2022, Abb. 3I). Im Vergleich zu den GSC Primärkulturen deuten diese Ergebnisse darauf hin, dass die molekulare mRNA-Signatur zwischen mesenchymal und proneural in Proben des gesamten Tumorgewebes - wie sie in den Datenbanken zur Verfügung stehen - die Eigenschaften der primär kultivierten Glioblastom-Stammzellsubpopulationen nur in gewissem und variablem Maße beschreibt.

*Studie 2. Ganser K, Stransky N, Abed T, Quintanilla-Martinez L, Gonzalez-Menendez I, Naumann U, Koch P, Krueger M, Ruth P, Huber SM, and Eckert F. K<sub>Ca</sub> channel targeting impairs DNA repair and invasion capability of patient-derived glioblastoma stem cells in culture and orthotopic mouse xenografts, submitted*

### 3.3 Expression von IK<sub>Ca</sub>-, BK<sub>Ca</sub> - und Stammzellmarkern in Primärkulturen von Glioblastom-Stammzellen aus Patientenresektaten

Wie in der Einleitung bereits beschrieben, weisen vorhergehende Erkenntnisse darauf hin, dass die Ca<sup>2+</sup>- aktivierten IK<sub>Ca</sub> - und BK<sub>Ca</sub> - Kanäle für die Biologie des Glioblastoms eine hohe funktionelle Bedeutung haben. Deswegen wurde die Abhängigkeit des Gesamtüberlebens der Patient:innen von den *KCNN4* (IK<sub>Ca</sub>) und *KCNMA1* (BK<sub>Ca</sub>) mRNA-Abundanzen in Glioblastomresektaten in mehreren Glioblastom-Datenbanken untersucht. Dazu wurden die Daten des „The Cancer Genome Atlas“ (TCGA), des „Chinese Glioma Genome Atlas“ (CGGA), der „Ivy Glioblastoma Atlas Project Datenbank“ und die „Repository for Molecular Brain Neoplasia Data“ (REMBRANDT) zunächst nach Patient:innen gefiltert, die eine Strahlentherapie erhalten hatten. Anschließend wurden die *KCNN4* und *KCNMA1* mRNA-Expressionsdaten nach dem ersten Quartil stratifiziert und gepoolt. In univariaten Tests ergab diese Meta-Analyse einen prognostischen / prädiktiven Stellenwert für *KCNN4* (Ganser et al. 2023, Abb. 1A, rechts) aber nicht für *KCNMA1* (Ganser et al. 2023, Abb. 1A, links), was auf eine etwas bessere

Gesamtüberlebenswahrscheinlichkeit von Patient:innen mit geringerer *KCNN4* mRNA Expression im Tumor hindeutet.

Eine Stratifizierung der Glioblastom-Patient:innen aus der Tübinger Kohorte (klinische Daten siehe Ganser et al 2022, Suppl. Tabelle S1) nach der medianen *KCNN4* - (Ganser et al. 2023, Abb. 1B, links) oder *KCNMA1* - (Ganser et al. 2023, Abb. 1B, rechts) mRNA-Häufigkeit der GSC-Kulturen zeigte dagegen, dass die Patient:innen mit einer niedrigeren *KCNN4* - oder *KCNMA1* mRNA-Abundanz in den jeweilig dazugehörigen Kulturen ein längeres medianes Gesamtüberleben aufwiesen. Dieses Ergebnis führt zu der Hypothese, dass *KCNN4* und *KCNMA1* in der GSC angereicherten Primärkultur eigenständige prognostische Marker für den Krankheitsverlauf sein und zudem das Ansprechen auf eine gegen diese  $K_{Ca}$ -Kanäle gerichteten Therapie voraussagen könnten. Deswegen wurden alle 24 GSC Primärkulturen der Tübinger Kohorte mittels RT-PCR auf ihre *KCNN4* und *KCNMA1* mRNA-Abundanz hin untersucht und zwei mit hoher *KCNN4* (LK7, LK13), zwei mit hoher *KCNMA1* (LK12, LK28) und zwei mit nicht nachweisbarer *KCNN4* und *KCNMA1* mRNA-Expression (LK19, LK39) für Experimente zur  $K_{Ca}$  Kanal-Blockade ausgewählt (Ganser et al. 2023, Abb 1C, rot umrandet). Die funktionelle Expression des  $IK_{Ca}$  und  $BK_{Ca}$  Kanals wurde wie in Abschnitt 3.1 stichprobenartig in LK13 (hohe  $IK_{Ca}$  mRNA Abundanz) und LK28 (hohe  $BK_{Ca}$  mRNA Abundanz) mit Hilfe der Patch-Clamp Methode nachgewiesen (Ganser et al.2023, Suppl. Abb. S3-5).

Da fraktionierte Bestrahlung die molekulare mRNA-Signatur, die  $IK_{Ca}$  und  $BK_{Ca}$  als mesenchymale Marker enthält, verändern (s. Abschnitt 3.2.1) oder langfristige  $K_{Ca}$  Blockaden durch Hochregulation eines anderen Kanaltyps kompensiert werden könnte, wurde getestet, ob die gewählte fraktionierte Bestrahlung (5x 0 oder 5x 2 Gy) und/oder pharmakologische  $IK_{Ca}$ - (TRAM-34) oder  $BK_{Ca}$  - (Paxilline) Blockade Veränderungen in den mRNA-Abundanzen beider Kanäle oder der molekularen proneural zu mesenchymalen Signatur hervorrufen. Wie in Ganser et al. 2023, Suppl. Abb. S1A+B gezeigt, führten weder eine fraktionierte Bestrahlung noch eine  $IK_{Ca}$ - oder  $BK_{Ca}$ -Hemmung über 5 Tage zu einer Veränderung der mRNA-Abundanzen von *KCNN4* und *KCNMA1*, noch der molekularen Signatur, obwohl bei zwei GSCs (LK39, LK12) die kombinierte Behandlung einen Anstieg (CXCR4, NOTCH1, MSI1) oder eine Abnahme (Nestin, FABP7) einzelner Marker der Signatur hervorrief (Ganser et al. 2023, Suppl Abb. S2).

Zusammenfassend wird geschlussfolgert, dass der individuelle GSC-Phänotyp während des Behandlungszeitraums erhalten bleibt.

### 3.4 Effekte einer IK<sub>Ca</sub> bzw. BK<sub>Ca</sub> Blockade auf GSC-Kulturen *in vitro*

#### 3.4.1 Funktionelle Bedeutung der IK<sub>Ca</sub> und BK<sub>Ca</sub> Kanäle für die DNA-Reparatur

Um die Rolle von IK<sub>Ca</sub> und BK<sub>Ca</sub> bei der Reparatur von DNA-Schäden zu testen, wurde IK<sub>Ca</sub> in den GSC-Primärkulturen LK7, LK13 und LK39 durch TRAM-34 blockiert, während BK<sub>Ca</sub> in LK12-, LK19- und LK28-GSCs durch Paxilline (beide jeweils 0 oder 5 µM in DMSO) gehemmt wurde. Während der Inkubation der Blocker wurde eine fraktionierte Bestrahlung mit 0 oder 2 Gy an 5 aufeinanderfolgenden (5x 0 oder 5x 2 Gy) Tagen durchgeführt. Verbleibende nukleäre γH2AX-Foci als Surrogatmarker für residuale DNA-Doppelstrangbrüche (DSBs) (Redon et al. 2010) wurden 24 h nach der letzten Bestrahlungsfraction immunhistochemisch bestimmt (Ganser et al. 2023, Suppl. Fig. S6). TRAM-34 allein induzierte in LK7 (hohe *KCNN4* mRNA-Expression, Ganser et al. 2023, Abb. 1D, Mitte) GSCs einen signifikanten Anstieg der Zellfraktion mit nukleären γH2AX-Foci im Vergleich zur Vehikel-Kontrolle, was auf eine Hemmung der DNA-DSB-Reparatur hinweist. In ähnlicher Weise tendierte der TRAM-34-Effekt (p = 0,058) in 5x 2 Gy-bestrahlten LK7-Zellen zu einem Anstieg der γH2AX-Foci-positiven Zellkernfraktion. In LK13 (hohe *KCNN4* mRNA-Expression, Ganser et al. 2023, Abb. 1D, Mitte) und LK39 (niedrige *KCNN4* mRNA-Expression, Ganser et al. 2023, Abb. S7, rechts) GSCs hatte TRAM-34 allein oder in Kombination mit fraktionierter Bestrahlung keinen Einfluss auf die verbleibenden γH2AX-Foci. In LK12 (Ganser et al. 2023, Suppl. Abb. S7, links) und LK28 (Ganser et al. 2023, Abb. 1D, rechts) GSCs (beide mit hohem *KCNMA1* mRNA-Expression) verringerte die Behandlung mit Paxilline (5 µM) allein den Anteil der Kerne mit γH2AX-Foci im Vergleich zur Vehikel-Kontrolle signifikant. In bestrahlten (5x 2 Gy) LK28 (Ganser et al. 2023, Abb. 1D, rechts), aber nicht in bestrahlten LK12 (Ganser et al. 2023, Suppl. Abb. S7, links), führte die Behandlung mit Paxilline zu einem signifikanten Anstieg dieser Fraktion, was auf eine Beeinträchtigung der DNA-DSB-Reparatur schließen lässt. In unbestrahlten (5x 0 Gy) und bestrahlten (5x 2 Gy) LK19-Zellen, in denen eine BK<sub>Ca</sub>-Expression nicht nachweisbar war, hatte Paxilline keinen Effekt (Ganser et al. 2023, Abb. S7 Mitte). Diese Daten könnten auf ein komplexes Zusammenspiel von BK<sub>Ca</sub> mit der DNA-Reparatur oder der Dynamik von γH2AX-Foci Bildung hindeuten

Der Vergleich der LK7- und LK13 bzw. LK12 und LK28 legt nahe, dass das Ausmaß der IK<sub>Ca</sub> bzw. BK<sub>Ca</sub> mRNA-Abundanzen allein nicht ausreicht, um die Wirkung von TRAM-34 bzw. Paxilline auf die DNA-DSB-Reparatur vorherzusagen.

### 3.4.2 Funktionelle Bedeutung der IK<sub>Ca</sub> und BK<sub>Ca</sub> Kanäle für das klonogene Überleben und den Zellzyklus

Bei Betrachtung der vorherigen Ergebnisse (Abschnitt 3.4.1), stellte sich die Frage, ob eine Hemmung der DNA-Reparatur durch IK<sub>Ca</sub> bzw. BK<sub>Ca</sub> Blockade mit einem verminderten klonogenen Überleben zusammenhängen könnte. Dies wird in den nächsten Experimenten untersucht.

Hierzu wurden pre-plated Limited Dilution Assays mit 0, 4 oder 8 Gy bestrahlten GSC Primärkulturen durchgeführt, die mit TRAM-34 (0 oder 5 µM, LK7, LK13, LK39) oder Paxilline (0 oder 5 µM, LK12, LK19, LK28) co-inkubiert wurden. Die Überlebensfraktionen der GSCs bei 4 Gy (SF4) korrelierten auch hier wieder mit der molekularen mRNA-Signatur (Pearson und Spearman Korrelationskoeffizienten von  $r = 0,76$  bzw.  $r = 0,48$ , Daten nicht gezeigt), womit unsere früheren Befunde bestätigt wurden (s. Abschnitt 3.2.1). Passend zu den beobachteten Effekten der applizierten Inhibitoren auf die DNA-Reparatur wurden nur LK7- (Ganser et al. 2023, Abb. 1E, links) und in der Tendenz ( $p = 0,1$ ) auch LK28- (Ganser et al. 2023, Abb. 1E, rechts) GSCs durch TRAM-34 bzw. Paxilline radiosensibilisiert, wohingegen keine Radiosensibilisierung bei den GSCs LK13 (Ganser et al. 2023, Abb. 1E, Mitte), LK12, LK19 und LK39 (Ganser et al. 2023, Suppl. Abb. S8) nachweisbar war.

Da wie beschrieben die Aktivität von K<sup>+</sup>-Kanälen erforderlich ist, um in bestrahlten Krebszellen einen Zellzyklusarrest auszulösen (Stegen'15, Palme'13, Palme'20), könnten die beobachteten Auswirkungen von TRAM-34 oder Paxilline auf die DNA-Reparatur und das klonogene Überleben von LK7 und LK28 auf eine vorzeitige Aufhebung des Zellzyklusarrests zurückzuführen sein. Daher haben wir die Wirkung der IK<sub>Ca</sub>- und BK<sub>Ca</sub>-Blockade auf die Verteilung der Zellzyklusphasen und den durch DNA-Schäden ausgelösten Zellzyklusarrests in unseren GSC-Kulturen mittels Durchflusszytometrie analysiert. Dafür wurde eine Nicoletti-Färbung der DNA 48 Stunden nach Bestrahlung mit einer Einzeldosis von 0, 4 oder 8 Gy durchgeführt. Darüber hinaus wurden die GSCs vor (1 h) und nach (48 h) der Bestrahlung mit TRAM-34 (0 oder 5 µM, LK7, LK13, LK39) oder Paxilline (0 oder 5 µM, LK12, LK19, LK28) inkubiert. In allen GSCs außer LK19 stimulierte die Bestrahlung dosisabhängig die

Akkumulation in der G2-Phase des Zellzyklus, unabhängig von der  $K_{Ca}$ -Kanal Blockade (Ganser et al. 2023, Abb. S9), was auf einen strahleninduzierten G2/M-Zellzyklusstillstand schließen lässt. Nur bei LK13 und LK39 waren signifikante, aber geringe Auswirkungen der Kanalblockade auf die Zellzyklusverteilung zu erkennen (Ganser et al. 2023, Abb. S9). Zusammengenommen deuten diese Daten darauf hin, dass eine gestörte Zellzyklusregulation höchstwahrscheinlich nicht die Ursache für die radiosensibilisierende Wirkung von TRAM-34 und Paxilline in LK7 bzw. LK28 Zellkulturen ist.

### 3.4.3 Funktionelle Bedeutung von $IK_{Ca}$ und $BK_{Ca}$ für die Gel-Invasion

Wie in Abschnitt 1.2.2 bereits erwähnt, spielen  $IK_{Ca}$  (Sciaccaluga et al. 2010, D'Alessandro et al. 2013, Catacuzzeno and Franciolini 2018) und  $BK_{Ca}$  (Wundergem and Bartley 2009, Cheng et al. 2016, Rosa et al. 2017) Kanäle eine zentrale Rolle bei der Migration von Glioblastomzellen und der Invasion in das Gehirn. Außerdem wurde in einigen Glioblastom-Modellen eine strahleninduzierte Hypermigration/Invasion beobachtet, die von  $IK_{Ca}$ - oder  $BK_{Ca}$ -Kanälen abhängig ist (Steinle et al. 2011, Edalat et al. 2016, D'Alessandro et al. 2019). Aus diesem Grund wurden die Effekte einer  $IK_{Ca}$ - und  $BK_{Ca}$ -Blockade (jeweils 0 oder 5  $\mu$ M in DMSO) auf die Invasion von Kontroll- (0 Gy) und bestrahlten (2 Gy) GSC-Kulturen in Fibringel untersucht. Hier wurden TRAM-34 und Paxilline in allen GSC-Kulturen unabhängig von deren *KCNN4* und *KCNMA1* mRNA-Expressionsleveln appliziert.

In unbehandelten Zellen war die Invasion, definiert durch die Zunahme der durch Glioblastomzellen invadierten Fläche pro Tag in den mikroskopischen Aufnahmen (Ganser et al. 2023, Abb. 2A) oder der maximalen Invasionsdistanz pro Tag (Abb. 2B), in der als höchst mesenchymal identifizierte GSC-Kultur LK7 (Ganser et al. 2023, Abb. 2, links) am höchsten, in LK13, LK28 (Abb. 2, Mitte und rechts) und LK12 (Ganser et al. 2023, Suppl. Abb. S11A, B, links) gering und in LK 19 und LK39 (Ganser et al. 2023, Suppl. Abb. S11, A, B, Mitte und rechts) fast nicht vorhanden. Die Korrelation der Invasivität mit der molekularen mRNA-Signatur der GSCs (Pearson und Spearman Korrelationskoeffizienten von  $r = 0,77$  bzw.  $r = 0,65$ , Daten nicht gezeigt), bestätigte frühere Befunde (Vergleiche mit Ganser et al 2022). Die Bestrahlung führte nur bei einer (LK7, Ganser et al. 2023, Abb. 2A, B links) der 6 getesteten GSC-Kulturen zu einer Tendenz zur Hyperinvasion und bei LK28 und LK12 GSCs sogar zu einer Hypoinvasion (Ganser et al. 2023, Abb. 2A, B Mitte und Suppl. Abb. S10 A, B, links).

TRAM-34 verringerte die Invasion von Kontroll- (0 Gy) oder bestrahlten (2 Gy) GSC-Kulturen, außer bei unbestrahlten (0 Gy) LK7-Zellen (Ganser et al. 2023, Abb. 2 und Supp. Abb. S10) nicht. Im Gegensatz dazu verringerte Paxilline die Invasion in Kontroll- und bestrahlten LK7 GSCs (Ganser et al. 2023, Abb. 2A, B, links) und bestrahlten LK13 und LK 28 GSCs (Ganser et al. 2023, Abb. 2A, B, Mitte und rechts), aber weder in LK12 (alle mit moderater oder hoher BK<sub>Ca</sub>-Expression) noch in LK19 oder LK39 Zellen (niedrige BK<sub>Ca</sub>-Expression, Ganser et al. 2023, Abb. S10).

Zusammengenommen zeigten die *in vitro*-Daten der GSC-Primärkulturen eine große Heterogenität in Bezug auf Strahlenempfindlichkeit und Invasivität. Eine K<sub>Ca</sub> Blockade der IK<sub>Ca</sub>- oder BK<sub>Ca</sub>-exprimierenden GSC-Kulturen konnte die DNA-Schadensreparatur beeinträchtigen, was eine Ursache für die Radiosensibilisierung und die Abschwächung der Gel-Invasion sein könnte.

### 3.5 Orthotope Xenotransplantation von aus Patienten stammenden GSCs in immunkompromittierte Mäuse und Überwachung der Glioblastombildung

Um die Durchführbarkeit und Wirksamkeit der gezielten K<sub>Ca</sub>-Kanal Hemmung bei gleichzeitiger fraktionierter Tumorbestrahlung im präklinischen *in-vivo* Modell zu testen, wurden mesenchymale LK7 (hohe *KCNN4* mRNA-Expression, TRAM-34-sensitiv), intermediäre proneurale/mesenchymale LK13 (hohe *KCNN4* und niedrige *KCNMA1* mRNA-Expression, TRAM-34-unempfindlich) und proneurale LK28 (niedrige *KCNN4*-und hohe *KCNMA1*-mRNA Expression, paxillinesensitiv) GSCs stereotaktisch im rechten Striatum von immunkompromittierten NSG-Mäusen nach Edalat et al. (2015) xenotransplantiert. Zur nicht-invasiven Kontrolle des Tumorwachstums wurde eine T2-gewichtete MRT-Sequenz entwickelt und der hyperintense Bereich als Tumor- und Ödemlokalisierung in MRT Aufnahmen definiert. Alle drei GSC-Kulturen entwickelten orthotope Tumore (wenn auch mit unterschiedlichen Anwachszeiten), was deren Fähigkeit zur Tumorbildung bestätigt (Ganser et al. 2023, Abb. 3A und 3B, links). Die Tumorbildung wurde (immun-)histochemisch als kernangereicherte Bereiche in der Standard-Hämatoxylin/Eosin (HE)-Färbung (Ganser et al. 2023, Abb. 3B, Mitte) und als humane Nucleolin-immunreaktive Zellen (Ganser et al. 2023, Abb. 3B, rechts) bestätigt.

Nach Sichtbarkeit der Tumore im MRT (1-5 Monate nach der Transplantation) wurden die Mäuse an fünf aufeinander folgenden Tagen mit einer täglichen Strahlenfraktion

von 0 oder 4 Gy (5x 0 oder 5x 4 Gy) bestrahlt und gleichzeitig mit  $IK_{Ca}$  - oder  $BK_{Ca}$  - Blockern behandelt. Hierfür wurden den Mäusen mit LK7- und LK13-Gliomen 6 Stunden vor jeder Bestrahlungsfraction intraperitoneal TRAM-34 (5x 0 oder 5x 120 mg/kg KG) injiziert. Mäusen mit LK28-Gliomen wurden 6 h vor und 6 h nach der täglichen Bestrahlungsfraction intraperitoneal Paxilline (10x 0 oder 10x 8 mg/kg KG) verabreicht (Abb. 3A). 24 Stunden nach der letzten Bestrahlungsfraction wurden die Mäuse sakrifiziert und die resezierten Gehirne für die Immunhistochemie vorbereitet.

### 3.5.1 Häufigkeit von ALDH1A3-exprimierenden GSCs *in vivo*

Wie in Abschnitt 1.1.4 bereits erwähnt, wurde eine erhöhte Expression des Aldehyd-Dehydrogenase-1-Familienmitglieds A3 (ALDH1A3) in mesenchymalen GSCs gefunden (Li et al. 2018). Um das Vorhandensein von mesenchymalen GSCs in unseren Gliom-Mausmodellen zu bestätigen, wurde die Verteilung des ALDH1A3 Proteins in Mausgehirnen analysiert, die mit den GSC-Kulturen LK7, LK13 bzw. LK28 *xenotransplantiert* und unter Kontrollbedingungen (5x 0 Gy, Vehikel) behandelt wurden. Wie die mikroskopischen Aufnahmen zeigten (Ganser et al. 2023, Suppl. Abb. S11A), waren die ALDH1A3-positiven Zellen im normalen Gewebe des Hippocampus, Kleinhirns und Mittelhirns stark vertreten. Auf zellulärer Ebene wurde ALDH1A3 immunhistochemisch in der Tumorkläsion (#), in gliaförmigen Zellen (\*) und in Blutgefäßen (§, Suppl. Abb. S10B) nachgewiesen. Um zwischen ALDH1A3 exprimierenden Glioblastomen und normalen Zellen zu unterscheiden, wurde die Co-Lokalisierung von ALDH1A3, hNucleolin, Iba1 (ionisiertes calciumbindendes Adaptermolekül-1) und GFAP in konsekutiven Paraffinschnitten analysiert (Ganser et al. 2023, Suppl. Abb. S11 C-H). Die Zellpopulationen wurden als mesenchymale GSCs (hNucleolin<sup>+</sup>/ALDH1A3<sup>+</sup>), glial differenzierte Tumorzellen (hNucleolin<sup>+</sup>/GFAP<sup>+</sup>), Mikroglia/Makrophagen (Iba1<sup>+</sup>) und Astrozyten (hNucleolin<sup>-</sup>/GFAP<sup>+</sup>) definiert. In Tumoren, stammend aus LK7, machten hNucleolin<sup>+</sup>-Zellen etwa die Hälfte der Tumorkläsion aus und waren außerdem in der Infiltrationszone um den Tumor herum verstreut. Die überwiegende Mehrheit der hNucleolin<sup>+</sup>-Glioblastomzellen zeigte einen "glial differenzierten" hNucleolin<sup>+</sup>/GFAP<sup>+</sup> Phänotyp, während nur wenige ALDH1A3-Immunreaktivität zeigten (rote Pfeile in Ganser et al. 2023, Abb. S11H,). Diese war vor allem in der äußeren Iba1<sup>+</sup>/hNucleolin<sup>-</sup>/GFAP<sup>+</sup>-Zone deutlich zu sehen. Die restlichen Zellen innerhalb der Tumorkläsion waren hNucleolin<sup>-</sup>/GFAP<sup>+</sup> Astrozyten. Iba1<sup>+</sup> Mikroglia/Makrophagen und hNucleolin<sup>-</sup>/GFAP<sup>+</sup> Astrozyten umschlossen die



Tumormasse und einen angrenzenden "ödematösen" Bereich mit geringer Zelldichte. (Suppl. Abb. 11C-H).

Um die Anzahl der mesenchymalen ALDH1A3<sup>+</sup> GSCs zwischen den GSC-Kulturen und abgeleiteten orthotopen *Xenotransplantaten* direkt zu vergleichen, wurde eine hNucleolin/ALDH1A3-Doppelfärbung mittels Immunfluoreszenzmikroskopie durchgeführt. In mesenchymalen LK7 war die Anzahl der ALDH1A3<sup>+</sup> Zellen in der GSC-Kultur und in den daraus abgeleiteten Tumor-*Xenotransplantaten* (Ganser et al. 2023, Abb. 4A, links) ähnlich. Im Gegensatz dazu waren in den intermediären proneuralen/mesenchymalen LK13 (Ganser et al. 2023, Abb. 4A, Mitte) und proneuralen LK28 (Ganser et al. 2023, Abb. 4A, rechts) GSC-Kulturen passend zu den mRNA-Expressionsdaten keine ALDH1A3 Immunreaktivität nachweisbar. Interessanterweise konnten jedoch hNucleolin<sup>+</sup>/ALDH1A3<sup>+</sup> Zellen in den dazugehörigen orthotopen *Xenotransplantaten* nachgewiesen werden. (Ganser et al. 2023, Abb. 4A, untere Zeile).

Zusammengenommen deuten diese immunhistologischen Daten auf einen moderaten Anteil ALDH1A3<sup>+</sup>, mesenchymaler GSCs (LK7) sowohl in GSC-Kulturen als auch in orthotopen *Xenotransplantaten* hin. Darüber hinaus könnten die Ergebnisse der Immunfluoreszenz-Färbung ein Hinweis auf eine "Mesenchymalisierung" der proneuralen GSCs durch die Mikroumgebung nach *Xenotransplantation* sein. Als Nächstes wurden die Effekte einer IK<sub>Ca</sub>- bzw. BK<sub>Ca</sub>-Blockade und/oder fraktionierter Bestrahlung auf die Gehirninvasion der implantierten Tumore ins gesunde Hirngewebe und die DNA-DSB-Reparatur *in vivo* untersucht.

### 3.6. Effekte einer *in vivo* IK<sub>Ca</sub> bzw. BK<sub>Ca</sub> Blockade auf *Xenotransplantate* von aus Patienten stammenden GSC Kulturen

#### 3.6.1 Abhängigkeit der Glioblastom-Hirninfiltration und der DNA-Doppelstrangbruch-Reparatur von IK<sub>Ca</sub> und BK<sub>Ca</sub> Kanälen *in vivo*

Das Invasionsverhalten von LK7-, LK13- und LK28- GSC *in vivo* wurde 24 Stunden nach Ende der letzten Bestrahlungsfraction (5x 0 oder 5x 4 Gy) analysiert. Dabei wurde die Anzahl der hNucleosin<sup>+</sup> Tumorzellen, die aus der primären Tumorkläsion ausgewandert waren, sowie der maximale Abstand der ausgewanderten Zellen aus der Tumorkläsion bestimmt (Ganser et al. 2023, Abb. 4B) Wie in Abb. 4C (Ganser et al. 2023) gezeigt, unterschied sich die basale (5x 0 Gy, Vehikel) Anzahl der

ausgewichenen Glioblastomzellen pro Tumorfläche nicht signifikant zwischen mesenchymalen LK7-, intermediären LK13- und proneuralen LK28-Glioblastomen. Eine fraktionierte Bestrahlung erhöhte in LK13 tendenziell diese Zellzahl (Ganser et al. 2023, Abb. 4C) und die maximale Invasionsdistanz (Ganser et al. 2023, Abb. 4D), während sie beide Invasionsparameter in LK7- und LK28-*Xenotransplantaten* verringerte. Die Kombination aus  $K_{Ca}$ -Kanal Blockade und fraktionierter Bestrahlung (5x 4 Gy) führte zwar nur bei LK13-Tumoren zu einer signifikanten Verringerung beider Invasionsparameter (Ganser et al. 2023, Abb. 4C und D, Mitte), war aber bei allen drei *Xenotransplantaten* mit der geringsten Anzahl migrierter Tumorzellen (außer bei LK7-Tumoren) und der kürzesten maximalen Invasionsdistanz sowie der geringsten Datenstreuung im Vergleich zu den anderen drei Behandlungsarmen verbunden (Ganser et al. 2023, Abb. 4C, D).

Zusammenfassend lässt sich sagen, dass die *in vivo* Invasionsdaten - wie auch die *in vitro* Invasionsexperimente - keinen Beweis für eine allgemeine strahleninduzierte Hyperinvasion/Hyperhirninfiltration liefern. Interessanterweise war in LK13 *Xenografts* eine Tendenz zur radiogenen Hyperinfiltration *in vivo* zu erkennen, während eine solche Tendenz *in vitro* nur bei LK7 GSC-Kulturen zu beobachten war. Eine weitere Diskrepanz zwischen den *in vitro* und den *in vivo* Daten bestand darin, dass TRAM-34 offenbar die Hirninfiltration von LK13 *Xenografts* abschwächte, während es die Gelinvasion in LK13 GSC-Kulturen nicht hemmte (vgl. Abb. 2A, B, Mitte mit Abb. 4C, D, Mitte in Ganser et al. 2023). Dennoch deuten die Daten zur Infiltration der *Xenotransplantate* auf eine Verlangsamung der Ausbreitung des Glioblastoms durch die gleichzeitige  $K_{Ca}$  Blockade mit fraktionierter Bestrahlung hin.

Um die Reaktion der orthotopen GSC-*Xenografts* auf fraktionierte Bestrahlung und/oder  $K_{Ca}$ -Kanal-Hemmung zu untersuchen, wurde die DNA-Doppelstrangbruch-Reparatur in der Tumorkläsion durch immunhistochemische Bestimmung der Anzahl der residualen  $\gamma$ H2AX-Foci 24 Stunden nach der letzten Bestrahlungsfraction analysiert (Ganser et al. 2023 Abb. 5A). Die Histogramme (Abb. 5B) zeigen die normalisierte Verteilung der Anzahl der Foci pro Zellkern, während in Abb. 5C (Ganser et al. 2023) die Anzahl der Foci pro Zellkern für alle drei *Xenotransplantatmodelle* (LK7, LK13; LK28) dargestellt ist. Wie erwartet, führte eine fraktionierte Bestrahlung (5x 4 Gy) mit oder ohne gleichzeitiger  $K_{Ca}$ -Kanal-Blockade in allen drei Modellen zu einem Anstieg der Anzahl der residualen  $\gamma$ H2AX-Foci pro Zellkern. Bemerkenswerterweise verstärkte, wie bereits bei LK28 und (tendenziell) bei LK7 GSC-Kulturen *in vitro*

beobachtet, die gleichzeitige Hemmung von IK<sub>Ca</sub> (LK7 und LK13) oder BK<sub>Ca</sub> (LK28) diesen Effekt.

Zusammengenommen deuten diese  $\gamma$ H2AX-Daten auf eine beeinträchtigte Reparatur von strahleninduzierten DNA-Doppelstrangbrüchen durch IK<sub>Ca</sub>- oder BK<sub>Ca</sub>-Blockade bei gleichzeitiger fraktionierter Strahlung hin. Zuletzt wurde der potenziell therapeutische Nutzen einer gezielten IK<sub>Ca</sub>-Kanal-Hemmung während der Strahlentherapie *in vivo* untersucht.

### 3.6.2 Auswirkungen einer IK<sub>Ca</sub>-Kanalblockade auf das Tumorwachstum (des LK7-Xenotransplantats) und das Überleben der Mäuse

Es ist bereits bekannt, dass das Tumor umgebende Ödem infiltrierende Tumorzellen beinhaltet (Hawkins-Daarud et al. 2013) und sein Volumen mit dem Gesamtüberleben von Glioblastom-Patienten zusammenhängt (Wu et al. 2018). Aus diesem Grund wurde auch das Ödemvolumen in diesem Projekt mit eingezogen, welches wie auch die Tumorkläsion in T2-gewichteten MR-Aufnahmen hyperintens abgebildet ist (Ganser et al. 2023, Abb. 6A). Die Tumor- und Ödemvolumina wurden durch Konturierung in aufeinanderfolgenden Schnittbildern halbautomatisch mit Hilfe der 3D-Slicer-Software bestimmt. Die MRT-Aufnahmen wurden vor (um Tag -20 und Tag 0) und nach (um Tag +20, +40, +60) der Behandlung der LK7-Xenografts an fünf konsekutiven Tagen (Tage 1-5) mit fraktionierter Tumorbestrahlung (5x 0 oder 5x 2 Gy) und gleichzeitiger intraperitonealer TRAM-34 Injektion (5x 0 oder 5x 120 mg/kg KG, 6 h vor den Bestrahlungsfractionen) aufgenommen. Die Strahlendosis wurde in den Langzeitexperimenten verringert, um die Schädigung von normalem Gewebe (Mundschleimhaut) zu minimieren, da bekannt ist, dass NSG-Mäuse sehr strahlenempfindlich sind (Shultz et al. 2007). In Ganser et al. 2023, Abb. 6B werden die Tumor- und Ödemvolumina vor, während (graue Linie) und nach Behandlung gezeigt. Unter Kontrollbedingungen (5x 0 Gy + Vehikel; Ganser et al. 2023, Abb. 6B, 1. Diagramm) nahm das Tumor- und Ödemvolumen exponentiell zu. Die TRAM-34 Behandlung (5x 0 Gy + TRAM-34) oder die fraktionierte Bestrahlung (5x 2 Gy + Vehikel) allein, hatten keine oder nur geringe Auswirkungen auf das Tumorwachstum (Ganser et al. 2023, Abb. 6B, 2. und 3. Diagramm), während die kombinierte Behandlung (5x 2 Gy + TRAM-34; Ganser et al. 2023, Abb. 6B, 4. Diagramm) zu einer deutlichen - wenn auch nicht signifikanten ( $p = 0,16$ ) - Verzögerung des Tumorwachstums im Vergleich zum Kontrollarm führte. Dies veranschaulicht auch

Abb. 6C (Ganser et al. 2023), in der die Steigungen zwischen Tag 0 und Tag 40 der  $\log_{10}$ -transformierten Volumenwerte für die einzelnen Tumore der vier Behandlungsarme angegeben sind. Die Verzögerung des Tumorwachstums bei kombiniert behandelten Mäusen (5x 2 Gy + TRAM-34) war bis zum Tag 40 nach Behandlungsbeginn erkennbar. Danach wuchsen Tumor und Ödeme beschleunigt und erreichten ähnliche Volumina wie in den anderen Behandlungsarmen (Ganser et al. 2023, Abb. 6B, nicht gezeigt). Das Überleben der Mäuse (bis zum Erreichen der Kriterien für die Beendigung des Tierversuchs) unterschied sich nicht zwischen den vier Behandlungsarmen (Ganser et al. 2023, Abb. 6D).

Studie 3: Eckert F, **Ganser K**, Bender B, et al. Potential of pre-operative MRI features in glioblastoma to predict for molecular stem cell subtype and patient overall survival [published online ahead of print, 2023 Aug 22]. *Radiother Oncol.* 2023;109865. doi:10.1016/j.radonc.2023.109865

### 3.7 Potentielle Aussagekraft von prä-operativen MRT-Aufnahmen auf die molekulare mRNA-Signatur

Die mRNA-Signatur der GSC-Kulturen könnte auch zur patientenindividuellen Anpassung der Strahlentherapie verwendet werden. Proneurale, wenig streuende Glioblastome, könnten durch eine Dosisescalation auf den Tumorbulk + Sicherheitssaum besser eradiziert werden, ohne bei entsprechender Strahlungsplanung das Normalgewebe zusätzlich zu schädigen. Leider dauert das Anzüchten der GSC-Kulturen zu lange, um die daraus gewonnen Erkenntnisse schon direkt bei der Radiotherapie des Glioblastompatienten anwenden zu können, die in der Regel innerhalb von 4 Wochen nach Tumorresektion beginnt. In der dritten Studie versuchten wir aus der prätherapeutischen Bildgebung Informationen über den wahrscheinlichen Phänotyp der vorherrschenden GSC-Subpopulation zu extrahieren. Hierzu berechneten wir aus den therapienativen MRT Aufnahmen die Volumina von Tumor-, Ödem- und Nekrose- Arealen des Glioblastoms (Eckert et al. 2023, Abb. 2A+B) und assoziierten diese bzw. eine aus diesen Volumen hervorgegangene Bildgebungssignatur mit der molekularen proneural zu mesenchymalen mRNA-Signatur und der Radiosensitivität der dazugehörigen GSC-Kulturen (Eckert et al. 2023, Abb. 3A-D). Dabei zeigte sich, dass insbesondere bei MGMT- Promotor unmethylierten Glioblastomen das Verhältnis des Nekrose zu Tumor-Vektors negativ mit der molekularen mRNA-Signatur (Eckert et al. Abb. 3B rechts) und der

Radioresistenz (Eckert et al. Abb. 3D rechts) korrelierte. Eine Signatur (Ödem-Vektor x Nekrose/Tumor Vektorratio) assoziierte am besten mit der molekularen mRNA-Signatur der gesamten Glioblastomkohorte (Eckert et al. 2023, Abb. 4A, links). Bemerkenswerterweise unterschied sich das Gesamtüberleben der Patienten:innen signifikant, wenn sie nach unserer Imaging-Signatur in zwei Gruppen stratifiziert wurden (Eckert et al. 2023, Abb 4B, rechts).

## 4. Diskussion

Im ersten Teil des Projekts wurde mit Hilfe von mRNA-Expressionsdaten von Stammzell-, Invasions- und Resistenzmarkern aus Glioblastomstammzell-Primärkulturen (GSCs) eine proneural zu mesenchymale mRNA Signatur definiert. Eine bereits publizierte Studie (Chandran et al. 2015) verglich mesenchymale und proneurale GSC-spezifische mRNA-Daten mit GBM-Transkriptomdaten und zeigte eine ausgeprägte Korrelation der Expressionsprofile mit den entsprechenden molekularen proneuralen und mesenchymalen Glioblastom-Subtypen. Diese Ergebnisse deuten darauf hin, dass die proneural zu mesenchymale Signatur der GSC-Subpopulation(en) zur molekularen Glioblastom-Subklassifizierung maßgeblich beiträgt. Im ersten Projektteil wurde eine Korrelation der molekularen proneuralen zu mesenchymalen mRNA-Signatur mit der intrinsischen Radioresistenz und dem Invasionsverhalten der GSC Kulturen aufgedeckt. Diesbezüglich konnte gezeigt werden, dass der GSC-Phänotyp umso maligner (bezogen auf Radioresistenz und Invasivität) war, desto mesenchymaler dessen mRNA-Signatur war.

Es wurde bereits berichtet, dass sich Phänotypen durch die Abwesenheit des Tumormikromilieus während der Kultivierung ändern können (Barnes et al. 2018). Dies war in unseren Experimenten nicht der Fall. Generell unterschieden sich jedoch die einzelnen GSC-Kulturen enorm in ihren funktionellen und molekularen Signaturen. Dies deutet darauf hin, dass ihre ursprüngliche Subtypenvielfalt zumindest bis zu einem gewissen Grad in den GSC-Kulturen erhalten blieb.

Klinisch relevant war, dass unsere molekulare mRNA-Signatur der GSC-Kulturen mit dem Rezidivierungsmuster (Ganser et al. 2022, Abb 3B) und dem Gesamtüberleben der entsprechenden Glioblastompatienten korrelierte. Dies lässt darauf schließen, dass der malignitätsbestimmende GSC-Phänotyp des Resektats während der Kultivierung und GSC-Anreicherung durch stammzellinduzierende Bedingungen

konserviert ist. In Übereinstimmung mit der bereits erwähnten Korrelation zwischen mesenchymalem Phänotyp und Malignität zeigten als mesenchymal identifizierte GSC Kulturen eine schlechtere Prognose der entsprechenden Patient:innen (univariater Test  $p = 0,001$ , Abb. 3E, rechts in Ganser et al. 2022). Ähnlich dazu wurden bereits in früheren Studien Epigenom- und Transkriptomdaten aus Glioblastomproben mit klinischen Daten in Assoziation gebracht, die ein kürzeres Gesamtüberleben von Patient:innen mit hochregulierten mesenchymalen Methylierungs- oder Expressionsmustern der Tumoren zeigten (Phillips et al. 2006, Colman et al. 2010, Bhat et al. 2013, Klumpp et al. 2018, Dejaegher et al. 2021).

Glioblastomzellen können einen glial-mesenchymalen Übergang (Mahabir et al. 2014) durchlaufen und einen infiltrativen Phänotyp annehmen (Yachi et al. 2018, Sha et al. 2020). Die ektopische Stimulierung von kultivierten GSC-Sphäroiden mit Retinsäure (gebildet durch ALDH1A3, siehe Abschnitt 1.1.5) induzierte neben der Herabregulierung von proneuralen Stammzellmarkern auch morphologische Veränderungen *in vitro*, wie eine Zellauswanderung aus den Neurosphären, die Bildung von Zellfortsätzen und des adhärenen Wachstums als Monolayer (Ying et al. 2011). *In vivo* infiltrieren auswandernde Glioblastomzellen das Gehirn, indem sie sich an Gefäße oder Axonbündel anheften und entlang dieser wie auf Bahnen wandern (Sontheimer 2008). Im ersten Projektteil wiesen GSC-Kulturen mit einer hohen mesenchymalen mRNA-Signatur neben einer erhöhten Invasivität (siehe Abb. 2F-H in Ganser et al. 2022) auch einen adhärenen Wachstumsphänotyp auf (siehe Abb. 1B, C in Ganser et al. 2022). Diese Beobachtungen deuten darauf hin, dass der adhärenen Wachstumsphänotyp der mesenchymalen GSC die promigratorische/invasive Eigenschaft dieser Zellen widerspiegelt.

Präklinische *in vitro* - und *in vivo*-Studien haben gezeigt, dass die Migration von Glioblastomzellen und die Infiltration ins umliegende Hirngewebe ein komplexes Zusammenspiel von zellvolumenregulierenden Strukturen erfordert, zu denen die  $\text{Ca}^{2+}$ -aktivierbaren  $\text{K}^{+}$ -Kanäle  $\text{IK}_{\text{Ca}}$  und  $\text{BK}_{\text{Ca}}$  gehören (Sontheimer 2008, Ruggieri et al. 2012, Turner and Sontheimer 2014, Edalat et al. 2016). In den GSC-Kulturen wurde eine moderate (*KCNN4*,  $\text{IK}_{\text{Ca}}$ ) bzw. schwache (*KCNMA1*,  $\text{BK}_{\text{Ca}}$ ) Korrelation zwischen den mRNA Expressionsleveln der erwähnten Kanäle und ALDH1A3 gefunden (Ganser et al. 2022, Abb 1A), was auf eine Hochregulation dieser Kaliumkanäle in mesenchymalen GSCs hinweist. Diese Hochregulation könnte das multifokale

Rezidivmuster der Tumore aus denen die mesenchymalen GSCs stammen, erklären (Ganser et al. 2022, Abb 3A, B). Da eine nochmalige Resektion oder Bestrahlung von multifokalen Rezidiven schwierig ist, ist wahrscheinlich eine erhöhte Invasivität der mesenchymalen GSCs mit einer schlechteren Prognose der Patienten verbunden (Park et al. 2019).

Ein anderer Grund für die schlechtere Prognose der Patienten der mesenchymalen GSCs könnte die erhöhte Radioresistenz des mesenchymalen Typs darstellen, welche mit der molekularen Signatur korreliert (Ganser et al. 2022, Abb. 2B, C). In früheren Arbeiten konnte bereits eine Assoziation zwischen einem mesenchymalen Subtyp und der Radioresistenz in GBM Zellen gezeigt werden (Sullivan et al. 2017, Barnes et al. 2018, Bhat et al. 2020). Auch innerhalb unserer Arbeitsgruppe wurde bereits eine  $IK_{Ca}$ -abhängige Strahlenresistenz durch Knockdown des proneuralen Stammzellmarkers MSI1 mit resultierender Hochregulation des  $IK_{Ca}$  Kanals in U87MG Zelllinie beobachtet (Stegen et al. 2016). Darüber hinaus scheint die radiogene  $IK_{Ca}$ -Aktivität die  $Ca^{2+}$ -Signalübertragung, den Zellzyklusarrest und die DNA-Reparatur in bestrahlten Glioblastomzellen zu beeinflussen und das klonogene Zellüberleben zu verbessern (Stegen et al. 2015).

Zusammenfassend deuten diese Erkenntnisse darauf hin, dass ein mesenchymaler GSC-Subtyp invasiver und therapieresistenter als andere Subtypen ist und somit zu einer schlechteren Prognose der Patienten führt. Die beiden  $Ca^{2+}$ -aktivierbaren  $K^+$ -Kanäle  $IK_{Ca}$  und  $BK_{Ca}$  scheinen zu diesem mesenchymalen Subtyp beizutragen, weswegen sie potentielle Zielstrukturen für neue Therapiestrategien darstellen könnten. Aus diesem Grund wurde im zweiten Teil des Projekts der mögliche Nutzen einer  $IK_{Ca}$  bzw.  $BK_{Ca}$  Blockade in GSC Kulturen *in vitro* und in deren *Xenografts in vivo* untersucht.

Dafür wurden zunächst sechs GSC-Kulturen aus der Tübinger GBM-Kohorte mit verschiedenen  $IK_{Ca}$ - und  $BK_{Ca}$  mRNA Expressionen (siehe Abb. 1C) und molekularen mRNA-Signaturen (siehe Ganser et al. 2023, Suppl. Abb. S1, S2) ausgewählt. Da sich diese auch in ihrer Radioresistenz (Ganser et al. 2023, Abb. 1 und S7, S8) und Gelinvasionen *in vitro* (Ganser et al. 2023, Abb. 2 und S11) unterschieden, wurde somit eine intertumorale GBM-Heterogenität der Patienten nachgeahmt.

Eine  $K_{Ca}$  Kanal Blockade zeigte in einigen dieser sechs GSC-Kulturen bezogen auf die Doppelstrangbruchreparatur, das klonogene Überleben und die Gelinvasion *in vitro* tatsächlich die erwartete radiosensibilisierende bzw. anti-invasive Wirkung. Jedoch war dafür eine hohe  $IK_{Ca}$  bzw.  $BK_{Ca}$  Expression allein nicht prädiktiv (Ganser et al. 2023, Abb. 1, 2 und Abb. S7, S8, S11). Beispielsweise wurde die höchst mesenchymal identifizierte (Ganser et al. 2023, Abb. S1B) LK7 GSC Kultur (hohe  $IK_{Ca}$ -, moderate  $BK_{Ca}$  Expression), welche die höchste Strahlenresistenz (Ganser et al. 2023, Abb 1E, Abb S8) und Invasivität (Ganser et al. 2023, Abb. 2, Abb S10) aufweist, durch TRAM-34 radiosensibilisiert und ihre Invasivität durch Paxilline und TRAM-34 gehemmt. Im Vergleich dazu wurde in LK13 GSCs mit mittlerer proneural zu mesenchymaler Signatur und hoher  $IK_{Ca}$ - aber geringer  $BK_{Ca}$ -Expression die Invasion nur durch Paxilline abgeschwächt, während TRAM-34 keinen Effekt zeigte. Paxilline zeigte außerdem in proneuralen LK28 GSCs Kulturen anti-invasive und (tendenziell) radiosensibilisierende Wirkung *in vitro*, was auf das hohe  $BK_{Ca}$  mRNA Expressionslevel zurückzuführen sein könnte.

Nach orthotoper *Xenotransplantation* von drei (LK7, LK13 und LK28) der sechs GSC-Kulturen in immunkompromittierte NSG-Mäuse wurden  $ALDH1A3^+/hNucleolin^+$  mesenchymale GSCs nicht nur in den mesenchymalen LK7-*Xenotransplantaten*, sondern auch in den Tumoren der LK13- und LK28-GSC-Kulturen mit intermediärer bzw. proneuraler molekularen Signaturen gefunden, welche *in vitro* noch nicht nachweisbar waren (Ganser et al. 2023, Abb. 4A). Dies könnte auf eine Induktion von mesenchymalen GSCs durch die Mikroumgebung des Tumors im Mausgehirn hindeuten.

Bei LK7- und LK13-*Xenotransplantaten* schwächte eine  $IK_{Ca}$ -Blockade mit intraperitonealer TRAM-34 Injektion bei gleichzeitiger fraktionierter Bestrahlung nicht nur (tendenziell) die Tumordinfiltration des Mäusegehirns ab, sondern erhöhte auch die Anzahl der verbleibenden Doppelstrangbrüche effizienter als die Bestrahlung allein, was auf eine Rolle von  $IK_{Ca}$  bei der Hirninvasion und der DNA DSB-Reparatur hindeutet. Da in der GSC-Kultur LK13 *in vitro* keine Effekte gegenüber TRAM-34 beobachtet werden konnte, ist die Hypothese erlaubt, dass es durch das Tumormikromilieu zu einer „Mesenchymalisierung“ gekommen sein könnte, welche zu einem Ansprechen gegenüber TRAM-34 geführt haben könnte.



In ähnlicher Weise hemmte die gezielte Blockade von BK<sub>Ca</sub> mit Paxilline in Kombination mit fraktionierter Bestrahlung tendenziell die Hirninfiltration *in vivo* und erhöhte die Anzahl der residualen Doppelstrangbrüche in proneuralen LK28-*Xenotransplantaten*, was auf eine Beteiligung von BK<sub>Ca</sub> an diesen beiden Prozessen hinweist.

Wie in der Einleitung (Abschnitt 1.2.2) bereits beschrieben, konnten sowohl IK<sub>Ca</sub> als auch BK<sub>Ca</sub> Kanäle mit der (strahlungsinduzierten) Zellmigration in Glioblastomzelllinien *in vitro* (Sciaccaluga et al. 2010, Steinle et al. 2011, Ruggieri et al. 2012, Cuddapah et al. 2013, D'Alessandro et al. 2013, D'Alessandro et al. 2019) und der radiogenen Hirninfiltration *in vivo* in Verbindung gebracht werden (Edalat et al. 2016, D'Alessandro et al. 2019, Stransky et al. 2023). Außerdem wurde bereits gezeigt, dass ein IK<sub>Ca</sub> Knockout im Brustkrebsmodell (Mohr et al. 2019), eine pharmakologische IK<sub>Ca</sub> Blockade von Glioblastomzelllinien *in vitro* (Stegen et al. 2015, Stegen et al. 2016) oder in ektopen *Xenotransplantaten in vivo* (Stegen et al. 2015) eine Radiosensibilisierung verursacht.

Die histologische Analyse der Tumorinvasion ins umliegende Hirngewebe und der residualen Doppelstrangbrüche im zweiten Teilprojekt lassen vermuten, dass eine gleichzeitig zur fraktionierten Tumorbestrahlung erfolgte IK<sub>Ca</sub>- oder BK<sub>Ca</sub>-Behandlung die therapeutische Wirksamkeit einer fraktionierten Bestrahlung im Glioblastommodell erhöhen könnte (Ganser et al. 2023, Abb. 4 und 5). Diesbezüglich konnte unter Doppelbehandlung (TRAM-34 mit fraktionierter Bestrahlung) tatsächlich eine vorübergehende Verzögerung des Tumorwachstums in LK7-*Xenografts* erreicht werden (Ganser et al. 2023, Abb. 6B, C). Aufgrund der beschleunigten Repopulation der mit TRAM-34 und Bestrahlung behandelten Tumoren ca. 35 Tage nach Ende der Behandlung, unterschied sich die Überlebensrate der Mäuse zwischen den vier Behandlungsarmen (siehe Abb. 6D) nicht. Dies ist auch nicht zu erwarten, da in der klinischen Situation die nach der Operation residualen Glioblastomzellen im Gehirn mit 60 Gy in 30 Fraktionen (mit gleichzeitiger Temozolomid-Chemotherapie und anschließenden Temozolomid-Erhalttherapie) nur äußerst selten vollständig eradiziert und der Tumor kontrolliert werden kann. Im Gegensatz zu einer früheren Studie, in welcher die Verabreichung der gleichen Menge TRAM-34 vom 8. bis zum 16. Tag nach der Tumortransplantation das Tumorwachstum im syngenem orthotopen GL261/C57BL/6-Gliom-Modell signifikant verzögerte (Grimaldi et al. 2016) zeigte

TRAM-34 alleine hier oder in früheren Arbeiten unserer Arbeitsgruppe (Stegen et al. 2015) keinen hemmenden Effekt auf das Tumorwachstum

Wie in Abschnitt 1.2.2 bereits beschrieben, gibt es bereits FDA-zugelassene Wirkstoffe, die (auch) eine hemmende Wirkung auf  $IK_{Ca}$  und  $BK_{Ca}$  Kanäle ausüben. Eine mögliche unerwünschte Nebenwirkung der  $IK_{Ca}$ -Blockade könnte jedoch die Beeinträchtigung der Immunantwort auf Glioblastomzellen darstellen, da auch Immunzellen einschließlich T-Zellen und NK-Zellen  $IK_{Ca}$ -Kanäle exprimieren. In diesen Zellen könnte  $IK_{Ca}$  eine Funktion bei der Regulation der Zellproliferation, Differenzierung, Migration und Zytokinproduktion im angeborenen und adaptiven Immunsystem einnehmen (Übersicht s. (Ohya and Kito 2018)). Unter dieser Annahme überraschte es, dass eine  $IK_{Ca}$  Blockade *in vivo* eine Erhöhung der Abtötungsrate von Tumorzellen durch eine Untergruppe natürlicher Killerzellen bewirkte (Koshy et al. 2013). In syngenen Mausmodellen konnte außerdem gezeigt werden, dass die von Gliomen verursachte Induktion eines tumorunterstützenden Phänotyps von Mikroglia und Makrophagen durch TRAM-34 wieder in einen tumorbekämpfenden Phänotyp umgekehrt werden kann (Grimaldi et al. 2016, Massenzio et al. 2022). Schließlich konnte unsere Arbeitsgruppe zuletzt eine TRAM-34 induzierte Hemmung der Gliom-Infiltration durch  $CD3^+$ ,  $CD8^+$  oder  $FoxP3^+$  T-Zellen ausschließen (Stransky et al. 2023). Diese Beispiele syngener Gliom-Mausmodelle deuten darauf hin, dass eine  $IK_{Ca}$  Blockade die Immunantwort gegen Gliome nicht beeinträchtigen würde.

In den durchgeführten *in vitro* Experimenten dieser Arbeit wurde jeweils nur eine von zwei GSC-Kulturen mit hoher  $IK_{Ca}$ - und  $BK_{Ca}$ -Expression durch TRAM-34 bzw. Paxilline radiosensibilisiert (siehe Abb. 1C, D und S7 und S8 Ganser et al. 2023), was darauf hindeutet, dass im Gegensatz zu der ersten Hypothese hohe  $IK_{Ca}$ - oder  $BK_{Ca}$ -mRNA Expressionslevel der GSC-Kulturen die Ansprechbarkeit auf  $K_{Ca}$ -Kanal Blockade nicht vorhersagen kann. Zudem zeigte TRAM-34 in LK13 GSCs *in vitro* keine Wirkung, während radiosensibilisierende und antiinvasive Effekte *in vivo* nach orthotopischer *Xenotransplantation* in NSG-Mäuse jedoch beobachtet werden konnten (Ganser et al. 2023, Abb. 1D, E, Mitte, Abb. 4C, D, Mitte und Abb. 5C, Mitte). Diese Befunde lassen darauf schließen, dass Glioblastompatient:innen anhand der  $IK_{Ca}$ - oder  $BK_{Ca}$  mRNA-Abundanz im Tumorsektat oder der Ansprechbarkeit ihrer GSC-Kulturen *in vitro* wahrscheinlich nicht für eine zukünftige zu erwägende  $K_{Ca}$  Kanal-

gerichtete Therapie stratifiziert werden können. Jedenfalls belegt die Erhöhung der residualen Doppelstrangbrüche *in vivo* durch fraktionierte Bestrahlung in Kombination mit systemischer TRAM-34 bzw. Paxilline Applikation in allen drei *Xenotransplantationsmodellen*, dass durch eine  $K_{Ca}$  Kanal Blockade wahrscheinlich eine Strahlensensibilisierung der Glioblastome erreicht werden kann.

## 5. Schlussfolgerung

Unsere beiden Studien bestätigen zum einen den Nutzen patientenstämmiger Glioblastom-Stammzell-angereicherter Kulturen und deren molekulare und funktionelle Charakterisierung für die klinische-relevante Einteilung der Glioblastome in Subklassen: sie zeigen direkt, dass Glioblastome die mesenchymale GSC bilden mit einer deutlich schlechteren Prognose des Krankheitsverlaufs einhergehen als Tumoren mit proneuraleren GSCs.

Zum anderen identifizieren die Studien zwei  $Ca^{2+}$ -aktivierte  $K^+$ -Kanäle,  $IK_{Ca}$  und  $BK_{Ca}$ , als mögliche molekulare Targets zur Radiosensibilisierung von Glioblastomen bei gleichzeitiger fraktionierter Strahlentherapie. Beide Kanäle sind in mesenchymalen Glioblastom-Stammzellen hochreguliert, die – wie gezeigt wurde – die radioresistenteste und invasivste Stammzell-Subpopulation darstellen. Hierzu konnte ich im orthotopen Gliom-Maus-Modell den „Proof-of-Concept“ erbringen, dass pharmakologisches  $K_{Ca}$ -Targeting konkomitant zur fraktionierten Strahlentherapie durchführbar ist und zur Strahlensensibilisierung und Immobilisierung der Glioblastomzellen führen kann.

## 6. Ausblick

Da beide  $K_{Ca}$ -Kanaltypen durch zugelassene oder in klinischen Studien gut verträgliche Wirkstoffe gehemmt werden können (s. Einleitung Abschnitt 1.2.2), könnte eine  $K_{Ca}$  Hemmung in der adjuvanten Therapie von Glioblastompatient:innen in Zukunft verwendet werden. Zuvor müssten in präklinischen Studien jedoch bessere Marker für das Ansprechen einer  $K_{Ca}$  Kanal gerichteten Therapie gefunden werden, um

diejenigen Patient:innen zu identifizieren, die von dieser Therapiestrategie profitieren könnten. GSC-Kulturen aus Resektionsmaterial können zwar während der Standardtherapie bis zum Ende der adjuvanten Radiochemotherapie herangezüchtet werden, sind jedoch mit sehr viel Aufwand verbunden und ihre  $IK_{Ca}$  bzw.  $BK_{Ca}$  Expression scheint nicht ausschlaggebend für ihre Empfindlichkeit gegenüber  $K_{Ca}$  Blockade zu sein. Eine schnellere Methode zur Stratifizierung der GBM-Patient:innen, könnte eine Vorhersage des molekularen Subtyps durch MRT Aufnahmen sein, wie sie in unserer neuesten Veröffentlichung postuliert wurde (Eckert et al. 2023). Diese Strategie wäre im Zuge einer Bildgebung vor Resektion oder Strahlentherapie leicht in den klinischen Ablauf integrierbar, an allen Zentren leicht verfügbar und könnte die molekulare Analyse des Subtyps somit untermauern oder sogar umgehen.

## Literaturverzeichnis

Alnahhas, I., M. Alsawas, A. Rayi, J. D. Palmer, R. Raval, S. Ong, P. Giglio, M. H. Murad and V. Puduvalli (2020). "Characterizing benefit from temozolomide in MGMT promoter unmethylated and methylated glioblastoma: a systematic review and meta-analysis." Neuro-Oncology Advances **2**(1).

Ataga, K. I., M. Reid, S. K. Ballas, Z. Yasin, C. Bigelow, L. S. James, W. R. Smith, F. Galacteros, A. Kutlar, J. H. Hull, J. W. Stocker and I. C. A. S. Investigators (2011). "Improvements in haemolysis and indicators of erythrocyte survival do not correlate with acute vaso-occlusive crises in patients with sickle cell disease: a phase III randomized, placebo-controlled, double-blind study of the Gardos channel blocker senicapoc (ICA-17043)." Br J Haematol **153**(1): 92-104.

Ataga, K. I., S. J. Staffa, C. Brugnara and J. W. Stocker (2021). "Haemoglobin response to senicapoc in patients with sickle cell disease: a re-analysis of the Phase III trial." Br J Haematol **192**(5): e129-e132.

Bagley, S. J., S. Kothari, R. Rahman, E. Q. Lee, G. P. Dunn, E. Galanis, S. M. Chang, L. B. Nabors, M. S. Ahluwalia, R. Stupp, M. P. Mehta, D. A. Reardon, S. A. Grossman, E. P. Sulman, J. H. Sampson, S. Khagi, M. Weller, T. F. Cloughesy, P. Y. Wen and M. Khasraw (2022). "Glioblastoma Clinical Trials: Current Landscape and Opportunities for Improvement." Clinical Cancer Research **28**(4): 594-602.

Bai, X., J. Ma, Z. Pan, Y. H. Song, S. Freyberg, Y. Yan, D. Vykoukal and E. Alt (2007). "Electrophysiological properties of human adipose tissue-derived stem cells." Am J Physiol Cell Physiol **293**(5): C1539-1550.

Barnes, J. M., S. Kaushik, R. O. Bainer, J. K. Sa, E. C. Woods, F. Kai, L. Przybyla, M. Lee, H. W. Lee, J. C. Tung, O. Maller, A. S. Barrett, K. V. Lu, J. N. Lakins, K. C. Hansen, K. Obernier, A. Alvarez-Buylla, G. Bergers, J. J. Phillips, D. H. Nam, C. R. Bertozzi and V. M. Weaver (2018). "A tension-mediated glycocalyx-integrin feedback loop promotes mesenchymal-like glioblastoma." Nat Cell Biol **20**(10): 1203-1214.

Battle, E. and H. Clevers (2017). "Cancer stem cells revisited." Nat Med **23**(10): 1124-1134.

Bhat, K., M. Saki, E. Vlashi, F. Cheng, S. Duhachek-Muggy, C. Alli, G. Yu, P. Medina, L. He, R. Damoiseaux, M. Pellegrini, N. R. Zemke, P. L. Nghiemphu, T. F. Cloughesy, L. M. Liau, H. I. Kornblum and F. Pajonk (2020). "The dopamine receptor antagonist trifluoperazine prevents phenotype conversion and improves survival in mouse models of glioblastoma." Proc Natl Acad Sci U S A **117**(20): 11085-11096.

Bhat, K. P. L., V. Balasubramanian, B. Vaillant, R. Ezhilarasan, K. Hummelink, F. Hollingsworth, K. Wani, L. Heathcock, J. D. James, L. D. Goodman, S. Conroy, L. Long, N. Lelic, S. Wang, J. Gumin, D. Raj, Y. Kodama, A. Raghunathan, A. Olar, K. Joshi, C. E. Pelloso, A. Heimberger, S. H. Kim, D. P. Cahill, G. Rao, W. F. A. Den Dunnen, H. Boddeke, H. S. Phillips, I. Nakano, F. F. Lang, H. Colman, E. P. Sulman and K. Aldape (2013). "Mesenchymal differentiation mediated by NF- $\kappa$ B promotes radiation resistance in glioblastoma." Cancer Cell **24**(3): 331-346.

Binda, E., A. Visioli, F. Giani, N. Trivieri, O. Palumbo, S. Restelli, F. Dezi, T. Mazza, C. Fusilli, F. Legnani, M. Carella, F. Di Meco, R. Duggal and A. L. Vescovi (2017). "Wnt5a Drives an Invasive Phenotype in Human Glioblastoma Stem-like Cells." Cancer Res **77**(4): 996-1007.

Carrasquel-Ursulaez, W., I. Segura, I. Diaz-Franulic, F. Echeverria, Y. Lorenzo-Ceballos, N. Espinoza, M. Rojas, J. A. Garate, E. Perozo, O. Alvarez, F. D. Gonzalez-Nilo and R. Latorre (2022). "Mechanism of voltage sensing in Ca(2+)- and voltage-activated K(+) (BK) channels." Proc Natl Acad Sci U S A **119**(25): e2204620119.

Catacuzzeno, L. and F. Franciolini (2018). "Role of KCa3.1 Channels in Modulating Ca(2+) Oscillations during Glioblastoma Cell Migration and Invasion." Int J Mol Sci **19**(10).

Chandran, U. R., S. Luthra, L. Santana-Santos, P. Mao, S. H. Kim, M. Minata, J. Li, P. V. Benos, M. DeWang, B. Hu, S. Y. Cheng, I. Nakano and R. W. Sobol (2015). "Gene expression profiling distinguishes proneural glioma stem cells from mesenchymal glioma stem cells." Genom Data **5**: 333-336.

Chen, Z., H. W. Wang, S. Wang, L. Fan, S. Feng, X. Cai, C. Peng, X. Wu, J. Lu, D. Chen, Y. Chen, W. Wu, D. Lu, N. Liu, Y. You and H. Wang (2019). "USP9X deubiquitinates ALDH1A3 and maintains mesenchymal identity in glioblastoma stem cells." J Clin Invest **129**(5): 2043-2055.

Cheng, P., J. Wang, I. Waghmare, S. Sartini, V. Coviello, Z. Zhang, S. H. Kim, A. Mohyeldin, M. S. Pavlyukov, M. Minata, C. L. Valentim, R. R. Chhipa, K. P. Bhat, B. Dasgupta, C. La Motta, M. Kango-Singh and I. Nakano (2016). "FOXD1-ALDH1A3 Signaling Is a Determinant for the Self-Renewal and Tumorigenicity of Mesenchymal Glioma Stem Cells." Cancer Res **76**(24): 7219-7230.

Cheng, Y. Y., C. M. Wright, M. B. Kirschner, M. Williams, K. H. Sarun, V. Sytnyk, I. Leshchynska, J. J. Edelman, M. P. Valley and B. C. McCaughan (2016). "KCa1. 1, a calcium-activated potassium channel subunit alpha 1, is targeted by miR-17-5p and modulates cell migration in malignant pleural mesothelioma." Molecular cancer **15**(1): 1-12.

Christie, M. J., R. A. North, P. B. Osborne, J. Douglass and J. P. Adelman (1990). "Heteropolymeric potassium channels expressed in Xenopus oocytes from cloned subunits." Neuron **4**(3): 405-411.

Colman, H., L. Zhang, E. P. Sulman, J. M. McDonald, N. L. Shooshtari, A. Rivera, S. Popoff, C. L. Nutt, D. N. Louis, J. G. Cairncross, M. R. Gilbert, H. S. Phillips, M. P. Mehta, A. Chakravarti, C. E. Pelloski, K. Bhat, B. G. Feuerstein, R. B. Jenkins and K. Aldape (2010). "A multigene predictor of outcome in glioblastoma." Neuro Oncol **12**(1): 49-57.

Cuddapah, V. A., K. L. Turner, S. Seifert and H. Sontheimer (2013). "Bradykinin-induced chemotaxis of human gliomas requires the activation of KCa3.1 and CIC-3." J Neurosci **33**(4): 1427-1440.

D'Alessandro, G., M. Catalano, M. Sciaccaluga, G. Chece, R. Cipriani, M. Rosito, A. Grimaldi, C. Lauro, G. Cantore, A. Santoro, B. Fioretti, F. Franciolini, H. Wulff and C. Limatola (2013). "KCa3.1 channels are involved in the infiltrative behavior of glioblastoma in vivo." Cell Death Dis **4**: e773.

D'Alessandro, G., A. Grimaldi, G. Chece, A. Porzia, V. Esposito, A. Santoro, M. Salvati, F. Mainiero, D. Ragozzino and S. Di Angelantonio (2016). "KCa3.1 channel inhibition sensitizes malignant gliomas to temozolomide treatment." Oncotarget **7**(21): 30781.

D'Alessandro, G., L. Monaco, L. Catacuzzeno, F. Antonangeli, A. Santoro, V. Esposito, F. Franciolini, H. Wulff and C. Limatola (2019). "Radiation Increases Functional KCa3.1 Expression and Invasiveness in Glioblastoma." Cancers (Basel) **11**(3).

Dejaegher, J., L. Solie, Z. Hunin, R. Sciote, D. Capper, C. Siewert, S. Van Cauter, G. Wilms, J. van Loon, N. Ectors, S. Fieuws, S. M. Pfister, S. W. Van Gool and S. De Vleeschouwer (2021). "DNA methylation based glioblastoma subclassification is related to tumoral T-cell infiltration and patient survival." Neuro Oncol **23**(2): 240-250.

Du, C., Z. Zheng, D. Li, L. Chen, N. Li, X. Yi, Y. Yang, F. Guo, W. Liu and X. Xie (2016). "BKCa promotes growth and metastasis of prostate cancer through facilitating the coupling between  $\alpha\beta3$  integrin and FAK." Oncotarget **7**(26): 40174.

Du, Y., W. Song, J. Chen, H. Chen, Z. Xuan, L. Zhao, J. Chen, C. Jin, M. Zhou, B. Tuo, Y. Zhao, S. Zheng and P. Song (2019). "The potassium channel KCa3.1 promotes cell proliferation by activating SKP2 and metastasis through the EMT pathway in hepatocellular carcinoma." Int J Cancer **145**(2): 503-516.

Eckerdt, F. and L. C. Plataniias (2023). "Emerging Role of Glioma Stem Cells in Mechanisms of Therapy Resistance." Cancers (Basel) **15**(13).

Eckert, F., K. Ganser, B. Bender, J. Schittenhelm, M. Skardelly, F. Behling, G. Tabatabai, N. Stransky, E. Hoffmann, D. Zips, S. M. Huber and F. Paulsen (2023). "Potential of pre-operative MRI features in glioblastoma to predict for molecular stem cell subtype and patient overall survival." Radiother Oncol: 109865.

Edalat, L., B. Stegen, L. Klumpp, E. Haehl, K. Schilbach, R. Lukowski, M. Kuhnle, G. Bernhardt, A. Buschauer, D. Zips, P. Ruth and S. M. Huber (2016). "BK K+ channel blockade inhibits radiation-induced migration/brain infiltration of glioblastoma cells." Oncotarget **7**(12): 14259-14278.

Emler, D. R., P. Gupta, M. Holgado-Madruga, C. A. Del Vecchio, S. S. Mitra, S. Y. Han, G. Li, K. C. Jensen, H. Vogel, L. W. Xu, S. S. Skirboll and A. J. Wong (2014). "Targeting a glioblastoma cancer stem-cell population defined by EGF receptor variant III." Cancer Res **74**(4): 1238-1249.

Fan, X., L. Khaki, T. S. Zhu, M. E. Soules, C. E. Talsma, N. Gul, C. Koh, J. Zhang, Y. M. Li, J. Maciaczyk, G. Nikkhah, F. Dimeco, S. Piccirillo, A. L. Vescovi and C. G. Eberhart (2010). "NOTCH pathway blockade depletes CD133-positive glioblastoma

cells and inhibits growth of tumor neurospheres and xenografts." Stem Cells **28**(1): 5-16.

Fareh, M., L. Turchi, V. Virolle, D. Debruyne, F. Almairac, S. de-la-Forest Divonne, P. Paquis, O. Preynat-Seaube, K. H. Krause, H. Chneiweiss and T. Virolle (2012). "The miR 302-367 cluster drastically affects self-renewal and infiltration properties of glioma-initiating cells through CXCR4 repression and consequent disruption of the SHH-GLI-NANOG network." Cell Death Differ **19**(2): 232-244.

Fioretti, B., E. Castigli, M. R. Micheli, R. Bova, M. Sciacaluga, A. Harper, F. Franciolini and L. Catacuzzeno (2006). "Expression and modulation of the intermediate-conductance Ca<sup>2+</sup>-activated K<sup>+</sup> channel in glioblastoma GL-15 cells." Cell Physiol Biochem **18**(1-3): 47-56.

Ganser, K., L. Klumpp, H. Bischof, R. Lukowski, F. Eckert and S. M. Huber (2021). "Potassium Channels in Cancer." Handb Exp Pharmacol **267**: 253-275.

Grimaldi, A., G. D'Alessandro, M. T. Golia, E. M. Grössinger, S. Di Angelantonio, D. Ragozzino, A. Santoro, V. Esposito, H. Wulff, M. Catalano and C. Limatola (2016). "KCa<sub>3.1</sub> inhibition switches the phenotype of glioma-infiltrating microglia/macrophages." Cell Death Dis **7**(4): e2174.

Hambardzumyan, D., D. H. Gutmann and H. Kettenmann (2016). "The role of microglia and macrophages in glioma maintenance and progression." Nat Neurosci **19**(1): 20-27.

Hammoud, M. A., R. Sawaya, W. M. Shi, P. F. Thall and N. E. Leeds (1996). "Prognostic significance of preoperative MRI scans in glioblastoma multiforme." Journal of Neuro-Oncology **27**(1): 65-73.

Hawkins-Daarud, A., R. C. Rockne, A. R. Anderson and K. R. Swanson (2013). "Modeling Tumor-Associated Edema in Gliomas during Anti-Angiogenic Therapy and Its Impact on Imageable Tumor." Front Oncol **3**: 66.

Herrlinger, U., T. Tzaridis, F. Mack, J. P. Steinbach, U. Schlegel, M. Sabel, P. Hau, R. D. Kortmann, D. Krex, O. Grauer, R. Goldbrunner, O. Schnell, O. Bähr, M. Uhl, C. Seidel, G. Tabatabai, T. Kowalski, F. Ringel, F. Schmidt-Graf, B. Suchorska, S. Brehmer, A. Weyerbrock, M. Renovanz, L. Bullinger, N. Galldiks, P. Vajkoczy, M. Misch, H. Vatter, M. Stuplich, N. Schäfer, S. Kebir, J. Weller, C. Schaub, W. Stummer, J. C. Tonn, M. Simon, V. C. Keil, M. Nelles, H. Urbach, M. Coenen, W. Wick, M. Weller, R. Fimmers, M. Schmid, E. Hattungen, T. Pietsch, C. Koch and M. Glas (2019). "Lomustine-temozolomide combination therapy versus standard temozolomide therapy in patients with newly diagnosed glioblastoma with methylated MGMT promoter (CeTeG/NOA-09): a randomised, open-label, phase 3 trial." Lancet **393**(10172): 678-688.

Huang, C. L. and B. H. Ruskin (1964). "Determination of Serum Chlorpromazine Metabolites in Psychotic Patients." J Nerv Ment Dis **139**: 381-386.



Ji, F., Y. Wang, J. Yuan, Q. Wu, J. Wang and D. Liu (2020). "The potential role of stromal cell-derived factor-1 $\alpha$ /CXCR4/CXCR7 axis in adipose-derived mesenchymal stem cells." J Cell Physiol **235**(4): 3548-3557.

Kaczmarek, L. K., R. W. Aldrich, K. G. Chandy, S. Grissmer, A. D. Wei and H. Wulff (2017). "International Union of Basic and Clinical Pharmacology. C. Nomenclature and Properties of Calcium-Activated and Sodium-Activated Potassium Channels." Pharmacol Rev **69**(1): 1-11.

Kahlert, U. D., D. Maciaczyk, S. Doostkam, B. A. Orr, B. Simons, T. Bogiel, T. Reithmeier, M. Prinz, J. Schubert, G. Niedermann, T. Brabletz, C. G. Eberhart, G. Nikkhah and J. Maciaczyk (2012). "Activation of canonical WNT/ $\beta$ -catenin signaling enhances in vitro motility of glioblastoma cells by activation of ZEB1 and other activators of epithelial-to-mesenchymal transition." Cancer Lett **325**(1): 42-53.

Karimi, S., J. A. Zuccato, Y. Mamatjan, S. Mansouri, S. Suppiah, F. Nassiri, P. Diamandis, D. G. Munoz, K. D. Aldape and G. Zadeh (2019). "The central nervous system tumor methylation classifier changes neurooncology practice for challenging brain tumor diagnoses and directly impacts patient care." Clinical Epigenetics **11**(1).

Khaitan, D., U. T. Sankpal, B. Weksler, E. A. Meister, I. A. Romero, P.-O. Couraud and N. S. Ningaraj (2009). "Role of KCNMA1 gene in breast cancer invasion and metastasis to brain." BMC Cancer **9**(1): 1-11.

Kim, H. J., J. Y. Kim, C. W. Jung, Y. S. Lee, J. Y. An, E. H. Kim, K. H. Kim, S. P. Lee, J. Y. Park and M. J. Park (2021). "ANO1 regulates the maintenance of stemness in glioblastoma stem cells by stabilizing EGFRvIII." Oncogene.

Klumpp, D., S. C. Frank, L. Klumpp, E. C. Sezgin, M. Eckert, L. Edalat, M. Bastmeyer, D. Zips, P. Ruth and S. M. Huber (2017). "TRPM8 is required for survival and radioresistance of glioblastoma cells." Oncotarget **8**(56): 95896-95913.

Klumpp, L., E. C. Sezgin, M. Skardelly, F. Eckert and S. M. Huber (2018). "KCa3.1 Channels and Glioblastoma: In Vitro Studies." Curr Neuropharmacol **16**(5): 627-635.

Korpi, E. R., J. E. Kleinman, D. T. Costakos, M. Linnoila and R. J. Wyatt (1984). "Reduced haloperidol in the post-mortem brains of haloperidol-treated patients." Psychiatry Res **11**(3): 259-269.

Koshy, S., D. Wu, X. Hu, R. B. Tajhya, R. Huq, F. S. Khan, M. W. Pennington, H. Wulff, P. Yotnda and C. Beeton (2013). "Blocking KCa3.1 channels increases tumor cell killing by a subpopulation of human natural killer lymphocytes." PLoS One **8**(10): e76740.

Kudulaiti, N., Z. Zhou, C. Luo, J. Zhang, F. Zhu and J. Wu (2021). "A nomogram for individualized prediction of overall survival in patients with newly diagnosed glioblastoma: a real-world retrospective cohort study." BMC Surg **21**(1): 238.

Lathia, J. D., S. C. Mack, E. E. Mulkearns-Hubert, C. L. L. Valentim and J. N. Rich (2015). "Cancer stem cells in glioblastoma." Genes & Development **29**(12): 1203-1217.

Lee, K., F. McKenna, I. C. Rowe and M. L. Ashford (1997). "The effects of neuroleptic and tricyclic compounds on BKCa channel activity in rat isolated cortical neurones." Br J Pharmacol **121**(8): 1810-1816.

Levesque, J. P. and I. G. Winkler (2008). "Mobilization of hematopoietic stem cells: state of the art." Curr Opin Organ Transplant **13**(1): 53-58.

Li, G., Y. Li, X. Liu, Z. Wang, C. Zhang, F. Wu, H. Jiang, W. Zhang, Z. Bao, Y. Wang, J. Cai, L. Zhao, U. D. Kahlert, T. Jiang and W. Zhang (2018). "ALDH1A3 induces mesenchymal differentiation and serves as a predictor for survival in glioblastoma." Cell Death Dis **9**(12): 1190.

Li, G. Z., Y. M. Li, X. Liu, Z. Wang, C. B. Zhang, F. Wu, H. Y. Jiang, W. L. Zhang, Z. S. Bao, Y. Z. Wang, J. Q. Cai, L. Zhao, U. D. Kahlert, T. Jiang and W. Zhang (2018). "ALDH1A3 induces mesenchymal differentiation and serves as a predictor for survival in glioblastoma." Cell death & disease **9**.

Liesche-Starnecker, F., K. Mayer, F. Kofler, S. Baur, F. Schmidt-Graf, J. Kempter, G. Prokop, N. Pfarr, W. Wei, J. Gempt, S. E. Combs, C. Zimmer, B. Meyer, B. Wiestler and J. Schlegel (2020). "Immunohistochemically Characterized Intratumoral Heterogeneity Is a Prognostic Marker in Human Glioblastoma." Cancers **12**(10).

Liu, X., Y. Chang, P. H. Reinhart, H. Sontheimer and Y. Chang (2002). "Cloning and characterization of glioma BK, a novel BK channel isoform highly expressed in human glioma cells." J Neurosci **22**(5): 1840-1849.

Ma, H., C. Zhao, Z. Zhao, L. Hu, F. Ye, H. Wang, Z. Fang, Y. Wu and X. Chen (2020). "Specific glioblastoma multiforme prognostic-subtype distinctions based on DNA methylation patterns." Cancer Gene Ther **27**(9): 702-714.

Mahabir, R., M. Tanino, A. Elmansuri, L. Wang, T. Kimura, T. Itoh, Y. Ohba, H. Nishihara, H. Shirato, M. Tsuda and S. Tanaka (2014). "Sustained elevation of Snail promotes glial-mesenchymal transition after irradiation in malignant glioma." Neuro Oncol **16**(5): 671-685.

Mao, P., K. Joshi, J. Li, S. H. Kim, P. Li, L. Santana-Santos, S. Luthra, U. R. Chandran, P. V. Benos, L. Smith, M. Wang, B. Hu, S. Y. Cheng, R. W. Sobol and I. Nakano (2013). "Mesenchymal glioma stem cells are maintained by activated glycolytic metabolism involving aldehyde dehydrogenase 1A3." Proc Natl Acad Sci U S A **110**(21): 8644-8649.

Massenzio, F., M. Cambiaghi, F. Marchiotto, D. Boriero, C. Limatola, G. D'Alessandro and M. Buffelli (2022). "In vivo morphological alterations of TAMs during KCa3.1 inhibition-by using in vivo two-photon time-lapse technology." Front Cell Neurosci **16**: 1002487.

Mesrati, M. H., A. B. Behrooz, A. Y. Abuhamad and A. Syahir (2020). "Understanding Glioblastoma Biomarkers: Knocking a Mountain with a Hammer." Cells **9**(5).

- Mikkelsen, V. E., O. Solheim, O. Salvesen and S. H. Torp (2021). "The histological representativeness of glioblastoma tissue samples." Acta Neurochirurgica **163**(7): 1911-1920.
- Mohr, C. J., D. Gross, E. C. Sezgin, F. A. Steudel, P. Ruth, S. M. Huber and R. Lukowski (2019). "KCa3.1 Channels Confer Radioresistance to Breast Cancer Cells." Cancers (Basel) **11**(9).
- Mohr, C. J., W. Schroth, T. E. Murdter, D. Gross, S. Maier, B. Stegen, A. Dragoi, F. A. Steudel, S. Stehling, R. Hoppe, S. Madden, P. Ruth, S. M. Huber, H. Brauch and R. Lukowski (2020). "Subunits of BK channels promote breast cancer development and modulate responses to endocrine treatment in preclinical models." Br J Pharmacol.
- Mohr, C. J., F. A. Steudel, D. Gross, P. Ruth, W. Y. Lo, R. Hoppe, W. Schroth, H. Brauch, S. M. Huber and R. Lukowski (2019). "Cancer-Associated Intermediate Conductance Ca(2+)-Activated K<sup>+</sup> Channel K(Ca)3.1." Cancers (Basel) **11**(1).
- Nam, Y. W., D. Kong, D. Wang, R. Orfali, R. T. Sherpa, J. Totonchy, S. M. Nauli and M. Zhang (2021). "Differential modulation of SK channel subtypes by phosphorylation." Cell Calcium **94**: 102346.
- Ohya, S., K. Kimura, S. Niwa, A. Ohno, Y. Kojima, S. Sasaki, K. Kohri and Y. Imaizumi (2009). "Malignancy grade-dependent expression of K<sup>+</sup>-channel subtypes in human prostate cancer." J Pharmacol Sci **109**(1): 148-151.
- Ohya, S. and H. Kito (2018). "Ca(2+)-Activated K(+) Channel K(Ca)3.1 as a Therapeutic Target for Immune Disorders." Biol Pharm Bull **41**(8): 1158-1163.
- Palchoudhuri, R., V. Nesterenko and P. J. Hergenrother (2008). "The complex role of the triphenylmethyl motif in anticancer compounds." J Am Chem Soc **130**(31): 10274-10281.
- Panaccione, A., Y. Guo, W. G. Yarbrough and S. V. Ivanov (2017). "Expression Profiling of Clinical Specimens Supports the Existence of Neural Progenitor-Like Stem Cells in Basal Breast Cancers." Clin Breast Cancer **17**(4): 298-306.e297.
- Parihar, A. S., M. J. Coghlan, M. Gopalakrishnan and C. C. Shieh (2003). "Effects of intermediate-conductance Ca<sup>2+</sup>-activated K<sup>+</sup> channel modulators on human prostate cancer cell proliferation." Eur J Pharmacol **471**(3): 157-164.
- Park, A. K., P. Kim, L. Y. Ballester, Y. Esquenazi and Z. Zhao (2019). "Subtype-specific signaling pathways and genomic aberrations associated with prognosis of glioblastoma." Neuro Oncol **21**(1): 59-70.
- Patel, A. P., I. Tirosh, J. J. Trombetta, A. K. Shalek, S. M. Gillespie, H. Wakimoto, D. P. Cahill, B. V. Nahed, W. T. Curry, R. L. Martuza, D. N. Louis, O. Rozenblatt-Rosen, M. L. Suva, A. Regev and B. E. Bernstein (2014). "Single-cell RNA-seq highlights intratumoral heterogeneity in primary glioblastoma." Science **344**(6190): 1396-1401.

Phillips, H. S., S. Kharbanda, R. Chen, W. F. Forrest, R. H. Soriano, T. D. Wu, A. Misra, J. M. Nigro, H. Colman, L. Soroceanu, P. M. Williams, Z. Modrusan, B. G. Feuerstein and K. Aldape (2006). "Molecular subclasses of high-grade glioma predict prognosis, delineate a pattern of disease progression, and resemble stages in neurogenesis." Cancer Cell **9**(3): 157-173.

Pillozzi, S., M. D'Amico, G. Bartoli, L. Gasparoli, G. Petroni, O. Crociani, T. Marzo, A. Guerriero, L. Messori, M. Severi, R. Udisti, H. Wulff, K. G. Chandy, A. Becchetti and A. Arcangeli (2018). "The combined activation of KCa3.1 and inhibition of Kv11.1/hERG1 currents contribute to overcome Cisplatin resistance in colorectal cancer cells." Br J Cancer **118**(2): 200-212.

Puram, S. V., I. Tirosh, A. S. Parikh, A. P. Patel, K. Yizhak, S. Gillespie, C. Rodman, C. L. Luo, E. A. Mroz, K. S. Emerick, D. G. Deschler, M. A. Varvares, R. Mylvaganam, O. Rozenblatt-Rosen, J. W. Rocco, W. C. Faquin, D. T. Lin, A. Regev and B. E. Bernstein (2017). "Single-Cell Transcriptomic Analysis of Primary and Metastatic Tumor Ecosystems in Head and Neck Cancer." Cell **171**(7): 1611-+.

Rabjerg, M., A. Olivan-Viguera, L. K. Hansen, L. Jensen, L. Sevelsted-Moller, S. Walter, B. L. Jensen, N. Marcussen and R. Kohler (2015). "High expression of KCa3.1 in patients with clear cell renal carcinoma predicts high metastatic risk and poor survival." PLoS One **10**(4): e0122992.

Redon, C. E., A. J. Nakamura, Y. W. Zhang, J. J. Ji, W. M. Bonner, R. J. Kinders, R. E. Parchment, J. H. Doroshow and Y. Pommier (2010). "Histone gammaH2AX and poly(ADP-ribose) as clinical pharmacodynamic biomarkers." Clin Cancer Res **16**(18): 4532-4542.

Reya, T., S. J. Morrison, M. F. Clarke and I. L. Weissman (2001). "Stem cells, cancer, and cancer stem cells." Nature **414**(6859): 105-111.

Riedel, A., L. Klumpp, A. Menegakis, C. De-Colle, S. M. Huber, J. Schittenhelm, M. Neumann, S. Noell, M. Tatagiba and D. Zips (2021). "γH2AX foci assay in glioblastoma: Surgical specimen versus corresponding stem cell culture." Radiother Oncol **159**: 119-125.

Rosa, P., L. Sforza, S. Carlomagno, G. Mangino, M. Miscusi, M. Pessia, F. Franciolini, A. Calogero and L. Catacuzzeno (2017). "Overexpression of Large-Conductance Calcium-Activated Potassium Channels in Human Glioblastoma Stem-Like Cells and Their Role in Cell Migration." J Cell Physiol **232**(9): 2478-2488.

Ruggieri, P., G. Mangino, B. Fioretti, L. Catacuzzeno, R. Puca, D. Ponti, M. Miscusi, F. Franciolini, G. Ragona and A. Calogero (2012). "The inhibition of KCa3.1 channels activity reduces cell motility in glioblastoma derived cancer stem cells." PLoS One **7**(10): e47825.

Rushing, E. J. (2021). "WHO classification of tumors of the nervous system: preview of the upcoming 5th edition." memo - Magazine of European Medical Oncology.

Sciaccaluga, M., B. Fioretti, L. Catacuzzeno, F. Pagani, C. Bertollini, M. Rosito, M. Catalano, G. D'Alessandro, A. Santoro, G. Cantore, D. Ragozzino, E. Castigli, F.

Franciolini and C. Limatola (2010). "CXCL12-induced glioblastoma cell migration requires intermediate conductance Ca<sup>2+</sup>-activated K<sup>+</sup> channel activity." Am J Physiol Cell Physiol **299**(1): C175-184.

Sha, Z., J. Zhou, Y. Wu, T. Zhang, C. Li, Q. Meng, P. P. Musunuru, F. You, Y. Wu, R. Yu and S. Gao (2020). "BYSL Promotes Glioblastoma Cell Migration, Invasion, and Mesenchymal Transition Through the GSK-3 $\beta$ / $\beta$ -Catenin Signaling Pathway." Front Oncol **10**: 565225.

Shultz, L. D., F. Ishikawa and D. L. Greiner (2007). "Humanized mice in translational biomedical research." Nature Reviews Immunology **7**(2): 118-130.

Song, P., Y. Du, W. Song, H. Chen, Z. Xuan, L. Zhao, J. Chen, J. Chen, D. Guo and C. Jin (2017). "KCa<sub>3.1</sub> as an effective target for inhibition of growth and progression of intrahepatic cholangiocarcinoma." Journal of Cancer **8**(9): 1568.

Sontheimer, H. (2008). "An unexpected role for ion channels in brain tumor metastasis." Exp Biol Med (Maywood) **233**(7): 779-791.

Stegen, B., L. Butz, L. Klumpp, D. Zips, K. Dittmann, P. Ruth and S. M. Huber (2015). "Ca<sup>2+</sup>-Activated IK K<sup>+</sup> Channel Blockade Radiosensitizes Glioblastoma Cells." Mol Cancer Res **13**(9): 1283-1295.

Stegen, B., L. Klumpp, M. Misovic, L. Edalat, M. Eckert, D. Klumpp, P. Ruth and S. M. Huber (2016). "K(+) channel signaling in irradiated tumor cells." Eur Biophys J **45**(7): 585-598.

Steinle, M., D. Palme, M. Misovic, J. Rudner, K. Dittmann, R. Lukowski, P. Ruth and S. M. Huber (2011). "Ionizing radiation induces migration of glioblastoma cells by activating BK K(+) channels." Radiother Oncol **101**(1): 122-126.

Stocker, J. W., L. De Franceschi, G. A. McNaughton-Smith, R. Corrocher, Y. Beuzard and C. Brugnara (2003). "ICA-17043, a novel Gardos channel blocker, prevents sickled red blood cell dehydration in vitro and in vivo in SAD mice." Blood **101**(6): 2412-2418.

Stocker, M. (2004). "Ca(2+)-activated K<sup>+</sup> channels: molecular determinants and function of the SK family." Nat Rev Neurosci **5**(10): 758-770.

Stransky, N., K. Ganser, U. Naumann, S. M. Huber and P. Ruth (2022). "Tumoricidal, Temozolomide- and Radiation-Sensitizing Effects of K(Ca)<sub>3.1</sub> K<sup>+</sup> Channel Targeting In Vitro Are Dependent on Glioma Cell Line and Stem Cell Fraction." Cancers **14**(24).

Stransky, N., K. Ganser, L. Quintanilla-Fend, I. Gonzalez Menendez, U. Naumann, F. Eckert, K. P., S. M. Huber and P. Ruth (2023). "TRAM-34 inhibits irradiation-induced hyperinvasion of glioma cells and prolongs survival in the SMA-560 VM/Dk mouse model without impairing immune cell infiltration." (unpublished observations).

Stupp, R., M. E. Hegi, W. P. Mason, M. J. van den Bent, M. J. Taphoorn, R. C. Janzer, S. K. Ludwin, A. Allgeier, B. Fisher, K. Belanger, P. Hau, A. A. Brandes, J. Gijtenbeek, C. Marosi, C. J. Vecht, K. Mokhtari, P. Wesseling, S. Villa, E.

Eisenhauer, T. Gorlia, M. Weller, D. Lacombe, J. G. Cairncross and R. O. Mirimanoff (2009). "Effects of radiotherapy with concomitant and adjuvant temozolomide versus radiotherapy alone on survival in glioblastoma in a randomised phase III study: 5-year analysis of the EORTC-NCIC trial." Lancet Oncol **10**(5): 459-466.

Stupp, R. and Z. Ram (2017). "Standard of Care Temozolomide Chemotherapy +/- Tumor Treating Fields (Ttfields) in Newly Diagnosed Glioblastoma. Final Results of the Phase Iii Ef-14 Clinical Trial." Neuro-Oncology **19**: 15-15.

Stupp, R., S. Taillibert, A. Kanner, S. Kesari, S. A. Toms, G. H. Barnett, K. L. Fink, A. Silvani, F. S. Lieberman, J. J. G. Zhu, L. P. Taylor, J. Honnorat, A. Hottinger, T. Chen, D. D. Tran, C. Y. Kim, H. W. Hirte, M. E. Hegi, Y. Palti and Z. Ram (2015). "Tumor treating fields (TTFields): A novel treatment modality added to standard chemo- and radiotherapy in newly diagnosed glioblastoma-First report of the full dataset of the EF14 randomized phase III trial." Journal of Clinical Oncology **33**(15).

Sullivan, K. E., K. Rojas, R. A. Cerione, I. Nakano and K. F. Wilson (2017). "The stem cell/cancer stem cell marker ALDH1A3 regulates the expression of the survival factor tissue transglutaminase, in mesenchymal glioma stem cells." Oncotarget **8**(14): 22325-22343.

Tang, X., C. Zuo, P. Fang, G. Liu, Y. Qiu, Y. Huang and R. Tang (2021). "Targeting Glioblastoma Stem Cells: A Review on Biomarkers, Signal Pathways and Targeted Therapy." Front Oncol **11**: 701291.

Todesca, L. M., S. Maskri, K. Brommel, I. Thale, B. Wunsch, O. Koch and A. Schwab (2021). "Targeting K(ca)3.1 Channels in Cancer." Cell Physiol Biochem **55**(S3): 131-144.

Turner, K. L., A. Honasoge, S. M. Robert, M. M. McFerrin and H. Sontheimer (2014). "A proinvasive role for the Ca(2+) -activated K(+) channel KCa3.1 in malignant glioma." Glia **62**(6): 971-981.

Turner, K. L. and H. Sontheimer (2014). "KCa3.1 modulates neuroblast migration along the rostral migratory stream (RMS) in vivo." Cereb Cortex **24**(9): 2388-2400.

Verhaak, R. G., K. A. Hoadley, E. Purdom, V. Wang, Y. Qi, M. D. Wilkerson, C. R. Miller, L. Ding, T. Golub, J. P. Mesirov, G. Alexe, M. Lawrence, M. O'Kelly, P. Tamayo, B. A. Weir, S. Gabriel, W. Winckler, S. Gupta, L. Jakkula, H. S. Feiler, J. G. Hodgson, C. D. James, J. N. Sarkaria, C. Brennan, A. Kahn, P. T. Spellman, R. K. Wilson, T. P. Speed, J. W. Gray, M. Meyerson, G. Getz, C. M. Perou and D. N. Hayes (2010). "Integrated genomic analysis identifies clinically relevant subtypes of glioblastoma characterized by abnormalities in PDGFRA, IDH1, EGFR, and NF1." Cancer Cell **17**(1): 98-110.

Villani, V., B. Casini, A. Tanzilli, M. Lecce, F. Rasile, S. Telera, A. Pace, F. Piludu, I. Terrenato, F. Rollo, F. De Nicola, M. Fanciulli, M. Pallocca, G. Ciliberto and M. Carosi (2023). "The Glioma-IRE project - Molecular profiling in patients with glioma: steps toward an individualized diagnostic and therapeutic approach." J Transl Med **21**(1): 215.

Wang, Q., B. Hu, X. Hu, H. Kim, M. Squatrito, L. Scarpace, A. C. deCarvalho, S. Lyu, P. Li, Y. Li, F. Barthel, H. J. Cho, Y. H. Lin, N. Satani, E. Martinez-Ledesma, S. Zheng, E. Chang, C. G. Sauv , A. Olar, Z. D. Lan, G. Finocchiaro, J. J. Phillips, M. S. Berger, K. R. Gabrusiewicz, G. Wang, E. Eskilsson, J. Hu, T. Mikkelsen, R. A. DePinho, F. Muller, A. B. Heimberger, E. P. Sulman, D. H. Nam and R. G. W. Verhaak (2017). "Tumor Evolution of Glioma-Intrinsic Gene Expression Subtypes Associates with Immunological Changes in the Microenvironment." Cancer Cell **32**(1): 42-56.e46.

Wongergem, R. and J. W. Bartley (2009). "Menthol increases human glioblastoma intracellular Ca<sup>2+</sup>, BK channel activity and cell migration." Journal of biomedical science **16**(1): 90.

Wu, W., J. Schecker, S. Wurstle, F. Schneider, M. Schonfelder and J. Schlegel (2018). "Aldehyde dehydrogenase 1A3 (ALDH1A3) is regulated by autophagy in human glioblastoma cells." Cancer Letters **417**: 112-123.

Yachi, K., M. Tsuda, S. Kohsaka, L. Wang, Y. Oda, S. Tanikawa, Y. Ohba and S. Tanaka (2018). "miR-23a promotes invasion of glioblastoma via HOXD10-regulated glial-mesenchymal transition." Signal Transduct Target Ther **3**: 33.

Yan, G. N., L. Yang, Y. F. Lv, Y. Shi, L. L. Shen, X. H. Yao, Q. N. Guo, P. Zhang, Y. H. Cui, X. Zhang, X. W. Bian and D. Y. Guo (2014). "Endothelial cells promote stem-like phenotype of glioma cells through activating the Hedgehog pathway." J Pathol **234**(1): 11-22.

Yin, J., G. Park, T. H. Kim, J. H. Hong, Y. J. Kim, X. Jin, S. Kang, J. E. Jung, J. Y. Kim, H. Yun, J. E. Lee, M. Kim, J. Chung, H. Kim, I. Nakano, H. S. Gwak, H. Yoo, B. C. Yoo, J. H. Kim, E. M. Hur, J. Lee, S. H. Lee, M. J. Park and J. B. Park (2015). "Pigment Epithelium-Derived Factor (PEDF) Expression Induced by EGFRvIII Promotes Self-renewal and Tumor Progression of Glioma Stem Cells." PLoS Biol **13**(5): e1002152.

Ying, M., S. Wang, Y. Sang, P. Sun, B. Lal, C. R. Goodwin, H. Guerrero-Cazares, A. Quinones-Hinojosa, J. Laterra and S. Xia (2011). "Regulation of glioblastoma stem cells by retinoic acid: role for Notch pathway inhibition." Oncogene **30**(31): 3454-3467.

Yoon, S. J., J. K. Shim, J. H. Chang, J. H. Moon, T. H. Roh, K. S. Sung, J. H. Lee, E. H. Kim, S. H. Kim, Y. K. Hong, S. J. Lee, Y. M. Huh and S. G. Kang (2016). "Tumor Mesenchymal Stem-Like Cell as a Prognostic Marker in Primary Glioblastoma." Stem Cells International **2016**.

Yusuf, S., P. Aretz, A. C. Nickel, P. Westhoff, A. Sharma, N. Qin, M. Remke, H. J. Steiger, D. Hanggi, H. Liu, H. Liu, S. Neumann, G. Reifenberger and J. Maciaczyk (2022). "WNT/beta-Catenin-Mediated Resistance to Glucose Deprivation in Glioblastoma Stem-like Cells." Cancers (Basel) **14**(13).

Zhang, Z. W., J. Chen, X. H. Huo, G. Zong, K. B. Huang, M. Cheng, L. B. Sun, X. Y. Yue, E. B. Bian and B. Zhao (2021). "Identification of a mesenchymal-related signature associated with clinical prognosis in glioma." Aging-U.S. **13**(9): 12431-12455.

# Danksagung

Zunächst möchte ich mich bei meinem Doktorvater, Herr Prof. Dr. Peter Ruth sowie meinem Betreuer Herr Prof. Dr. Stephan Huber für das Überlassen dieses hoch interessanten Themas meiner Dissertation bedanken. Auch durch die Möglichkeit der Teilnahme von Kongressen und Fortbildungen konnte ich mich in den letzten fünf Jahren fachlich und persönlich immer weiterentwickeln.

Vielen Dank, Stephan, für dein stets offenes Ohr, deine Unterstützung und Beratung zu jeder Zeit und die tolle Atmosphäre, die du so in deiner Arbeitsgruppe geschafften hast.

Bei Herr Prof. Matthias Schwab möchte ich mich für die Bereiterklärung als Drittgutachter und Prüfer meiner mündlichen Promotionsprüfung bedanken. In diesem Zuge auch vielen Dank an Herrn Prof. Dr. Harald Groß, welcher das Prüfungskomitee vervollständigt.

Außerdem möchte ich mich bei Frau PD Dr. Franziska Eckert für die Integration in ihr Forschungsprojekt bedanken, sodass ich auch vieles über Weichteilsarkome lernen und einen Einblick in den Ablauf klinischer Studien bekommen konnte.

In der Abteilung der Radioonkologie und darüber hinaus durfte ich durch mein translationales Projekt viele tolle Kolleg:innen kennenlernen, die leider nicht alle namentlich genannt werden können. Deswegen vielen Dank an alle Weggefährt:innen für die schöne Zeit sowie allen Koauthor:innen der gemeinsamen Publikationen für die gute Zusammenarbeit und der „Laborjugend“ für viele lustige Tage und Nächte auch außerhalb des Arbeitsalltags. Ich hoffe wir bleiben weiterhin in Kontakt.

Vielen Dank, Heidi, für deine mentale und professionelle Unterstützung während meines Projektes. Du fehlst hier, aber ich weiß du schaust „der Jugend“ auf ihren weiteren Wegen jetzt von oben zu.

Schließlich möchte ich meiner Familie für ihre Unterstützung danken und, dass sie mich bei meiner Entscheidung für eine Promotion nach dem Studium bestärkt haben.

Juli, Felix, Miriam und Sarah, danke für die wöchentlichen „Pharmietreffen“ bei denen wir Frust aber auch Freude austauschen konnten. Ihr gehört mittlerweile zur „gewählten“ Familie.

Zu guter Letzt vielen Dank Pepe - meiner Konstante die letzten zehn Jahre. Mit dir an meiner Seite weiß ich, dass ich auch in Zukunft alle Herausforderungen meistern kann.



## Anhang - Publikationen

Der Inhalt dieser kumulative Promotionsschrift umfasst die Studien Ganser et al. 2022, Ganser et al. 2023 und Eckert et al 2023 (in der ausführlichen „Liste der Publikationen“ blau markiert). Aus diesem Grund, sind nur diese drei ausgewählten Publikationen der Dissertation angehängt.



### Akzeptierte Publikationen

1. **Ganser K**, Eckert F, Riedel A, Stransky N, Paulsen F, Noell S, Krueger M, Schittenhelm J, Beck-Wödl S, Zips D, Ruth P, Huber SM, Klumpp L. Patient-individual phenotypes of glioblastoma stem cells are conserved in culture and associate with radioresistance, brain infiltration and patient prognosis. *Int J Cancer*. 2022 May 15;150(10):1722-1733. doi: 10.1002/ijc.33950. Epub 2022 Feb 14. PMID: 35085407.
2. Eckert F, **Ganser K**, Bender B, et al. Potential of pre-operative MRI features in glioblastoma to predict for molecular stem cell subtype and patient overall survival [published online ahead of print, 2023 Aug 22]. *Radiother Oncol*. 2023;109865. doi:10.1016/j.radonc.2023.109865

### Eingereichtes Manuskript

1. **Ganser K**, Stransky N, Abed T, Quintanilla-Martinez L, Gonzalez-Menendez I, Naumann U, Koch P, Krueger M, Ruth P, Huber SM, and Eckert F. KCa channel targeting impairs DNA repair and invasion capability of patient-derived glioblastoma stem cells in culture and orthotopic mouse xenografts 2023 (*submitted*)

# Patient-individual phenotypes of glioblastoma stem cells are conserved in culture and associate with radioresistance, brain infiltration and patient prognosis

Katrin Ganser<sup>1</sup> | Franziska Eckert<sup>1</sup> | Andreas Riedel<sup>1</sup> | Nicolai Stransky<sup>1,2</sup>  | Frank Paulsen<sup>1</sup> | Susan Noell<sup>3</sup> | Marcel Krueger<sup>4</sup> | Jens Schittenhelm<sup>5</sup> | Stefanie Beck-Wödl<sup>6</sup> | Daniel Zips<sup>1</sup> | Peter Ruth<sup>2</sup> | Stephan M. Huber<sup>1</sup>  | Lukas Klumpp<sup>1</sup>

<sup>1</sup>Department of Radiation Oncology, University of Tübingen, Tübingen, Germany

<sup>2</sup>Department of Pharmacology, Toxicology and Clinical Pharmacy, Institute of Pharmacy, University of Tübingen, Tübingen, Germany

<sup>3</sup>Department of Neurosurgery, University of Tübingen, Tübingen, Germany

<sup>4</sup>Preclinical Imaging and Radiopharmacy, Werner Siemens Imaging Center, University of Tübingen, Tübingen, Germany

<sup>5</sup>Department of Neuropathology, University of Tübingen, Tübingen, Germany

<sup>6</sup>Institute of Medical Genetics und Applied Genomics, University of Tübingen, Tübingen, Germany

## Correspondence

Stephan M. Huber, Department of Radiation Oncology, University of Tübingen, Hoppe-Seyler-Str. 3, 72076 Tübingen, Germany.  
Email: stephan.huber@uni-tuebingen.de

## Funding information

Deutsche Krebshilfe, Grant/Award Numbers: 70112872, 70113144; Else-Kroener-Fresenius Research Foundation, Grant/Award Number: Grant 2015\_Kolleg.14; Gesellschaft für Kinderkrebsforschung; ICEPHA Graduate Program

## Abstract

Identification of prognostic or predictive molecular markers in glioblastoma resection specimens may lead to strategies for therapy stratification and personalized treatment planning. Here, we analyzed in primary glioblastoma stem cell (pGSC) cultures the mRNA abundances of seven stem cell (MSI1, Notch1, nestin, Sox2, Oct4, FABP7 and ALDH1A3), and three radioresistance or invasion markers (CXCR4, IK<sub>Ca</sub> and BK<sub>Ca</sub>). From these abundances, an mRNA signature was deduced which describes the mesenchymal-to-proneural expression profile of an individual GSC culture. To assess its functional significance, we associated the GSC mRNA signature with the clonogenic survival after irradiation with 4 Gy and the fibrin matrix invasion of the GSC cells. In addition, we compared the molecular pGSC mRNA signature with the tumor recurrence pattern and the overall survival of the glioblastoma patients from whom the pGSC cultures were derived. As a result, the molecular pGSC mRNA signature correlated positively with the pGSC radioresistance and matrix invasion capability in vitro. Moreover, patients with a mesenchymal (>median) mRNA signature in their pGSC cultures exhibited predominantly a multifocal tumor recurrence and a significantly (univariate log rank test) shorter overall survival than patients with proneural (≤median mRNA signature) pGSCs. The tumors of the latter recurred predominantly unifocally. We conclude that our pGSC cultures induce/select those cell subpopulations of the heterogeneous brain tumor that determine disease progression and therapy outcome. In addition, we further postulate a clinically relevant

Abbreviations: ACTB,  $\beta$ -actin; ALDH1A3, aldehyde dehydrogenase-1A3; Cp, crossing point; DFS, disease free survival; EGFRvIII, epidermal growth factor receptor variant III; FABP7, fatty acid binding protein-7; GAPDH, glyceraldehyde-3-phosphate dehydrogenase; GFAP, glial fibrillary acidic protein; GSC, glioblastoma stem cell; HNSCC, head and neck squamous carcinoma cells; Ivy GAP, Ivy Glioblastoma Atlas Project; MGMT, O6-methylguanine-DNA-methyltransferase; MMP2, -9, matrix metalloproteinase-2 and -9; MSI1, Musashi-1; OS, overall survival; PBS, phosphate buffered saline; Pcc, Pearson correlation coefficient; PDHB, pyruvate dehydrogenase- $\beta$ ; PE, plating efficiency; pGSC, primary glioblastoma stem cell; REMBRANDT, Repository of Molecular Brain Neoplasia Data; RT-PCR, real-time reverse-transcriptase polymerase chain reaction; SDF1, stromal cell derived factor-1; SF, survival fractions; TCGA, The Cancer Genome Atlas; TRPM8, melastatin family member-8 of the transient receptor potential nonselective cation channels.

This is an open access article under the terms of the Creative Commons Attribution-NonCommercial-NoDerivs License, which permits use and distribution in any medium, provided the original work is properly cited, the use is non-commercial and no modifications or adaptations are made.

© 2022 The Authors. *International Journal of Cancer* published by John Wiley & Sons Ltd on behalf of UICC.

prognostic/predictive value for the 10 mRNAs-based mesenchymal-to-proneural signature of the GSC subpopulations in glioblastoma.

#### KEYWORDS

brain infiltration, glioblastoma stem cells, ionizing radiation, overall survival

#### What's new?

Individualized treatment for glioblastoma could help improve survival for this cancer, which generally has a poor prognosis. Here, the authors measured abundances of 10 mRNAs in primary cultures of glioblastoma stem cells (pGSCs) and identified an RNA signature that correlates with radiation resistance and invasiveness. They also found that the mRNA signature correlated with the tumor recurrence pattern and overall survival of the glioblastoma patients that the pGSCs came from. Thus, culturing pGSCs may provide a platform for predicting response to treatment or determining prognosis.

## 1 | INTRODUCTION

(Epi)genome and transcriptome analysis of glioblastoma biopsies or resection specimens revealed a high intertumoral heterogeneity and led to the identification of distinct molecular glioblastoma subtypes.<sup>1-9</sup> Among those, classical, proneural, neural and mesenchymal molecular subtypes were identified<sup>2,7</sup> which differ in immune micro-environment<sup>7</sup> and to some extent in patient prognosis when analysis is restricted to glioblastomas with low transcriptional heterogeneity. Later on, the neural subgroup has been shown to artificially arise from a high fraction of normal brain tissue in brain areas with loosely disseminated tumor cells.<sup>7</sup> Moreover, the proneural subgroup accumulates IDH-mutated tumors with highly methylated CpG island phenotype<sup>5,10</sup> and better prognosis of disease outcome. IDH-mutated gliomas are now a distinct molecular tumor class and no longer rated as glioblastoma according to the upcoming 5th edition of WHO classification.<sup>11</sup>

Beyond transcriptome and (epi)genetic subclass profiles, further markers that are prognostic or predictive for the clinical outcome and therapy response in glioblastoma have been identified. Among those is the promoter methylation of the temozolomide resistance gene *MGMT* (O6-methylguanine-DNA-methyltransferase) that is associated with better prognosis.<sup>12</sup> The identification of molecular subclasses and prognostic/predictive markers, however, has hardly<sup>13</sup> been translated into the clinical routine for glioblastoma patient stratification and personalized adaptation of therapy regimens. Despite multimodal therapy, median survival of glioblastoma patients remains still below 2 years. A highly immunosuppressive tumor microenvironment in concert with the infiltrative growth and the therapy resistance of glioblastoma cells has been proposed to contribute to the bad prognosis and high therapy failure rate. The latter is in particular caused by the properties of stem cell-like glioblastoma cells.<sup>7</sup>

Glioblastoma comprise a small cell fraction with stem cell-like phenotype (GSCs) and tumor-initiating capability.<sup>14</sup> The overwhelming portion of the brain tumor is formed by "differentiated" glioblastoma bulk cells, microglia and tumor-associated macrophages. The

latter two build up 30% to 50% of all cells within the tumor.<sup>15</sup> Cancer stem cell-like cells including GSCs have been proposed to be the most therapy-resistant subpopulation of a tumor due to (compared to bulk cells) downregulated apoptotic pathways, upregulated DNA repair and oxidative defense, and better adaptation to stress factors of the tumor microenvironment arising from inflammation, hypoxia, low pH values and nutrient shortage. In addition, GSCs have the possibility to survive during therapy by entering cell quiescence and to repopulate more accelerated than bulk tumor cells after therapy by pursuing ontogenetic pathways.<sup>16,17</sup> This might suggest that the efficacy of an anti-glioblastoma treatment is limited by the therapy resistance of the GSC subpopulation(s).

At least two distinct subpopulations of GSCs have been described by gene expression profiling and functional analysis that differ in expression of proneural and mesenchymal markers. Aldehyde dehydrogenase-1A3 (*ALDH1A3*) that contributes to a molecular mesenchymal GSC phenotype<sup>18-21</sup> has been reported to oxidize retinal to retinoic acid.<sup>22</sup> Retinoic acid, in turn, has been shown to downregulate Notch1 signaling<sup>23</sup> and expression of the proneural stem cell markers *prominin-1* (*CD133*), *MSI1*, *nestin* and *Sox2* in glioblastoma cells.<sup>22</sup> The epidermal growth factor receptor variant III (*EGFRvIII*), in contrast, reportedly induces in glioblastoma cells the proneural stem cell markers *Notch1*, *Sox2*, *nestin* and *prominin-1* (*CD133*) and suppresses expression of the astrocytic differentiation marker *GFAP* (glial fibrillary acidic protein).<sup>24-26</sup> In primary culture a mesenchymal GSC phenotype is characterized beyond its transcriptional profile (that includes upregulation of *ALDH1A3*) by a more cell culture-dish adherent growth morphology, and a higher radioresistance<sup>18</sup> as well as by faster migration and invasion<sup>27,28</sup> than the proneural GSC phenotype that is characterized in culture by formation of neuro(glioma)spheres.

Since GSCs represent only a minor fraction of the tumor, GSC-specific markers with potentially prognostic or predictive value for disease outcome are diluted in transcriptome data from glioblastoma biopsy and resection specimens. Single cell mRNA sequencing of identified GSC cells is one elaborate approach to acquire GSC-specific transcriptome data.<sup>7</sup> Alternatively, the GSCs fraction of a tumor

sample can be tremendously expanded by primary culture of the cells in a serum-free medium that has been designed to select or induce neural stem/progenitor cells.<sup>4,29</sup> Primary GSC cultures, however, carry the risk of culture-induced changes in gene expression pattern considering the suggested high plasticity within the different GSCs and “differentiated” (ie, downregulation of stem cell marker expression) phenotypes.<sup>30</sup> Moreover, primary cultures lack the reciprocal interaction between GSCs and the tumor microenvironment, for example, within perivascular stem cell niches, which reportedly contributes to induction and/or maintenance of the GSC phenotype.<sup>31</sup> Only few data are available<sup>32</sup> on the degree transcriptional GSC subtypes dedifferentiate or transdifferentiate during isolated primary culture. One important aspect that argues for the use of primary GSC cultures is that enriched GSCs allow the functional characterization of GSC phenotypes *in vitro*.

Preclinical *in vitro* and animal studies disclosed cellular mechanisms of therapy-resistance and invasiveness that are upregulated in GSCs. ALDH1A3-expressing mesenchymal GSCs reportedly overexpress Ca<sup>2+</sup>-activated intermediate conductance IK<sub>Ca</sub> K<sup>+</sup> channels.<sup>33</sup> IK<sub>Ca</sub> channels have been demonstrated *in vitro* and in an ectopic mouse model to confer radioresistance to glioblastoma cells.<sup>34,35</sup> In addition, IK<sub>Ca</sub> is required for glioblastoma cell migration<sup>36</sup> and maintenance of the proinvasive GSC phenotype.<sup>37</sup> Finally, expression profiling of tumor specimens has associated IK<sub>Ca</sub> with a stem cell subpopulation of breast cancer<sup>38</sup> and electrophysiological data suggest upregulation of IK<sub>Ca</sub> by normal adipose tissue-derived mesenchymal stem cells.<sup>39</sup>

Likewise, beyond retaining mesenchymal hematopoietic stem cells in bone marrow niches,<sup>40</sup> the chemokine receptor CXCR4 reportedly exerts self-renewal, promigratory, proinfiltrative and radio-protecting functions in glioblastoma cells and is, therefore, presumed as a stem cell marker in glioblastoma.<sup>41</sup> Furthermore, stem cell growth culture conditions highly upregulate Ca<sup>2+</sup>-activated high conductance BK<sub>Ca</sub> K<sup>+</sup> channels in U87-MG glioblastoma cells<sup>42</sup> and activation of BK<sub>Ca</sub> K<sup>+</sup> channels by radiogenic CXCR4 signaling has been demonstrated to promote glioblastoma migration *in vitro* and brain infiltration in an orthotopic glioblastoma mouse model.<sup>43</sup> Similarly, blockade of BK<sub>Ca</sub> reportedly lowers spontaneous<sup>42</sup> and hypoxia-induced<sup>44</sup> migration of U87-MG glioblastoma cells *in vitro*. Like IK<sub>Ca</sub>, BK<sub>Ca</sub><sup>39</sup> and CXCR4<sup>45</sup> have been associated with normal adipose tissue-derived mesenchymal stem cells which might hint to a specific function of IK<sub>Ca</sub>, BK<sub>Ca</sub> and CXCR4 in mesenchymal GSCs.

The present study aimed to define GSC subtypes and their phenotypes in primary culture from a cohort of 23 glioblastoma patients by the use of a molecular mRNA signature derived from expression patterns of proneural and mesenchymal stem cell markers combined with above mentioned markers of radioresistance and invasiveness. This signature was used to define whether GSCs conserve their transcriptional subtype diversity in primary culture and during fractionated radiotherapy. In addition, the present study analyzes the differences in intrinsic radioresistance and invasiveness between the transcriptional GSC subtypes *in vitro* and the association with their molecular mRNA signature herein. Finally, the functional significance of the

molecular mRNA GSC signature for the clinical outcome of the patients (the GSC cultures were derived from) was addressed.

## 2 | MATERIALS AND METHODS

### 2.1 | Patient data and cell culture

Glioblastoma stem (cell-like) cells (GSCs) were grown from 24 resection specimens of 23 isocitrate dehydrogenase (IDH) wildtype glioblastoma and one IDH-mutated grade-4 astrocytoma (see Table S1 in part A of the Supporting Information) who underwent surgery at the Department of Neurosurgery, University of Tübingen, Germany, in the time from 2016 to 2018.

Primary GSC cultures (pGSCs) were grown from glioblastoma specimens in stem cell-enriching/selecting supplemented complete human NeuroCult NS-A Proliferation Medium (STEMCELL Technologies, Cologne, Germany) as described.<sup>33</sup> For detail, see part B of the Supporting Information. All pGSCs were recently authenticated using short tandem repeat (STR) profiling and unique STR profiles were obtained for all pGSCs (profiling was performed in November to December 2021, data not shown). Clinical and neuropathological data were retrieved by chart review. Patients with recurrent glioblastoma or differing histologies in the final pathology report were excluded. Progression was defined as new or larger contrast enhancing lesion and/or initiation of a new line of therapy. Follow-up data were retrieved from the medical chart. Images and radiotherapy plans were extracted from the imaging archive and radiotherapy planning system. The patient with the IDH-mutated grade-4 astrocytoma showed an overall survival of 2.7 years that was close to median survival (2.6 years, data not shown) of our total Tübingen patient cohort (the latter exceeded the median overall survival reported for historical cohorts<sup>12</sup> due to the fact that our patients were restricted to a subpopulation with resectable tumors and, therefore, better prognosis) and was, therefore, maintained in our analysis.

### 2.2 | Calculation of the molecular mesenchymal-to-proneural mRNA signature

For every mRNA of a pGSC, the log<sub>10</sub> values (*L*) of the housekeeper-normalized abundance ( $L = \log_{10}A$ ) was further normalized (*N*) to the corresponding minimal (*L*<sub>min</sub>) and maximal (*L*<sub>max</sub>) values among all pGSCs by the use of the following equation:  $N = (L - L_{min}) / (L_{max} - L_{min}) + 1$ . The molecular signature was then deduced by the geometric mean of N<sub>KCNNA4</sub>, N<sub>KCNMA1</sub>, N<sub>ALDH1A3</sub>, N<sub>CXCR4</sub> and N<sub>Oct4</sub>, divided by the geometric mean of N<sub>Nestin</sub>, N<sub>Sox2</sub>, N<sub>MSI1</sub>, N<sub>FABP7</sub> and N<sub>Notch1</sub>. Since we used log<sub>10</sub> values of the mRNA abundances, geometrical means were chosen instead of arithmetical means. The individual values of the molecular mRNA ranged from 0.74 to 1.20.

RNA isolation, RT-PCR and calculation of the molecular mesenchymal-to-proneural mRNA signature, was performed as described.<sup>33</sup> Templates were amplified using the following primers:

KCNN4 (IK<sub>Ca</sub>, QT00003780, QuantiTect Primer Assay, QIAGEN, Venlo, Netherlands), KCNMA1 (QT00024157), ALDH1A3 (QT00077588), CXCR4 (QT00223188), Sox2 (QT00237601), Notch1 (QT01005109), Oct4 (QT00210840), MS11 (QT00025389), nestin (QT00235781), FABP7 (QT00007322), Nanog (QT01025850), CD133 (QT00075586), GFAP (QT00081151), SDF1 (QT00087591), MMP2 (QT00088396), MMP9 (QT00040040), TRPM8 (QT00038906), as well as for the housekeepers glyceraldehyde-3-phosphate dehydrogenase GAPDH (QT01192646), ACTB (QT00095431) and PDHB (QT00031227). For detail, see part B of the Supporting Information.

Ionizing radiation (6 MV photons) was applied with a linear accelerator (LINAC SL15, Philips, Eindhoven, The Netherlands) and clonogenic survival was determined by preplating limited dilution assay as described.<sup>46</sup> A hypofractionated radiation protocol (5x 8 Gy) was defined dose-equivalent to normofractionated radiotherapy (60 Gy in 30 fractions). For details, see part B of the Supporting Information.

Fibrin gel invasion by pGSC cells, querying glioblastoma data bases and statistics were performed as described in detail in part B of the Supporting Information.

### 3 | RESULTS

#### 3.1 | Identifying a molecular mesenchymal-to-proneural pGSC mRNA signature

Given the low number of glioblastoma patients in the Tübingen cohort, the statistical probability is extremely low to identify by transcriptome analysis mRNA markers or derived molecular signatures that associate with functional parameters of our pGSC cultures. Therefore, we pursued another approach. We analyzed in our pGSC cultures the mRNA abundances of established stem cell markers. In addition, we determined mRNAs encoding for proteins that confer radioresistance and/or promote glioblastoma spreading as identified in our previous work.<sup>33-35,43,47-49</sup> In particular, abundances of mRNAs encoding for stem cell markers Nanog (transcription factor), CD133 (prominin-1, glycoprotein), nestin (intermediate filament), Notch1 (membrane receptor), Sox2 (transcription factor), Oct4 (POU5F1, transcription factor), MS11 (Musashi-1, RNA-binding protein) and ALDH1A3 (aldehyde dehydrogenase), of the neural stem cell-/glial precursor marker FABP7 (cytoplasmic fatty acid binding protein-7), of the astrocyte differentiation marker GFAP (glial fibrillary acidic protein, intermediate filament), respectively, and of the invasion markers CXCR4 (chemokine receptor), SDF1 (stromal cell derived factor-1, CXCL12, chemokine),<sup>43</sup> MMP2, -9, (matrix metalloproteinase-2 and -9) and the promigratory ion channels IK<sub>Ca</sub> (KCNN4),<sup>37</sup> BK<sub>Ca</sub> (KCNMA1),<sup>43,49</sup> and TRPM8 (melastatin family member-8 of the transient receptor potential nonselective cation channels)<sup>47</sup> were determined by RT-PCR, to characterize the heterogeneity of the pGSC cultures derived from n = 24 resection specimens of n = 23 patients. As a result, the abundances of these mRNAs varied considerably between the individual pGSC cultures. Associating these mRNA abundances to each other exhibited several positive and negative correlations. Among those, nestin correlated weakly to moderately positively with FABP7, Notch1, Sox2 and MS11 (Pearson correlation

coefficients  $P_{cc} = .47-.65$ ; Figure 1A, upper row). ALDH1A3, in contrast, correlated weakly negatively with MS11 and nestin ( $P_{cc} = -.42$  and  $-.35$ , respectively) and weakly positively with IK<sub>Ca</sub> and BK<sub>Ca</sub> ( $P_{cc} = .43$  and  $.30$ , respectively; Figure 1A, middle row) while CXCR4 correlated weakly positively with Oct4 and GFAP ( $P_{cc} = .47$  and  $.34$ , respectively; Figure 1A, lower row).

In addition to the differing mRNA expression profiles, pGSC cultures showed distinct growth phenotypes ranging from free floating neurospheres to adherent cell monolayers (Figure 1B). One pGSC culture (LK3) grew with two different phenotypes and expression profiles (LK3<sub>a</sub> in adherent monolayer and LK3<sub>s</sub> in spheres, see Figure 1F). We scored the growth phenotypes between 1 (free floating spheres) and 4 (monolayer adherent to the Petri dish bottom, Figure 1B). Given the reported differing morphological growth phenotypes of mesenchymal and proneural GSC subpopulations in primary culture,<sup>18</sup> we used this scoring to identify a molecular mesenchymal-to-proneural mRNA signature. In particular, under consideration of the mRNA correlations shown in Figure 1A, mRNA abundances were allocated to “mesenchymal” and “proneural” markers and molecular mesenchymal-to-proneural mRNA signatures were computed by forming the ratio between their mean abundances (using the averaged mRNA abundances of the “proneural” marker group as denominator and that of the “mesenchymal” group as numerator). By iterating analyses of Pearson correlation between growth score and molecular signature during modification of the “mesenchymal” and/or “proneural” marker groups, a molecular mesenchymal-to-proneural signature (based on the “mesenchymal” markers ALDH1A3, IK<sub>Ca</sub>, BK<sub>Ca</sub>, CXCR4 and Oct4 and the “proneural” markers Notch1, Sox2, MS11, nestin and FABP7) could be identified that correlated best (Pearson coefficient for linear correlation,  $P_{cc} = .82$ ) with the growth morphology (Figure 1C). The heatmap (Figure 1D) visualizes the dependence of the mRNA abundances and our molecular 10 mRNA signature.

At least in theory, small differences in gene expression might determine whether a pGSC culture forms spheres or grows as adherent monolayer. The contact to the plastic surface, in turn, might induce the mesenchymal expression profile. If so, adherent mesenchymal cells forced to grow in spheres should lose their mesenchymal signature. To test this hypothesis, adherent mesenchymal pGSC cultures were seeded on low-attachment surfaces resulting in the formation of free-floating spheres (Figure 1E, inserts). Notably, the molecular mRNA signature of three mesenchymal and adherently growing pGSCs did not change when forced into a spheroidal growth phenotype (Figure 1E). This strongly suggests that adherent growth is a consequence of a mesenchymal mRNA signature and not vice versa. Moreover, these data indicate that albeit growing in identical NeuroCult neural stem cell medium, pGSCs were induced/selected that differ considerably between the individual cultures in their mesenchymal-to-proneural molecular mRNA signature. To test how stably these transcriptional pGSC subtypes are maintained during continuous culture, the molecular signature was monitored up to >50 passages of cell culture (Figure 1F). The data indicate that individual pGSC cultures maintain their mesenchymal-to-proneural molecular mRNA signature. Next, the protein and functional expression of selected marker RNAs were studied. As shown in part C of the Supporting Information (Figures S1-S4), the studied marker mRNAs (ALDH1A3, CXCR4, nestin and IK<sub>Ca</sub>) associated



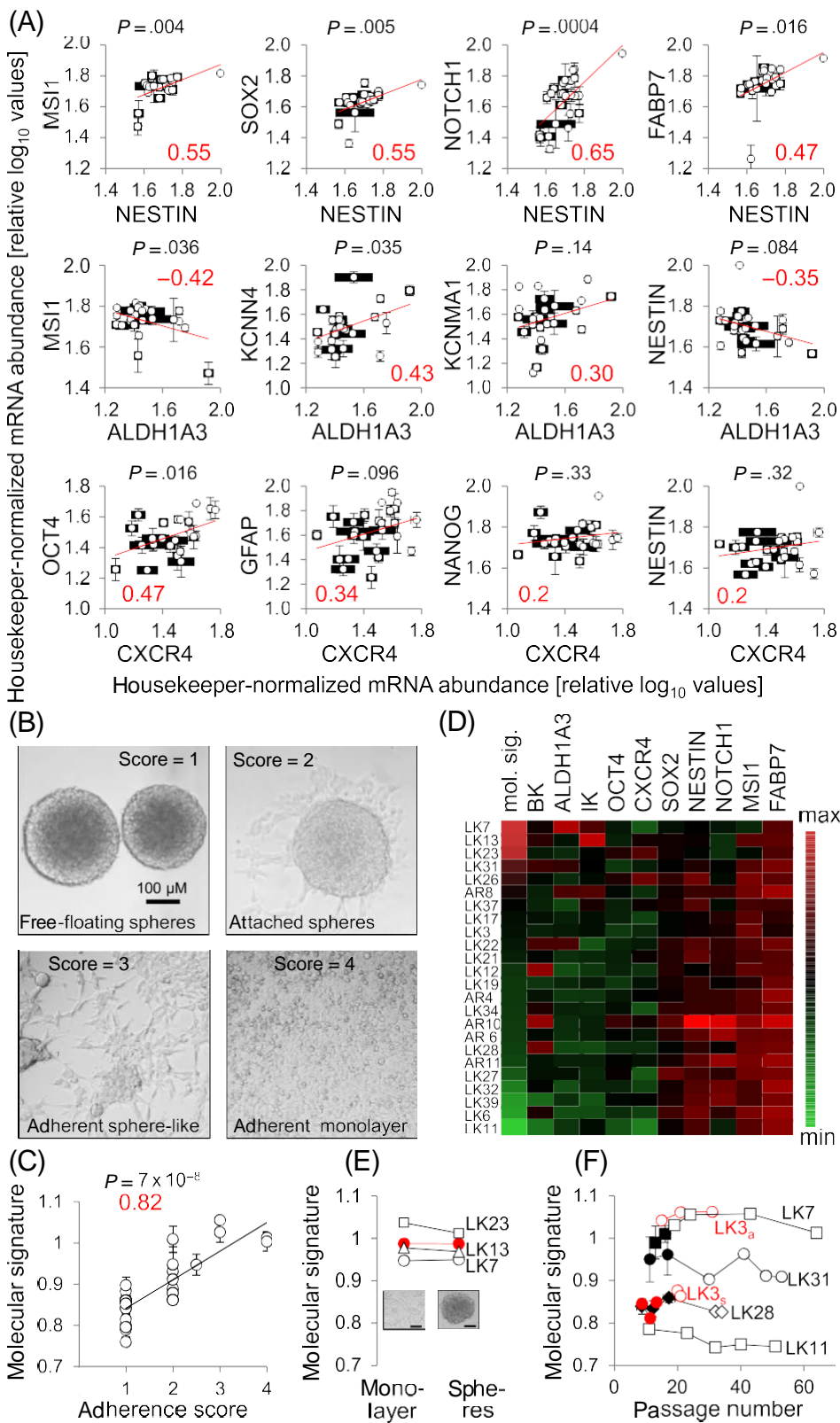


**FIGURE 1** Identifying a molecular mRNA signature in patient-derived pGSC cultures. (A) Associations of several mRNA abundances in pGSC cultures. Minimum/maximum-adjusted relative log<sub>10</sub> data of housekeeper-normalized mRNA abundances are shown for 24 pGSC cultures. Data are individual values for AR10 and AR11 and means ± SE, n = 3-15 for all other pGSCs. (B) Light micrographs of the different growth phenotypes and their adherence scoring. (C) Relationship between molecular mRNA signature (individual values for AR10 and AR11 and means ± SE, n = 3-15 for all other pGSCs) and adherence score. (D) Heatmap visualizing correlations of the molecular signature with each mRNA abundance used for signature calculation. (E) Dependence of the molecular mRNA signature on the growth phenotype. Shown are three pGSC cultures simultaneously grown as adherent monolayer (left) and as neurospheres (right) as depicted by the light micrographs (inserts; bars indicate 100 μm). Data are individual (open black symbols) or mean (±SE, n = 8) values (closed red symbols). For the latter the data of all three cultures determined for two to three passages each were pooled. (F) Culture passaging-dependent change in molecular mRNA signature. Mean (±SE, n = 3-6; closed symbols) and individual values (open symbols) of five pGSC cultures. The red symbols indicate a pGSC line (LK3) that grew adherent (LK3<sub>a</sub>) and as spheres (LK3<sub>s</sub>). The red numbers and P-values in (A) and (C) indicate the Pearson correlation coefficients and the significance levels for the difference of the correlation coefficient from 0, respectively.

positively with their (surface) protein abundances or functions indicating protein/functional expression of the tested marker mRNAs. To assess stem cell properties of our pGSC cultures, we transplanted LK7, LK13, LK19, LK28 and LK39 in the right striatum of immunocompromised mice. All cultures tested developed large brain infiltrating

orthotopic glioblastoma indicating their tumor-initiating capability. An example is given in part C of the Supporting Information (Figure S5). Next, the functional significance of the molecular mRNA signature for the in vitro radioresistance and matrix invasion of the pGSC cultures was defined.

### 3.2 | Functional significance of the molecular pGSC mRNA signature for in vitro radioresistance and matrix invasion

To define the intrinsic radiosensitivity of the pGSC cultures, the clonogenic survival of irradiated pGSC cells was determined by preplating limited dilution assay. In these assays, minimal cell number

required to maintain the culture could be measured for both, the spheroid and adherent monolayer cultures, allowing us to directly compare plating efficiencies and survival fraction between all growth phenotypes. Notably, the individual pGSC cultures differed markedly in their intrinsic radiosensitivity (Figure 2A) and the survival fractions of 4 Gy-irradiated pGSC cells ( $SF_{4Gy}$ ) correlated moderately positively with their molecular mRNA signature ( $P_{cc} = .62$ ; Figure 2B). Stratifying the  $SF_{4Gy}$  values by

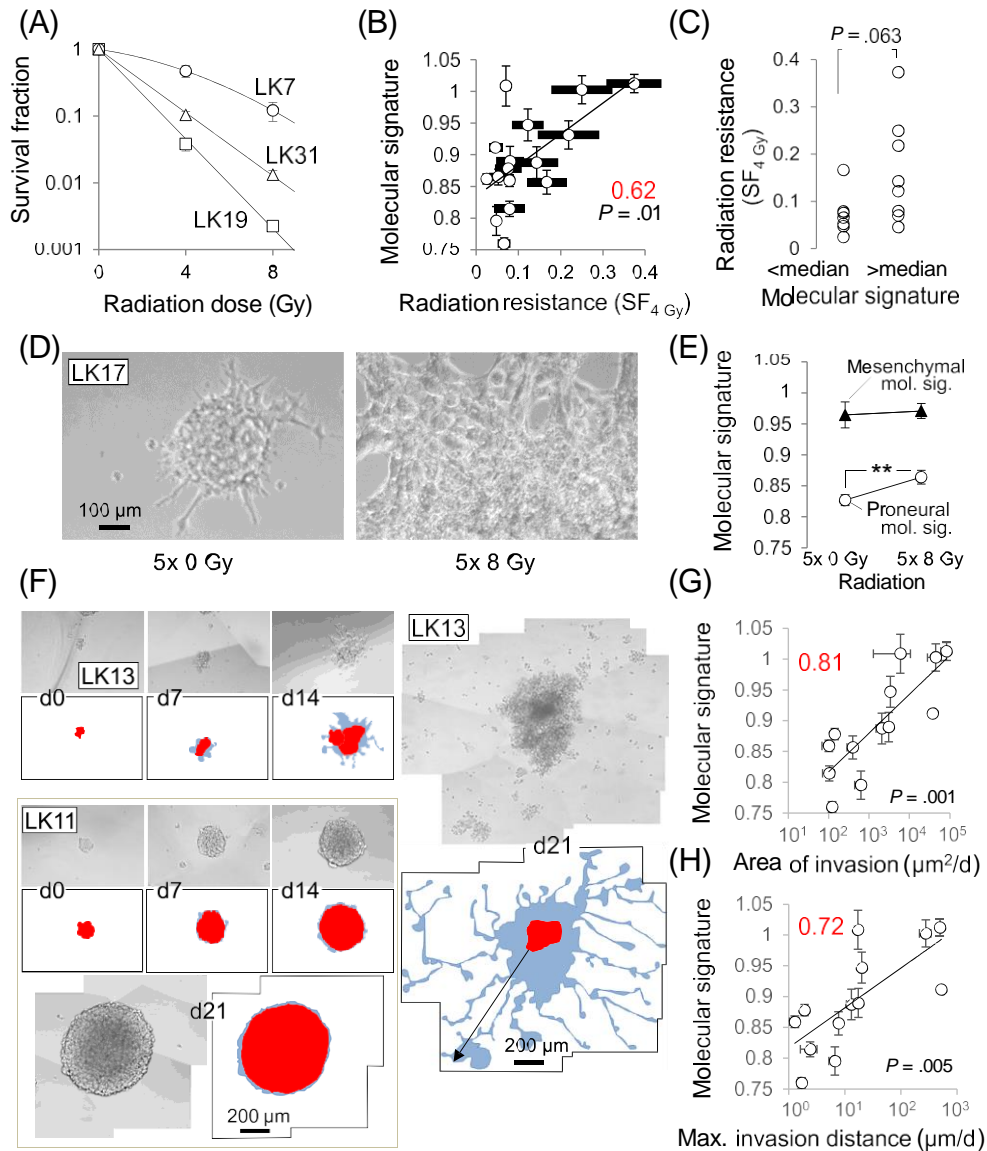


**FIGURE 2** Functional significance of the molecular pGSC mRNA signature for in vitro radioresistance and matrix invasion. (A) Dependence of the mean ( $\pm$ SE,  $n = 24$ -44) survival fraction of LK7 (circles), LK31 (triangles) and LK19 (squares) pGSCs on radiation dose as analyzed by preplating limited dilution assay. (B) Relationship between mean ( $\pm$ SE,  $n = 3$ -15) molecular mRNA signature and mean ( $\pm$ SE,  $n = 3$ -7) survival fraction (determined as in (A)) after irradiation with 4 Gy ( $SF_{4Gy}$ ) in a cohort of 16 pGSC cultures. (C)  $SF_{4Gy}$  values (means without error bars) of pGSC lines with higher and lower mesenchymal-to-proneural mRNA signature stratified by the median. (D) Light micrographs of LK17 pGSC treated with 5x 0 Gy (left) and 5x 8 Gy (right). Note, that fractionated radiation induced a shift in growth phenotype from attached spheres to adherent monolayer. (E) Mean ( $\pm$ SE,  $n = 12$ -14) molecular RNA signature of five mesenchymal (closed triangles) and five proneural (open circles) pGSC cultures treated with 5x 0 Gy (left) and 5x 8 Gy (right). \*\* indicates  $zP \leq .01$ , Welch-corrected two-tailed  $t$ -test with  $z = 2$  pairwise comparisons. (F) Light micrographs and drawing of LK13 (top) and LK11 (bottom) pGSC spheres taken on day 0, 7, 14 and 21 after embedding in fibrin gel. The drawings (below and right, respectively) outline the 2D projected sphere (red) and invasion area (blue) The arrow (drawing of LK13 on day 21) indicates the maximal invasion distance. (G,H) Relationship between mean ( $\pm$ SE,  $n = 3$ -15) molecular mRNA signature and mean ( $\pm$ SE,  $n = 3$ -102) 2D projected invasion area (G) and maximal invasion distance (H) in a cohort of 13 pGSC cultures. Red numbers and  $P$  values in (B), (G) and (H) indicate the Pearson correlation coefficients and the significance levels for the difference of the correlation coefficient from 0, respectively

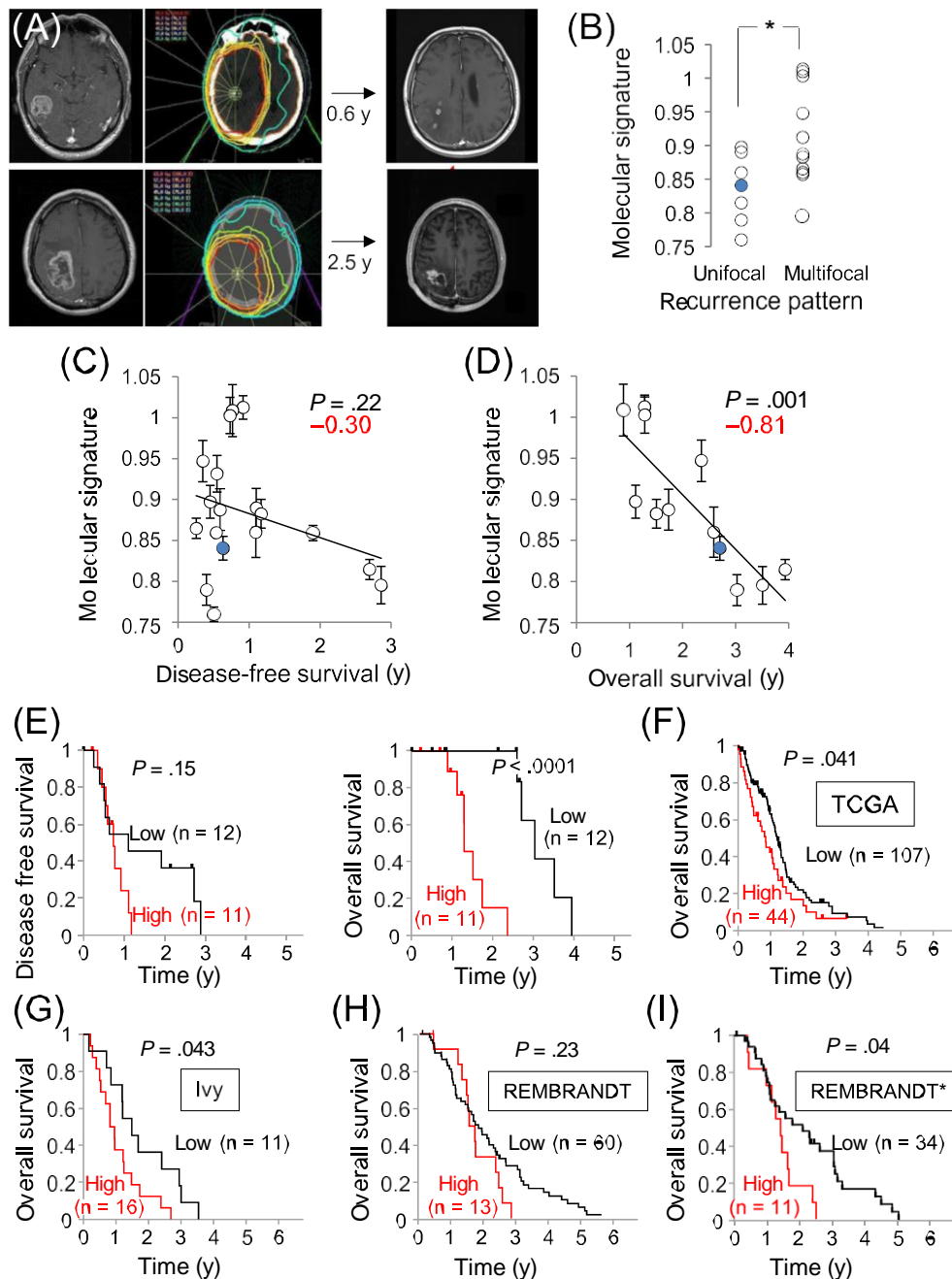


**FIGURE 3** Pattern of glioblastoma recurrence and patient overall survival associates with the molecular pGSC mRNA signature. (A) MRI at diagnosis (left) and glioblastoma recurrence (right), and planning CT of radiotherapy (middle) for two patients with mesenchymal (upper line) and proneural pGSC mRNA signature (lower line), respectively. (B) Molecular pGSC mRNA signatures of patients with unifocally (left) and multifocally recurring glioblastoma (\* indicates  $P \leq .05$ , Welch-corrected two-tailed  $t$ -test). (C,D) Relationships between disease-free (C) and overall survival (D) of the Tübingen glioblastoma cohort and the molecular pGSC mRNA signature (mean  $\pm$  SE,  $n = 3$ -15 or single value for AR10 in (C)); red numbers and  $P$  values give the Pearson correlation coefficients and the significance levels for the difference of the correlation coefficient from 0, respectively. The data points of the patient with the IDH-mutated grade-4 astrocytoma are labeled in blue. (E) Disease-free (left) and overall survival (right) of the Tübingen glioblastoma patients stratified by median in groups with high (red) and low (black) molecular pGSC mRNA signature. (F-I) Kaplan-Meier curves giving the overall survival of glioblastoma patients from the glioblastoma data base of The Cancer Genome Atlas (TCGA, F), Ivy Glioblastoma Atlas Project database (G) and Repository for Molecular Brain Neoplasia Data (REMBRANDT, H, I) with high (red) and low (black) molecular RNA signature (upwards deflections indicate censored patients). In REMBRANDT\* data (I) only patients scheduled for radiation and temozolomide treatment were included. For the calculation of the molecular RNA signature, RNASeqV2 mRNA abundances of the glioblastoma specimens were used and patients stratified by threshold optimization (indicated error probability ( $P$ ) values were calculated by log rank test)



the median molecular pGSC mRNA signature resulted in a (not significantly,  $P = .063$ ) lower intrinsic radioresistance of proneural as compared to mesenchymal pGSCs (Figure 2C). Together, this points to a functional significance of the molecular mesenchymal-to-proneural mRNA signature for the intrinsic radiosensitivity of the pGSC cultures.

To estimate the effect of radiotherapy on the molecular mesenchymal-to-proneural mRNA signature, we applied fractionated radiotherapy of 5x 8 Gy within 5 days that was assumed to be dose-equivalent to the standard normofractionated radiotherapy of 60 Gy in 30 fractions during 6 weeks. Applying 5x 8 Gy led to an increase in molecular mesenchymal-to-proneural mRNA signature in proneural ( $\leq$ median signature, Figure 2D,E, open circles) pGSCs. Mesenchymal pGSCs ( $>$ median molecular mRNA signature), in contrast, did not exhibit such a radiation-induced increase in signature (Figure 2E, closed triangles) suggesting mesenchymal progression of proneural and intermediate but not mesenchymal pGSC cultures during and after fractionated radiation.

To associate the molecular mRNA signature with matrix invasion, proneural and (low attachment surface-pregrown) mesenchymal spheres were embedded in a fibrin gel and invasion area and the maximal invasion distances of matrix-infiltrating cells were analyzed on days 0, 7, 14 and 21 after embedding (Figure 2F). As a result, the 2D-projected invasion area/time (in  $\mu\text{m}^2/\text{d}$ , Figure 2G) and the maximal invasion distance/time (in  $\mu\text{m}/\text{d}$ , Figure 2H) correlated positively with the molecular pGSC mRNA signature ( $P_{cc} = .81$  and  $.72$ , respectively), suggesting additional functional significance of the molecular pGSC mRNA signature for the invasiveness of the pGSC cells. Next, we associated the molecular mesenchymal-to-proneural pGSC mRNA signature with the clinical data from the Tübingen cohort of glioblastoma patients the pGSC cultures were derived of.

### 3.3 | Functional significance of the molecular pGSC mRNA signature for tumor recurrence pattern and patient survival

To identify prognostic or predictive values of the molecular pGSC mRNA signature for the disease outcome, glioblastoma occurrence and recurrence pattern (unifocal vs multifocal) as well as disease-free and overall survival of the Tübingen glioblastoma patients (clinical data in Table S1) were associated with the molecular pGSC mRNA signature. Since our pGSC cultures were grown from resection material and not from biopsies and since many multifocal glioblastomas were not surgically resected, patients with primarily multifocal tumors were probably underrepresented in our Tübingen cohort. In particular, only three multifocal glioblastomas were surgically resected and grown to pGSCs. These cultures exhibited mesenchymal (rank 7/24 and 9/24) and intermediate (rank 13/24) molecular mRNA signatures which did not result in a significant correlation between tumor occurrence pattern and molecular mRNA signature (data not shown). The molecular pGSC mRNA signatures of multifocally recurring glioblastomas ( $n = 11$ ), in contrast, were significantly higher than of unifocally recurring tumors ( $n = 7$ ; Figure 3A,B) which might hint at a mesenchymal stem cell-associated tumor spreading.

For 17 out of our 23 patients (one patient developed two glioblastomas, a MGMT promotor-unmethylated frontal tumor with a mesenchymal pGSC mRNA signature and a MGMT promotor-methylated temporo-occipital tumor with a proneural pGSC mRNA signature) clinical follow-up data  $\geq 10$  month were available. Altogether, 19 of the 23 patients received fractionated radiation therapy in different regimens (see Table S1). We associated the pGSC signature with disease-free and overall survival of the glioblastoma patients (Figure 3C-E). As a result, disease-free survival showed a weak tendency ( $P = .22$ ) to correlate negatively with the molecular pGSC mRNA signature ( $P_{cc} = -.30$ ; Figure 3C). In contrast to disease-free survival, overall survival correlated strongly negatively with the molecular pGSC mRNA signature ( $P_{cc} = -.81$ ; Figure 3D). This is also shown by the Kaplan-Meier survival curves in Figure 3E, left, where disease-free survival did not differ significantly between patients with proneural ( $\leq$ median molecular mRNA signature) pGSCs as compared to those with mesenchymal pGSCs ( $>$ median). Overall survival of patients with proneural ( $\leq$ median molecular mRNA signature) pGSCs, in contrast, significantly exceeded ( $P \leq .001$ , log rank test) that of patients with mesenchymal ( $>$ median) pGSCs in univariate testing (Figure 3E, right). Importantly, the molecular mRNA signature did not correlate with established prognostic/predictive factors such as patient age or MGMT promotor methylation status (data not shown).

Finally, we queried the TCGA, Ivy GAP and REMBRANDT glioblastoma databases to confirm associations between patients' overall survival and the molecular mesenchymal-to-proneural signature based on the 10 mRNA abundances of the glioblastoma resection specimens. Here, in the TCGA and Ivy GAP database, a superior survival of patients with "proneural" glioblastomas over that of patients with "mesenchymal" tumors was only evident in univariate testing if patient stratification has been performed by best threshold finding (Figure 3F,G). For the REMBRANDT database, in contrast, no difference between patients with "proneural" and "mesenchymal" glioblastomas was apparent (Figure 3H). When, however, constraining the analysis to the patient subcohort of the REMBRANDT database that were scheduled for radiation plus temozolomide chemotherapy (REMBRANDT\*) in order to decrease the heterogeneity of the patient cohort, survival curves pointed again to a better prognosis for patients with "proneural" as compared to those with "mesenchymal" tumors (Figure 3I). Combined, these analyses suggest that the molecular 10 mRNA mesenchymal-to-proneural signature in specimens of the whole tumor tissue describes the properties of the primary cultured glioblastoma stem cell subpopulations only to some and variable extent.

## 4 | DISCUSSION

### 4.1 | Mesenchymal and proneural transcriptional subtypes of GSCs

The present study characterized in primary culture of resection specimens from 23 glioblastoma patients under neural stem cell-selecting/inducing conditions the mRNA expression of stem cell-

invasion- and resistance markers. An mRNA signature calculated from the abundances of these 10 marker mRNAs disclosed pGSC cultures with mesenchymal or proneural molecular signature confirming earlier studies.<sup>4,50</sup> In the latter study,<sup>50</sup> comparison of mesenchymal and proneural pGSC-specific mRNA data with glioblastoma transcriptome data sets indicated a pronounced correlation of the expression profiles with the corresponding molecular proneural and mesenchymal glioblastoma subtypes. These data suggest that the mesenchymal-to-proneural signature of the GSC subpopulation(s) is a determinant of the molecular glioblastoma subclassification.

In addition, the molecular mesenchymal-to-proneural mRNA signature correlated in the present study with the degree of in vitro intrinsic radioresistance and invasiveness of the pGSC cultures (see Figure 2) suggesting both: (a) the pathophysiological significance of the mesenchymal-to-proneural pGSC mRNA signature and (b) that the more mesenchymal the more malignant the functional pGSC phenotype is in terms of tumor dissemination and therapy resistance.

#### 4.2 | Primary cultures conserve individual transcriptional GSC subtypes

The present study also demonstrated that the chosen culture conditions conserved the mesenchymal-to-proneural pGSC mRNA signature over several cell culture passages (see Figure 1E). A previous study reported a loss of mesenchymal characteristic and a higher proneural signature in mesenchymal subtype-derived pGSCs as compared to the parental glioblastoma specimens pointing to a GSC phenotypic assimilation by loss of micro(environmental) input in primary GSC culture.<sup>32</sup> Nevertheless, the individual pGSC cultures of the present study differed tremendously in their functional and molecular signatures suggesting maintenance of their original subtype diversity at least to some extent. Moreover, and most importantly, the molecular mesenchymal-to-proneural mRNA signature of the pGSC cultures correlated in the present study with the clinical pattern of tumor recurrence (see Figure 3B) and the overall survival (see Figure 3D) of the glioblastoma patients from whom the pGSC cultures had been derived. This clearly indicates that the malignancy-determining functional pGSC phenotype was not only conserved during continued culture but also during GSC enrichment by taking glioblastoma specimens in primary culture under stem cell-inducing/ selecting conditions.

#### 4.3 | Mesenchymal glioblastoma associates with a worse patient prognosis than proneural tumors

In our Tübingen cohort, patients with glioblastoma that gave rise to mesenchymal (ie, with numerically high mRNA signature) pGSCs exhibited in univariate testing a significantly ( $P = .001$ ) shorter overall survival than patients with proneural (ie, low mRNA signature) pGSC cultures (see Figure 3E, right). In accordance to this observations, previous retrospective associations of epigenome and transcriptome data

from glioblastoma resection specimens/biopsies with clinical data similarly pointed to a shorter overall survival of patients with upregulated vs downregulated mesenchymal methylation- or expression patterns of the tumor.<sup>1,3,4,7,32,51</sup>

Likewise, stratifying (best threshold) in the present study the TCGA (see Figure 3F), Ivy GAP cohort (see Figure 3G) and prefiltered (radiation and temozolomide) REMBRANDT\* (see Figure 3I) glioblastoma patient cohort by the molecular mesenchymal-to-proneural mRNA signature used to characterize our pGSC cultures might hint in univariate analysis at a shorter ( $P = .04$ ) overall survival of patients with mesenchymal as compared to those with proneural glioblastomas. Notably, the disease-free survival of our Tübingen glioblastoma cohort correlated only weakly with the molecular pGSC mRNA signature (see Figure 3C) suggesting similar recurrence times of mesenchymal and proneural glioblastomas.

#### 4.4 | A mesenchymal transcriptional GSC subtype facilitates glioblastoma spreading

In analogy to carcinoma cells where tissue infiltration and metastasis has been postulated to require epithelial-mesenchymal transition, glioblastoma cells may undergo glial-mesenchymal transition<sup>52</sup> and adopt a migratory, infiltrative phenotype.<sup>53,54</sup> Notably, ectopic stimulation of cultured glioblastoma neurospheres with retinoic acid (which is formed by the mesenchymal enzyme ALDH1A3, see Section 1) induces beyond downregulation of proneural stem cell markers morphological changes including evasion from neurospheres, formation of cell processes and dish bottom-adherent monolayer-like growth.<sup>22</sup> In vivo, evading glioblastoma cells infiltrate the brain by attaching to and migrating along vessels or axon bundles which function as tracks.<sup>55</sup> In the present study, pGSC cultures with high mesenchymal molecular mRNA signature exhibited besides elevated invasiveness (see Figure 2F-H) an adherent growth phenotype (see Figure 1B,C). Combined, these observations suggest that the nonspheroid, adherent growth phenotype of mesenchymal pGSC reflects the promigratory/ invasive property of these cells.

Preclinical in vitro and orthotopic mouse models have demonstrated that glioblastoma cell migration and brain infiltration requires an efficient cell volume regulation machinery that includes  $IK_{Ca}$  and  $BK_{Ca}$   $Ca^{2+}$ -activated  $K^{+}$  channel types as key regulatory elements.<sup>36,37,43,55</sup> The present study observed in the pGSC cultures a moderately ( $IK_{Ca}$ ) or weakly ( $BK_{Ca}$ ) positive correlation between the mRNA abundances of these channels and the mesenchymal stem cell marker ALDH1A3 (see Figure 1A) while correlations were not apparent between the  $Ca^{2+}$ -activated  $K^{+}$  channels and the tested proneural stem cell markers (data not shown). This hints to an upregulation of both proinvasive  $K^{+}$  channel types in mesenchymal GSCs. Accordingly, glioblastoma leading to mesenchymal pGSCs recurred in the present study more often multifocally as compared to tumors that gave rise to proneural pGSCs (see Figure 3A,B). Since glioblastoma multilocal brain spreading is thought to impede tumor control by surgery and radiation therapy, an enhanced invasiveness of

mesenchymal GSCs probably is one reason for the above discussed worse prognosis of the mesenchymal as compared to the other glioblastoma subtype(s). In line with that conclusion, an invasive mRNA expression signature of the tumor has been directly demonstrated to associate with poor prognosis of glioblastoma patients.<sup>56</sup> Another probable reason for the higher malignancy of mesenchymal compared to other glioblastoma subtypes is an elevated therapy resistance.

#### 4.5 | The mesenchymal transcriptional glioblastoma subtype confers radioresistance

In the present study, the intrinsic radioresistance of the pGSC cultures differed by more than 10-fold and correlated positively with the molecular mesenchymal-to-proneural mRNA signature (see Figure 2B, C). The latter observation is in line with previous reports demonstrating that mesenchymal transition of glioblastoma cells promotes radioresistance.<sup>4,32,57</sup> Previous reports of our group have demonstrated beyond co-expression of ALDH1A3 and IK<sub>Ca</sub> in pGSCs (see Figure 1A and Reference 33), an upregulation of IK<sub>Ca</sub>-dependent radioresistance by knockdown of the proneural stem cell marker MS11 in a human glioblastoma cell line.<sup>35</sup> Radiogenic IK<sub>Ca</sub> activity in turn regulates Ca<sup>2+</sup> signaling, cell cycle arrest and DNA repair in irradiated glioblastoma cells and contributes to clonogenic cell survival<sup>34</sup> suggesting a possible cellular mechanism of mesenchymal transcriptional subtype-associated radioresistance.

Like glioblastoma, ALDH1A3-associated mesenchymal transition has been shown to promote radioresistance in head and neck squamous carcinoma cells (HNSCC)<sup>16,58</sup> suggesting homologous resistance pathways in tumor entities from epithelial and glial origin. The studies on HNSCC also demonstrate a radiotherapy-induced mesenchymal transition of the cancer stem cells similarly to the mesenchymal shift in molecular mRNA signature observed in the present study in proneural pGSC cultures treated with 5x 8 Gy ionizing radiation (see Figure 2D,E).

#### 4.6 | Transcriptional glioblastoma subtypes and temozolomide sensitivity

IK<sub>Ca</sub><sup>59</sup> and CXCR4<sup>60</sup> have been reported to confer temozolomide resistance to glioblastoma cells. Therefore, the contribution of the IK<sub>Ca</sub> and CXCR4 abundances to the molecular mesenchymal-to-proneural mRNA signature might suggest a correlation between temozolomide sensitivity and molecular pGSC signature. The major determinant of temozolomide sensitivity in glioblastoma, however, is the MGMT promoter methylation state and the latter did not differ between mesenchymal and proneural pGSC stratified by the median of the molecular mRNA signature (data not shown). Furthermore, initial experiments on clonogenic survival in the absence and presence of temozolomide (30 μM) of two MGMT promotor-unmethylated and four-methylated pGSC did not show any correlation between temozolomide sensitivity and molecular mesenchymal-to-proneural mRNA signature (data not shown). Together, this suggests that the

molecular mRNA signature of the pGSCs is not predictive for the response to temozolomide.

#### 4.7 | Fractionated radiochemotherapy may induce mesenchymal progression of glioblastoma

In accordance with our observation, several but not all<sup>7</sup> studies have shown by pairwise analysis of initial and recurrent glioblastoma resection/biopsy specimens as well as in vitro irradiation-induced glial-mesenchymal transition.<sup>1,32,50,52,61</sup> Notably, radiation reportedly induces upregulation of ALDH1A3 and inhibition of ALDH1A3 attenuates radiation induced mesenchymal progression<sup>50</sup> suggesting a pivotal function of ALDH1A3 in the maintenance of the mesenchymal functional phenotype. In line with a radiogenic mesenchymal transition are reports on radiogenic hypermigration/invasion of glioblastoma cells. In particular, auto-/paracrine CXCL12/CXCR4 signaling,<sup>43</sup> IK<sub>Ca</sub>-<sup>34</sup> and BK<sub>Ca</sub> channel-regulated<sup>43</sup> electro-signaling, Ca<sup>2+</sup> signaling and cell-volume changes have been demonstrated to program and motorize radiogenic hypermigration/invasion.

## 5 | CONCLUSION

A 10 mRNA-based molecular mesenchymal-to-proneural signature of glioblastoma stem cell-like cells in primary culture (pGSCs) correlated with the intrinsic radioresistance and invasiveness indicating its high functional significance. The differences in molecular mRNA signature, radioresistance and invasiveness between individual pGSC cultures suggest the maintenance of phenotypic GSC diversity in primary culture. Importantly, the individual pGSC signatures correlated with glioblastoma recurrence pattern and overall survival of the corresponding patients indicating a high prognostic value of the molecular pGSC mRNA signature. Since pGSC cultures can be grown with high yield during standard therapy until the end of adjuvant radiochemotherapy, pGSC cultures may be used as an in vitro platform to test experimental therapy strategies in a patient individualized manner. This may be applied for predicting therapy response to optional treatments, or re-irradiation and second line chemotherapies upon tumor relapse.

#### ACKNOWLEDGMENT

The authors thank Heidrun Faltin (from the Department of Radiation Oncology, University Hospital, Tübingen, Germany) for excellent technical assistance. Open Access funding enabled and organized by Projekt DEAL.

#### CONFLICT OF INTEREST

Research and educational grants by Elekta, Philips, Siemens, Sennewald, Kaikuu and TheraPanacea (Franziska Eckert, Frank Paulsen, Daniel Zips). All other authors declare no competing interests.

#### AUTHOR CONTRIBUTION

Conception and design: Katrin Ganser, Lukas Klumpp, Franziska Eckert, Daniel Zips, Peter Ruth, Stephan M. Huber. Development of

methodology: Lukas Klumpp, Katrin Ganser. Acquisition of data: Katrin Ganser, Lukas Klumpp, Andreas Riedel, Nicolai Stransky, Franziska Eckert, Frank Paulsen, Stefanie Beck-Wödl. Analysis and interpretation of data: Katrin Ganser, Lukas Klumpp, Franziska Eckert, Frank Paulsen, Marcel Krueger, Peter Ruth, Stephan M. Huber. Writing, review and/or revision of the article: all authors. Administrative, technical or material support: Susan Noell, Study supervision: Lukas Klumpp and Stephan M. Huber. Other (pathology review and analysis): Jens Schittenhelm.

#### DATA AVAILABILITY STATEMENT

The datasets used or analyzed during the current study are available from the corresponding author on reasonable request. Analyzed data sets are available under following links: TCGA: <https://portal.gdc.cancer.gov/> (Date of data download: 10.02.2020). IVY: [https://glioblastoma.alleninstitute.org/api/v2/well\\_known\\_file\\_download/305873915](https://glioblastoma.alleninstitute.org/api/v2/well_known_file_download/305873915) (date of data download: July 27, 2021). Rembrandt: <https://www.ncbi.nlm.nih.gov/geo/query/acc.cgi?acc=GSE108474> (date of data download: July 27, 2021).

#### ETHICS STATEMENT

The use of patient data and glioblastoma resection material have been approved by the ethical review commission of the Faculty of Medicine, University of Tübingen, at the University Hospital Tübingen (project # 579/2015B02 and B02-2, 184/2015B01). A written informed consent was obtained from all patients.

#### ORCID

Nicolai Stransky  <https://orcid.org/0000-0002-0872-5220>

Stephan M. Huber  <https://orcid.org/0000-0002-9430-8334>

#### REFERENCES

- Phillips HS, Kharbanda S, Chen R, et al. Molecular subclasses of high-grade glioma predict prognosis, delineate a pattern of disease progression, and resemble stages in neurogenesis. *Cancer Cell*. 2006;9:157-173.
- Verhaak RG, Hoadley KA, Purdom E, et al. Integrated genomic analysis identifies clinically relevant subtypes of glioblastoma characterized by abnormalities in PDGFRA, IDH1, EGFR, and NF1. *Cancer Cell*. 2010;17:98-110.
- Colman H, Zhang L, Sulman EP, et al. A multigene predictor of outcome in glioblastoma. *Neuro Oncol*. 2010;12:49-57.
- Bhat KPL, Balasubramanian V, Vaillant B, et al. Mesenchymal differentiation mediated by NF- $\kappa$ B promotes radiation resistance in glioblastoma. *Cancer Cell*. 2013;24:331-346.
- Brennan CW, Verhaak RG, McKenna A, et al. The somatic genomic landscape of glioblastoma. *Cell*. 2013;155:462-477.
- Ceccarelli M, Barthel FP, Malta TM, et al. Molecular profiling reveals biologically discrete subsets and pathways of progression in diffuse glioma. *Cell*. 2016;164:550-563.
- Wang Q, Hu B, Hu X, et al. Tumor evolution of glioma-intrinsic gene expression subtypes associates with immunological changes in the microenvironment. *Cancer Cell*. 2017;32:42-56.e6.
- Capper D, Jones DTW, Sill M, et al. DNA methylation-based classification of central nervous system tumours. *Nature*. 2018;555:469-474.
- Ma H, Zhao C, Zhao Z, et al. Specific glioblastoma multiforme prognostic-subtype distinctions based on DNA methylation patterns. *Cancer Gene Ther*. 2020;27:702-714.
- Malta TM, de Souza CF, Sabedot TS, et al. Glioma CpG Island methylator phenotype (G-CIMP): biological and clinical implications. *Neuro-Oncol*. 2018;20:608-620.
- Rushing EJ. WHO classification of tumors of the nervous system: preview of the upcoming 5th edition. *Memo*. 2021;14:188-191.
- Stupp R, Mason WP, van den Bent MJ, et al. Radiotherapy plus concomitant and adjuvant temozolomide for glioblastoma. *N Engl J Med*. 2005;352:987-996.
- Herrtinger U, Tzaridis T, Mack F, et al. Lomustine-temozolomide combination therapy versus standard temozolomide therapy in patients with newly diagnosed glioblastoma with methylated MGMT promoter (CeTeG/NOA-09): a randomised, open-label, phase 3 trial. *Lancet*. 2019;393:678-688.
- Singh SK, Clarke ID, Terasaki M, et al. Identification of a cancer stem cell in human brain tumors. *Cancer Res*. 2003;63:5821-5828.
- Hambardzumyan D, Gutmann DH, Kettenmann H. The role of microglia and macrophages in glioma maintenance and progression. *Nat Neurosci*. 2016;19:20-27.
- Cojoc M, Peitzsch C, Kurth I, et al. Aldehyde dehydrogenase is regulated by  $\beta$ -catenin/TCF and promotes radioresistance in prostate cancer progenitor cells. *Cancer Res*. 2015;75:1482-1494.
- Battle E, Clevers H. Cancer stem cells revisited. *Nat Med*. 2017;23:1124-1134.
- Mao P, Joshi K, Li J, et al. Mesenchymal glioma stem cells are maintained by activated glycolytic metabolism involving aldehyde dehydrogenase 1A3. *Proc Natl Acad Sci U S A*. 2013;110:8644-8649.
- Cheng P, Wang J, Waghmare I, et al. FOXD1-ALDH1A3 signaling is a determinant for the self-renewal and tumorigenicity of mesenchymal glioma stem cells. *Cancer Res*. 2016;76:7219-7230.
- Li G, Li Y, Liu X, et al. ALDH1A3 induces mesenchymal differentiation and serves as a predictor for survival in glioblastoma. *Cell Death Dis*. 2018;9:1190.
- Chen Z, Wang HW, Wang S, et al. USP9X deubiquitinates ALDH1A3 and maintains mesenchymal identity in glioblastoma stem cells. *J Clin Invest*. 2019;129:2043-2055.
- Ying M, Wang S, Sang Y, et al. Regulation of glioblastoma stem cells by retinoic acid: role for Notch pathway inhibition. *Oncogene*. 2011;30:3454-3467.
- Fan X, Khaki L, Zhu TS, et al. NOTCH pathway blockade depletes CD133-positive glioblastoma cells and inhibits growth of tumor neurospheres and xenografts. *Stem Cells*. 2010;28:5-16.
- Emler DR, Gupta P, Holgado-Madruga M, et al. Targeting a glioblastoma cancer stem-cell population defined by EGF receptor variant III. *Cancer Res*. 2014;74:1238-1249.
- Yin J, Park G, Kim TH, et al. Pigment epithelium-derived factor (PEDF) expression induced by EGFRvIII promotes self-renewal and tumor progression of glioma stem cells. *PLoS Biol*. 2015;13:e1002152.
- Kim HJ, Kim JY, Jung CW, et al. ANO1 regulates the maintenance of stemness in glioblastoma stem cells by stabilizing EGFRvIII. *Oncogene*. 2021;40:1490-1502.
- Kahlert UD, Maciaczyk D, Doostkam S, et al. Activation of canonical WNT/ $\beta$ -catenin signaling enhances in vitro motility of glioblastoma cells by activation of ZEB1 and other activators of epithelial-to-mesenchymal transition. *Cancer Lett*. 2012;325:42-53.
- Binda E, Visioli A, Giani F, et al. Wnt5a drives an invasive phenotype in human glioblastoma stem-like cells. *Cancer Res*. 2017;77:996-1007.
- Riedel A, Klumpp L, Menegakis A, et al.  $\gamma$ H2AX foci assay in glioblastoma: surgical specimen versus corresponding stem cell culture. *Radiother Oncol*. 2021;159:119-125.
- Bhat K, Saki M, Vlashi E, et al. The dopamine receptor antagonist trifluoperazine prevents phenotype conversion and improves survival in mouse models of glioblastoma. *Proc Natl Acad Sci U S A*. 2020;117:11085-11096.



31. Yan GN, Yang L, Lv YF, et al. Endothelial cells promote stem-like phenotype of glioma cells through activating the hedgehog pathway. *J Pathol.* 2014;234:11-22.
32. Barnes JM, Kaushik S, Bainer RO, et al. A tension-mediated glycocalyx-integrin feedback loop promotes mesenchymal-like glioblastoma. *Nat Cell Biol.* 2018;20:1203-1214.
33. Klumpp L, Sezgin EC, Skardelly M, Eckert F, Huber SM. KCa3.1 channels and Glioblastoma: in vitro studies. *Curr Neuropharmacol.* 2018; 16:627-635.
34. Stegen B, Butz L, Klumpp L, et al. Ca<sup>2+</sup>-activated IK K<sup>+</sup> channel blockade radiosensitizes glioblastoma cells. *Mol Cancer Res.* 2015;13:1283-1295.
35. Stegen B, Klumpp L, Misovic M, et al. K<sup>+</sup> channel signaling in irradiated tumor cells. *Eur Biophys J.* 2016;45:585-598.
36. Turner KL, Honasoge A, Robert SM, McFerrin MM, Sontheimer H. A proinvasive role for the Ca<sup>2+</sup>-activated K<sup>+</sup> channel KCa3.1 in malignant glioma. *Glia.* 2014;62:971-981.
37. Ruggieri P, Mangino G, Fioretti B, et al. The inhibition of KCa3.1 channels activity reduces cell motility in glioblastoma derived cancer stem cells. *PLoS One.* 2012;7:e47825.
38. Panaccione A, Guo Y, Yarbrough WG, Ivanov SV. Expression profiling of clinical specimens supports the existence of neural progenitor-like stem cells in basal breast cancers. *Clin Breast Cancer.* 2017;17: 298-306.e7.
39. Bai X, Ma J, Pan Z, et al. Electrophysiological properties of human adipose tissue-derived stem cells. *Am J Physiol Cell Physiol.* 2007;293: C1539-C1550.
40. Levesque JP, Winkler IG. Mobilization of hematopoietic stem cells: state of the art. *Curr Opin Organ Transplant.* 2008;13:53-58.
41. Fareh M, Turchi L, Virolle V, et al. The miR 302-367 cluster drastically affects self-renewal and infiltration properties of glioma-initiating cells through CXCR4 repression and consequent disruption of the SHH-GLI-NANOG network. *Cell Death Differ.* 2012;19: 232-244.
42. Rosa P, Sforna L, Carlomagno S, et al. Overexpression of large-conductance calcium-activated potassium channels in human glioblastoma stem-like cells and their role in cell migration. *J Cell Physiol.* 2017;232:2478-2488.
43. Edalat L, Stegen B, Klumpp L, et al. BK K<sup>+</sup> channel blockade inhibits radiation-induced migration/brain infiltration of glioblastoma cells. *Oncotarget.* 2016;7:14259-14278.
44. Rosa P, Catacuzzeno L, Sforna L, et al. BK channels blockage inhibits hypoxia-induced migration and chemoresistance to cisplatin in human glioblastoma cells. *J Cell Physiol.* 2018;233:6866-6877.
45. Ji F, Wang Y, Yuan J, Wu Q, Wang J, Liu D. The potential role of stromal cell-derived factor-1 $\alpha$ /CXCR4/CXCR7 axis in adipose-derived mesenchymal stem cells. *J Cell Physiol.* 2020;235:3548-3557.
46. Eckert M, Klumpp L, Huber SM. Cellular effects of the antiepileptic drug valproic acid in glioblastoma. *Cell Physiol Biochem.* 2017;44:1591-1605.
47. Klumpp D, Frank SC, Klumpp L, et al. TRPM8 is required for survival and radioresistance of glioblastoma cells. *Oncotarget.* 2017;8: 95896-95913.
48. Klumpp D, Misovic M, Szteyn K, Shumilina E, Rudner J, Huber SM. Targeting TRPM2 channels impairs radiation-induced cell cycle arrest and fosters cell death of T cell leukemia cells in a Bcl-2-dependent manner. *Oxid Med Cell Longev.* 2016;2016:8026702.
49. Steinle M, Palme D, Misovic M, et al. Ionizing radiation induces migration of glioblastoma cells by activating BK K<sup>+</sup> channels. *Radiother Oncol.* 2011;101:122-126.
50. Chandran UR, Luthra S, Santana-Santos L, et al. Gene expression profiling distinguishes proneural glioma stem cells from mesenchymal glioma stem cells. *Genom Data.* 2015;5:333-336.
51. Dejaeger J, Solie L, Hunin Z, et al. DNA methylation based glioblastoma subclassification is related to tumoral T-cell infiltration and patient survival. *Neuro-Oncol.* 2021;23:240-250.
52. Mahabir R, Tanino M, Elmansuri A, et al. Sustained elevation of snail promotes glial-mesenchymal transition after irradiation in malignant glioma. *Neuro-Oncol.* 2014;16:671-685.
53. Yachi K, Tsuda M, Kohsaka S, et al. miR-23a promotes invasion of glioblastoma via HOXD10-regulated glial-mesenchymal transition. *Signal Transduct Target Ther.* 2018;3:33.
54. Sha Z, Zhou J, Wu Y, et al. BYSL promotes glioblastoma cell migration, invasion, and mesenchymal transition through the GSK-3 $\beta$ / $\beta$ -catenin signaling pathway. *Front Oncol.* 2020;10:565225.
55. Sontheimer H. An unexpected role for ion channels in brain tumor metastasis. *Exp Biol Med (Maywood).* 2008;233:779-791.
56. Park J, Shim JK, Yoon SJ, Kim SH, Chang JH, Kang SG. Transcriptome profiling-based identification of prognostic subtypes and multi-omics signatures of glioblastoma. *Sci Rep.* 2019;9:10555.
57. Sullivan KE, Rojas K, Cerione RA, Nakano I, Wilson KF. The stem cell/cancer stem cell marker ALDH1A3 regulates the expression of the survival factor tissue transglutaminase, in mesenchymal glioma stem cells. *Oncotarget.* 2017;8:22325-22343.
58. Peitzsch C, Cojoc M, Hein L, et al. An epigenetic reprogramming strategy to resensitize radioresistant prostate cancer cells. *Cancer Res.* 2016;76:2637-2651.
59. D'Alessandro G, Grimaldi A, Chece G, et al. KCa3.1 channel inhibition sensitizes malignant gliomas to temozolomide treatment. *Oncotarget.* 2016;7:30781-30796.
60. Wang S, Chen C, Li J, Xu X, Chen W, Li F. The CXCL12/CXCR4 axis confers temozolomide resistance to human glioblastoma cells via up-regulation of FOXM1. *J Neurol Sci.* 2020;414:116837.
61. Wood MD, Reis GF, Reuss DE, Phillips JJ. Protein analysis of glioblastoma primary and posttreatment pairs suggests a mesenchymal shift at recurrence. *J Neuropathol Exp Neurol.* 2016;75:925-935.

#### SUPPORTING INFORMATION

Additional supporting information may be found in the online version of the article at the publisher's website.

How to cite this article: Ganser K, Eckert F, Riedel A, et al. Patient-individual phenotypes of glioblastoma stem cells are conserved in culture and associate with radioresistance, brain infiltration and patient prognosis. *Int. J. Cancer.* 2022;150(10): 1722-1733. doi:10.1002/ijc.33950



## Supplementary Material

Patient-individual phenotypes of glioblastoma stem cells are conserved in culture and associate with radioresistance, brain infiltration and patient prognosis

Katrin Ganser, Franziska Eckert, Andreas Riedel, Nicolai Stransky, Frank Paulsen, Susan Noell, Marcel Krueger, Jens Schittenhelm, Stefanie Beck-Wödl, Daniel Zips, Peter Ruth, Stephan M. Huber, and Lukas Klumpp

### Table of content

#### A. Supplementary Tables

- **Suppl. Tab. S1.** Clinical data of Tübingen glioblastoma cohort

#### B. Supplementary material and methods

- pGSC culture
- RNA Isolation and real-time reverse-transcriptase polymerase chain reaction (RT-PCR)
- Clonogenic survival of irradiated cells
- Hypo-fractionated radiation protocol that is dose-equivalent to the normo-fractionated radiotherapy
- Fibrin gel invasion
- Querying The Cancer Genome Atlas (TCGA), the Ivy Glioblastoma Atlas Project (Ivy GAP), and the Repository of Molecular Brain Neoplasia Data (REMBRANDT)
- Statistics

#### C. Protein and functional expression of markers used to calculate the molecular pGSC mRNA signature.

- **Suppl. Fig. S1.** Protein expression of ALDH1A3 and nestin in pGSCs
- **Suppl. Fig. S2.** CXCR4 surface expression of pGSCs
- **Suppl. Fig. S3.** ALDH activity of pGSCs
- **Suppl. Fig. S4.** Functional expression of  $IK_{Ca}$   $K^+$  channels in the plasma membrane of pGSCs

#### D. Tumor-initiating capability of the pGSC cultures

- **Suppl. Fig. S5.** In paraffin embedded brain sections. Hematoxylin and eosin (HE) staining and immunohistochemical detection of human nucleolin

## A. Supplementary Tab. S1. Clinical data of the Tübingen glioblastoma cohort

pGSC	Mol sig	Age at diagnosis (years)	Sex	Complete resection	MGMT promoter status	IDH1	Radiotherapy	Concomitant systemic therapy	Sequencial Temozolomide courses	Recurrence	Multi-focal recurrence	Last follow up status
AR4	0.8610	63	M	Yes	meth	WT	normof	Tem	6	No		NED
AR6	0.8591	56	M	Yes	meth	WT	normof	Tem +/- Nivo*	5	Yes	No	AWD
AR8	0.9114	72	M	Yes	unmeth	WT	hypof	Tem	5	No	Yes	NED
AR10	0.8594	46	M	No	unmeth	WT	unknown sch	Tem		Yes		AWD
AR11	0.8525	75	M	Yes	meth	WT	normof	Tem		unknown		alive
LK3	0.8874	56	M	No	meth	WT	normof	Tem	3	Yes	Yes	DOD
LK6	0.7895	48	F	Yes	meth	WT	normof	Tem	2	Yes	No	DOD
LK7	1.0125	66	M	Yes	unmeth	WT	normof	No		Yes	Yes	DOD
LK11	0.7598	71	M	Yes	unmeth	WT	unknown sch	No		Yes	No	alive
LK12	0.8649	69	F	No	meth	WT	No		1	Yes	Yes	alive, BSC
LK13	1.0087	71	M	Yes	meth	WT	No		6	Yes	Yes	DOD
LK17	0.8896	54	M	Yes	unmeth	WT	normof	Tem	6	Yes	No	alive, BSC
LK19	0.8616	63	F	Yes	meth	WT	No			unknown		unknown
LK21	0.8781	74	F	No	unmeth	WT	No			No		NED
LK22	0.8825	51	M	Yes	unmeth	WT	normof	Tem	6	Yes	Yes	DOD
LK23	1.0026	66	M	Yes	meth	WT	hypof	No	6	Yes	Yes	DOD
<u>LK26</u>	0.9315	75	F	Yes	unmeth	WT	hypof	Tem		see LK28		alive
LK27	0.8404	37	M	Yes	unmeth	mut	unknown sch	Tem		Yes	No	DOD
<u>LK28</u>	0.8566	75	F	Yes	meth	WT	hypof	Tem		Yes	Yes	alive
LK31	0.9470	46	M	Yes	meth	WT	normof	Tem	1	Yes	Yes	DOD
LK32	0.8145	64	M	Yes	meth	WT	normof	Tem	12	Yes	No	DOD
LK34	0.8600	65	M	Yes	unmeth	WT	normof	Nivo*		Yes	Yes	DOD
LK37	0.8972	54	F	Yes	unmeth	WT	normof	Nivo*	2	Yes	No	DOD
LK39	0.7954	56	F	Yes	meth	WT	normof	Tem + Nivo*	6	Yes	Yes	DOD

LK26 and LK28 were tumors from the same patient that had been resected and subsequently irradiated in a consecutive manner. Mol sig: molecular mesenchymal-to-proneural mRNA signature, M: male, F: female, (un)meth: (un)methylated, normo(hypo)f: normo(hypo)fractionated, unknown sch: unknown schedule, Tem: temozolomide, Nivo: nivolumab, \* indicates patients who were enrolled in clinical trials, NED: no evidence of disease, AWD: alive with disease, DOD: dead of disease, BSC: best supportive care.

## B. Supplementary material and methods

**pGSC culture.** Tumor specimens were washed three times in sterile phosphate buffered saline (PBS), minced and digested (15 min, 37°C) in 0.05% trypsin/EDTA (Thermo Fisher Scientific, Karlsruhe, Germany). Digestion was stopped with an equal volume of trypsin inhibitor (Sigma Aldrich, Taufkirchen, Germany) with a concentration of 0.5 mg/ml in NeuroCult NS-A Basal Medium (STEMCELL Technologies, Cologne, Germany). Afterwards, samples were centrifuged (110 g, 5 min) and the supernatant was discarded. Pellets were resuspended in 1 ml of NeuroCult NS-A Basal Medium and remaining clumps were



dissociated by pipetting up and down a few times. Thereafter, 14 ml of Basal Medium were added and the suspensions were filtrated through a cell strainer (mesh width 40  $\mu\text{m}$ , BD, Heidelberg, Germany) and recentrifuged (110 g, 5 min). The supernatant was removed and isolated cells were resuspended in complete human NeuroCult NS-A Proliferation Medium including 20 ng/ml rhEGF, 10 ng/ml rhFGF and 0.0002% heparin (STEMCELL Technologies) and transferred to 25  $\text{cm}^2$  cell culture flasks. Primary GSC (pGSC) sphere or monolayer cultures were obtained in about 75% of all attempts within 9 weeks on average between surgery and 1<sup>st</sup> passaging of the pGSC cultures. To isolate cells from spheres, spheres were rinsed in PBS, pelleted (110 g, 5 min), and resuspended in accutase (5 min, 37°C; Sigma Aldrich). Cell isolation was further facilitated mechanically by up- and down pipetting of the sphere/cell suspension. Adherent pGSC cultures (e.g., LK7) were rinsed and detached by accutase (5 min, 37°C). Accutase digestion was stopped by adding excess volume of PBS. After washing with PBS, cells were counted in a Neubauer chamber. To grow adherent monolayer (e.g., LK7) as spheres, detached cells were re-plated on low-attachment surfaces.

*RNA Isolation and real-time reverse-transcriptase polymerase chain reaction (RT-PCR).* RNA was isolated from pGSCs ( $\sim 10^6$  cells) by using NucleoSpin RNA Isolation Kit (Macherey-Nagel, Düren, Germany) following the manufacturer's instructions. The concentration of the eluted RNA was measured by NanoDrop ND-100 spectrometer (PEQLAB Biotechnologies GmbH, Erlangen, Germany) and samples were adjusted to 3 ng/ $\mu\text{l}$  in RNase-free water. To determine mRNA abundances of KCNN4, KCNMA1, ALDH1A3, CXCR4, Sox2, Notch1, Oct4, MSI1, nestin, FABP7, Nanog, CD133, GFAP, SDF1, MMP2, -9, TRPM8, as well as of the housekeepers glyceraldehyde-3-phosphate dehydrogenase (GAPDH),  $\beta$ -actin (ACTB) and pyruvate dehydrogenase- $\beta$  (PDHB) in a 20 ng RNA sample, fragments specific for KCNN4 (IK<sub>Ca</sub>, QT00003780, QuantiTect Primer Assay, QIAGEN, Venlo, Netherlands), KCNMA1 (QT00024157), ALDH1A3 (QT00077588), CXCR4 (QT00223188), Sox2 (QT00237601), Notch1 (QT01005109), Oct4 (QT00210840), MSI1 (QT00025389), nestin (QT00235781), FABP7 (QT00007322), Nanog (QT01025850), CD133 (QT00075586), GFAP (QT00081151), SDF1 (QT00087591), MMP2 (QT00088396), MMP9 (QT00040040), TRPM8 (QT00038906), as well as for the housekeepers GAPDH (QT01192646), ACTB (QT00095431) and PDHB (QT00031227) were amplified by SYBR Green-based real-time PCR (1Step RT qPCR Green ROX L Kit, highQu, Kraichtal, Germany) in a LightCycler480 (Roche, Mannheim, Germany). Crossing point ( $C_p$ ) values and melt curves were analyzed by LightCycler-480 software and abundances of the individual mRNAs (A) were normalized to the geometric mean of the three housekeeper mRNAs.

*Clonogenic survival of irradiated cells.* Isolated pGSC cells were sequentially 1:2 diluted in 96-well plates resulting in 12 cell dilutions (1024 to 0.5 cells in 100 µl complete human NeuroCult NS-A Proliferation Medium). Four hours after dilution, cells were irradiated with 0, 4 or 8 Gy given by 6 MV photons with a linear accelerator (LINAC SL15, Philips, Eindhoven, The Netherlands) at a dose rate of 4 Gy/min at room temperature. Two (LK7 which exhibited fastest growth kinetics) and 4 weeks (other pGSC cultures) after irradiation, the minimal cell number required to restore the culture (pGSCs growing with score 3-4) or for sphere formation (pGSCs growing with score 1-2) was determined. The reciprocal value of this minimal number defined the plating efficiency (PE). To calculate the survival fractions (SF), the PEs at the different radiation doses were normalized to the corresponding PE<sub>0Gy</sub> of the mock-irradiated control:

$$SF_{0-8 \text{ Gy}} = PE_{0-8 \text{ Gy}}/PE_{0 \text{ Gy}}$$

The survival fractions (SF) thus obtained were plotted against the radiation dose (d) and fitted according the linear quadratic model with the following equation derived from the linear quadratic model:

$$SF = e^{-(\alpha \cdot d + \beta \cdot d^2)}$$

with  $\alpha$ ,  $\beta$ : cell type-specific parameters.

*Hypo-fractionated radiation protocol that is dose-equivalent to the normo-fractionated radiotherapy.* To imitate changes of the molecular mesenchymal-to-proneural mRNA signature during standard normo-fractionated radiotherapy (60 Gy in 30 fractions) *in vitro*, a radiation protocol was defined, that applies a biologically equivalent radiation dose in 5 fractions by the following equation:

$$(d + \alpha/\beta)/(2 \text{ Gy} + \alpha/\beta) \times 5d = 60 \text{ Gy}$$

with d: radiation dose of a single fraction. Assuming an  $\alpha/\beta$  ratio of 10 Gy for glioblastoma results in a single fraction dose of d = 8 Gy suggesting that 40 Gy in 5 fractions (5x 8 Gy) are biologically dose-equivalent to 60 Gy in 30 fractions (30x 2 Gy). Mesenchymal-to-proneural mRNA signatures were analyzed 24 h after the last fraction of 5x 8 Gy and, for control, 5x 0 Gy mock-radiation.

*Fibrin gel invasion.* The extracellular matrix of healthy brain mainly consists of proteoglycans, hyaluronan, tenascins and link proteins (Ruoslahti E. Brain extracellular matrix. Glycobiology. 1996; 6(5):489-492). In order to mimic the *in vivo* brain infiltration of healthy brain by glioblastoma cells, we assessed the *in vitro* invasion of pGSC cells into a non-collagen matrix. For this purpose, adherent cultures were pre-grown to free-floating spheres on low attachment plates. Fibrinogen (3 µg/ml, Millipore, Darmstadt, Germany) and thrombin (4 U/ml, Sigma Aldrich) solution (both in complete NeuroCult NS-A Proliferation Medium) were

mixed 1+1 in a 96-well plate, casting a 2 mm thick layer of fibrin gel. Thereafter, pGSC spheres were suspended in fibrinogen-containing medium and placed on top of the fibrinogen layers, before adding the same volume of thrombin-containing medium. After polymerization, the embedded spheres were overlaid with complete NeuroCult NS-A Proliferation Medium to prevent dehydration during incubation time (21 d). Spheres were imaged directly after seeding (day 0) and after 7, 14 and 21 days by light microscopy. Two dimension (2D)-projected sphere and surrounding invasion area and maximal invasion distance around the spheres were semi-quantitatively analyzed with ImageJ software (open source). Only spheres with a 2D-projected area that correspond to a circle with  $\leq 100 \mu\text{m}$  radius were analyzed to minimize potential (repellent or mesenchymal-progression-inducing) effects of hypoxia that arises in the core of large spheres.

*Querying The Cancer Genome Atlas (TCGA), the Ivy Glioblastoma Atlas Project (Ivy GAP), and the Repository of Molecular Brain Neoplasia Data (REMBRANDT).* To expose the dependence of the overall survival (OS) of glioblastoma patients on the molecular mesenchymal-to-proneural mRNA signature of tumor specimens, the available RNA expression data sets were queried for the respective mRNA abundances (for links see in *Availability of data and materials*). In the Ivy data set, mesenchymal-to-proneural signatures were calculated separately for multiple cellular tumor samples of an individual tumor and then averaged to compute the molecular signature of this tumor. In the REMBRANDT data set, mRNA abundance data were averaged for multiply probed mRNA species. For survival analysis, patients were stratified by the mesenchymal-to-proneural signature calculated from these 10 mRNA abundances by applying a “best” threshold that yielded the clearest survival differences between both groups for each data set.

*Statistics.* Pearson correlation coefficients ( $P_{cc}$ ) were calculated to estimate linear correlations between two parameters. A  $P_{cc}$  value of  $\geq 0.3$  ( $\leq -0.3$ ),  $\geq 0.5$  ( $\leq -0.5$ ), and  $0.8$  ( $\leq -0.8$ ) was assumed as weakly, moderately or strongly positively (negatively) correlating, respectively. Error probability ( $p$ ) values of the Pearson correlations were indicated in the Figs. and show the significance level for the difference of the correlation coefficient from 0.

Differences between sample groups were assessed by unpaired two-tailed t-test and Bonferroni correction for two pairwise testing (Fig. 2E) or unpaired two-tailed Welch-corrected t-test in case of differing standard deviations (Figs. 2C, 3B, S4E). Kaplan-Meier survival curves were compared by log-rank test. Error probabilities of  $z_p \leq 0.05$  were assumed to indicate statistical significance ( $z$  = number of pairwise comparisons in Bonferroni correction).  $P_{cc}$

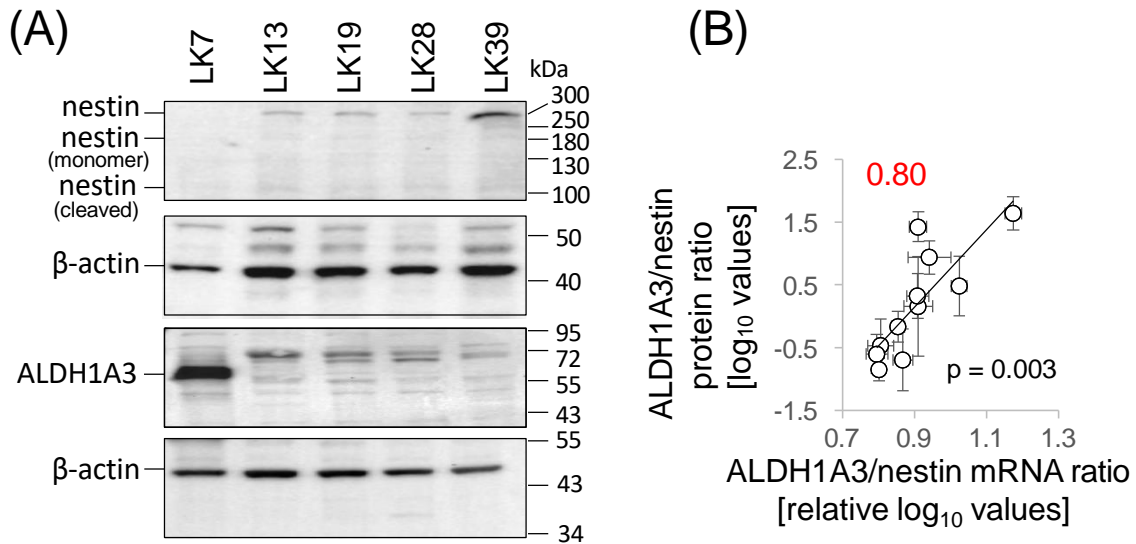
calculation, and statistical tests were performed with Microsoft Excel (version 2019) and GraphPad Prism (version 8.4.0).

### **C. Protein and functional expression of markers used to calculate the molecular pGSC mRNA signature.**

To define the mRNA/protein correlation for ALDH1A3 and nestin, protein abundances of nestin, ALDH1A3, and the housekeeper  $\beta$ -actin were determined in our pGSC cultures by immunoblotting (Suppl. Fig. S1A). The results indicate a strong correlation between the ALDH1A3/nestin mRNA and protein ratio in the analyzed cohort of 10 pGSC cultures ( $P_{cc} = 0.80$ , Suppl. Fig. S1B). Similarly, CXCR4 mRNA abundance correlated with CXCR4 surface expression ( $P_{cc} = 0.81$ , Suppl. Fig. S2A, B) in a cohort of 19 pGSC cultures as defined in flow cytometry by the differential binding of fluorochrome-linked CXCR4-specific and unspecific isotype control antibody (Suppl. Fig. S2A).

Furthermore, the functional expression of the mesenchymal stem cell marker ALDH1A3 was measured by Aldefluor assay in flow cytometry (Suppl. Fig. S3A). Plotting the mean number of cells that exhibited DEAB-sensitive ALDH enzyme activity against the mean ALDH1A3 mRNA abundance revealed a strongly positive correlation ( $P_{cc} = 0.86$ ; Suppl. Fig. S3B) in a cohort of 16 tested pGSC cultures.

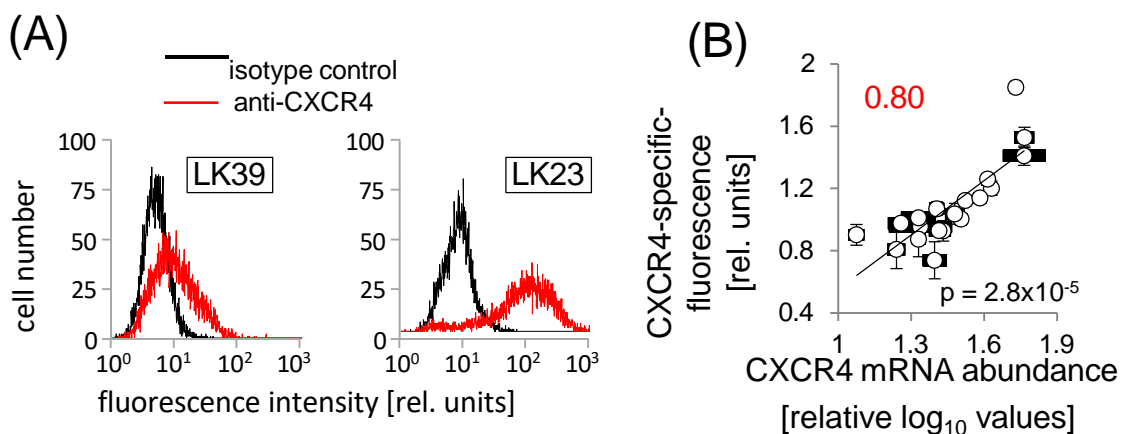
Finally, functional expression of  $I_{K_{Ca}}$   $K^+$  channels was analyzed by patch-clamp on-cell recording in two GSC cultures with high (LK7) and low (LK19) KCNN4 mRNA abundance, respectively. To this end, macroscopic  $I_{K_{Ca}}$  on-cell currents were activated and inhibited by the consecutive administration of the  $I_{K_{Ca}}$  opener 1-EBIO (100  $\mu$ M) and the  $I_{K_{Ca}}$  inhibitor TRAM-34 (5  $\mu$ M), respectively (Suppl. Fig. S4A-D). As shown in Suppl. Fig. S4E, 1-EBIO-induced macroscopic on-cell conductance was higher in LK7 than in LK19 cells. Combined, these data indicate protein and/or functional expression of the marker genes tested.



**Suppl. Fig. S1.** Protein expression of ALDH1A3 and nestin in pGSCs. (A) Immunoblots of whole lysates from 5 pGSC cultures probed against nestin (1<sup>st</sup> blot), ALDH1A3 (3<sup>rd</sup> blot) and for corresponding loading control  $\beta$ -actin (2<sup>nd</sup> and 4<sup>th</sup> blots). (B) Relationship between the ALDH1A3/nestin protein and mRNA ratio as a measure of mesenchymal-to-proneural GSC differentiation of 10 pGSC cultures. Protein ratios are means (n = 2, AR6) or means  $\pm$  SE (n = 3-9 for all other pGSCs), mRNA ratios are means  $\pm$  SE (n = 4-15). Red number and p value indicate the Pearson correlation coefficient and the significance level for the difference of the correlation coefficients from 0, respectively.

For immunoblotting, protein lysates were prepared by solubilizing pGSCs ( $\sim 10^6$  cells) in radioimmunoprecipitation assay buffer (RIPA-buffer) containing (in mM) 25 Tris/NaOH (pH 7.6), 150 NaCl, 35 sodium dodecyl sulphate (SDS), 12 sodium deoxycholate, additionally supplemented with Triton x-100 (1.0 %), proteinase inhibitor (complete tablets Mini EDTA-free, Roche), and phosphatase inhibitor cocktail-2 (Sigma Aldrich). Lysates were heated (5 min, 70°C) after adding 4x sample-buffer containing (in mM) 14 SDS, 200 Tris/NaOH (pH 6.8), 10 dithiothreitol further containing glycerol (20%) and bromophenol blue (0.005%). Proteins were separated by SDS-polyacrylamide gel (10%) electrophoresis and blotted onto a Roti polyvinylidene fluoride (PVDF) membrane (0.45  $\mu$ m, Carl Roth, Karlsruhe, Germany). Membranes were washed (3x 5 min) in TBS-Tween (150 mM NaCl, 0.1% Tween-20, 10 mM Tris(hydroxymethyl)aminomethane (Tris)/HCl, pH 8.0) and unspecific binding sites blocked (60 min, 21°C) in 5% bovine serum albumin (BSA, Carl Roth)/TBS-Tween. Membranes were probed (4°C, overnight) against ALDH1A3, nestin, and  $\beta$ -actin using 5% BSA/TBS-Tween-diluted primary rabbit polyclonal anti-nestin- (#N5413, batch number SLCC3419, 1:500, Sigma Aldrich), rabbit polyclonal anti-ALDH1A3- (#PA5-29188, batch number TH2617862, 1:1000, Thermo Scientific), and mouse monoclonal anti- $\beta$ -actin-antibody (#A554, 1:20.000,

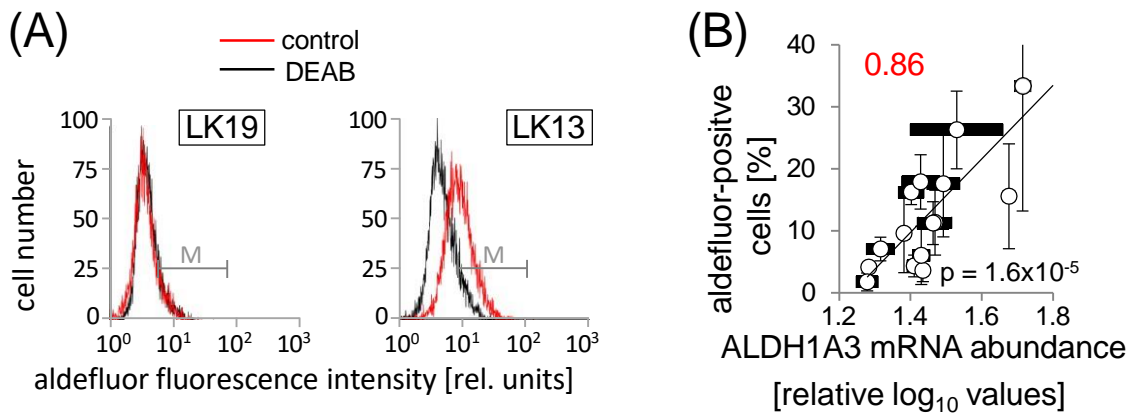
Sigma Aldrich), respectively, washed (3x 5 min in TBS-Tween), and incubated (60 min, 21°C) with 5% BSA/TBS-Tween-diluted horseradish peroxidase (HRP)-linked anti-mouse IgG (#NA931V, 1:2000, GE Healthcare, Buckinghamshire, UK) or anti-rabbit IgG (#70749, 1:2000, Cell Signaling Technology, Frankfurt a. Main, Germany) secondary antibody. After washing (3x 5min in TBS-Tween), antibody binding was detected with Immobilon Western HRP-substrate (Merck Millipore) and recorded with ChemiDoc Imaging System (BioRad Laboratories, Feldkirchen, Germany). Digitalized protein bands were semiquantified with ImageLab 5.2.1 software (BioRad).



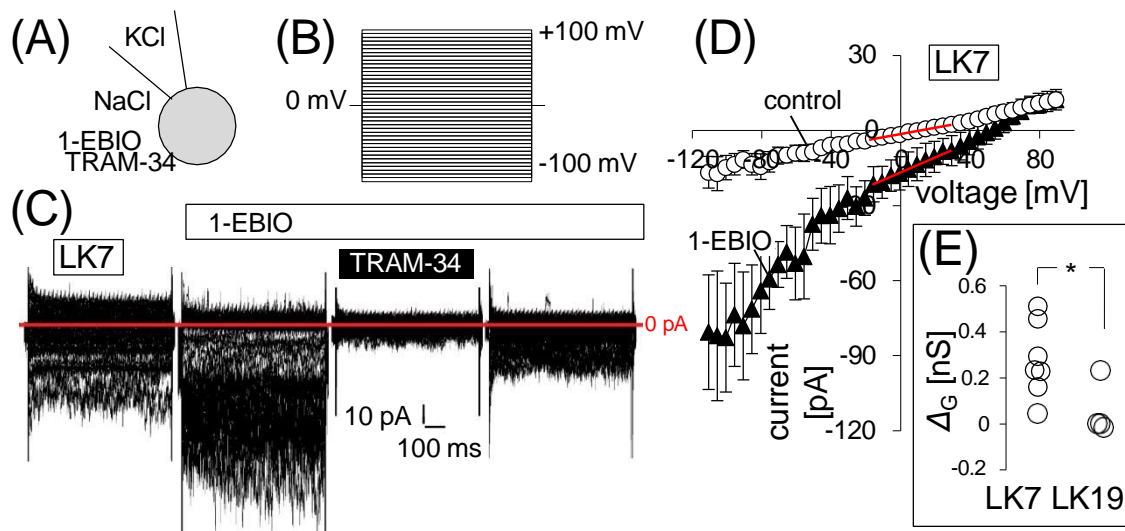
**Suppl. Fig. S2.** CXCR4 surface expression of pGSCs. (A) Flow cytometry histograms of fluorescence intensities following binding of fluorescence-labelled anti-CXCR4- (red) or isotype control (black) antibody to the surface of LK39 (left) and LK23 (right) pGSCs. (B) Relationship between CXCR4-specific fluorescence (as determined as in (A) by subtracting the geometric mean of the black from that of the red histogram) and the CXCR4 mRNA abundance of 19 pGSC cultures. Data are means  $\pm$  SE (n = 3-8). Red number and p value in indicate the Pearson correlation coefficient and the significance level for the difference of the correlation coefficient from 0, respectively.

To analyze CXCR4 surface expression, aliquots of single pGSC cell suspensions ( $2.5 \times 10^5$  cells/250  $\mu$ l) were stained (30 min, on ice) with R-phycoerythrin-linked monoclonal mouse anti-CXCR4 (#MHCXCR404) or IgG isotype (#12472482) control antibody (both 1:500 in PBS, both from Thermo Fisher Scientific). After washing and resuspending the pGSC cells in 0.5% BSA/PBS, antibody binding was recorded by flow cytometry (FACS Calibur with CellQuest software, BD) with 488/10 nm excitation and 585/42 nm emission. The geometric mean of fluorescence intensity was analyzed by FCS Express-3 software (De Novo Software, Pasadena, CA, USA) for anti-CXCR4- and isotype control antibody binding and the difference between both geometric mean values used as a measure for CXCR4 surface

expression. Red number and p value indicate the Pearson correlation coefficient and the significance level for the difference of the correlation coefficient from 0, respectively.



**Suppl. Fig. S3.** ALDH activity of pGSCs. (A) Flow cytometry histograms showing the ALDH-dependent conversion of Aldefluor substrate into a fluorescent product in the absence (control, red) and presence of the ALDH-inhibitor DEAB (3  $\mu$ M, black) in LK19 (left) and LK13 (right) pGSCs. (B) Relationship between percentage of ALDH-positive cells (as defined as in (A) by the DEAB-blockable population fraction marked by (M)) and the ALDH1A3 mRNA abundance of 16 pGSCs. Data are means  $\pm$  SE (n = 3-8). Red number and p value indicate the Pearson correlation coefficient and the significance level for difference of the correlation coefficients from 0, respectively. The Aldefluor Kit (STEMCELL Technologies) was used to determine ALDH activity of pGSC cells ( $3 \times 10^5$  cells/500  $\mu$ l assay buffer). In particular, conversion of the fluorescent substrate bodipy-aminoacetaldehyde by ALDH into the intracellularly trapped bodipy-aminoacetate during incubation (45 min, 37°C) with ALDH inhibitor DEAB (0 or 3  $\mu$ M) was measured by flow cytometry (FACSscalibur with CellQest software, BD) at 488 nm excitation and 530/30 nm emission. The cell fraction showing DEAB-sensitive fluorescence was defined as ALDH-positive cell population (in %) by FCS Express-3 software.



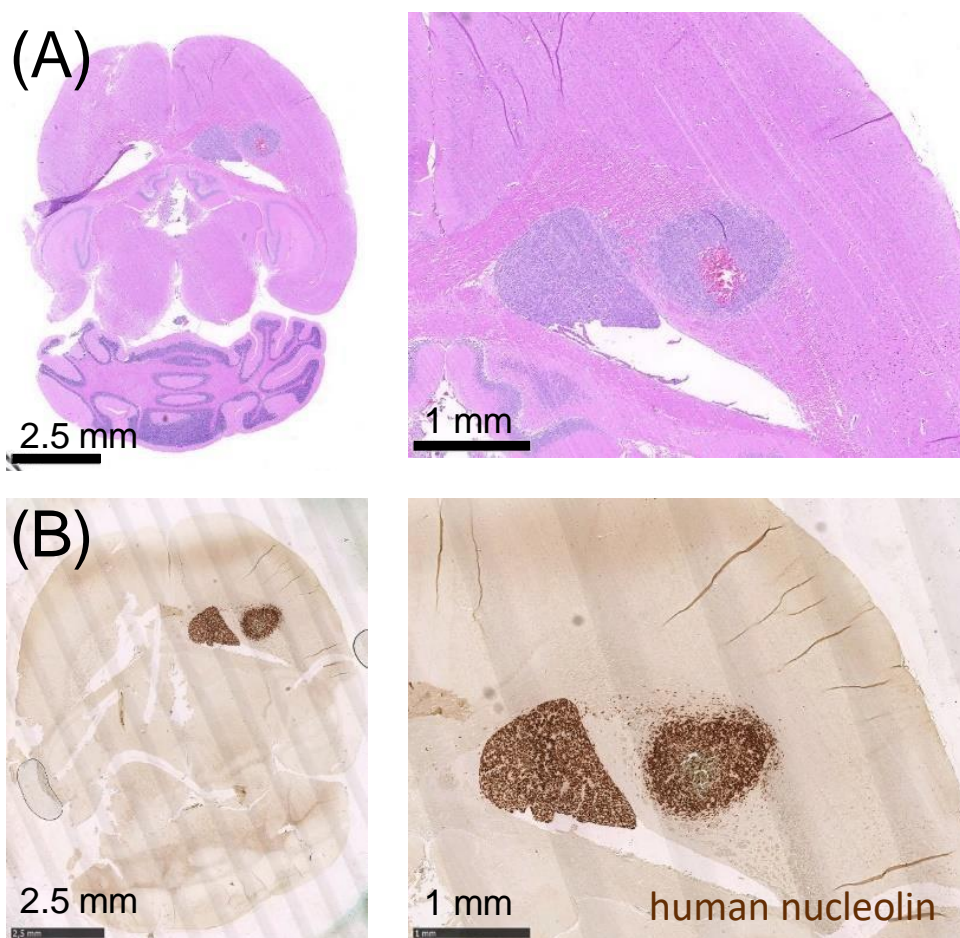
**Suppl. Fig. S4.** Functional expression of  $I_{KCa}$   $K^+$  channels in the plasma membrane of pGSCs. (A-C) Ionic composition and channel modulators of pipette and bath solution (A) and applied voltage pulse protocol (B) used to record from a LK7 pGSC in on cell (cell-attached) mode the current tracings shown in (C). The latter were obtained before (outer left) and during bath application of the  $I_{KCa}$   $K^+$  channel opener 1-EBIO (100  $\mu$ M, middle left and outer right) alone or in combination with the  $I_{KCa}$  inhibitor TRAM-34 (5  $\mu$ M, middle right). (D) Clamp-voltage dependence of macroscopic on cell currents in LK7 pGSC cells recorded before (control, open circles) and during bath application of 1-EBIO (closed triangles). (E) 1-EBIO-stimulated increase in cell-attached conductance ( $\Delta G$ , as calculate for the macroscopic inward currents for the voltage range shown by red lines in (D)) for LK7 (left) and LK19 (right) cells (given are). Data in (D) are means  $\pm$  SE ( $n = 4-7$ ) and in (E) individual values; \* indicates  $p \leq 0.05$ , Welch corrected two-tailed t-test.

Patch-clamp macroscopic on-cell (cell-attached) currents from LK19 and LK7 pGSC cells were recorded (10 kHz sampling rate) and 3 kHz low-pass-filtered by an EPC-9 amplifier (Heka, Lambrecht, Germany) using Pulse software (Heka) and an ITC-16 Interface (Instrutech, Port Washington, NY, USA). Borosilicate glass pipettes ( $\sim 5$  M $\Omega$  pipette resistance; GC150 TF-10, Clark Medical Instruments, Pangbourne, UK) manufactured by a microprocessor-driven DMZ puller (Zeitz, Augsburg, Germany) were used in combination with a STM electrical micromanipulator (Lang, Gießen, Germany). Cells were continuously superfused at 37°C with NaCl solution (in mM: 125 NaCl, 32 N-2-hydroxyethylpiperazine-N-2-ethanesulfonic acid (HEPES), 5 KCl, 5 D-glucose, 1 MgCl<sub>2</sub>, 1 CaCl<sub>2</sub>, titrated with NaOH to pH 7.4) additionally containing the  $I_{KCa}$   $K^+$  channel activator 1-ethyl-2-benzimidazolinone (1-EBIO, 0 or 100  $\mu$ M) and the  $I_{KCa}$  inhibitor triarylmethane-34 (Tram-34, 0 or 5  $\mu$ M). The pipette solution contained (in mM) 130 KCl, 32 HEPES, 5 D-glucose, 1 MgCl<sub>2</sub>, 1 CaCl<sub>2</sub>, titrated with



KOH to pH 7.4. Currents were elicited by 41 voltage square pulses (700 ms each) from 0 mV holding potential to voltages between -100 mV and +100 mV delivered in 5 mV increments. Clamp voltages refer to the cytosolic face of the plasma membrane and were corrected offline for the applying liquid junction potential according to Barry and Lynch (Barry PH, Lynch JW. Liquid junction potentials and small cell effects in patch-clamp analysis. *J Membr Biol.* 1991; 121:101-117). For analysis, macroscopic on-cell currents were averaged between 100 and 700 ms of each voltage sweep. Inward currents are defined as influx of cations into the cells (or efflux of anions out of the cell), depicted as downward deflections of the current tracings, and defined as negative currents in the current voltage relationships. Macroscopic on-cell conductance was calculated for the inward currents between -15 mV and +25 mV clamp voltage. The 1-EBIO-stimulated conductance increase was used as a measure of functional  $IK_{Ca}$  channel expression in the plasma membrane.

#### D. Tumor-initiating capability of the pGSC cultures.



**Suppl. Fig. S5.** Human pGSCs developed orthotopic glioblastoma in NSG (NOD/SCID/IL2Ry<sup>null</sup>) mice visualized in 5  $\mu$ m paraffin embedded brain sections. Hematoxylin

and eosin (HE) staining (A) and immunohistochemical detection of human nucleolin (B). Arrows indicate invasive growing tumor cells. Stereotactic *xenotransplantation* of primary GCSs was performed as previously described (Edalat L et al. BK K<sup>+</sup> channel blockade inhibits radiation-induced migration/brain infiltration of glioblastoma cells. *Oncotarget* 2016;7(12):14259-78). Tumor formation was monitored by a 7 Tesla MRT ClinScan (Bruker Corporation, Massachusetts, USA) in the Werner Siemens Imaging Center Tübingen (data not shown).

Glioblastoma cells expressing human nucleolin were stained immunohistochemically by the use of an Animal Research Kit (ARK, Dako, Hamburg, Germany) as described previously (Riedel A et al.  $\gamma$ H2AX foci assay in glioblastoma: Surgical specimen versus corresponding stem cell culture. *Radiother Oncol* 2021;159:119-25) and an anti-nucleolin antibody (Enzo ADI-KAM-CP100-E, Lot Nr.11151717, 1:100 in PBS).



Contents lists available at ScienceDirect

Radiotherapy and Oncology

journal homepage: [www.thegreenjournal.com](http://www.thegreenjournal.com)

Original Article

## Potential of pre-operative MRI features in glioblastoma to predict for molecular stem cell subtype and patient overall survival



Franziska Eckert<sup>a,b,†</sup>, Katrin Ganser<sup>a</sup>, Benjamin Bender<sup>c</sup>, Jens Schittenhelm<sup>d</sup>, Marco Skardelly<sup>e,f</sup>, Felix Behling<sup>e</sup>, Ghazaleh Tabataba'i<sup>f</sup>, Elgin Hoffmann<sup>a</sup>, Daniel Zips<sup>a,g</sup>, Stephan M. Huber<sup>a</sup>, Frank Paulsen<sup>a</sup>

<sup>a</sup> Department of Radiation Oncology, University of Tübingen, Germany; <sup>b</sup> Medical University Vienna, Department of Radiation Oncology, Comprehensive Cancer Center Vienna, Vienna, Austria; <sup>c</sup> Department of Diagnostic and Interventional Neuroradiology, University of Tübingen, Tübingen, Germany; <sup>d</sup> Department of Pathology and Neuropathology, University of Tübingen, Germany; <sup>e</sup> Department of Neurosurgery, University of Tübingen, Germany; <sup>f</sup> Centre for Neurooncology, University of Tübingen, Germany; <sup>g</sup> Department of Radiation Oncology, Charité Universitätsmedizin Berlin, Germany

### article info

#### Article history:

Received 17 April 2023

Received in revised form 31 July 2023 Accepted 14 August 2023

14 August 2023

Available online 22 August 2023

#### Keywords:

Glioblastoma

MGMT promoter methylation Stem cells

Mesenchymal

Proneural MRI

### abstract

**Aim of the study:** A molecular signature based on 10 mRNA abundances that characterizes the mesenchymal-to-proneural phenotype of glioblastoma stem(like) cells (GSCs) enriched in primary culture has been previously established. As this phenotype has been proposed to be prognostic for disease outcome the present study aims to identify features of the preoperative MR imaging that may predict the GSC phenotype of individual tumors.

**Material/Methods:** Molecular mesenchymal-to-proneural mRNA signatures and intrinsic radioresistance (SF<sub>4</sub>, survival fraction at 4 Gy) of primary GSC-enriched cultures were associated with survival data and pre-operative MR imaging of the corresponding glioblastoma patients of a prospective cohort (n = 24). The analyzed imaging parameters comprised linear vectors derived from tumor volume, necrotic volume and edema as contoured manually.

**Results:** A necrosis/tumor vector ratio and to a weaker extent the product of this ratio and the edema vector were identified to correlate with the mesenchymal-to-proneural mRNA signature and the SF<sub>4</sub> of the patient-derived GSC cultures. Importantly, both parameter combinations were predictive for overall survival of the whole patient cohort. Moreover, the combination of necrosis/tumor vector ratio and edema vector differed significantly between uni- and multifocally recurring tumors.

**Conclusion:** Features of the preoperative MR images may reflect the molecular signature of the GSC population and might be used in the future as a prognostic factor and for treatment stratification especially in the MGMT promoter-unmethylated sub-cohort of glioblastoma patients.

© 2023 Elsevier B.V. All rights reserved. Radiotherapy and Oncology 188 (2023) 109865

Diagnosis and treatment of glioblastoma is based on MR (magnetic resonance) imaging to define macroscopic tumor volume (contrast enhancing volume in T1 weighted images) and edema (hyperintense volume in T2 FLAIR (fluid-attenuated inversion recovery) images) [1]. In postoperative or primary radiotherapy planning, these volumes (resection cavity/macroscopic tumor and edema in the US guideline) are used to derive the clinical target volume [2,3]. In addition, numerous attempts have been made to predict patient prognosis and/or molecular tumor characteristics from pre-therapeutic imaging features. Two possible strategies are radiomics/radiogenomics approaches as reviewed in [4,5] or image analysis with clinically used approaches such as contouring of volumes of interest and volumetric analysis. In well-defined

patient populations with prospective imaging at designated MR scanners and comparable sequence parameters, radiomics approaches are very promising to explore possible correlations of imaging features with patient outcome and biologic tumor features far beyond volumetric analysis. However, in mixed patient cohorts with MR imaging performed at several different institutions, with different MR scanners and imaging protocols, robustness of radiomics approaches is rather limited [6]. Thus, simple and robust volumetric image analysis approaches based on contouring such as used in radiotherapy planning is still an attractive research strategy to explore correlations between MRI features and biological properties of the respective tumors.

Molecular properties of glioblastoma have entered daily clinical practice and are incorporated in the 2021 WHO (world health organization) classification [7]. IDH (isocitrate dehydrogenase) status is crucial for neuropathological diagnosis and a strong prognostic marker [8]. IDH-1/-2 mutated grade-4 astrocytomas are now no

<sup>†</sup> Corresponding author at: Medical University Vienna, Department of Radiation Oncology, Waehringer Guertel 18-20 1090, Vienna, Austria.

E-mail address: [franziska.eckert@meduniwien.ac.at](mailto:franziska.eckert@meduniwien.ac.at) (F. Eckert).

longer considered as glioblastoma. Additional prognostic markers for the diagnosis of glial tumors are ATRX (ATP-dependent helicase) and TERT (telomerase reverse transcriptase) [9,10]. For IDH wildtype glioblastoma, the prognostic as well as predictive significance of MGMT (O<sup>6</sup>-methylguanine DNA-methyltransferase) promoter methylation for therapy response to temozolomide has been established [11]. A 2017 meta-analysis confirmed the significantly better overall survival of patients with methylated MGMT promoter status [12].

With the data of the NORDIC trial in 2012, treatment for elderly glioblastoma patients was stratified to hypofractionated radiotherapy for patients with unmethylated MGMT promoter status and temozolomide monotherapy for patients with methylated MGMT promoter status [13]. In 2017 with the data by Perry et al. hypofractionated radiochemotherapy with concurrent temozolomide was introduced into clinical practice for the latter patient population [14]. For newly diagnosed glioblastoma in young patients with ECOG performance status 0 or 1 and methylated MGMT promoter, temozolomide and CCNU (chloroethyl-cyclohexyl-nitroso-urea, Lomustin) is an option for concomitant and sequential chemotherapy in addition to radiotherapy [15]. Thus, molecular tumor properties are used for treatment stratification in routine clinical practice.

Moreover, several molecular subgroups of glioblastomas were established, mostly based on transcriptome and methylome analysis of tumor biopsy/resection material (e.g. [16–18]). Mostly, mesenchymal compared to proneural phenotype of glioblastoma stem (cell-like) cells has been associated with poor patient prognosis [19,20]. In order to simplify the diagnosis of molecular subgroups, different approaches were used, such as immunohistochemistry or quantitative PCR of a limited number of markers [21,22].

As reviewed by Fathi Kazerooni et al., several molecular features have been associated with imaging features [4]. Multiparametric and multiregional MR imaging features reportedly correlate with molecular characteristics, however, not with sufficient strength to pursue the model in further projects [23]. An analysis of the TCGA dataset and imaging material of 75 patients pointed to associations of diameters of contrast-enhanced tumor and non-enhanced tumor with molecular subgroups, but not of edema and necrosis diameters [23].

In a prospective cohort of patients, for whom a molecular score of mesenchymal versus proneural stem cell properties on a continuous scale as well as radiosensitivity were evaluated in primary, stem cell enriched glioblastoma cultures [24], pretherapeutic MR images were collected for the present study. In an intraindividual comparison, manually contoured tumor, edema and necrosis volumes as well as derived parameters were correlated with patient survival as well as with the biological *in vitro* properties of the corresponding stem cell enriched glioblastoma cultures.

## Materials and methods

### Patient cohort

For 24 patients with high grade gliomas undergoing resection at our institution, stem cell-enriched primary cultures were established from tumor resection specimens. All patients had given written informed consent, the study was approved by the ethics committee of our institution (project numbers 579/20015BO2 and BO2-2, 184/2015BO1). Clinical and neuropathologic features were analyzed for all patients, as well as oncologic outcome. Neuropathologic features showed typical findings for glioblastoma with IDH wildtype tumors in all but one (grade-4 astrocytoma) cases and ATRX retention in all tumors. Eleven tumors showed unmethylated MGMT promoters, 14 tumors had methylated MGMT promoters. Most patients (n = 21) underwent macroscopic

complete resection. Postoperative treatment varied according to patient age and ECOG status. Four patients did not undergo any additive therapy while 14 patients underwent normofractionated radiotherapy and three hypofractionated radiotherapy (data not available for three patients). Concurrent and sequential systemic therapy mostly consisted of temozolomide, however, some patients were enrolled in clinical trials and treated with immune checkpoint inhibitors. With an estimated median follow up of 1.9 years 18 tumors had developed recurrences, 2 tumors were controlled (lost to follow up: 5). Patient characteristics are summarized in Table 1. Progression-free and overall survival of the patients was assessed for the whole cohort as well as subgroups.

### Glioblastoma stem cell-enriched cultures

As described previously [24] primary, stem-cell enriched glioblastoma cultures were established from fresh resection specimens. Individual cultures differed significantly in their growth pattern and biological properties. For all samples, a molecular score was determined calculated from mRNA abundances of ten markers with a low score referring to a proneural, non-invasive subtype, a high score referring to a mesenchymal, highly invasive subtype. For 18 cell cultures *in vitro* intrinsic radiosensitivity was determined by limited dilution assay comparing unirradiated and 4 Gy (6 MV photons)-irradiated cells. Individual cell cultures exhibited a broad range of survival fraction after 4 Gy (SF<sub>4</sub>).

### Contouring

Preoperative MR images were available in the imaging database of our institution for all patients. T1 weighted, contrast enhanced sequences (T1ce) and FLAIR sequences were imported to the radiation treatment planning systems MONACO version 5.11.03 (Elekta AB, Stockholm, Sweden) and RayStation (RaySearch Laboratories, Stockholm, Sweden). Tumor volumes were contoured as hyperintense volumes on T1ce. Necrosis was defined as T1ce hypointense volume inside the tumor volume. Edema was contoured as hyperintense volume on FLAIR images. All contouring was done by an experienced radiation oncologist. Volume parameters were extracted from the radiation treatment planning system for all contoured volumes. Cell division or migration of glioblastoma cells can be assumed to occur along monodimensional axes suggesting that the behavior of the cells (bulk proliferation with necrotic core and brain infiltration) is better represented by linear vectors rather than by three-dimensional volumes. To translate volumes into linear vectors, determined volumes were considered as ideal spheres and linear vectors (S<sub>tumor</sub>, S<sub>necrosis</sub>, and S<sub>edema</sub>) defined by the third root of the sphere volume. To analyze the functional significance of these image features, S<sub>edema</sub>, the S<sub>necrosis</sub>/S<sub>tumor</sub> ratio, and  $\ln$

Table 1

		n	%
Sex	Male	16	67%
	Female	8	33%
Age	< 65	14	58%
	> 65	10	42%
Multifocal tumor	Yes	5	21%
	No	19	79%
Resection	Complete	21	88%
	Subtotal	3	12%
MGMT promoter	Methylated	13	54%
	Unmethylated	11	46%
Postoperative radiotherapy	Yes	19	79%
	No	5	21%
Postoperative temozolomide	Yes	17	71%
	No	7	29%

MRI index derived thereof ( $ind_{MR} = \text{Sedema} \times \text{S}_{necrosis}/\text{S}_{tumor}$ ) of the glioblastomas were associated with the molecular mesenchymal-to-proneural mRNA signatures and the SF<sub>4</sub> values of the corresponding primary GSC-enriched cultures as well as oncologic outcome. These analyses were performed for the whole patient cohort as well as separately for the MGMT promoter-methylated and -unmethylated subgroups. In addition to that,  $ind_{MR}$  values of the whole patient cohort for uni- and multifocally recurring glioblastomas were compared and the dependence of the MRI volumes on the MGMT promoter methylation status analyzed.

## Statistics

For pairwise comparison, data were tested for normal distribution by Kolmogorow-Smirnov-test. Means were compared with (Welch-corrected) student's t-test in case of normally distributed values, otherwise with Mann-Whitney-U test. Progression-free (PFS) and overall survival (OS) were depicted by Kaplan-Meier plots and differences between curves calculated by log-rank test in univariate testing and Cox regression for multivariate analysis. Error probabilities of  $p < 0.05$  were considered statistically significant in all analyses but those shown in Fig. 1E and 1F. Here, the significance level was raised to a value of  $p < 0.025$  due to the repeated analysis of the updated cohort of glioblastoma patients referring to the previous publication.

Pearson coefficient ( $r$ ) for linear correlation was calculated for the associations of continuous variable. Values of  $r_P > 0.3$  (or  $< -0.3$ ),  $r_P > 0.5$  (or  $< -0.5$ ) and  $r_P > 0.8$  (or  $< -0.8$ ) were considered as weak, moderate and strong (negative) correlation, respectively.

## Results

As described in our recent study stem cell enriched glioblastoma cell cultures were established of a prospective glioblastoma patient cohort with mixed clinical features and therapies [24], with a median overall survival of  $2.6 \pm 0.8$  years and a median progression-free survival of  $0.9 \pm 0.3$  years (Fig. 1A). Cell cultures were characterized by a mesenchymal-to-proneural mRNA signature (Fig. 1B) initially published by Ganser et al. [24]. A second analysis for the survival data of the Tübingen patient cohort with longer follow-up periods and increased patient number was performed. The mesenchymal-to-proneural signature significantly influenced PFS and OS with a cut-off at median (Fig. 1C, D). MGMT promoter methylated glioblastoma displayed a longer PFS and OS although without statistical significance (Fig. 1E). Mesenchymal-to-proneural signature was not different for MGMT promoter methylated and unmethylated tumors (Fig. 1F). Tumors with multifocal recurrences led to shorter OS (Fig. 1G) and displayed significantly higher (i.e., more mesenchymal) molecular signatures (Fig. 1H).

MR images were available and suitable for contouring and analysis in all cases. Examples of contours on T1ce and T2FLAIR images are given in Fig. 2A. The volumes of the contours were transformed to one-dimensional measures (Fig. 2B). Whereas tumor volumes and tumor vectors correlated significantly with edema plus tumor as well as necrosis volumes and vectors (Fig. 2C-F), edema vectors and necrosis/tumor vector ratio were not significantly dependent on tumor vector (Fig. 2G, H). Thus, edema vector and necrosis/tumor vector are not merely reflecting tumor size. Moreover, none of the vector parameters differed significantly between MGMT promoter methylated and unmethylated tumors (Fig. 2I).

Edema vector and necrosis/tumor vector ratio were correlated with mesenchymal-to-proneural mRNA signature (Fig. 3A-B) and *in vitro* radioresistance (SF<sub>4</sub>, Fig. 3C-D) of the respective stem-cell enriched glioblastoma cell lines. While there were no correlations

with edema vector, in the subgroup of glioblastomas with unmethylated MGMT promoter status, necrosis/tumor vector significantly correlated with mesenchymal-to-proneural mRNA signature and radioresistance. Larger edema vector showed a tendency towards better OS (Fig. 3E), higher necrosis/tumor vector ratios significantly correlated with better OS (Fig. 3F). In multivariate analysis of OS including the parameters molecular score, MGMT methylation status, necrosis/tumor vector ratio, and multifocal recurrence, necrosis/tumor vector ratio showed a trend to significance ( $p = 0.087$ ), data not shown.

To identify imaging parameters that correlate with the functional and molecular characteristics of stem cell cultures as well as patient prognosis, a more complex imaging index was defined by combining the edema vector and the necrosis/tumor vector ratio. This index (edema vector  $\times$  necrosis/tumor vector ratio,  $ind_{MR}$ ) correlated weakly ( $r_P = -0.3$  to  $-0.37$ ) but non-significantly with the mesenchymal-to-proneural mRNA signature in the whole, the MGMT-methylated, and the unmethylated cohort. In addition,  $ind_{MR}$  correlated moderately ( $r_P = -0.52$ ) but also non-significantly with the radioresistance of MGMT-unmethylated cultures. In contrast,  $ind_{MR}$  did not correlate with radioresistance of the whole cohort and the MGMT-methylated cohort (Fig. 4A). Most importantly, Kaplan-Meier curves diverged highly significantly when stratifying the whole glioblastoma patient cohort by  $ind_{MR}$ :  $ind_{MR}$  above the median was associated with a doubling of median OS as compared to patients with low  $ind_{MR}$  (Fig. 4B, right). In contrast,  $ind_{MR}$  was not prognostic for PFS (Fig. 4B, left). Finally, tumors recurring multifocally had significantly lower  $ind_{MR}$  than tumors with unifocal recurrence pattern (Fig. 4C).

## Discussion

Our analysis suggests that *in vitro* radiosensitivity as well as mesenchymal stem cell properties (as compared to proneural) correlate with volumetric imaging parameters in a prospective cohort of glioblastoma patients. These correlations were more pronounced in the subgroup of patients with MGMT promoter-unmethylated tumors, even if this subgroup analysis is limited by small sample size. In the whole cohort necrosis/tumor vector ratio as well as  $ind_{MR}$  (edema vector  $\times$  necrosis/tumor vector ratio) correlated with overall survival.

Volumetric analysis of tumor volume and necrosis based on T1 weighted contrast-enhanced MR imaging and edema in T2 FLAIR imaging was possible in all cases as these sequences are routinely acquired for all patients [25] and the analysis is not limited by different MR scanners and imaging protocols. In concordance with Palpan Flores et al. [26] tumor, necrosis and edema volume strongly correlated with each other [26]. Notably, in our study the tumor vector did not correlate with the edema vector as well as the necrosis/tumor vector ratio suggesting that these parameters are not mere epiphenomena of tumor size. Standard imaging (T1 weighted contrast-enhanced sequences and FLAIR sequence) had also already been used for an analysis focusing on the shape of necrosis, tumor and edema regions. The more complex volumes (quantified by fractal dimension and lacunarity) were, the worse the prognosis of the patients [27]. The main limitations of our study are the small patient cohort and the heterogeneity of postoperative treatments. Especially the subgroup analysis of glioblastomas with methylated versus unmethylated MGMT promoter subtypes is merely hypothesis-generating. However, the size of the cohort is limited by the availability of fresh tumor material at the time of resection, establishment of primary stem-cell enriched cell lines and molecular and biological analysis.



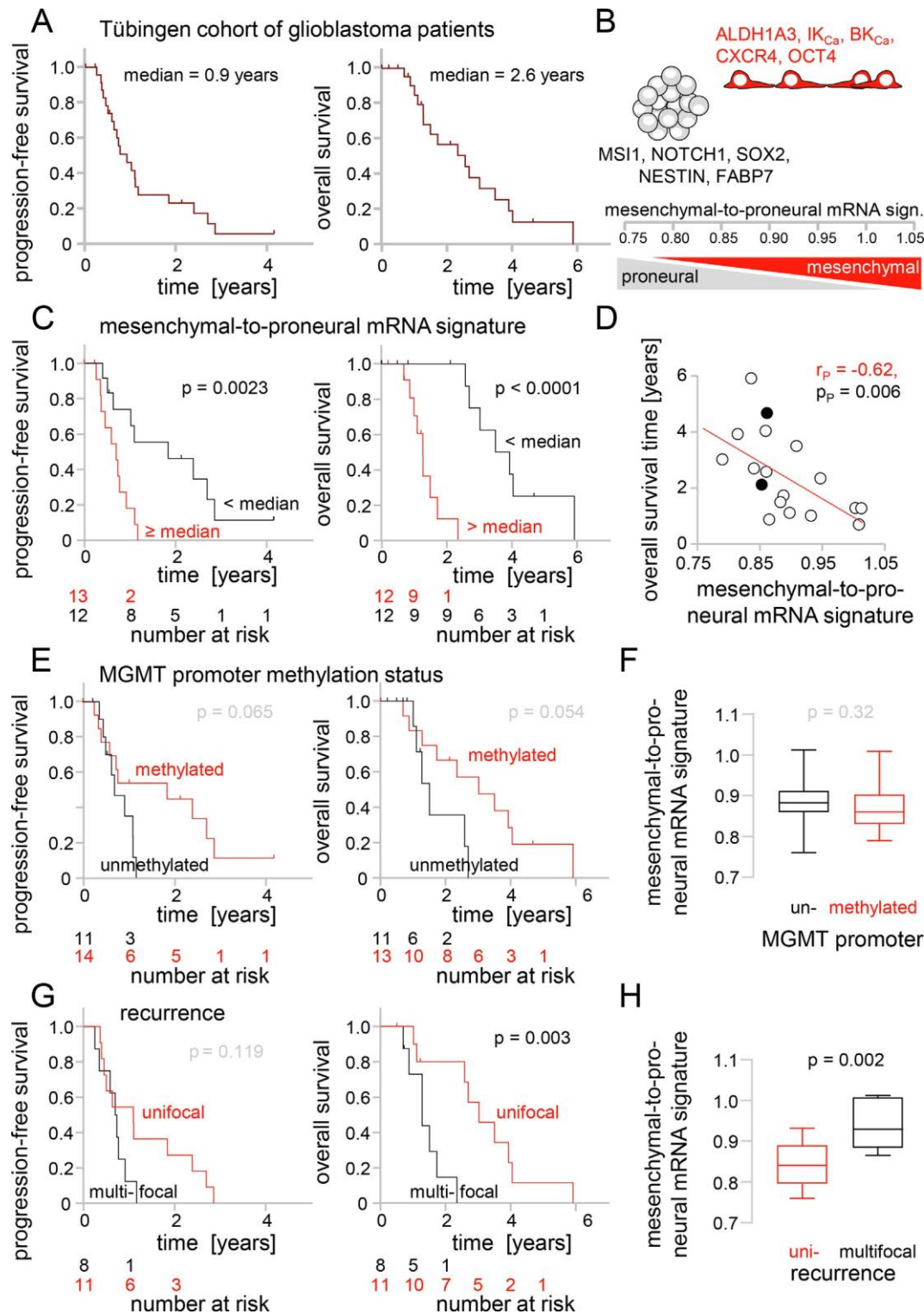


Fig. 1. The molecular mesenchymal-to-proneural mRNA signature of patient-derived GSC-enriched primary cultures is prognostic for the survival of glioblastoma patients. A. PFS and OS are shown for the whole cohort analyzed (updated follow-up after publication of Gansler et al. [24]). B. The mesenchymal-to-proneural score developed in Gansler et al. is calculated from mRNA abundances of five genes known to be expressed in mesenchymal and five genes known to be expressed in proneural glioblastoma stem cells. High and low values indicate mesenchymal and proneural phenotype of the individual cell lines, respectively. C. Patients whose tumors were characterized by a mesenchymal-to-proneural signature above the median showed significantly worse PFS and OS. D. Correlation of the mesenchymal-to-proneural signature with overall survival times was highly significant (closed symbols: censored patients). E. Patient stratification by the known prognostic factor of MGMT promoter methylation separated Kaplan-Meier curves albeit without statistical significance. F. The mesenchymal-to-proneural signature did not differ in tumors with unmethylated and methylated MGMT- promoter status. G. Patients whose tumors recurred multifocally had a significantly worse OS and (H) had significantly higher mesenchymal-to-proneural signature as compared to patients with unifocal glioblastoma recurrence. Red and black numbers indicate the coefficient of linear correlation and the error probability, respectively, as determined by Pearson correlation in (D), log-rank test in (C, E, G), and two-tailed t-test in (H).

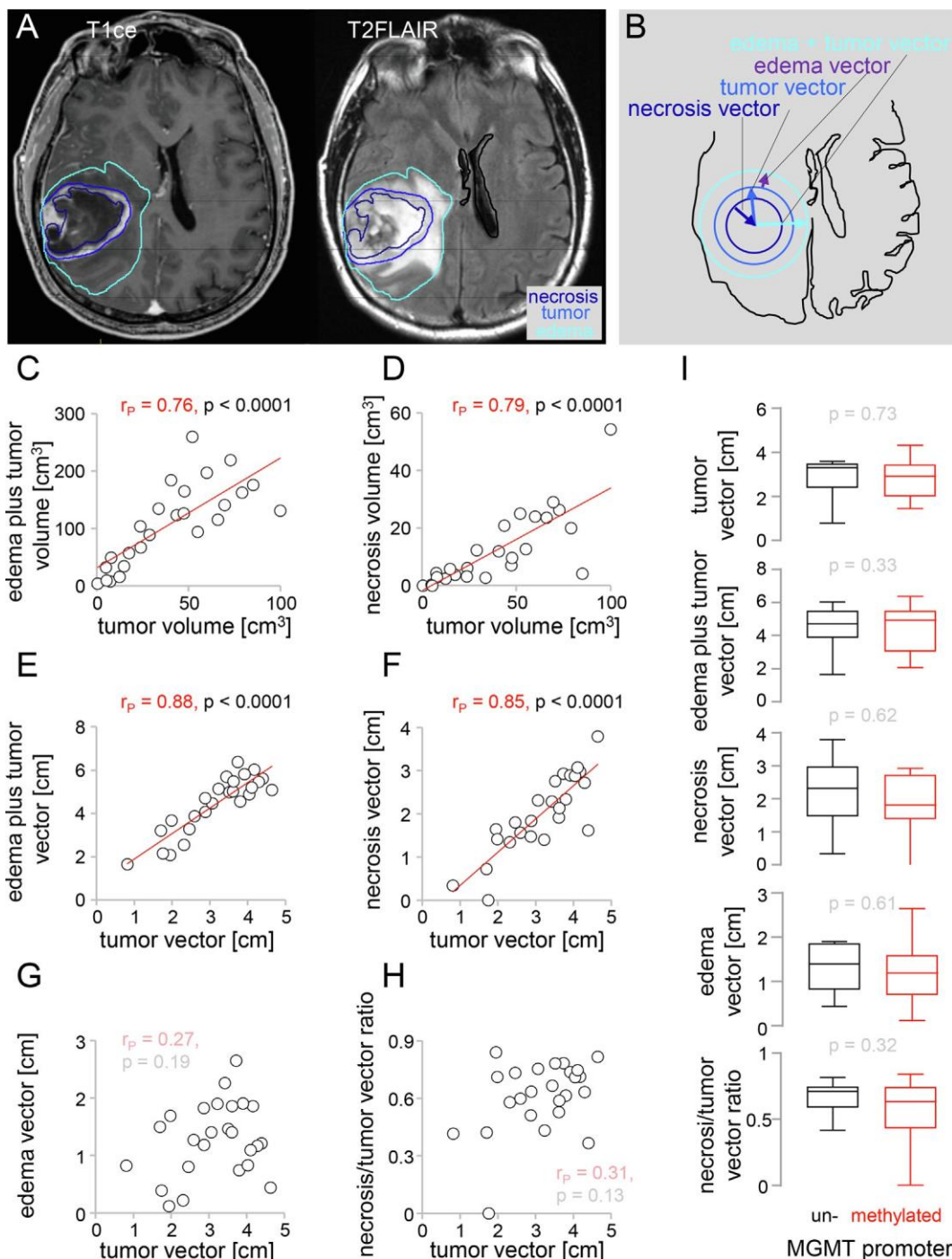
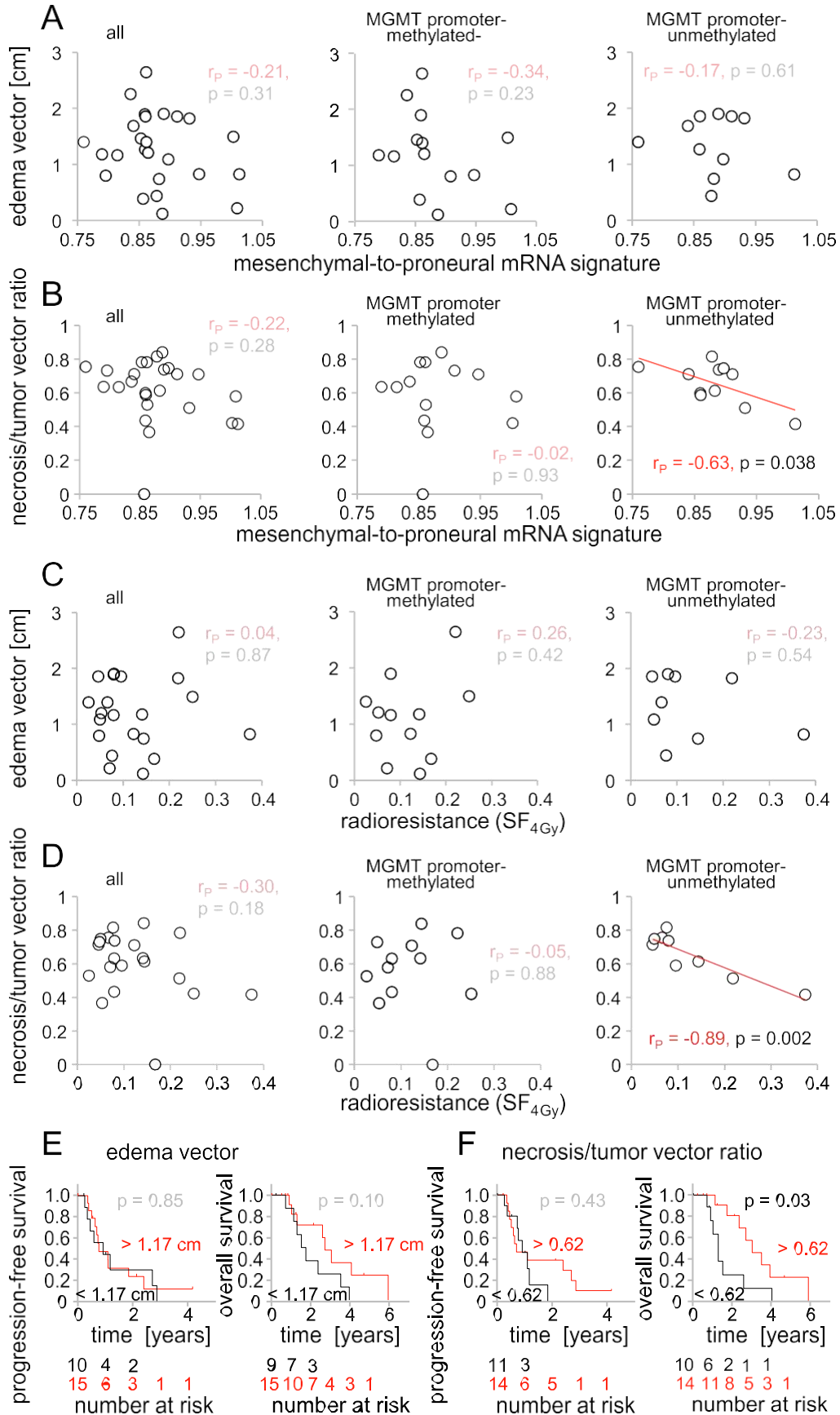


Fig. 2. Volumes contoured on preoperative MR imaging were transformed to one-dimensional vectors and were correlated with each other as well as with MGMT promoter methylation status. Preoperative MR images (T1 weighted sequence with contrast agent (T1ce) and T2FLAIR sequence) were imported to the radiation treatment planning system. A. Tumor volume was contoured as hyperintense volume on T1ce images. Necrosis was defined as hypointense volume on T1ce enclosed by the tumor volume. Edema was contoured as hyperintense volume on T2FLAIR images. B. In order to correlate the volumes with unidimensional cell movements, volume parameters were transformed to vectors representing the third root of the contoured volume. Edema plus tumor volume (C) as well as necrosis volume (D) correlated strongly with tumor volume (including necrosis). Even higher correlations were observed between edema plus tumor vector (E) or necrosis vector (F) with tumor vector. Edema vector (G) and necrosis/tumor vector ratio (H) did not significantly correlate with tumor vector. I. None of the volume parameters differed significantly between tumors with methylated and unmethylated MGMT promoter status. Red and black numbers indicate the coefficient of linear correlation and the error probability, respectively, as determined by Pearson correlation test.

In our study, volumetric features, vectors and ratios did not correlate with MGMT promoter methylation status. This is in line with the available literature. In a meta-analysis of 753 patients in 10 studies, MR features seemed to have the potential to predict MGMT promoter methylation status. However, in addition to

edema, diffusion and perfusion imaging (not analyzed in our cohort) showed the best predictive value [28]. Most published studies predicting MGMT promoter methylation status from MR imaging used radiomics approaches [29–31] or special MR sequences such as amide proton transfer-weighted CEST-MRI





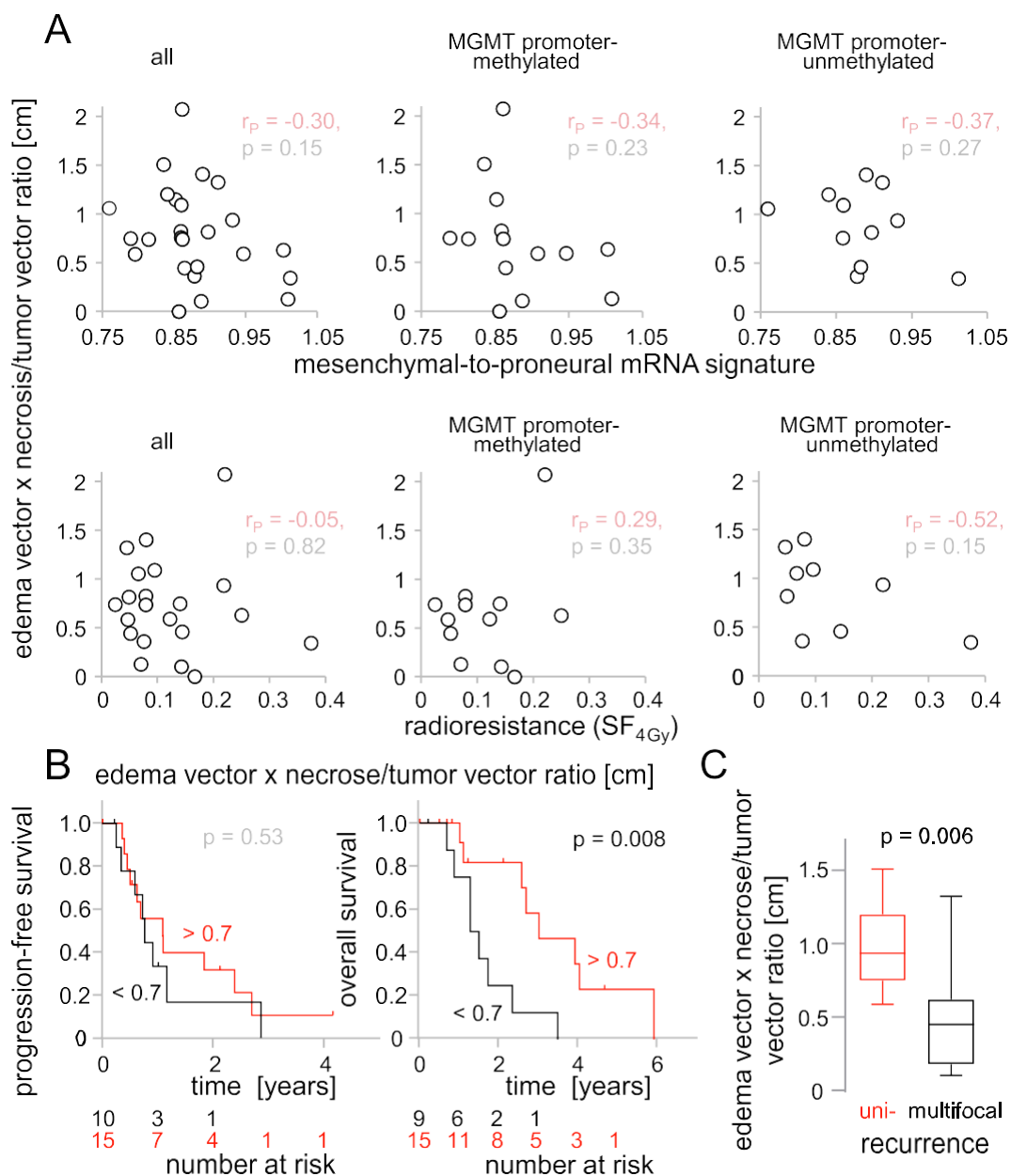


Fig. 4. A complex imaging index (edema vector x necrosis/tumor vector ratio,  $ind_{MR}$ ) is prognostic for OS and recurrence pattern of the whole patient cohort. A. The edema vector x necrosis/tumor vector ratio index ( $ind_{MR}$ ) associates weakly (and non-significantly) with the mesenchymal-to-proneural mRNA signature in the whole glioblastoma patient cohort and in patients with MGMT-methylated tumors but not the cohort of MGMT unmethylated tumors. No correlations were found between  $ind_{MR}$  and radioresistance in either patient cohort.  $ind_{MR}$  was not prognostic for PFS but for OS (B). Tumors recurring multifocally had significantly lower  $ind_{MR}$  compared to tumors recurring unifocally (C). Upper black numbers and lower black and red numbers in (B) indicate the error probability in log-rank test and the stratification threshold, respectively. Number in (C) indicates the error probability as calculated by Welch-corrected t-test.

[32]. Estimated PFS of our cohort was in line with published data with  $9.2 \pm 0.23$  months for a patient cohort with diverse clinical features and postoperative treatment schedules [33]. Methylated MGMT promoter status did not predict for a significantly better

PFS, but showed a trend to discriminate patients with better PFS and OS. As MGMT promoter methylation status is one of the best-known predictors of survival in glioblastoma [11,12], a lack of statistical significance due to small patient numbers and

3

Fig. 3. Necrosis/tumor vector ratio correlates with mesenchymal to proneural mRNA signature and radioresistance in MGMT promoter unmethylated tumors as well as overall survival. The edema vector did not correlate with the mesenchymal-to-proneural mRNA signature (A), or with the radioresistance (B) of the derived primary GSC cultures neither in the whole cohort, nor in glioblastoma with methylated or unmethylated MGMT promoter status. While there was no correlation between the mRNA signature (C) or the radioresistance (D) and the necrosis/tumor vector ratio in the whole cohort or in the cohort with methylated MGMT promoter status significant correlations occurred for tumors with unmethylated MGMT promoter. For the whole cohort edema vector showed a trend to statistical significance for OS but not for PFS (E), necrosis/tumor vector ratio had a significant influence on OS but not on PFS (F). Red and black numbers in (B) indicate the coefficient of linear correlation and the error probability, respectively, as determined by Pearson correlation test (A-D). Upper black numbers and lower black and red numbers in (E, F) indicate the error probability in log-rank test and the stratification threshold, respectively.

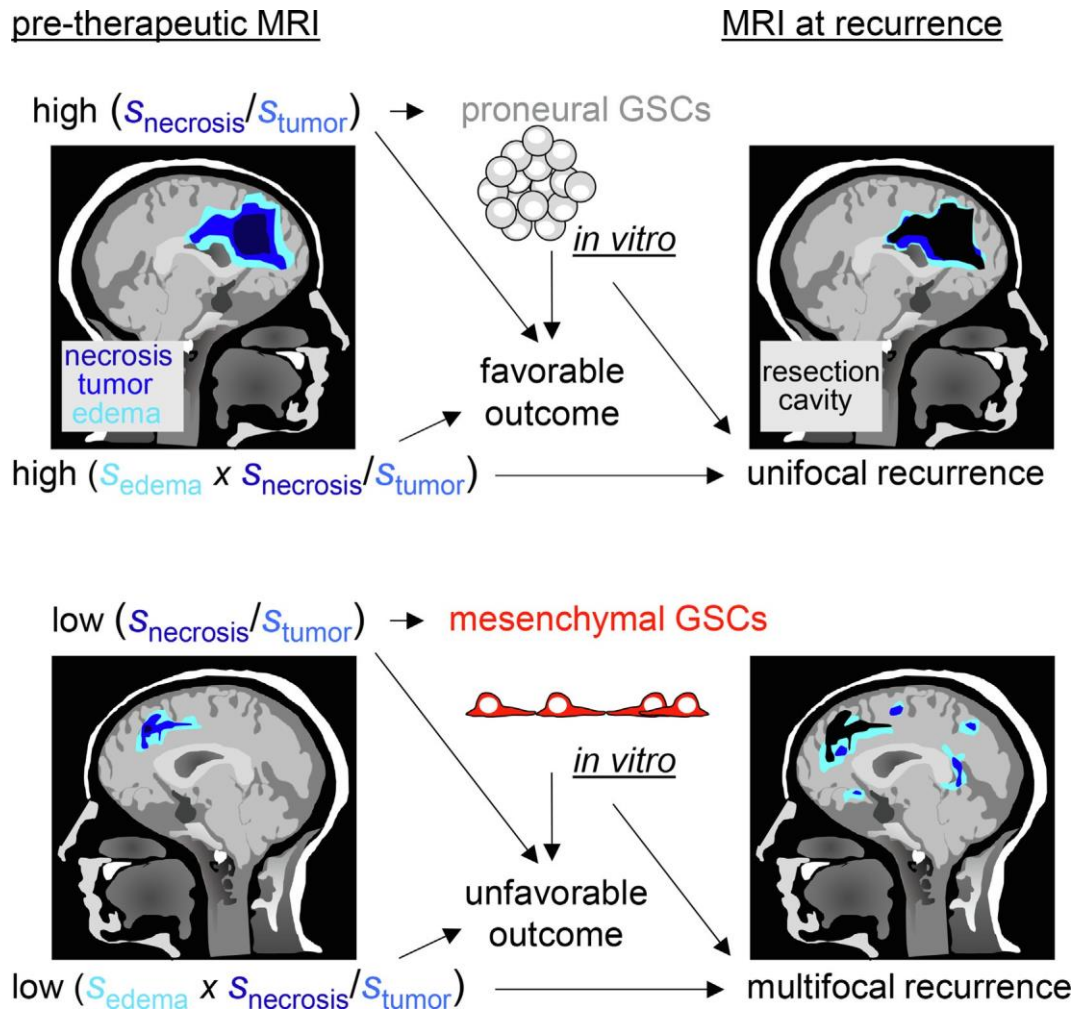


Fig. 5. Scheme depicting the prognostic/predictive value of the identified imaging parameters for molecular tumor features and patient prognosis.  $S_{necrosis}/S_{tumor}$ : necrosis/tumor vector ratio,  $S_{edema} \times S_{necrosis}/S_{tumor}$ : edema vector x necrosis/tumor vector ratio ( $ind_{MR}$ ).

heterogeneous treatment is assumed. In our analysis of the whole cohort, high necrosis/tumor vector ratio as well as high  $ind_{MR}$  predicted for better OS. In contrast, most imaging parameters were only able to predict for patient outcome in combination with clinical factors [34,35].

Imaging differences between tumors with methylated and unmethylated MGMT promoter have been described by several groups [28,36]. In conventional MR imaging glioblastoma with methylated MGMT promoters have been described to show less edema [37,38] and mixed-nodular contrast enhancing tumors [39]. Imaging analysis stratified by MGMT promoter methylation has been described for the diagnosis of pseudoprogression with a higher prognostic accuracy in the subgroup with methylated MGMT promoters [40]. In the present study, a correlation between necrosis/tumor vector ratio and mesenchymal-to-proneural molecular signature was only found in tumors with unmethylated MGMT promoters.

The described findings are in line with the biological properties of mesenchymal versus proneural glioblastoma stem cells as analyzed for the same patient cohort [24] and others [41]. The pronounced necrosis in proneural tumors might be associated with a less invasive phenotype and more solid growth pattern [42].

Higher  $ind_{MR}$  combining edema, necrosis and tumor volume parameters was associated with better overall survival as well as unifocal recurrences. The reduced PFS in patients with radioresistance

might also be explained by the radioresistance of mesenchymal stem cell subtypes and the known fact that patients with mesenchymal glioblastoma subtypes display a poorer prognosis [43].

## Conclusions

Volumetric MR image analysis of simple parameters is feasible in all cases with clinical standard imaging. In this small and exploratory cohort, volumetric MR parameters correlated with molecular and biological features of stem cell enriched cultures derived from the tumors of the respective patients. A possible explanation might be more invasive growth and infiltration of normal brain tissue as described for mesenchymal glioblastoma subtype (Fig. 5). MR parameters also correlated with patient outcome. Thus, volumetric analysis of standard MRIs might be useful to predict molecular and radiobiological stem cell characteristics of IDH-wildtype glioblastoma (especially with unmethylated MGMT promoter status) as well as patient outcome.

## Funding

F. Eckert was partly supported by the Gesellschaft fuer KinderKrebsforschung. The project was supported by the Deutsche

Krebshilfe (grants 70,112,872 and 70113144) and the Deutsche Forschungsgemeinschaft (grants EC 575/2–1; HU 781/7–1).

### Conflicts of interest

FE, FP, EH have research and educational grants from Elekta, Philips, Siemens, Dr. Sennewald GmbH. FE received speaker's fees of Dr. Sennewald GmbH. BB is co-founder, CTO and shareholder of AIRamed GmbH. DZ has research and educational grants from Elekta, Philips, Siemens, Sennewald, Therapanacea and Kaikuu. GT advisory boards (Bayer, Boehringer Ingelheim, CureVac), as a consultant (Bayer, Boehringer Ingelheim, CureVac), as steering committee member in non-interventional trials (Bayer, Novocure) and financial compensation for all these activities was provided as institutional funding to the University Hospital Tübingen.

### CRedit authorship contribution statement

Franziska Eckert: Conceptualization, Investigation, Writing – original draft, Writing – review & editing. Katrin Ganser: Methodology, Investigation, Resources, Data curation, Writing – review & editing. Benjamin Bender: Resources, Writing – review & editing. Jens Schittenhelm: Resources, Investigation, Writing – review & editing. Marco Skardelly: Resources, Writing – review & editing. Felix Behling: . Ghazaleh Tabatabai: Resources, Writing – review & editing. Elgin Hoffmann: Resources, Writing – review & editing. Daniel Zips: Resources, Writing – review & editing. Stephan M. Huber: Methodology, Formal analysis, Investigation, Visualization, Supervision, Writing – review & editing. Frank Paulsen: Conceptualization, Investigation, Resources, Supervision, Writing – review & editing.

### Declaration of Competing Interest

The authors declare that they have no known competing financial interests or personal relationships that could have appeared to influence the work reported in this paper.

### References

- [1] Shukla G et al. Advanced magnetic resonance imaging in glioblastoma: a review. *Chin Clin Oncol* 2017;6:40.
- [2] Kruser TJ et al. NRG brain tumor specialists consensus guidelines for glioblastoma contouring. *J Neurooncol* 2019;143:157–66.
- [3] Niyazi M et al. ESTRO-ACROP guideline “target delineation of glioblastomas”. *Radiother Oncol* 2016;118:35–42.
- [4] Fathi Kazerooni A et al. Imaging signatures of glioblastoma molecular characteristics: A radiogenomics review. *J Magn Reson Imaging* 2020;52:54–69.
- [5] Migliozi S et al. *Integrative multi-omics networks identify PKCδ and DNA-PK as master kinases of glioblastoma subtypes and guide targeted cancer therapy*. *Nat Cancer* 2023.
- [6] Suter Y et al. Radiomics for glioblastoma survival analysis in pre-operative MRI: exploring feature robustness, class boundaries, and machine learning techniques. *Cancer Imaging* 2020;20:55.
- [7] Louis DN et al. The 2016 World Health Organization Classification of Tumors of the Central Nervous System: a summary. *Acta Neuropathol* 2016;131:803–20.
- [8] Ohgaki H, Kleihues P. The definition of primary and secondary glioblastoma. *Clin Cancer Res* 2013;19:764–72.
- [9] Pekmezci M et al. Adult infiltrating gliomas with WHO 2016 integrated diagnosis: additional prognostic roles of ATRX and TERT. *Acta Neuropathol* 2017;133:1001–16.
- [10] Reuss DE et al. ATRX and IDH1-R132H immunohistochemistry with subsequent copy number analysis and IDH sequencing as a basis for an “integrated” diagnostic approach for adult astrocytoma, oligodendroglioma and glioblastoma. *Acta Neuropathol* 2015;129:133–46.
- [11] Hegi ME et al. MGMT gene silencing and benefit from temozolomide in glioblastoma. *N Engl J Med* 2005;352:997–1003.
- [12] Binabaj MM et al. The prognostic value of MGMT promoter methylation in glioblastoma: A meta-analysis of clinical trials. *J Cell Physiol* 2018;233:378–86.
- [13] Malmström A et al. Temozolomide versus standard 6-week radiotherapy versus hypofractionated radiotherapy in patients older than 60 years with glioblastoma: the Nordic randomised, phase 3 trial. *Lancet Oncol* 2012;13:916–26.
- [14] Perry JR et al. Short-course radiation plus temozolomide in elderly patients with glioblastoma. *N Engl J Med* 2017;376:1027–37.
- [15] Herrlinger U et al. Lomustine-temozolomide combination therapy versus standard temozolomide therapy in patients with newly diagnosed glioblastoma with methylated MGMT promoter (CeTeG/NOA-09): a randomised, open-label, phase 3 trial. *Lancet* 2019;393:678–88.
- [16] Capper D et al. DNA methylation-based classification of central nervous system tumours. *Nature* 2018;555:469–74.
- [17] Phillips HS et al. Molecular subclasses of high-grade glioma predict prognosis, delineate a pattern of disease progression, and resemble stages in neurogenesis. *Cancer Cell* 2006;9:157–73.
- [18] Verhaak RG et al. Integrated genomic analysis identifies clinically relevant subtypes of glioblastoma characterized by abnormalities in PDGFRA, IDH1, EGFR, and NF1. *Cancer Cell* 2010;17:98–110.
- [19] Fedele M et al. Proneural-mesenchymal transition: Phenotypic plasticity to acquire multitherapy resistance in glioblastoma. *Int J Mol Sci* 2019;20.
- [20] Shahar T et al. Percentage of mesenchymal stem cells in high-grade glioma tumor samples correlates with patient survival. *Neuro Oncol* 2017;19:660–8.
- [21] Orzan F et al. A simplified integrated molecular and immunohistochemistry-based algorithm allows high accuracy prediction of glioblastoma transcriptional subtypes. *Lab Invest* 2020;100:1330–44.
- [22] Stepanaitis G et al. Glioblastoma molecular classification tool based on mRNA analysis: From wet-lab to subtype. *Int J Mol Sci* 2022;23.
- [23] Kickingeder P et al. Radiomic subtyping improves disease stratification beyond key molecular, clinical, and standard imaging characteristics in patients with glioblastoma. *Neuro Oncol* 2018;20:848–57.
- [24] Ganser K et al. Patient-individual phenotypes of glioblastoma stem cells are conserved in culture and associate with radioresistance, brain infiltration and patient prognosis. *Int J Cancer* 2022;150:1722–33.
- [25] Ellingson BM et al. Consensus recommendations for a standardized Brain Tumor Imaging Protocol in clinical trials. *Neuro Oncol* 2015;17:1188–98.
- [26] Palpan Flores A et al. Assessment of pre-operative measurements of tumor size by MRI methods as survival predictors in wild type IDH glioblastoma. *Front Oncol* 2020;10:1662.
- [27] Curtin L et al. Shape matters: morphological metrics of glioblastoma imaging abnormalities as biomarkers of prognosis. *Sci Rep* 2021;11:23202.
- [28] Suh CH et al. Clinically relevant imaging features for MGMT promoter methylation in multiple glioblastoma studies: A systematic review and meta-analysis. *AJNR Am J Neuroradiol* 2018;39:1439–45.
- [29] Kanas VG et al. Learning MRI-based classification models for MGMT methylation status prediction in glioblastoma. *Comput Methods Programs Biomed* 2017;140:249–57.
- [30] Levner J et al. Predicting MGMT methylation status of glioblastomas from MRI texture. *Med Image Comput Assist Interv* 2009;12:522–30.
- [31] Li ZC et al. Multiregional radiomics features from multiparametric MRI for prediction of MGMT methylation status in glioblastoma multiforme: A multicentre study. *Eur Radiol* 2018;28:3640–50.
- [32] Jiang S et al. Discriminating MGMT promoter methylation status in patients with glioblastoma employing amide proton transfer-weighted MRI metrics. *Eur Radiol* 2018;28:2115–23.
- [33] Kelly C et al. Estimating progression-free survival in patients with glioblastoma using routinely collected data. *J Neurooncol* 2017;135:621–7.
- [34] Brancato V et al. Predicting survival in glioblastoma patients using diffusion MR imaging metrics-A systematic review. *Cancers (Basel)* 2020;12.
- [35] Burth S et al. Clinical parameters outweigh diffusion- and perfusion-derived MRI parameters in predicting survival in newly diagnosed glioblastoma. *Neuro Oncol* 2016;18:1673–9.
- [36] Faghani S et al. A comparison of three different deep learning-based models to predict the MGMT promoter methylation status in glioblastoma using brain MRI. *J Digit Imaging* 2023.
- [37] Ellingson BM et al. Anatomic localization of O6-methylguanine DNA methyltransferase (MGMT) promoter methylated and unmethylated tumors: a radiographic study in 358 de novo human glioblastomas. *Neuroimage* 2012;59:908–16.
- [38] Li WB et al. Relationship between magnetic resonance imaging and molecular pathology in patients with glioblastoma multiforme. *Chin Med J (Engl)* 2011;124:2589–92.
- [39] Eoli M et al. Methylation of O6-methylguanine DNA methyltransferase and loss of heterozygosity on 19q and/or 17p are overlapping features of secondary glioblastomas with prolonged survival. *Clin Cancer Res* 2007;13:2606–13.
- [40] Yoon RG et al. Different diagnostic values of imaging parameters to predict pseudoprogression in glioblastoma subgroups stratified by MGMT promoter methylation. *Eur Radiol* 2017;27:255–66.
- [41] Behnan J, Finocchiaro G, Hanna G. The landscape of the mesenchymal signature in brain tumours. *Brain* 2019;142:847–66.
- [42] Orteni B et al. Cancer stem cell contribution to glioblastoma invasiveness. *Stem Cell Res Ther* 2013;4:18.
- [43] Stanzani E et al. Radioresistance of mesenchymal glioblastoma initiating cells correlates with patient outcome and is associated with activation of inflammatory program. *Oncotarget* 2017;8:73640–53.



**K<sub>Ca</sub> channel targeting impairs DNA repair and invasiveness of patient-derived glioblastoma stem cells in culture and orthotopic mouse xenografts.**

Katrin Ganser<sup>1</sup>, Nicolai Stransky<sup>1,2</sup>, Tayeb Abed<sup>1</sup>, Leticia Quintanilla-Martinez<sup>3</sup>, Irene Gonzalez-Menendez<sup>3</sup>, Ulrike Naumann<sup>4</sup>, Pierre Koch<sup>5</sup>, Marcel Krueger<sup>6</sup>, Peter Ruth<sup>2</sup>, Stephan M. Huber<sup>1\*</sup>, and Franziska Eckert<sup>1,7</sup>

<sup>1</sup>Department of Radiation Oncology, University Hospital of Tübingen, Germany

<sup>2</sup>Department of Pharmacology, Toxicology and Clinical Pharmacy, Institute of Pharmacy, University of Tübingen, Germany

<sup>3</sup>Institute of Pathology and Neuropathology, Comprehensive Cancer Center, Eberhard Karls University of Tübingen, 72076 Tübingen, Germany and Cluster of Excellence iFIT (EXC 2180) "Image-Guided and Functionally Instructed Tumor Therapies", Eberhard Karls University, Tuebingen, Germany

<sup>4</sup>Molecular Neurooncology, Hertie Institute for Clinical Brain Research and Center Neurology, University of Tübingen, 72076 Tübingen, Germany


<sup>5</sup>Department of Pharmaceutical/Medicinal Chemistry II, Institute of Pharmacy, University of Regensburg, 93040 Regensburg, Germany

<sup>6</sup>Department of Preclinical Imaging and Radiopharmacy, Werner Siemens Imaging Center, University of Tübingen, Germany

<sup>7</sup>Department of Radiation Oncology, Medical University Vienna, AKH, Comprehensive Cancer Center, Vienna, Austria

**Running Title:** IK<sub>Ca</sub> and BK<sub>Ca</sub> targeting in glioblastoma therapy

**\*Correspondence to:** Stephan Huber, Department of Radiation Oncology, University Hospital of Tübingen, Hoppe-Seyler-Str. 3, 72076 Tübingen, Germany, Phone: +49 7071 29-

82183, Fax: +49 7071 29-4944, E-mail: stephan.huber@uni-tuebingen.de, ORCID  0000-0002-9430-8334

**Keywords.** glioma, BK<sub>Ca</sub>, IK<sub>Ca</sub>, orthotopic *xenograft* mouse model, ionizing radiation, TRAM-34, paxilline, DNA damage response, brain invasion,

**Article category.** Cancer Therapy and Prevention

**Novelty and Impact.** Here, we analyzed the radiosensitizing and anti-invasive effects of IK<sub>Ca</sub>- or BK<sub>Ca</sub>- targeting concomitant to glioblastoma irradiation. As model systems, patient-derived glioblastoma stem cell cultures with differing transcriptional profiles and thereof developed orthotopic glioma mouse models were used. As a result, pharmacological IK<sub>Ca</sub>- or BK<sub>Ca</sub>- targeting may radiosensitize and immobilize glioblastoma tumors *in vitro* and *in vivo*, and – due to the druggability of the two channels – might be translatable to future treatment of glioblastoma patients.

### Abbreviations

ALDH1A3	aldehyde dehydrogenase-1A3
BK <sub>Ca</sub>	Maxi-K Ca <sup>2+</sup> -activated potassium channel
DSBs	DNA double strand breaks
(p)GSC	(patient derived) glioblastoma stem cell
IDH	Isocitrate dehydrogenase
IK <sub>Ca</sub>	Intermediate conductance calcium-activated potassium channel
<i>KCNN4</i>	gene encoding IK channel protein
<i>KCNMA1</i>	gene encoding BK channel protein
MRI	magnetic resonance imaging
SF	survival fraction
TRAM-34	1-[(2-chlorophenyl)diphenylmethyl]-1H-pyrazole
γH2AX	phosphor-histone H2AX

## Abstract

Prognosis of glioblastoma patients is still poor despite multimodal therapy. The highly brain infiltrating growth in concert with a pronounced therapy resistance particularly of mesenchymal glioblastoma stem-like cells (GSCs) has been proposed to contribute to therapy failure. Recently, we have shown that a mesenchymal-to-proneural mRNA signature of patient derived GSC-enriched (pGSC) cultures associates with *in vitro* radioresistance and gel invasion. Importantly, this pGSC mRNA signature is prognostic for patients' tumor recurrence pattern and overall survival. Two mesenchymal markers of the mRNA signature encode for  $IK_{Ca}$  and  $BK_{Ca}$   $Ca^{2+}$ -activated  $K^+$  channels. Therefore, we analyzed here the effect of  $IK_{Ca}$ - and  $BK_{Ca}$ -targeting concomitant to (fractionated) irradiation on radioresistance and glioblastoma spreading in pGSC cultures and in pGSC-derived orthotopic *xenograft* glioma mouse models. To this end, *in vitro* gel invasion, clonogenic survival, *in vitro* and *in vivo* DNA double strand breaks (DSBs), tumor growth, and brain invasion were assessed in the dependence on tumor irradiation and  $K^+$  channel targeting. As a result, the  $IK_{Ca}$  and  $BK_{Ca}$  blocker TRAM-34 and paxilline, respectively, increased number of residual DSBs and (numerically) decreased clonogenic survival in some but not in all  $IK_{Ca}$ - and  $BK_{Ca}$ -expressing pGSC cultures, respectively. In addition,  $BK_{Ca}$  but not  $IK_{Ca}$  blockade slowed-down gel invasion *in vitro*. Moreover, systemic administration of TRAM-34 or paxilline concomitant to fractionated tumor irradiation increased in the *xenograft* model(s) residual number of DSBs and (numerically) attenuated tumor growth and glioblastoma brain invasion. We conclude, that  $K_{Ca}$  blockade concomitant to fractionated radiotherapy might be a promising new strategy in glioblastoma therapy.

## Introduction

Glioblastoma multiforme represents the most prevalent malignant primary brain tumor in adults. Standard therapy of newly diagnosed glioblastoma comprises tumor resection followed by irradiation (60 Gy in 30 fractions) with concomitant and maintenance temozolomide chemotherapy. Despite the multimodal therapy, prognosis of glioblastoma patients stays still poor with a median survival of below two years<sup>1</sup>. Multi-omics analyses of glioblastoma biopsies/resection specimens suggest various molecular subgroups which probably differ in patient prognosis and therapy response. In particular, classical, mesenchymal, proneural, and initially also neural subtypes have been distinguished by transcriptome analysis<sup>2-5</sup>.

Within these subtypes, several glioblastoma stem cell (GSC) phenotypes have been described recently that differ in their transcriptional profile<sup>5</sup>. In analogy to epithelial-to-mesenchymal transition as a proposed prerequisite for metastases of carcinomas, mesenchymal transition is thought to promote glioblastoma brain infiltration<sup>6</sup>. This assumption is corroborated by our previous studies<sup>7,8</sup> where in patient-derived GSC-enriched (pGSC) cultures a simple mesenchymal-to-proneural mRNA signature has been defined. Patient-derived GSCs with a mesenchymal mRNA signature exhibited *in vitro* higher invasiveness and higher radioresistance than proneural pGSC cultures. Strikingly, patients with glioblastomas that developed mesenchymal pGSCs had more often multifocal tumor recurrences and showed significantly worse clinical outcome than patients with proneural glioblastoma-derived pGSC cultures<sup>7,8</sup>. Along with aldehyde dehydrogenase-1A3 (ALDH1A3), a reported key marker of the mesenchymal stem-cell phenotype<sup>9</sup>, mesenchymal GSCs up-regulate two types of Ca<sup>2+</sup>-activated K<sup>+</sup> channels, IK<sub>Ca</sub> (IK, K<sub>Ca</sub>3.1, SK4, Gardos-channel, *KCNN4*) and BK<sub>Ca</sub> (BK, Maxi-K, K<sub>Ca</sub>1.1, Slo1, *KCNMA1*)<sup>8,10</sup>. Multiple lines of evidence suggest that IK<sub>Ca</sub> and BK<sub>Ca</sub> channels are also upregulated in further tumor entities classifying them as "oncochannels" (for review see<sup>11</sup>). Functionally, these channels



have been shown to play crucial roles in cell cycle control <sup>12</sup>, malignant progression <sup>13</sup>, tissue invasion <sup>14-17</sup>, distant metastasis <sup>18, 19</sup>, chemo- <sup>20, 21</sup> and radioresistance <sup>12, 22-24</sup> of cancer cells.

Hence, pharmacological IK<sub>Ca</sub>- or BK<sub>Ca</sub>-targeting might be a promising new strategy in cancer treatment and in particular in glioblastoma therapy. The latter suggestion is supported by the previous reports demonstrating that IK<sub>Ca</sub> inhibition by TRAM-34 (1-[(2-chlorophenyl)diphenylmethyl]-1H-pyrazole) or BK<sub>Ca</sub> blockade by paxilline may effectively impair radioresistance and tumor spreading in glioblastoma cell lines T98G <sup>14</sup>, U87MG, <sup>25</sup>, U521 <sup>23, 26</sup>, GL261 <sup>27</sup>, GL-15 <sup>28</sup> *in vitro* or in ectopic or orthotopic glioma *in vivo*-models <sup>12, 14, 17, 29</sup>.

Considering the proposed highly malignant and therapy-resistant phenotype of in particular mesenchymal GSCs and further the up-regulation of IK<sub>Ca</sub> and BK<sub>Ca</sub> K<sup>+</sup> channels by this glioblastoma GSC subpopulation <sup>8, 10</sup>, the present study aimed to define the feasibility, as well as the anti-invasive and radiosensitizing efficacy of pharmacological K<sup>+</sup> channel blockade in pGSC cultures and derived orthotopic *xenograft* mouse models.

## Material and Methods

Patient-derived glioblastoma stem (cell-like) cells (pGSCs) were grown from resection specimens of six patients with isocitrate dehydrogenase wildtype glioblastoma who underwent surgery at the Department of Neurosurgery, University of Tübingen, Germany, in the time from February to November, 2016. All pGSCs were authenticated in November/December 2021 using short tandem repeat (STR) profiling and unique STR profiles were obtained for all pGSCs<sup>8</sup> and regularly probed against mycoplasma by MycoAlert™ Mycoplasma Detection Kit (LT07-2108, Lonza, Cologne, Germany).

Meta-analysis of glioblastoma transcriptome- and clinical databases, Tübingen cohort of glioblastoma patients, pGSC culture conditions, irradiation and  $K_{Ca}$   $K^+$  channel targeting, RNA isolation and reverse-transcriptase polymerase chain reaction, calculation of the molecular mesenchymal-to-proneural mRNA signature, patch-clamp recording, analysis of residual DSBs, clonogenic survival, cell cycle and fibrin gel invasion *in vitro*, as well as establishment and monitoring of orthotopic pGSC *xenograft* glioma mouse models, fractionated tumor irradiation,  $K_{Ca}$  channel targeting, analysis of tumor growth, glioma brain infiltration and residual DSBs *in vivo*, and the applied statistics are described in detail in Part B of the Supplementary Material.

## Results

Initially, we queried several glioblastoma databases to analyse the dependence of patient survival on *KCNN4* and *KCNMA1* mRNA abundance in glioblastoma resection specimens (Fig. 1A). In particular, data from four databases were filtered for patients that received radiation therapy, stratified by the lower quartile of *KCNN4* (Fig. 1A, left) or *KCNMA1* (Fig. 1A, right) mRNA abundance, and pooled. In univariate testing, this meta-analysis suggested a prognostic value for *KCNN4* (Fig. 1A, left) but not for *KCNMA1* (Fig. 1A, right). Stratifying the glioblastoma patients of the Tübingen cohort <sup>7,8</sup> by the median *KCNN4* (Fig. 1B, left) or *KCNMA1* (Fig. 1B, right) mRNA abundance of the pGSC cultures, in contrast, showed that patients with both lower *KCNN4* or *KCNMA1* mRNA in the derived cultures exhibited longer median overall survival. Due to the observed high *KCNN4* or *KCNMA1* abundance of the glioma sub-cohort with shorter overall survival, we hypothesized that especially those patients with poor prognosis might benefit from K<sub>Ca</sub> channel drug targeting.

Fig. 1C depicts the basal *KCNN4* and *KCNMA1* mRNA abundances in a panel of 24 individual pGSCs from the Tübingen patient cohort <sup>7,8</sup> as determined by RT-PCR. IK<sub>Ca</sub> and BK<sub>Ca</sub> mRNA abundances varied considerably between the pGSCs. Two pGSC cultures with high *KCNN4* (LK7, LK13), two with high *KCNMA1* (LK12, LK28), as well as two with undetectable *KCNN4* and *KCNMA1* mRNA expression (LK19, LK39) were selected for further experiments (Fig. 1C, outlined in red). Reportedly, fractionated radiation may alter the mesenchymal-to-proneural mRNA signature of pGSCs that includes *KCNN4* and *KCNMA1* as mesenchymal markers <sup>8</sup>. In addition, pGSCs might compensate long-term blockages of one of the Ca<sup>2+</sup>-activated K<sup>+</sup> channels by upregulation of the other channel type. Therefore, we tested whether fractionated irradiation (5x 2 Gy in comparison to sham irradiation with 5x 0 Gy) and/or pharmacological IK<sub>Ca</sub> or BK<sub>Ca</sub> targeting induce alterations in the mRNA abundance of both channels. As shown in Suppl. Fig. S1A, neither fractionated irradiation nor IK<sub>Ca</sub> or BK<sub>Ca</sub> inhibition over 5 days elicited changes in *KCNN4* and *KCNMA1* mRNA

abundances. Likewise, the mesenchymal-to-proneural mRNA signature was not affected by fractionated radiation and channel targeting (Suppl. Fig. S1B) albeit in some (LK39 and LK12) pGSCs, fractionated irradiation combined with channel targeting induced minute changes of individual stem cell markers used to calculate the mRNA signature (Suppl. Fig. S2). Together, these data hinted to a maintenance of the individual GSC phenotype during the period of treatment.

To spot-check for functional expression of  $IK_{Ca}$  and  $BK_{Ca}$   $K^+$  channels in the plasma membrane of pGSCs, on-cell and whole-cell currents were recorded in LK13 (high  $IK_{Ca}$  expression) and LK28 (high  $BK_{Ca}$  expression) cells by the use of the patch-clamp technique. As a result, LK13 exhibited 1-EBIO (1-ethyl-1,3-dihydro-2H-benzimidazol-2-one, 200  $\mu$ M)-stimulated and TRAM-34 (1  $\mu$ M)-sensitive inwardly rectifying currents (Suppl. Fig.3). LK28, in contrast, showed voltage-dependent and paxilline (5  $\mu$ M)-sensitive outwardly rectifying currents that were generated by high conductance ( $\sim$ 200 pS) channels (Suppl. Figs. S4, S5). These properties were typical for those reported for  $IK_{Ca}$  and  $BK_{Ca}$ , respectively, confirming the functionality of these channels in the plasma membrane of pGSCs.

In experiments addressing the role of  $IK_{Ca}$  and  $BK_{Ca}$  in DNA damage response,  $IK_{Ca}$  blocker TRAM-34 was applied to pGSC cultures LK7, LK13 and LK39, while  $BK_{Ca}$  inhibitor paxilline was administered in LK12, LK19 and LK28 cultures (both inhibitors were dissolved at 0 or 5  $\mu$ M in DMSO) concomitant to fractionated radiation (5x 0 or 5x 2 Gy) during 5 consecutive days. Residual nuclear  $\gamma$ H2AX-foci as a surrogate marker of unfixed DSBs<sup>30</sup> were determined immunohistochemically (Suppl. Fig. S6) 24 h after the last radiation fraction. All data of LK12, LK19 and LK39 are given in the Supplementary Material). As shown in Fig. 1D, left, TRAM-34 alone induced in LK7 pGSCs a significant increase in the cell fraction with nuclear  $\gamma$ H2AX foci as compared to vehicle control, indicative of either increased formation or impaired repair of DSBs. Similarly, the TRAM-34 effect trended ( $p = 0.058$ ) in 5x 2 Gy-irradiated LK7 cells towards an increase in the  $\gamma$ H2AX foci-positive nucleus fraction. In LK13

(high  $IK_{Ca}$ , Fig 1D, middle) and in LK39 (low  $IK_{Ca}$ , Suppl. Fig. S7, right) pGSCs, in sharp contrast, TRAM-34 alone or in combination with fractionated irradiation did not affect residual  $\gamma$ H2AX foci. Notably, comparing the LK7 and LK13 data suggests that  $IK_{Ca}$  abundance alone is not sufficient to predict a TRAM-34 action on DSB formation/repair.

In LK12 (Suppl. Fig. S7, left) and LK28 (Fig. 1D, right) pGSCs (both with high  $BK_{Ca}$ ), paxilline treatment (5  $\mu$ M) alone significantly decreased the basal fraction of nuclei with  $\gamma$ H2AX foci as compared to vehicle control. In irradiated (5x 2 Gy) LK28 (Fig. 1D, right) but not in irradiated LK12 (Suppl. Fig. S7, left), paxilline application resulted in a significant increase in this fraction suggestive of an involvement of  $BK_{Ca}$  in radiogenic DSB formation or repair. Again,  $K_{Ca}$  expression was not predictive for this paxilline effect. In unirradiated and irradiated LK19 cells which lack  $BK_{Ca}$  expression, paxilline did not influence the fraction of nuclei with  $\gamma$ H2AX foci (Suppl. Fig. S7, left and middle).

To test whether an increase in residual DSB number by channel targeting translates into a diminished clonogenic survival of irradiated pGSCs, (pre-plated) limited dilution assays were performed with 0, 4, or 8 Gy single dose-irradiated cells co-incubated with TRAM-34 (0 or 5  $\mu$ M in LK7, LK13, and LK39) or paxilline (0 or 5  $\mu$ M in LK12, LK19, and LK28). Consistent with the observed inhibitor responses on residual DSB number, only LK7 (Fig. 1E, left) and in tendency ( $p = 0.11$ , Welch-corrected t-test) also LK28 (Fig. 1E, right) pGSCs were radiosensitized by TRAM-34 or paxilline, respectively. In contrast to these two pGSC cultures, the channel inhibitors did not exert radiosensitizing effects in highly  $IK_{Ca}$ -expressing LK13 (Fig. 1E, middle), highly  $BK_{Ca}$ -expressing LK12, and very low  $K_{Ca}$ -expressing LK19 and LK39 pGSCs (Suppl. Fig. S8).

Since activity of  $K^+$  channels reportedly may be required to execute cell cycle arrest in irradiated cancer cells<sup>12</sup>, the observed effects of TRAM-34 or paxilline on DNA repair and clonogenic survival of LK7 and LK28 might result from a pre-mature release from cell cycle

arrest. Therefore, we analyzed the effect of  $IK_{Ca}$  and  $BK_{Ca}$  blockade on DNA damage-induced cell cycle arrest in our pGSC cultures by flow cytometry. In particular, Nicoletti staining of DNA was performed 48 h after irradiation with a single dose of 0, 4, or 8 Gy. In addition, pGSCs were incubated 1 h prior to and until 48 h after irradiation with TRAM-34 (0 or 5  $\mu$ M, LK7, LK13, LK39) or paxilline (0 or 5  $\mu$ M, LK12, LK19, LK28). In all pGSCs but LK19, irradiation stimulated a dose-dependent accumulation in  $G_2$  phase of cell cycle independently of  $K_{Ca}$  channel targeting (Suppl. Fig. S9) consistent with a radiation-induced  $G_2/M$  cell cycle arrest. Only in LK13 and LK39, significant but minute effects of channel blockade on cell cycle distribution were apparent (Suppl. Fig. S9). Combined, these data suggest that impaired cell cycle regulation most probably does not underlie the radiosensitizing action of TRAM-34 and paxilline in LK7 and LK28 cells, respectively.

Next, we studied the effect of  $IK_{Ca}$ - and  $BK_{Ca}$ -targeting on invasion of the pGSC cultures. In particular, 3D fibrin gel invasion assays were performed in control (0 Gy) and irradiated (2 Gy) pGSCs in the presence of TRAM-34 or paxilline (0 or 5  $\mu$ M, each). We applied both inhibitors in all pGSC cultures independent of their *KCNN4* and *KCNMA1* mRNA abundances. Basal invasion as defined by increase in invasion area per day (Fig. 2A) or in maximal invasion distance per day (Fig. 2B) was highest in the most mesenchymal pGSC culture LK7 (Fig. 2, left), low in LK13, LK28 (Fig. 2, middle and right), and LK12 (Suppl. Fig. S10 left), and almost absent in LK 19 and LK39 (Suppl. Fig. S10, middle and right). TRAM-34 did not decrease invasion of control (0 Gy) or irradiated (2 Gy) pGSCs in either culture (Fig. 2 and Suppl. Fig. S10) except in unirradiated (0 Gy) LK7 cells (Fig. 2B). Paxilline, in contrast, decreased gel invasion in control and irradiated LK7 pGSCs (Fig. 2, left) and irradiated LK13 and LK28 GSCs (Fig. 2, middle and right) but not in LK12 (the latter two with high  $BK_{Ca}$  expression), and also not in LK19 or LK39 cells (both with low  $BK_{Ca}$  expression, Suppl. Fig. S10). Combined, the *in vitro* data on  $IK_{Ca}$ - or  $BK_{Ca}$ -expressing pGSC cultures revealed heterogeneity regarding radiosensitization and impairment of invasion by  $K_{Ca}$ -targeting.

To assess the feasibility and efficacy of K<sub>Ca</sub> channel targeting concomitant to fractionated tumor irradiation in *in vivo* models we *xenotransplanted* mesenchymal LK7 (high *KCNN4* mRNA abundance, TRAM-34-responsive), intermediate proneural/mesenchymal LK13 (high *KCNN4* and low *KCNMA1* mRNA abundance, TRAM-34-insensitive) and proneural LK28 (low *KCNN4* and high *KCNMA1* mRNA abundance, paxilline-responsive) pGSCs orthotopically in immunocompromised NSG mice as described previously<sup>14</sup>. A T2-weighted MRI sequence was established for detecting intracranial tumor growth at regular intervals. Specifically, tumor and edema localization in the brain was defined as hyperintense area in T2 weighted MR images. All three pGSCs developed orthotopic tumors (albeit with differing engraftment times) confirming their tumor-initiating capability (Fig. 3A and 3B left). Tumor formation was confirmed (immuno)histochemically as nuclei enriched area in standard hematoxylin/eosin staining (Fig. 3B, middle) and as human nucleolin-positive cells in immunohistochemistry (Fig. 3B, right). Upon detection of gliomas (1-5 months after transplantation), tumors were treated on five consecutive days with a daily radiation fraction of 0 or 4 Gy (5x 0 or 5x 4 Gy) concomitant to IK<sub>Ca</sub> or BK<sub>Ca</sub> targeting. To this end, TRAM-34 was injected intraperitoneally (5x 0 or 5x 120 mg/kg B.W.) into mice with LK7 and LK13 gliomas 6 h prior to the radiation fractions. Paxilline (10x 0 or 10x 8 mg/kg B.W.) was administered intraperitoneally to mice bearing LK28 gliomas 6 h prior and 6 h after the daily radiation fraction (Fig. 3A). For immunohistochemical analyses, mice were sacrificed 24 h after the last radiation fraction and the excised brains prepared for immunohistochemistry.

Since ALDH1A3 is upregulated in mesenchymal GSCs<sup>9</sup>, we analyzed the distribution of ALDH1A3 protein in mouse brain *xenografted* with pGSC LK7, LK13, and LK28 under control conditions (5x 0Gy, vehicle), in order to confirm the presence of mesenchymal GSCs in our glioma mouse models that can be targeted by IK<sub>Ca</sub> or BK<sub>Ca</sub> blockers. As shown in low magnification micrographs (Suppl. Fig. S11A) for LK7 *xenografts* (LK13 and LK28 tumors gave identical results, data not shown), ALDH1A3 immunoreactivity occurred in normal

tissue of hippocampus, cerebellum and midbrain. On cellular resolution, ALDH1A3 immunoreactivity was detected in the tumor infiltration areas (#), in glia-shaped cells (\*), and in blood vessels (§) (Suppl. Fig. S11B).

To distinguish between ALDH1A3-expressing glioblastoma and normal cells, colocalization of ALDH1A3, hNucleolin, Iba1 (ionized calcium-binding adapter molecule-1), and GFAP (glial fibrillary acidic protein) was analyzed using consecutive paraffin sections (Suppl. Fig. 11C-G). Cell populations were defined as mesenchymal GSCs (hNucleolin<sup>+</sup>/ALDH1A3<sup>+</sup>), glial differentiated tumor cells (hNucleolin<sup>+</sup>/GFAP<sup>+</sup>), microglia/macrophage (Iba1<sup>+</sup>), and astrocytes (hNucleolin<sup>-</sup>/GFAP<sup>+</sup>) (Suppl. Fig. S11H). The serial sections of Suppl. Fig. S11C-G suggest in LK7 *xenografts* that hNucleolin<sup>+</sup> cells formed about half of the tumor bulk cell mass and loosely scattered in the infiltration zone around the tumor. Although not valid to deduce cell types by multiple staining obtained from different series sections, the vast majority of glioblastoma cells (hNucleolin<sup>+</sup>) in Suppl. Fig. S11D coincided with a “glial differentiated” GFAP<sup>+</sup> phenotype (Suppl. Fig. S11H). The remaining cells of the tumor bulk probably were GFAP<sup>+</sup> astrocytes as deduced by their higher number as compared to the hNucleolin<sup>+</sup> cells in the series section. Iba1<sup>+</sup> microglia/macrophages and GFAP<sup>+</sup> astrocytes encapsulated the tumor bulk and an adjacent “edematous” area with low cell density. ALDH1A3 immunoreactivity was limited to few cells (red arrows in Suppl. Fig. S11H) in the tumor bulk, while it was prominent present in the outer Iba1-positive, hNucleolin-negative and GFAP-positive zone (Suppl. Fig. S11H).

To directly compare the number of mesenchymal ALDH1A3<sup>+</sup> GSCs between pGSC cultures and derived orthotopic *xenografts* by immunofluorescence microscopy, hNucleolin/ALDH1A3 double staining was applied. In the mesenchymal LK7 cells, numbers of ALDH1A3<sup>+</sup> in GSC culture (Fig. 4A, left) and in its derived tumors *xenografts* were similar. ALDH1A3<sup>+</sup> glioblastoma cells, in contrast, were absent in the intermediate proneural/mesenchymal LK13 (Fig. 4A, middle) and proneural LK28 (Fig. 4A, right) pGSC cultures but detectable upon



orthotopic *xenografting* (Fig. 4A, lower line). Combined, these immunohistological data pointed to a low abundance of mesenchymal GSCs (LK7) in both pGSC culture and orthotopic *xenografts*. In addition, it might hint to a mesenchymal progression of proneural GSCs by the mouse brain environment upon *xenografting*. Next, we analyzed the effect of IK<sub>Ca</sub> or BK<sub>Ca</sub> targeting concomitant to fractionated irradiation on glioblastoma brain invasion and residual DSBs *in vivo*.

Brain invasion of LK7, LK13 and LK28 glioblastoma cells was assessed by counting the number of hNucleosin<sup>+</sup> glioblastoma cells that had evaded from the tumor bulk and by determining the maximal distance of the evaded cells from the bulk surface (Fig. 4B) 24 h after end of the last irradiation fraction (5x 0 or 5x 4 Gy). As shown in Fig. 4C, basal (5x 0 Gy, vehicle) number of evaded glioblastoma cells per tumor area did not differ significantly (Dunn's multiple comparison test) between mesenchymal LK7, intermediate LK13, and proneural LK28 glioblastomas. Fractionated irradiation numerically increased this number (Fig. 4C) and also the maximal invasion distance (Fig. 4D) in LK13 and decreased both invasion parameters in LK7 and LK28 *xenografts*.

Albeit resulting in significant reductions of both invasion parameters only in LK13 tumors (Fig. 4C and D, middle), the combination of K<sub>Ca</sub> channel targeting and fractionated irradiation (5x 4 Gy) was associated in all three *xenografts* with lowest number of tumor bulk-evaded cells (except Fig. 4C, upper left) and shortest maximal invasion distance as well as smallest data scattering as compared to the other three treatment arms (Fig 4C, D) hinting at a reduction of glioblastoma spreading by concomitant K<sub>Ca</sub> targeting and fractionated irradiation. The fact that TRAM-34 apparently attenuated brain infiltration of LK13 *xenografts* while it did not inhibit gel invasion in LK13 pGSC cultures (compare Fig 2A, B, middle with Fig. 4C, D, middle) might again hint at a phenotypic transformation by the mouse brain environment.

To define the response of the GSC orthotopic *xenografts* to fractionated irradiation and/or  $K_{Ca}$  channel targeting, residual DSBs were analyzed in the tumor bulk by determining immunohistochemically number of residual  $\gamma$ H2AX foci 24 h after the last radiation fraction (Fig. 5A). In Fig. 5B, the histograms show the normalized distribution of foci number per nucleus while in Fig. 5C, the foci number per nucleus is depicted for all three *xenograft* models (LK7, LK13; LK28). Predictably, fractionated irradiation (5x 4 Gy) with or without concomitant  $K_{Ca}$  channel targeting led to an increase in number of residual  $\gamma$ H2AX foci per nuclei in all three models. Importantly, concomitant  $IK_{Ca}$  (LK7 and LK13) or  $BK_{Ca}$  (LK28) inhibition enhanced this effect, as already observed in LK28 and (in tendency) in LK7 pGSC cultures *in vitro* (Fig. 1C). Together, these  $\gamma$ H2AX data suggest an increased formation or impaired repair of DSBs by  $IK_{Ca}$ - or  $BK_{Ca}$ -targeting concomitant to fractionated radiation. Finally, we addressed in the LK7 *xenograft* model the potential therapeutic benefit of  $K_{Ca}$  channel targeting during radiotherapy.

Tumor bulk-surrounding edema has been demonstrated to include infiltrative tumor cells<sup>31</sup>. To calculate volumes of LK7 *xenografts*, the present study contoured tumor plus surrounding edema as defined by in hyperintense brain lesions in consecutive T2 weighted MRIs (Fig 6A). LK7 *xenografts* were imaged in regular intervals before and after treatment on five consecutive days (days 1-5) with fractionated tumor irradiation (5x 0 or 5x 2 Gy) and concomitant  $IK_{Ca}$  targeting (5x 0 or 5x 120 mg TRAM-34 /kg B.W. intraperitoneally, 6 h prior to the radiation fractions). For these long-term experiments, we decreased the radiation dose in order to minimize damaging of normal tissue (oral mucosa) because of the reported high radiosensitivity of NSG mice<sup>32</sup>.

Fig. 6B shows the volumes of tumor plus edema before, during (indicated by vertical grey line), and after application of all 4 treatment arms. Under control conditions (5x 0 Gy plus vehicle; Fig. 6B, 1<sup>st</sup> plot) tumor/edema volumes expanded exponentially. TRAM-34 treatment alone (5x 0 Gy plus TRAM-34) or fractionated radiation (5x 2 Gy plus vehicle) had no or only

little effect on volume expansion (Fig. 6B, 2<sup>nd</sup> and 3<sup>rd</sup> plot), while the combined treatment (5x 2 Gy plus TRAM-34; Fig. 6B, 4<sup>th</sup> plot) resulted in a pronounced – albeit insignificant ( $p = 0.16$ ) – delay in tumor growth as compared to the control arm. This is shown by Fig. 6C, where the slopes between day 0 and day 40 of the  $\log_{10}$ -transformed volume values are given for the individual tumors/edemas of the four treatment arms. The delay in tumor/edema growth in combined treated (5x 2 Gy plus TRAM-34) mice was apparent until day 40 after treatment start. Thereafter, tumor/edema volumes expanded in an accelerated manner and regained volumes similar to those of the other treatment arms (Fig. 6B, and not shown). Consistently, mouse survival (until reaching the termination criteria of animal experimentation) did not differ between the four treatment arms (Fig. 6D).

## Discussion

Multi-omics analysis of GBM resection specimens or biopsies suggests several molecular tumor sub-classes that have been proposed to differ in patient prognosis. Our approach was to define patient-individual tumor sub-classes by growing GSC-enriched cultures from GBM resection specimens. The recent molecular and functional characterization of these pGSC cultures suggests that i) the individual pGSCs differ in their mesenchymal-to-proneural mRNA signature, ii) this signature remains stable over several passages of the pGSC culture (and was in the present study also stable, even after fractionated irradiation and  $K_{Ca}$   $K^+$  channel targeting, see Suppl. Fig. S1C), iii) the signature correlates with the *in vitro* radioresistance and gel invasiveness, and most importantly, iv) the signature is prognostic for patients' tumor recurrence pattern and overall survival. The latter correlations might hint to the possibility that v) our pGSC culture conditions induce/select the most malignant tumor cell subpopulation that is limiting for the therapy response probably even in heterogenous tumors with mixed molecular sub-class profiles. Hence, it is tempting to speculate that the *in vitro* properties of the pGSC cultures can be used for patient stratification to individualized therapies <sup>8</sup>.

A potential new therapy strategy for the GBM patient subgroup that develops predominantly mesenchymal pGSC cultures with high  $IK_{Ca}$  and/or  $BK_{Ca}$  expression might be - at least in theory - the pharmacological targeting of  $K_{Ca}$   $K^+$  channels. In the present study, we selected six pGSC cultures from the Tübingen GBM cohort with differing  $IK_{Ca}$  and  $BK_{Ca}$  mRNA abundances (see Fig. 1C), differing mesenchymal-to-proneural mRNA signatures (see Suppl. Fig. S1, S2), and differing *in vitro* radioresistance (see Fig. 1 and Suppl. Fig. S7, S8) and gel invasion (see Fig. 2 and Suppl. Fig. S11) in order to mimic intertumoral GBM heterogeneity of the patients. Our *in vitro* experiments on DSBs, clonogenic survival and gel invasion suggested that  $K_{Ca}$ -targeting indeed may radiosensitize pGSC cultures and may attenuate gel invasion in some but not all pGSC cultures. Notably, high  $IK_{Ca}$  or  $BK_{Ca}$  mRNA

abundance alone was not predictive for this effect (see Fig. 1, 2 and Suppl. Fig. S7, S8, S11). In particular, the most mesenchymal (see Suppl Fig. S1B), most radioresistant (compare Fig 1E with Suppl. Fig. S8), most migratory (compare Fig 2 with Suppl. Fig. S10) LK7 pGSC culture with high  $IK_{Ca}$  and  $BK_{Ca}$  expression was radiosensitized by TRAM-34 and inhibited in invasion by paxilline and partly also by TRAM-34, while the intermediate proneural/mesenchymal LK13 cells with high  $IK_{Ca}$  but low  $BK_{Ca}$  expression was not radiosensitized by TRAM-34 but invasion-inhibited by paxilline. A further conclusion of these experiments was that also proneural (LK28) pGSCs may be targeted by  $BK_{Ca}$  channel inhibitors which might be due to the high  $KCNMA1$  mRNA abundance of this pGSC culture.

Upon *xenografting* three (LK7, LK13 and LK28) out of these six pGSC cultures orthotopically into immunocompromised mice,  $ALDH1A3^+/hNucleolin^+$  mesenchymal GSCs were detected not only in the mesenchymal LK7 *xenografts* but also in the tumors derived from the LK13 and LK28 pGSC cultures with more proneural molecular signatures (see Fig. 4A). This might suggest an induction of mesenchymal GSCs by the mouse brain microenvironment. One might speculate that this mesenchymal progression might have contributed to the transition of TRAM-34-insensitive LK13 pGSC cultures into TRAM-34-responding (see next paragraph) LK13 *xenografts* (TRAM-34 was not administered to LK28-bearing mice).

In LK7 and LK13 *xenografts*,  $IK_{Ca}$ -targeting with TRAM-34 concomitant to fractionated radiation did not only (at least numerically) impair tumor infiltration of the mouse brain but also increase number of residual DSBs more efficiently than irradiation alone, suggestive of a role of  $IK_{Ca}$  in brain invasion and DSB formation/repair. Likewise,  $BK_{Ca}$ -targeting with paxilline concomitant to fractionated irradiation tendentially inhibited brain infiltration and increased number of residual DSBs in proneural LK28 *xenografts* which – on the other hand – points to an involvement of  $BK_{Ca}$  in these two processes.

Both, BK<sub>Ca</sub> or IK<sub>Ca</sub> channel activity has been demonstrated previously to be required for basal or radiogenic glioblastoma cell migration<sup>25, 27, 29, 33-35</sup> in some but not all glioblastoma *in vitro* models and for (radiogenic) brain infiltration in orthotopic glioblastoma mouse models<sup>14, 17, 35</sup>. Moreover, pharmacological IK<sub>Ca</sub> targeting may reportedly radiosensitize glioblastoma cell lines *in vitro*<sup>12, 23</sup> and in ectopic xenografts<sup>12</sup>. Similarly, knock-down of IK<sub>Ca</sub> has been shown to radiosensitize breast cancer cells in a genetic tumor mouse model<sup>22</sup>.

Although the mode of action is ill-defined, the histological analysis of tumor spreading and residual DSBs of the present study suggests that concomitant IK<sub>Ca</sub> or BK<sub>Ca</sub> targeting might increase the therapeutic efficacy of fractionated glioblastoma radiation (see Fig. 4 and 5). As a matter of fact, concomitant TRAM-34 administration and fractionated tumor irradiation numerically delayed growth of LK7 xenografts in a transient manner (see Fig.6B, C). Due to accelerated repopulation of the TRAM-34 co-treated irradiated tumors 35 days after the end of treatment, mouse survival did not differ between the four treatment arms (see Fig. 6D). An effect on mouse survival of the here applied 10 Gy in 5 fractions, however, could not be expected as deduced from the clinical situation, where glioblastoma patients usually receive 60 Gy in 30 fractions.

In the present and our previous study<sup>12</sup>, TRAM-34 treatment alone had no effect on tumor plus edema volume (see Fig. 6C). This is in contrast to a previous report, where TRAM-34 administered (in identical daily doses as in our previous and present studies) from day 8 until day 16 after tumor transplantation significantly delayed tumor growth in the syngeneic orthotopic GL261/C57BL/6 glioma model<sup>36</sup>. Of note, the authors of the latter study proposed that the inhibitory effect on tumor growth of IK<sub>Ca</sub>-targeting is exerted by remodeling of the tumor immuno-microenvironment (see below) which can not be observed in immunocompromised mice used in the present study.

Our data on LK7 *xenograft* volumes did not prove statistically significant additive effects of fractionated irradiation and concomitant TRAM-34 administration (see Fig. 6C).

Nevertheless, they confirm feasibility of pharmacological  $IK_{Ca}$  targeting in the brain concomitant to fractionated radiation in orthotopic glioma mouse models. Likewise, TRAM-34 was well tolerated in a recent study of our group using the orthotopic SMA560/VM/Dk glioma mouse model<sup>17</sup> where TRAM-34 administered concomitantly to fractionated radiation blocked radiogenic tumor spreading and extended mouse survival. In patients, senicapoc, an  $IK_{Ca}$  inhibitor, has been well tolerated in clinical trials studying the effect of pharmacological  $IK_{Ca}$  channel targeting on sickle cell crisis<sup>37</sup>.

Like  $IK_{Ca}$ ,  $BK_{Ca}$  also seems to be druggable by, e.g., FDA-approved neuroleptics such as haloperidol or chlorpromazine which inhibit  $BK_{Ca}$  with low micromolar  $IC_{50}$ s<sup>38</sup>. Notably, these drugs reach  $BK_{Ca}$ -activity modulating concentrations in the brain<sup>39, 40</sup>. Ataxia or other movement disorders may be side effects of haloperidol or chlorpromazine and may involve  $BK_{Ca}$  inhibition in the cerebellum as shown for paxilline in mouse models<sup>41</sup>. A phase I dose escalation study is currently investigating the re-purposing of chlorpromazine adjuvant to radio-chemotherapy with temozolomide for the treatment of newly diagnosed glioblastoma (ClinicalTrials.gov identifier number NCT05190315) and will answer whether chlorpromazine therapy at putatively  $BK_{Ca}$ -inhibiting brain concentrations, in principle, is feasible in glioblastoma patients.

A possible therapeutically unwanted side effect of  $IK_{Ca}$  blockade might be impairment of the anti-glioblastoma immune response since immune cells including T cells and NK cells express  $IK_{Ca}$  channels. Importantly,  $IK_{Ca}$  has been proposed to regulate cell proliferation, differentiation, migration, and cytokine production in innate and adaptive immune systems (for review see: <sup>42</sup>). Saying that, it is surprising that  $IK_{Ca}$  blockage by TRAM-34 *in vivo* reportedly boosts tumor cell killing by a subpopulation of human natural killer lymphocytes<sup>43</sup>. Moreover, the already mentioned study by Grimaldi and colleagues<sup>36</sup> has demonstrated that

IK<sub>Ca</sub> targeting by TRAM-34 reversed the glioma-induced polarization of M/MΦ microglia/macrophages from an anti-inflammatory into an inflammatory phenotype. Similarly, TRAM-34 has been shown in the GL261-RFP / Cx3cr1GFP/WT glioma mouse model to convert the phenotype of tumor associated macrophages (TAMs) from a pro- into anti-tumor phenotype<sup>44</sup>. Furthermore, our recent study on SMA560 / VM/Dk mice did not observe inhibition of glioma infiltration by CD3<sup>+</sup>, CD8<sup>+</sup> or FoxP3<sup>+</sup> T cells associated with IK<sub>Ca</sub> targeting<sup>24</sup>. Combined, these few studies in syngeneic glioma mouse models might suggest that IK<sub>Ca</sub> targeting does not impair anti-glioma immune response.

In our *in vitro* experiments, only one of two highly IK<sub>Ca</sub>- or BK<sub>Ca</sub>-expressing pGSC cultures each, were radiosensitized by TRAM-34 or paxilline, respectively (see Fig. 1C, D and Suppl. Figs. S7 and S8), suggesting that, in contrast to our working hypothesis, high IK<sub>Ca</sub> or BK<sub>Ca</sub> mRNA abundance of the pGSC cultures does not necessarily predict responsiveness to K<sub>Ca</sub> channel targeting. Unexpectedly, the *in vitro* non-TRAM-34-responding LK13 pGSCs responded in the present study to TRAM-34 when orthotopically *xenografted* in NSC mice (see Fig. 1D, E, middle, Fig. 4C, D, middle and Fig. 5C, middle) which somehow questions the strategy that stratifies glioblastoma patients to second line therapies by the *in vitro* responsiveness of their pGSC cultures. Nevertheless, the fact that systemic administration of TRAM-34 or paxilline increased the number of residual DSBs of irradiated cells in all three *xenografts* models including our most mesenchymal LK7 glioblastoma proofs the concept of glioblastoma radiosensitization by concomitant pharmacological K<sub>Ca</sub> channel targeting.

In conclusion, our orthotopic *xenograft* models confirmed the feasibility and effectiveness of pharmacological targeting of the K<sub>Ca</sub> K<sup>+</sup> channels IK<sub>Ca</sub> and BK<sub>Ca</sub> *in vivo*. Given the druggability of both K<sub>Ca</sub> channel types by approved (or in clinical trials well tolerated) drugs, this therapy strategy might be translatable into adjuvant therapy of glioblastoma patients. Specifically, K<sub>Ca</sub> channel targeting might lower the malignancy of mesenchymal glioblastoma stem cells, thereby reducing glioblastoma spreading in the brain and sensitizing the tumor to



standard therapy. Prior to that, better markers in tumor resection specimens or derived pGSC cultures have to be defined in future preclinical studies to predict the responsiveness to adjuvant K<sub>Ca</sub> channel-targeted therapy in order to identify those glioblastoma patients that may benefit from this therapy strategy.

**Acknowledgements.** The authors thank Heidrun Faltin (from the Department of Radiation Oncology, University Hospital, Tübingen, Germany) for excellent technical assistance.

**Author Contributions.** The work reported in the paper has been performed by the authors, unless clearly specified in the text. *Conception and design:* KG, FE, PR, SMH. *Development of methodology:* KG. *Acquisition of data:* KG, IGM, TA, NS, SMH. *Analysis and interpretation of data:* KG, IGM, LQM, FE, MK, PR, SMH. *Writing, review, and/or revision of the manuscript:* all authors. *Administrative, technical, or material support:* MK, UN, PK. *Study supervision:* SMH. *Other (pathology review and analysis):* IGM, LQM

**Conflict of Interest.** Research and educational grants by Elekta, Philips, Siemens, Sennewald, Kaikuu, and TheraPanacea (FE). All other authors declare no competing interests.

**Data Availability Statement.** The datasets used or analyzed during the current study (Main Manuscript and Supplementary Material) are available from the corresponding author (SMH) on reasonable request. Analyzed public data sets are available under following links: The Cancer Genome Atlas (TCGA): <https://portal.gdc.cancer.gov/> (data download on 10.02.2020), The Ivy Glioblastoma Atlas Project (Ivy GAP): [https://glioblastoma.alleninstitute.org/api/v2/well\\_known\\_file\\_download/305873915](https://glioblastoma.alleninstitute.org/api/v2/well_known_file_download/305873915) (data download on 20.07.2023), Repository of Molecular Brain Neoplasia Data (REMBRANDT): <https://www.ncbi.nlm.nih.gov/geo/query/acc.cgi?acc=GSE108474> (data download on

20.07.2023), The Chinese Glioma Genome Atlas (CGGA):

<http://www.cgga.org.cn/analyse/RNA-data.jsp> (data download on 10.08.2021).

**Ethics Statement.** The use of patient data and glioblastoma resection material have been approved by the ethical review commission of the Faculty of Medicine, University of Tübingen, at the University Hospital Tübingen (project # 579/2015BO2 and BO2-2, 184/2015BO1). A written informed consent was obtained from all patients. Animal experiments were carried out according to the German animal protection law and approved by the local authorities (reference number of the Regierungspräsidium Tübingen: R13/18 G).

**Funding.** The project was supported by the German Cancer Aid (grants 70112872 and 70113144), the German Research foundation (grants EC 575/2-1 and HU 781/7-1), and by the Gesellschaft für Kinderkrebsforschung.

## References

1. Stupp R, Hegi ME, Mason WP, van den Bent MJ, Taphoorn MJB, Janzer RC, Ludwin SK, Allgeier A, Fisher B, Belanger K, Hau P, Brandes AA, et al. Effects of radiotherapy with concomitant and adjuvant temozolomide versus radiotherapy alone on survival in glioblastoma in a randomised phase III study: 5-year analysis of the EORTC-NCIC trial. *Lancet Oncol* 2009;**10**: 459-66.
2. Phillips HS, Kharbanda S, Chen R, Forrest WF, Soriano RH, Wu TD, Misra A, Nigro JM, Colman H, Soroceanu L, Williams PM, Modrusan Z, et al. Molecular subclasses of high-grade glioma predict prognosis, delineate a pattern of disease progression, and resemble stages in neurogenesis. *Cancer Cell* 2006;**9**: 157-73.
3. Verhaak RGW, Hoadley KA, Purdom E, Wang V, Qi Y, Wilkerson MD, Miller CR, Ding L, Golub T, Mesirov JP, Alexe G, Lawrence M, et al. Integrated Genomic Analysis Identifies Clinically Relevant Subtypes of Glioblastoma Characterized by Abnormalities in PDGFRA, IDH1, EGFR, and NF1. *Cancer Cell* 2010;**17**: 98-110.
4. Wang QH, Hu BL, Hu X, Kim H, Squatrito M, Scarpace L, deCarvalho AC, Lyu S, Li PP, Li Y, Barthel F, Cho HJ, et al. Tumor Evolution of Glioma-Intrinsic Gene Expression Subtypes Associates with Immunological Changes in the Microenvironment. *Cancer Cell* 2017;**32**: 42-+.
5. De Bacco F, Orzan F, Crisafulli G, Prelli M, Isella C, Casanova E, Albano R, Reato G, Erriquez J, D'Ambrosio A, Panero M, Dall'Aglio C, et al. Coexisting cancer stem cells with heterogeneous gene amplifications, transcriptional profiles, and malignancy are isolated from single glioblastomas. *Cell Rep* 2023;**42**: 112816.
6. Liu RZ, Choi WS, Jain S, Xu X, Elsherbiny ME, Glubrecht DD, Tessier AG, Easaw JC, Fallone BG, Godbout R. Stationary-to-migratory transition in glioblastoma stem-like cells driven by a FABP7-RXR $\alpha$  neurogenic pathway. *Neuro Oncol* 2023.
7. Eckert F, Ganser K, Bender B, Schittenhelm J, Skardelly M, Behling F, Tabatabai G, Stransky N, Hoffmann E, Zips D, Huber SM, Paulsen F. Potential of pre-operative MRI features in glioblastoma to predict for molecular stem cell subtype and patient overall survival. *Radiother Oncol* 2023: 109865.
8. Ganser K, Eckert F, Riedel A, Stransky N, Paulsen F, Noell S, Krueger M, Schittenhelm J, Beck-Wodl S, Zips D, Ruth P, Huber SM, et al. Patient-individual phenotypes of glioblastoma stem cells are conserved in culture and associate with radioresistance, brain infiltration and patient prognosis. *Int J Cancer* 2022;**150**: 1722-33.
9. Li GZ, Li YM, Liu X, Wang Z, Zhang CB, Wu F, Jiang HY, Zhang WL, Bao ZS, Wang YZ, Cai JQ, Zhao L, et al. ALDH1A3 induces mesenchymal differentiation and serves as a predictor for survival in glioblastoma. *Cell Death & Disease* 2018;**9**.

10. Klumpp L, Sezgin EC, Skardelly M, Eckert F, Huber SM. K(Ca)<sub>3.1</sub> Channels and Glioblastoma: In Vitro Studies. *Current Neuropharmacology* 2018;**16**: 627-35.
11. Ganser K, Klumpp L, Bischof H, Lukowski R, Eckert F, Huber SM. Potassium Channels in Cancer. *Handb Exp Pharmacol* 2021;**267**: 253-75.
12. Stegen B, Butz L, Klumpp L, Zips D, Dittmann K, Ruth P, Huber SM. Ca<sup>2+</sup>-Activated IK<sub>K</sub> Channel Blockade Radiosensitizes Glioblastoma Cells. *Mol Cancer Res* 2015;**13**: 1283-95.
13. Song P, Du Y, Song W, Chen H, Xuan Z, Zhao L, Chen J, Chen J, Guo D, Jin C, Zhao Y, Tuo B, et al. KCa<sub>3.1</sub> as an Effective Target for Inhibition of Growth and Progression of Intrahepatic Cholangiocarcinoma. *J Cancer* 2017;**8**: 1568-78.
14. Edalat L, Stegen B, Klumpp L, Haehl E, Schilbach K, Lukowski R, Kuhnle M, Bernhardt G, Buschauer A, Zips D, Ruth P, Huber SM. BK K<sup>+</sup> channel blockade inhibits radiation-induced migration/brain infiltration of glioblastoma cells. *Oncotarget* 2016;**7**: 14259-78.
15. Rosa P, Sforna L, Carlomagno S, Mangino G, Miscusi M, Pessia M, Franciolini F, Calogero A, Catacuzzeno L. Overexpression of Large-Conductance Calcium-Activated Potassium Channels in Human Glioblastoma Stem-Like Cells and Their Role in Cell Migration. *J Cell Physiol* 2017;**232**: 2478-88.
16. Catacuzzeno L, Franciolini F. Role of KCa<sub>3.1</sub> Channels in Modulating Ca<sup>2+</sup> Oscillations during Glioblastoma Cell Migration and Invasion. *Int J Mol Sci* 2018;**19**.
17. Stransky N, Ganser K, Quintanilla-Fend L, Gonzalez Menendez I, Naumann U, Eckert F, P. K, Huber SM, Ruth P. TRAM-34 inhibits irradiation-induced hyperinvasion of glioma cells and prolongs survival in the SMA-560 VM/Dk mouse model without impairing immune cell infiltration. (*unpublished observations*) 2023.
18. Khaitan D, Sankpal UT, Weksler B, Meister EA, Romero IA, Couraud PO, Ningaraj NS. Role of KCNMA1 gene in breast cancer invasion and metastasis to brain. *BMC Cancer* 2009;**9**: 258.
19. Rabjerg M, Olivan-Viguera A, Hansen LK, Jensen L, Sevelsted-Moller L, Walter S, Jensen BL, Marcussen N, Kohler R. High expression of KCa<sub>3.1</sub> in patients with clear cell renal carcinoma predicts high metastatic risk and poor survival. *PLoS One* 2015;**10**: e0122992.
20. D'Alessandro G, Grimaldi A, Chece G, Porzia A, Esposito V, Santoro A, Salvati M, Mainiero F, Ragozzino D, Di Angelantonio S, Wulff H, Catalano M, et al. KCa<sub>3.1</sub> channel inhibition sensitizes malignant gliomas to temozolomide treatment. *Oncotarget* 2016;**7**: 30781-96.
21. Pillozzi S, D'Amico M, Bartoli G, Gasparoli L, Petroni G, Crociani O, Marzo T, Guerriero A, Messori L, Severi M, Udisti R, Wulff H, et al. The combined activation of K(Ca)<sub>3.1</sub> and

- inhibition of K(v)11.1/hERG1 currents contribute to overcome Cisplatin resistance in colorectal cancer cells. *Br J Cancer* 2018;**118**: 200-12.
22. Mohr CJ, Gross D, Sezgin EC, Steudel FA, Ruth P, Huber SM, Lukowski R. KCa3.1 Channels Confer Radioresistance to Breast Cancer Cells. *Cancers (Basel)* 2019;**11**.
  23. Stegen B, Klumpp L, Misovic M, Edalat L, Eckert M, Klumpp D, Ruth P, Huber SM. K(+) channel signaling in irradiated tumor cells. *Eur Biophys J* 2016;**45**: 585-98.
  24. Stransky N, Ganser K, Naumann U, Huber SM, Ruth P. Tumoricidal, Temozolomide- and Radiation-Sensitizing Effects of K(Ca)3.1 K+ Channel Targeting In Vitro Are Dependent on Glioma Cell Line and Stem Cell Fraction. *Cancers* 2022;**14**.
  25. Steinle M, Palme D, Misovic M, Rudner J, Dittmann K, Lukowski R, Ruth P, Huber SM. Ionizing radiation induces migration of glioblastoma cells by activating BK K(+) channels. *Radiother Oncol* 2011;**101**: 122-6.
  26. Turner KL, Honasoge A, Robert SM, McFerrin MM, Sontheimer H. A proinvasive role for the Ca(2+) -activated K(+) channel KCa3.1 in malignant glioma. *Glia* 2014;**62**: 971-81.
  27. Ruggieri P, Mangino G, Fioretti B, Catacuzzeno L, Puca R, Ponti D, Miscusi M, Franciolini F, Ragona G, Calogero A. The inhibition of KCa3.1 channels activity reduces cell motility in glioblastoma derived cancer stem cells. *PLoS One* 2012;**7**: e47825.
  28. Fioretti B, Castigli E, Micheli MR, Bova R, Sciaccaluga M, Harper A, Franciolini F, Catacuzzeno L. Expression and modulation of the intermediate- conductance Ca2+-activated K+ channel in glioblastoma GL-15 cells. *Cell Physiol Biochem* 2006;**18**: 47-56.
  29. D'Alessandro G, Catalano M, Sciaccaluga M, Chece G, Cipriani R, Rosito M, Grimaldi A, Lauro C, Cantore G, Santoro A, Fioretti B, Franciolini F, et al. KCa3.1 channels are involved in the infiltrative behavior of glioblastoma in vivo. *Cell Death Dis* 2013;**4**: e773.
  30. Redon CE, Nakamura AJ, Zhang YW, Ji JJ, Bonner WM, Kinders RJ, Parchment RE, Doroshov JH, Pommier Y. Histone gammaH2AX and poly(ADP-ribose) as clinical pharmacodynamic biomarkers. *Clin Cancer Res* 2010;**16**: 4532-42.
  31. Hawkins-Daarud A, Rockne RC, Anderson AR, Swanson KR. Modeling Tumor-Associated Edema in Gliomas during Anti-Angiogenic Therapy and Its Impact on Imageable Tumor. *Front Oncol* 2013;**3**: 66.
  32. Shultz LD, Ishikawa F, Greiner DL. Humanized mice in translational biomedical research. *Nat Rev Immunol* 2007;**7**: 118-30.
  33. Sciaccaluga M, Fioretti B, Catacuzzeno L, Pagani F, Bertollini C, Rosito M, Catalano M, D'Alessandro G, Santoro A, Cantore G, Ragozzino D, Castigli E, et al. CXCL12-induced glioblastoma cell migration requires intermediate conductance Ca2+-activated K+ channel activity. *Am J Physiol Cell Physiol* 2010;**299**: C175-84.

34. Cuddapah VA, Turner KL, Seifert S, Sontheimer H. Bradykinin-induced chemotaxis of human gliomas requires the activation of KCa3.1 and ClC-3. *J Neurosci* 2013;**33**: 1427-40.
35. D'Alessandro G, Monaco L, Catacuzzeno L, Antonangeli F, Santoro A, Esposito V, Franciolini F, Wulff H, Limatola C. Radiation Increases Functional KCa3.1 Expression and Invasiveness in Glioblastoma. *Cancers (Basel)* 2019;**11**.
36. Grimaldi A, D'Alessandro G, Golia MT, Grössinger EM, Di Angelantonio S, Ragozzino D, Santoro A, Esposito V, Wulff H, Catalano M, Limatola C. KCa3.1 inhibition switches the phenotype of glioma-infiltrating microglia/macrophages. *Cell Death Dis* 2016;**7**: e2174.
37. Ataga KI, Smith WR, De Castro LM, Swerdlow P, Sauntharajah Y, Castro O, Vichinsky E, Kutlar A, Orringer EP, Rigdon GC, Stocker JW. Efficacy and safety of the Gardos channel blocker, senicapoc (ICA-17043), in patients with sickle cell anemia. *Blood* 2008;**111**: 3991-7.
38. Lee K, McKenna F, Rowe IC, Ashford ML. The effects of neuroleptic and tricyclic compounds on BKCa channel activity in rat isolated cortical neurones. *Br J Pharmacol* 1997;**121**: 1810-6.
39. Korpi ER, Kleinman JE, Costakos DT, Linnoila M, Wyatt RJ. Reduced haloperidol in the post-mortem brains of haloperidol-treated patients. *Psychiatry Res* 1984;**11**: 259-69.
40. Huang CL, Ruskin BH. DETERMINATION OF SERUM CHLORPROMAZINE METABOLITES IN PSYCHOTIC PATIENTS. *J Nerv Ment Dis* 1964;**139**: 381-6.
41. Sausbier U, Sausbier M, Sailer CA, Arntz C, Knaus HG, Neuhuber W, Ruth P. Ca<sup>2+</sup> - activated K<sup>+</sup> channels of the BK-type in the mouse brain. *Histochem Cell Biol* 2006;**125**: 725-41.
42. Ohya S, Kito H. Ca(2+)-Activated K(+) Channel K(Ca)3.1 as a Therapeutic Target for Immune Disorders. *Biol Pharm Bull* 2018;**41**: 1158-63.
43. Koshy S, Wu D, Hu X, Tajhya RB, Huq R, Khan FS, Pennington MW, Wulff H, Yotnda P, Beeton C. Blocking KCa3.1 channels increases tumor cell killing by a subpopulation of human natural killer lymphocytes. *PLoS One* 2013;**8**: e76740.
44. Massenzio F, Cambiaghi M, Marchiotta F, Boriero D, Limatola C, D'Alessandro G, Buffelli M. In vivo morphological alterations of TAMs during KCa3.1 inhibition-by using in vivo two-photon time-lapse technology. *Front Cell Neurosci* 2022;**16**: 1002487.

## Figures and Figure Legends

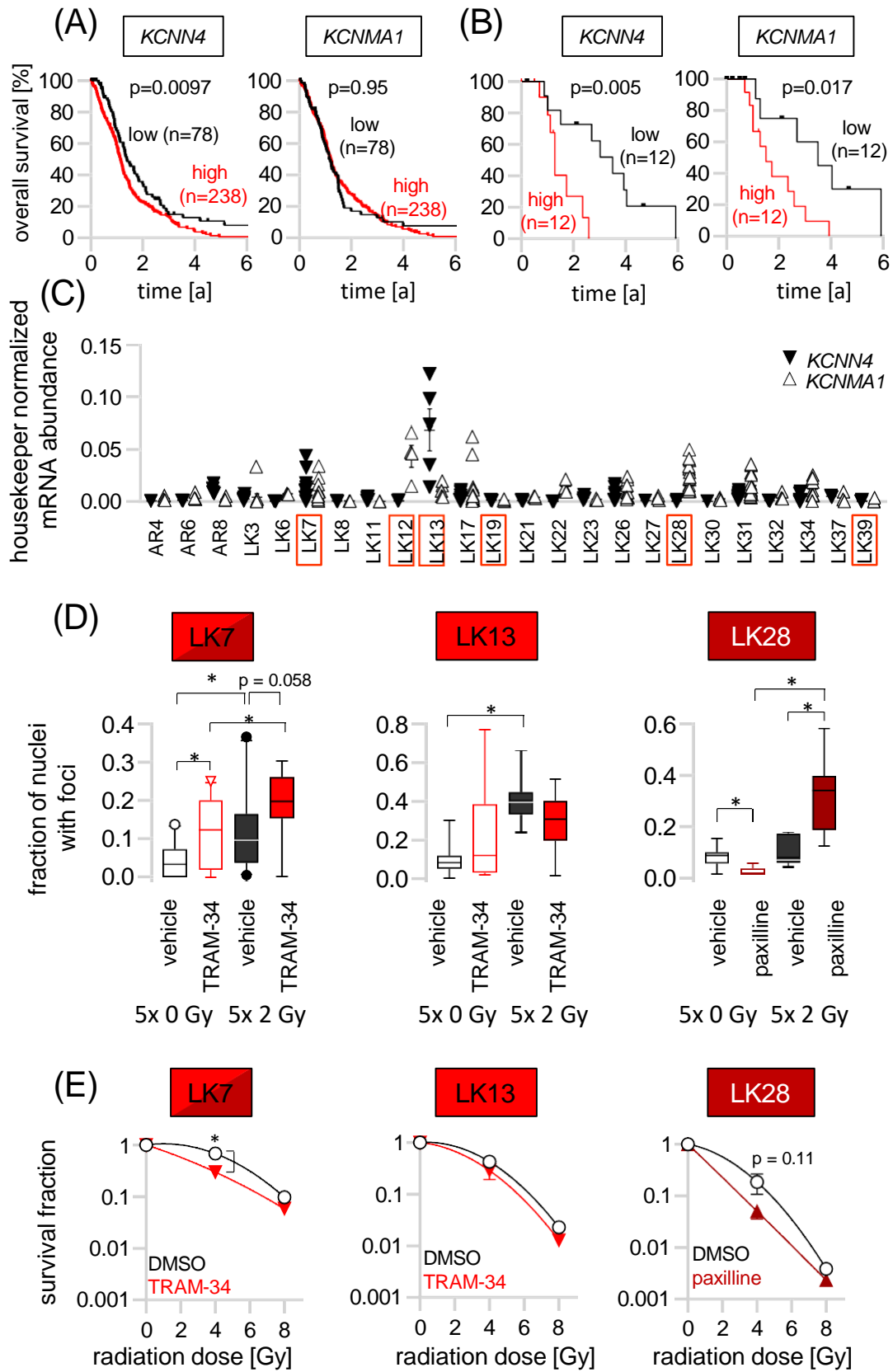


**Fig. 1.** Expression and functional significance of  $IK_{Ca}$  and  $BK_{Ca}$  channels in glioblastoma resection specimens and patient-derived cultures enriched in glioblastoma stem cells (pGSCs). **(A)** Overall survival of glioblastoma patients filtered for received radiation therapy and stratified by the upper quartile of *KCNN4* (left) and *KCNMA1* (right) mRNA abundance in glioblastoma resection specimens. For this meta-analysis, patient stratification was implemented separately for every database and data from 4 databases were pooled (for details see Data Availability Statement). **(B)** Overall survival of glioblastoma patients of the Tübingen cohort stratified by the median *KCNN4* (left) and *KCNMA1* (right) mRNA abundance in the patient-derived pGSC cultures (log-rank test). Univariate error probabilities ( $p$ ) of (A, B) were calculated by log-rank test. **(C)** Housekeeper-normalized *KCNN4* (inverted closed triangles) and *KCNMA1* (open triangles) mRNA abundances in pGSCs derived from the Tübingen glioblastoma patient cohort. Data are individual values and superimposed means ( $\pm$  SE  $n = 3-15$ ). Red boxes depict those pGSC cultures that were further analyzed in the present study. **(D)** Fraction of nuclei with residual nuclear  $\gamma$ H2AX foci 24 h after treatment on 5 consecutive days with  $K^+$  channel blockers TRAM-34 or paxilline (5x 0 or 5x 5  $\mu$ M, each) concomitant to fractionated irradiation (5x 0 or 5x 2 Gy) as indicated. Data (box plots with median and 5-95% whiskers,  $n = 15$  microscopic fields with 30-115 nuclei/field) are given for LK7 (left), LK13 (middle), and LK28 (right) pGSCs. For determination of nuclear  $\gamma$ H2AX foci by immunohistochemistry, 15 randomly chosen microscopic fields with 30-115 nuclei/field were analyzed in each of  $n = 3$  experiments. **(E)** Mean ( $\pm$  SE,  $n = 12-20$ ) survival fractions ( $S$ ) as determined by preplating limited dilution assay of irradiated (single dose ( $D$ ) of 0, 4, or 8 Gy) LK7 (left), LK13 (middle), and LK28 (pGSCs) pre-, co- and post-treated with TRAM-34 (LK7 and LK13) or paxilline (LK28) (0 or 5  $\mu$ M, each). \* indicates  $p \leq 0.05$  as calculated by Welch ANOVA- with Dunnett's T3 multiple comparison test or non-parametric Kruskal-Wallis- with Dunn's multiple comparison test, where appropriate, in **(D)** and (Welch-corrected) two-tailed t-test in **(E)**.



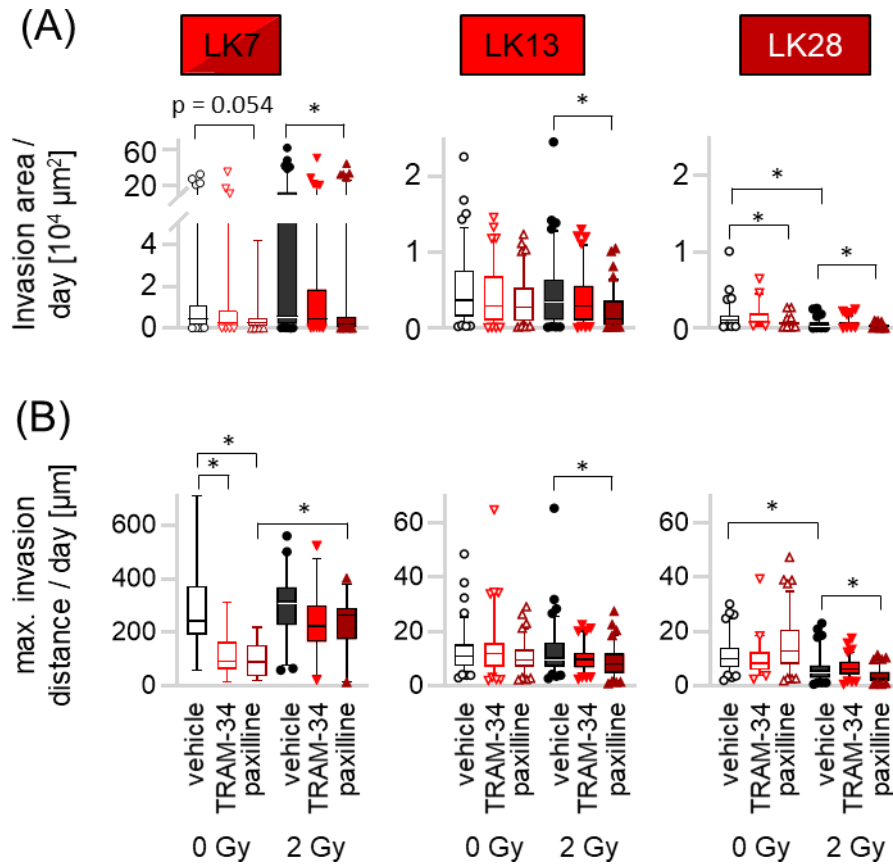


**Fig. 2.** BK<sub>Ca</sub> but not IK<sub>Ca</sub> targeting inhibits gel invasion of LK7 (left), LK13 (middle), and LK28 (right) pGSCs independently of BK<sub>Ca</sub> mRNA abundance. **(A, B)** Evasion of LK7 (left) LK13 (middle) and LK28 (right) glioblastoma cells from fibrin-imbbed spheres<sup>8</sup>. The increase in infiltrated sphere-surrounding area per day **(A)** and the maximal invasion velocity (maximal daily distance increase, **B**) were analyzed on days 0, 7, 14, and 24 after radiation (0 or 2 Gy) and co- and post treatment with TRAM-34 or paxilline (0 or 5  $\mu\text{M}$ , each). Pooled data are given as box plots with median and 5-95% whiskers (n = 30-90 spheres). \* indicates  $p \leq 0.05$ , as analyzed by non-parametric Kruskal-Wallis- with Dunn's multiple comparison test.

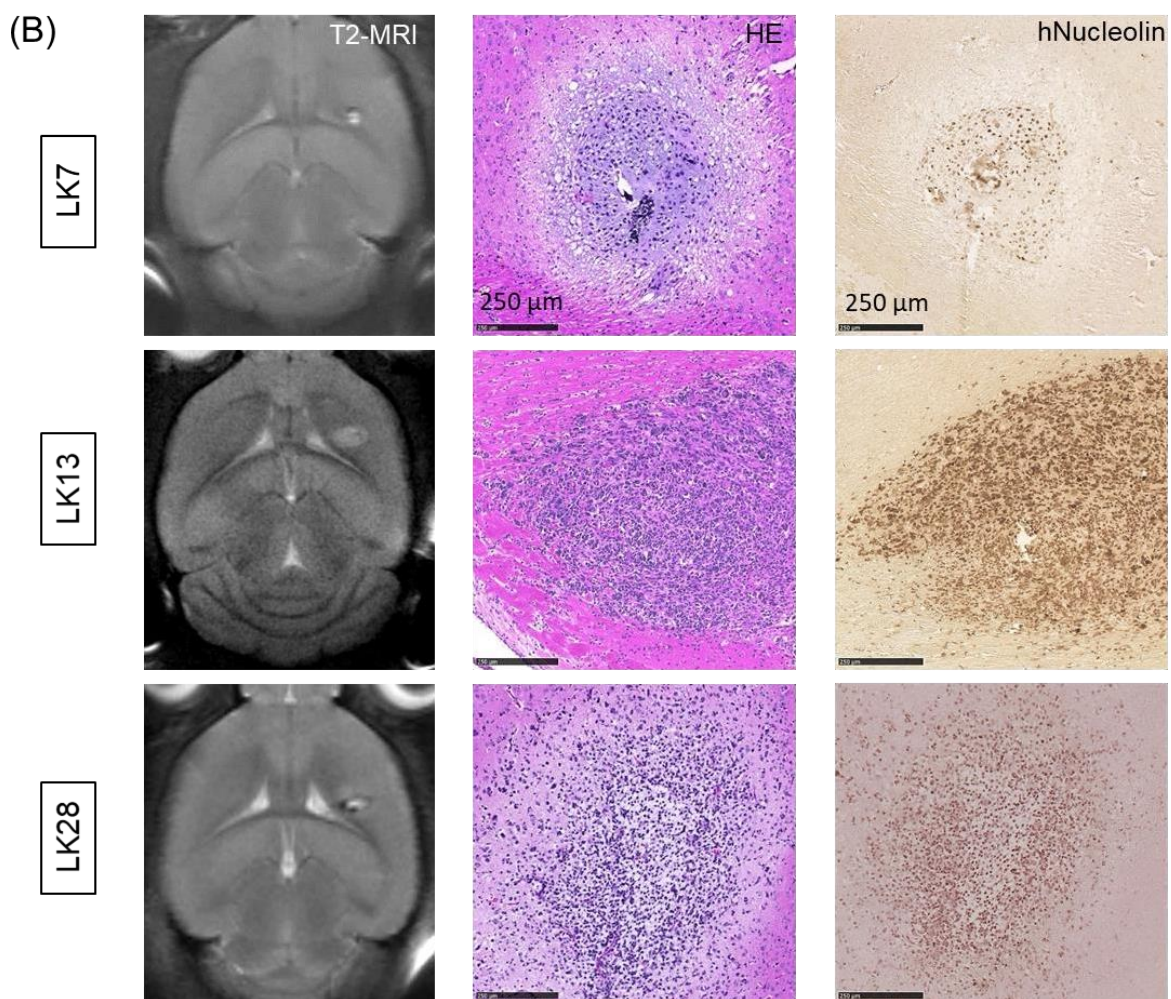
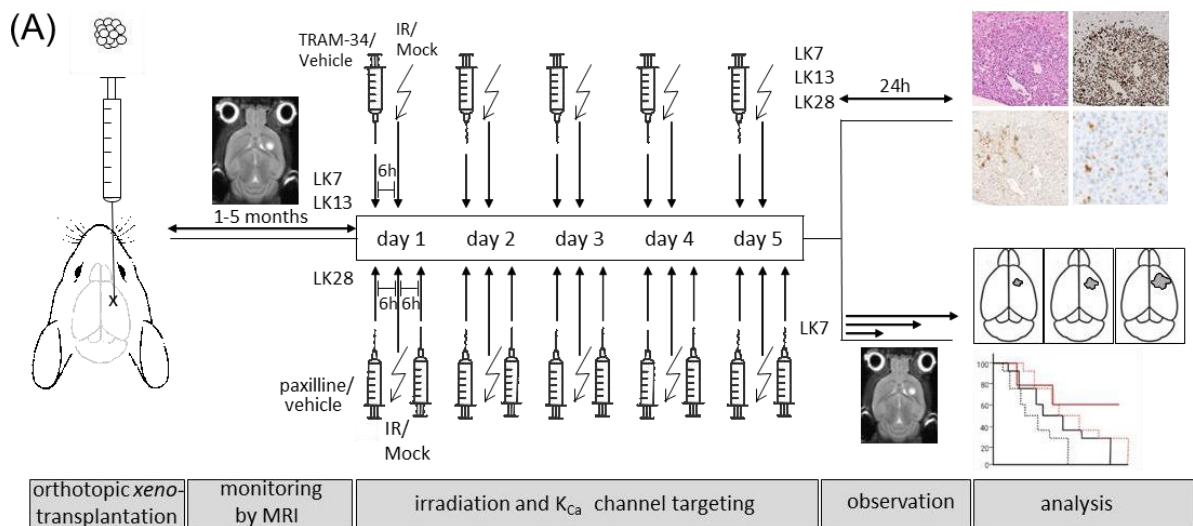


**Fig. 3.** Orthotopic GSC *xenograft* mouse models. (A) Scheme depicting generation of glioma mouse model and treatment protocols (for details see main text). (B) Identification of engrafted LK7 (top row), LK13 (middle row) and LK28 (bottom row) tumors by T2-weighted

MR imaging (left column), and corresponding histological analysis (middle and right columns). Hematoxylin/eosin staining (HE, middle) of brain paraffine sections show nuclei (blue)-rich tumor bulks that exhibited in immunohistochemistry hNucleolin immunoreactivity (brown) used as specific glioblastoma marker (right column).

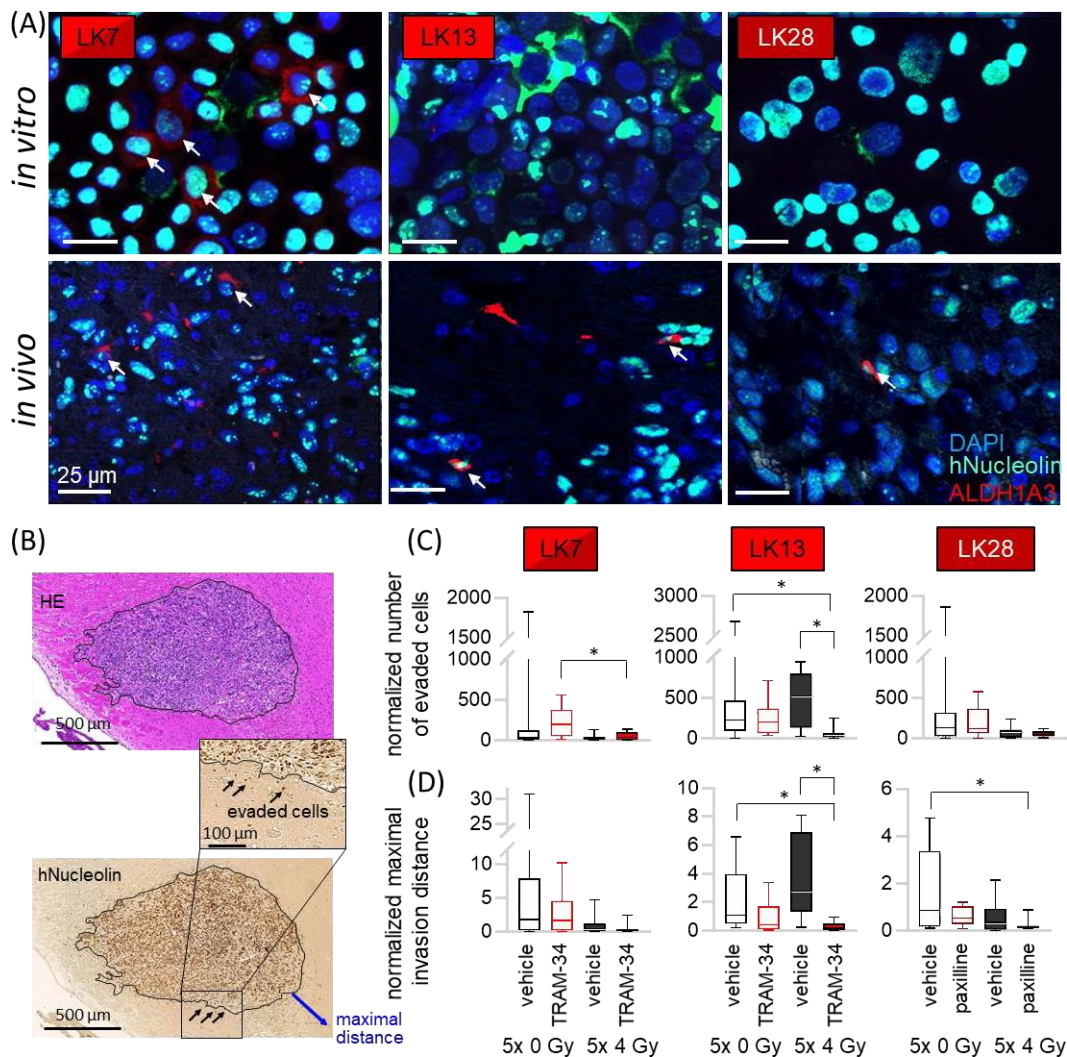


**Fig 4.** Brain spreading of GSC xenograft (**A**) Abundance of cells positive for the mesenchymal stem cell marker ALDH1A3 in LK7 (left), LK13 (middle) and LK28 (right) pGSC cultures (upper row) and upon *xenografting* into mouse brain (lower row) as indicated by white arrows. Shown are immunofluorescence micrographs of object slide-fixed singularized pGSC cells (upper row) and paraffine brain sections (lower row). Cells were double-probed against hNucleolin (green) and ALDH1A3 (red) as glioblastoma and mesenchymal markers, respectively. Nuclei were counterstained with DAPI (blue). hNucleolin was used to differentiate human cancer cells from murine cells in the *in vivo* setting. (**B**) Quantification of glioblastoma brain invasion. Tumor bulk was contoured in hematoxylin/eosin-stained paraffine sections (top) and the bulk-outline superimposed to a consecutive section that had been immunohistochemically probed against hNucleolin (bottom). The number and the

maximal invasion distance (blue arrow) of tumor bulk-evaded hNucleolin<sup>+</sup> cells (black arrows) were analyzed and normalized to the bulk area. **(C-D)** Box plots (with median and 5-95% whiskers, n = 8-12) depicting normalized number **(C)** and maximal distance **(D)** of LK7 (left), LK13 (middle), and LK28 (right) cells evaded from the tumor bulk as analyzed 24 h after the last radiation fraction (5x 0 or 5x 4Gy). Concomitant to fractionated irradiation mice received TRAM-34 (5x 0 or 5x 120 mg/kg B.W.) or paxilline (10x 0 or 10x 8 mg/kg B.W.) 6 h prior as well as 6 h after each radiation fraction, respectively. \* indicate  $p \leq 0.05$  as analyzed by non-parametric Kruskal-Wallis- with Dunn's multiple comparison test.



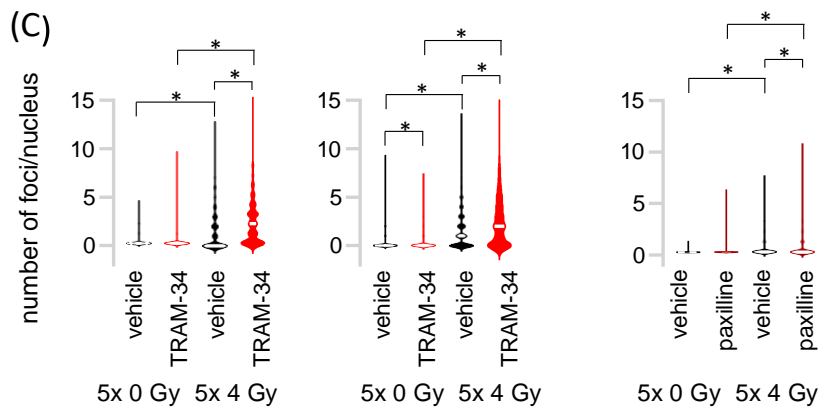
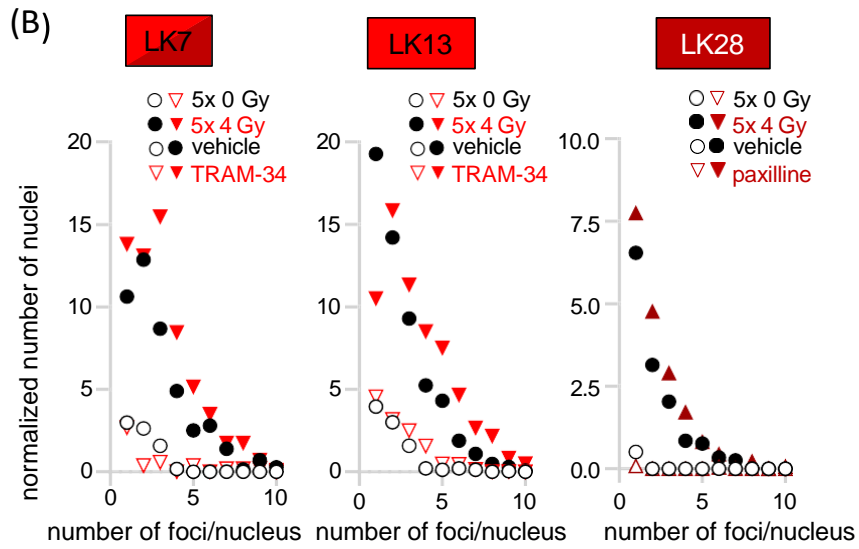
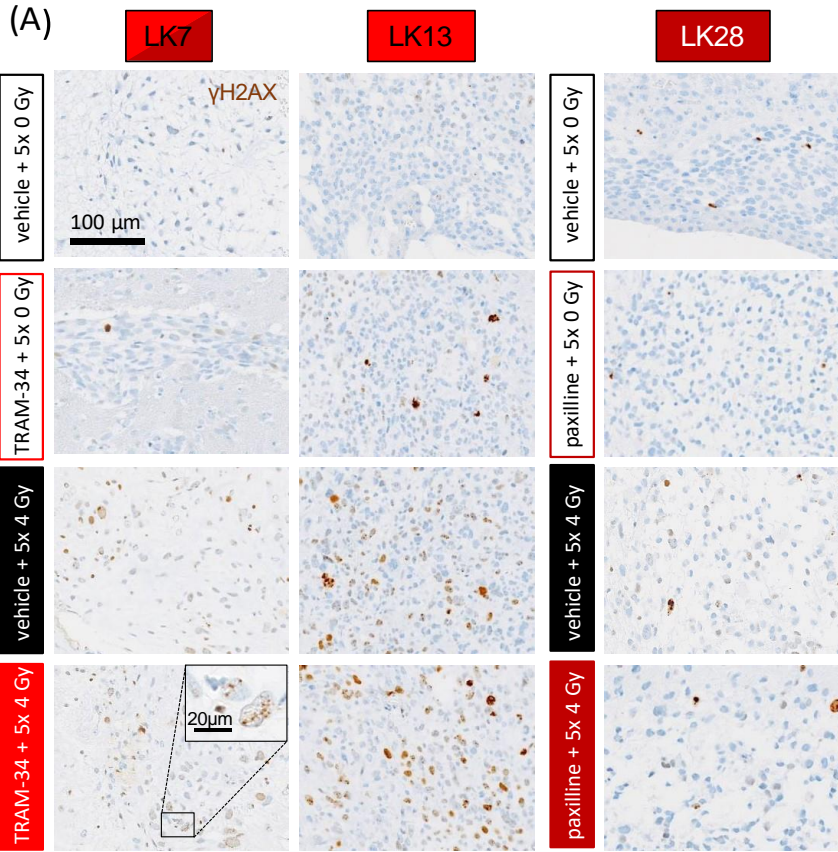


**Fig. 5.** K<sub>Ca</sub> channel targeting during fractionated tumor irradiation increases number of residual DNA DSBs in orthotopic GSC *xenografts*. **(A)** Representative micrographs of brain paraffine sections (5  $\mu$ m) probed against  $\gamma$ H2AX protein (brown) by immunohistochemistry. Nucleus (blue in hematoxylin counter-staining)-residing  $\gamma$ H2AX foci were counted 24 h after the last radiation fraction (5x 0 or 5x 4Gy). Concomitant to fractionated irradiation, mice received TRAM-34 (5x 0 or 5x 120 mg/Kg B.W.) 6 h prior or paxilline (10x 0 or 10x 8 mg/kg B.W.) 6 h prior as well as 6 h after each radiation fraction, respectively. **(B)** Histograms depicting the distribution of nuclear residual  $\gamma$ H2AX foci of all treatment arms (nuclei without foci were not plotted) recorded as in **(A)** in LK7, LK13 and LK28 *xenografts* (N = 3 tumors, each). Since absolute numbers of nuclei analyzed (n = 150-1864) differed between the treatment arms, data were scaled by setting maximal values to 100 nuclei. X-axis was cutted by 10 foci/nucleus since differences between treatment arms were no more visible at higher values. **(C)** Number of  $\gamma$ H2AX foci/nucleus (data from **(B)** including 0 focus/nucleus given as violin plots with medians as depicted by white lines, n = 519-2651 nuclei). \* indicates  $p \leq 0.05$  as analyzed by non-parametric Kruskal-Wallis- with Dunn's multiple comparison test.

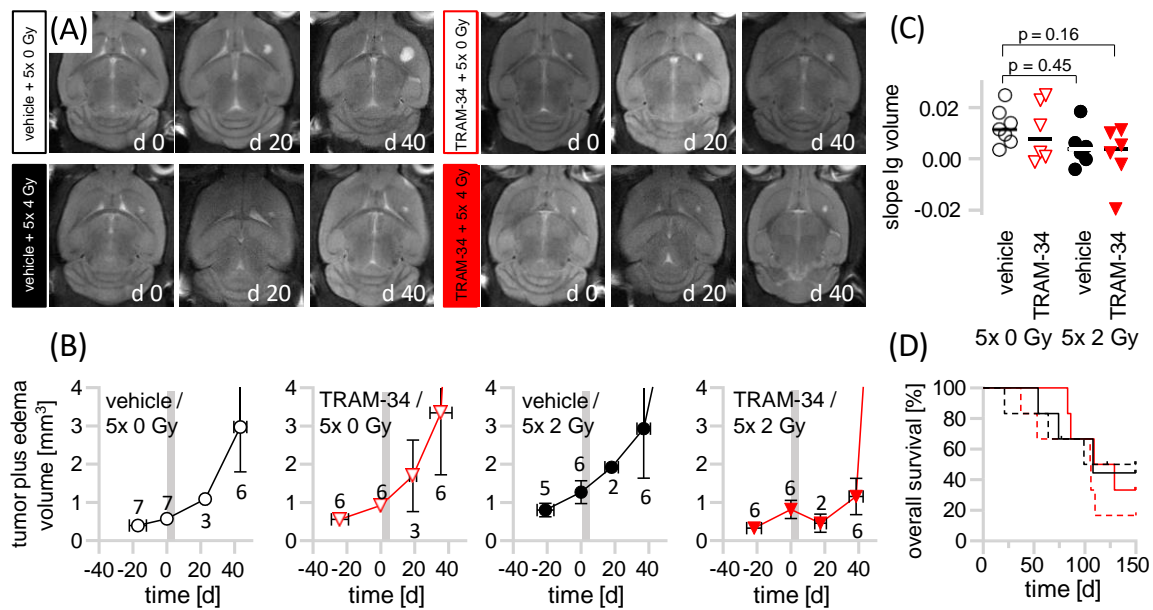


**Fig. 6.** Targeting of  $IK_{Ca}$  concomitant to fractionated radiation might delay growth of orthotopic GSC *xenografts*. **(A)** T2 weighted MR images of orthotopic LK7 *xenografts* (before, day -20, d0) and after (d20, d40) fractionated irradiation (5x 0 or 5x 2 Gy) and concomitant  $IK_{Ca}$  channel targeting with TRAM-34 (5x 0 or 5x 120 mg/kg B.W) on days 1-5, as indicated. **(B)** Time-dependent increase of LK7 *xenograft* (tumor plus edema) volume in all 4 treatment arms. Data are means  $\pm$  SE, 6-7 mice, each. Vertical grey bar shows the time interval of treatment. **(C)** Individual slopes (plus medians) of the increase in LK7 tumor plus edema volumes. Slopes were calculated for all 4 treatment arms from the  $\log_{10}$  (lg) volume values between day 0 and day 40 after treatment start. Error probability (p) values were calculated by ordinary ANOVA and Šídák's multiple comparisons post hoc test corrected for 4 pairwise comparisons. **(D)** Kaplan-Meier survival curves of LK7-challenged mice given for all 4 treatment arms (n = 6-7 mice each). 5x 0 Gy, 5x 2 Gy, vehicle and TRAM-34 treatments are symbolized by dashed, continuous, black and red line, respectively.

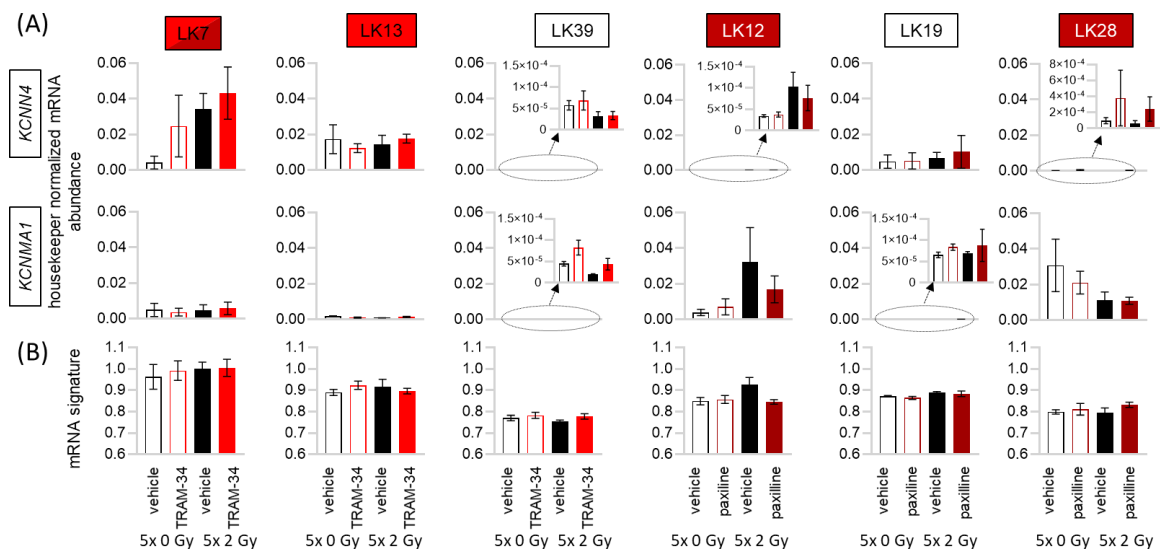


## Supplementary Material

### **K<sub>Ca</sub> channel targeting impairs DNA repair and invasiveness of patient-derived glioblastoma stem cells in culture and orthotopic mouse *xenografts*.**

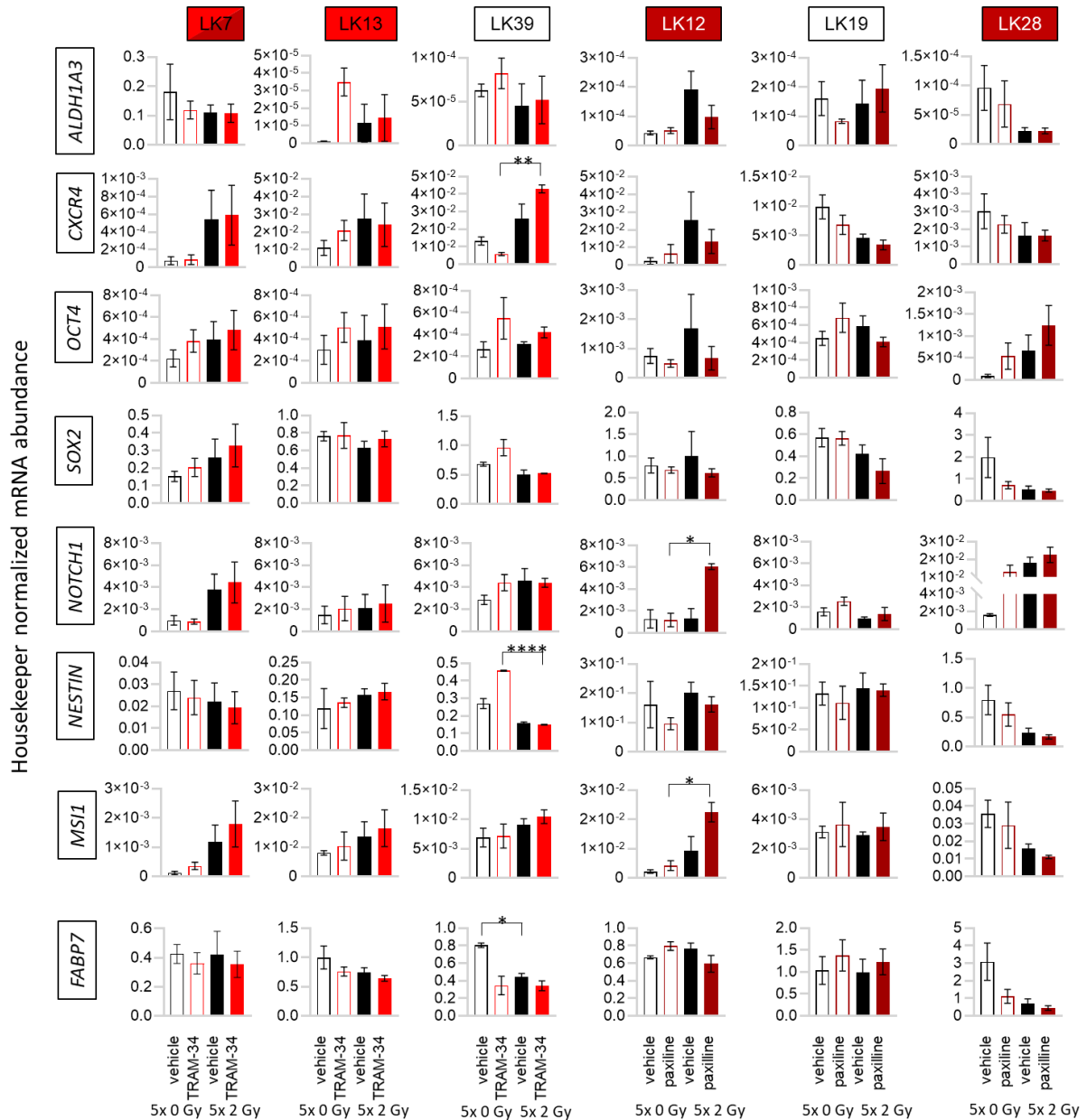
Katrin Ganser, Nicolai Stransky, Tayeb Abed, Leticia Quintanilla-Martinez, Irene Gonzalez-Menendez, Ulrike Naumann, Pierre Koch, Marcel Krueger, Peter Ruth, Stephan M. Huber, and Franziska Eckert

#### Part A - Supplementary Data



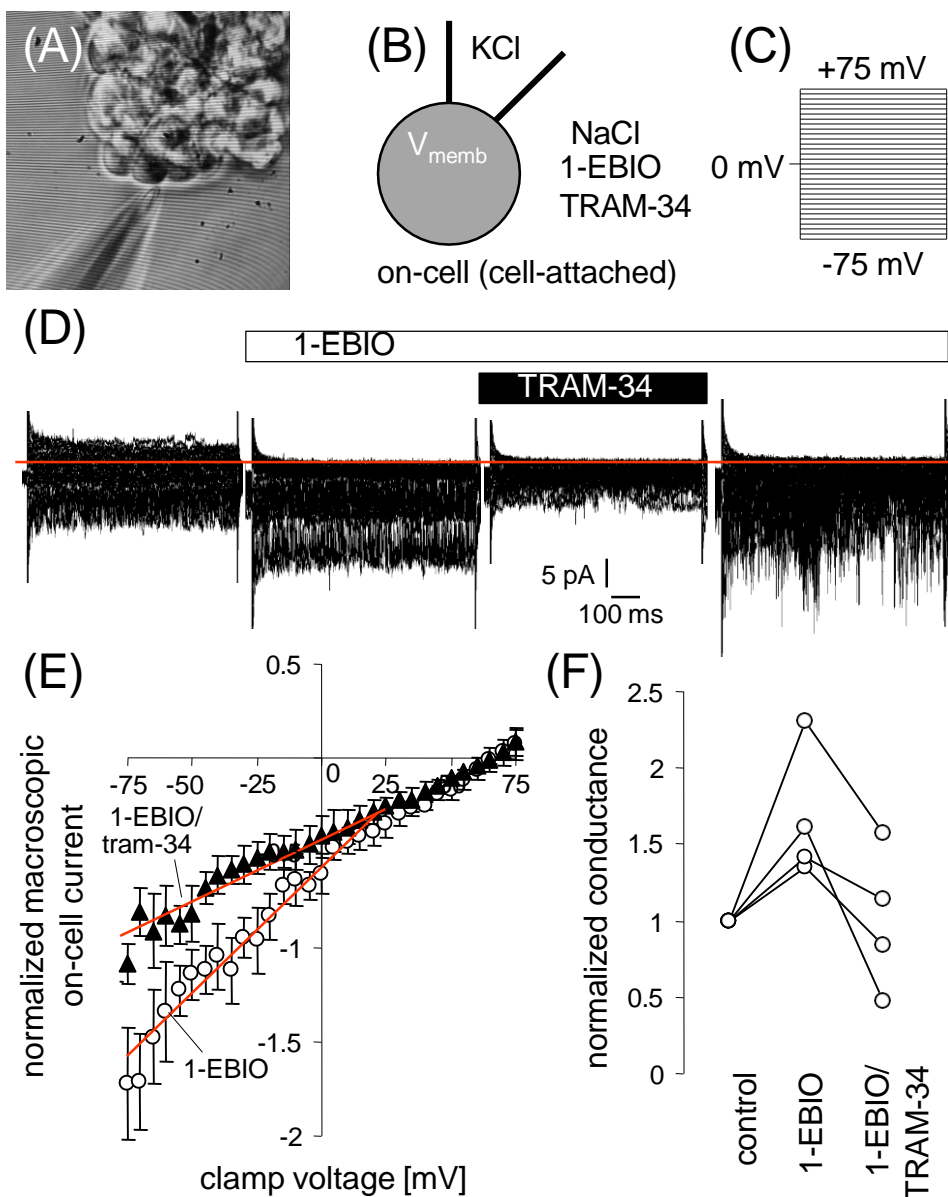
**Suppl. Fig. S1.** IK<sub>Ca</sub> or BK<sub>Ca</sub> channel inhibition and/or fractionated irradiation do not affect *KCNN4* (IK<sub>Ca</sub>) and *KCNMA1* (BK<sub>Ca</sub>) mRNA abundance or mesenchymal-to-proneural mRNA signature of selected pGSC cultures. **(A, B)** Mean ( $\pm$  SE, n = 3) housekeeper-normalized *KCNN4* (upper row) and *KCNMA1* (lower row) mRNA abundances (A) and mesenchymal-to-proneural mRNA signature (B) following fractionated irradiation (5x 0 or 5x 2 Gy) combined with pharmacological IK<sub>Ca</sub> (LK7, L13 and LK39) or BK<sub>Ca</sub> (LK12, LK19 and LK28) targeting by TRAM-34 (1-[(2-chlorophenyl)diphenylmethyl]-1H-pyrazole) and paxilline, respectively (both 0 or 5  $\mu$ M in DMSO). Data were not significantly different (Welch ANOVA and Dunnett's T3

multiple comparison or non-parametric Kruskal-Wallis and Dunn's T3 multiple comparison test depending on normal distribution as assessed by Kolmogorov-Smirnov test)

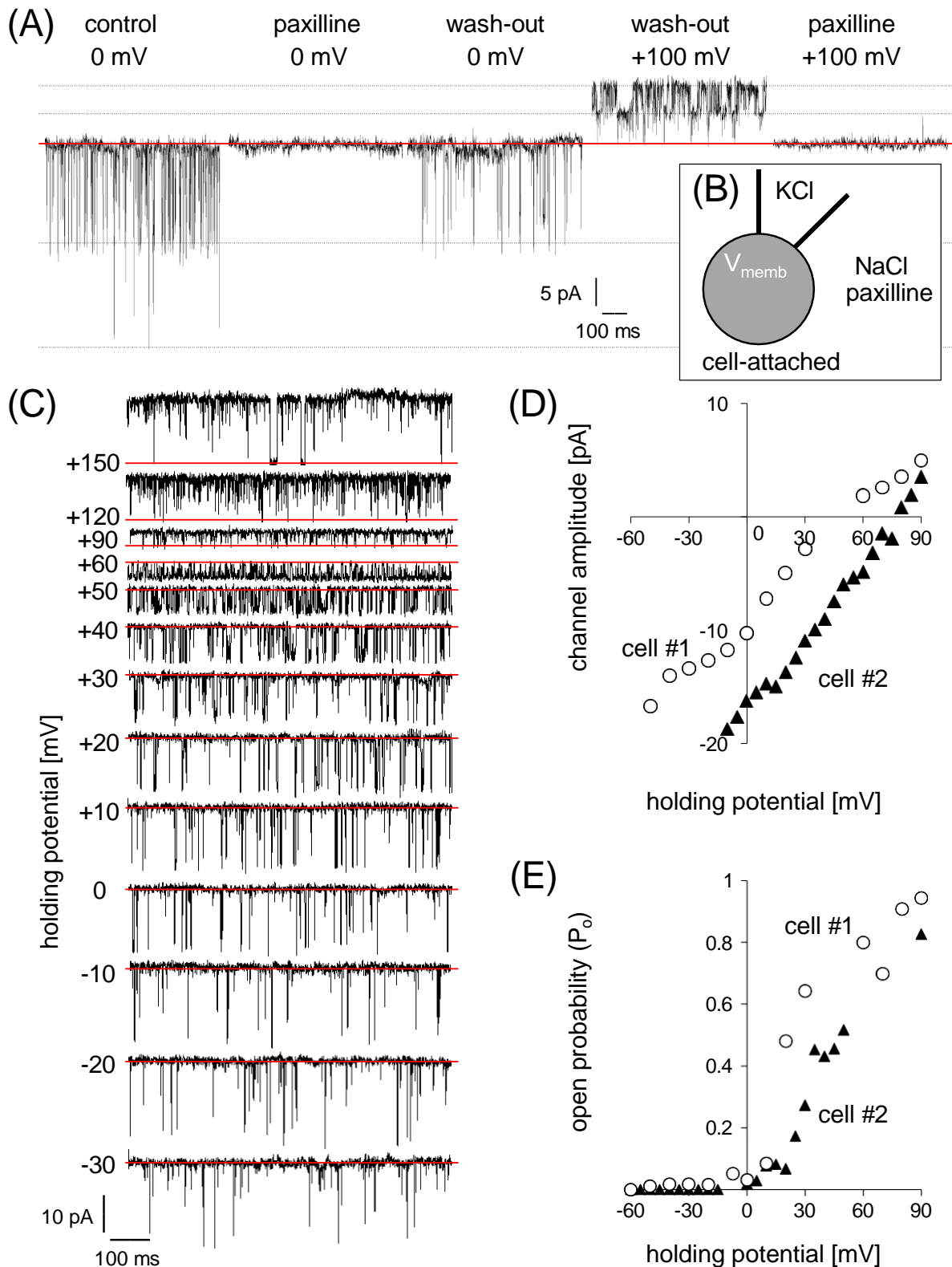


**Suppl. Fig S2.** Effects of pharmacological  $IK_{Ca}$  or  $BK_{Ca}$  targeting and/or fractioned irradiation on the mRNA abundances of stem cell markers. These markers were used together with the *KCNN4* and *KCNMA1* mRNA abundances to calculate the mesenchymal-to-proneural mRNA signature of the individual pGSC cultures. Data are means ( $\pm$  SE,  $n = 3$ ) of housekeeper-normalized *ALDH1A3* (aldehyde dehydrogenase 1 family member-A3), *CXCR4* (*Cx*-chemokine receptor-4), *OCT4* (octamer-binding transcription factor 4), *Sox2* (sex determining

region Y (SRY)- box-2), *NOTCH1*, *Nestin*, *MSI1* (Musashi-1), and *FABP7* (Fatty acid binding protein-7) mRNA abundance following fractionated irradiation (5x 0 or 5x 2 Gy) combined with pharmacological  $IK_{Ca}$  (LK7, L13 and LK39) or  $BK_{Ca}$  (LK12, LK19 and LK28) targeting by TRAM-34 and paxilline, respectively (both 0 or 5  $\mu$ M in DMSO). \*, \*\*, and \*\*\*\* indicate  $p \leq 0.05$ ,  $p \leq 0.01$ , and \*\*\*\*  $p \leq 0.0001$ , respectively (Welch ANOVA and Dunnett's T3 multiple comparison or non-parametric Kruskal-Wallis and Dunn's T3 multiple comparison test where appropriate).

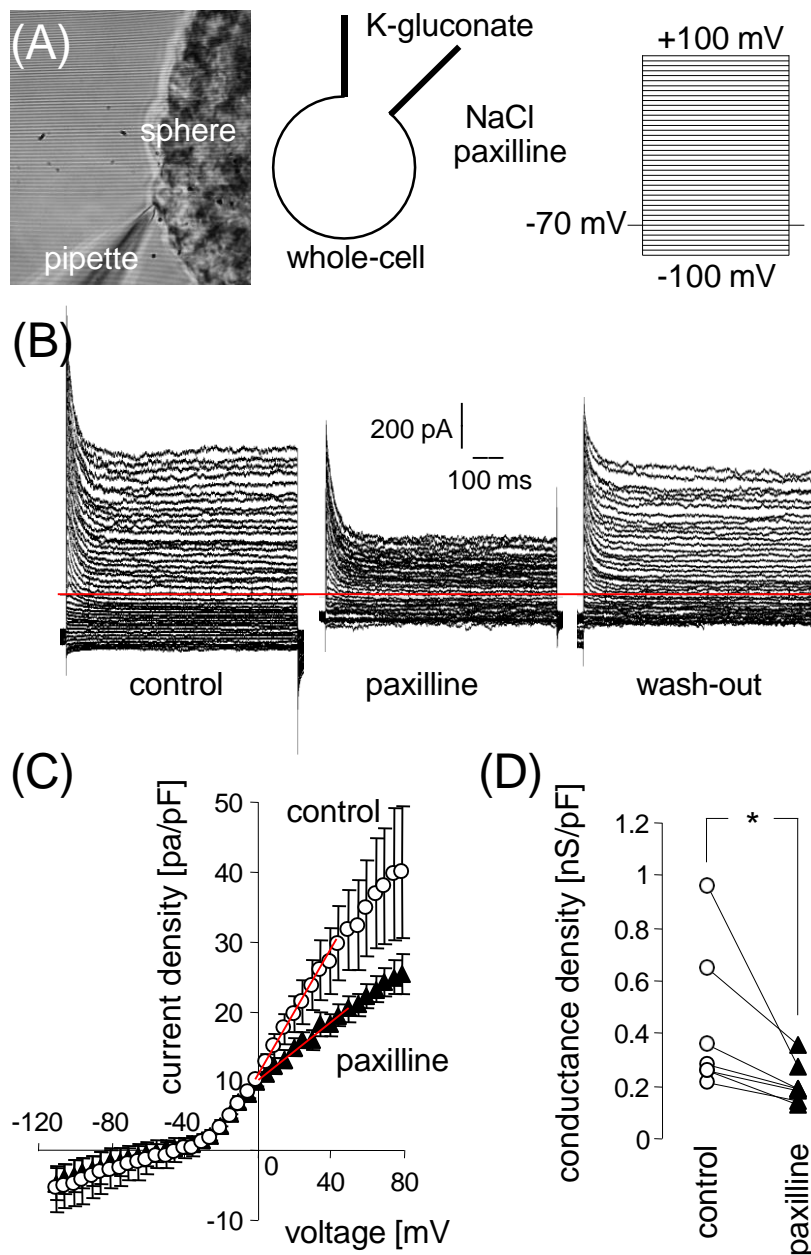


**Suppl. Fig. S3.** LK13 pGSCs functionally express  $I_{K_{Ca}}$   $K^+$  channels in the plasma membrane as analyzed by patch-clamp on-cell (cell-attached) recording. **(A)** Light micrograph of a LK13 spheroid during on-cell recording. **(B)** Ionic composition of pipette and bath solution and channel modulators applied, and **(C)** voltage pulse protocol used. **(D)** Macroscopic on-cell current tracings recorded as shown in (A-C) from a LK13 pGSC before (outer left) and during bath application of the  $I_{K_{Ca}}$   $K^+$  channel opener 1-EBIO (1-ethyl-1,3-dihydro-2H-benzimidazol-2-one), 200  $\mu$ M, middle left to outer right) alone, or in combination with the  $I_{K_{Ca}}$  inhibitor TRAM-34 (1  $\mu$ M, middle right). **(E)** Dependence of macroscopic on cell currents on clamp-voltage. Data were recorded as shown in (D) in the presence of 1-EBIO alone (control, open circles) or of 1-EBIO and TRAM-34 (closed triangles). Please note, given the high  $K^+$  concentration in the cytosol of the recorded cell, an electrochemical equilibrium potential for  $K^+$  ions ( $E_K$ ) across the recorded membrane in the range of 0 mV can be assumed when using high  $K^+$  concentration in the pipette solution. Per definition,  $K^+$ -selective currents exhibit a reversal potential ( $V_{rev}$ , i.e., the voltage where the current/voltage(I/V)-curve crosses the x-axis) at  $E_K$ . In on-cell mode, the physiological membrane potential applies in addition to the clamp voltage at the recorded, i.e., electrically sealed membrane patch. As a consequence, the negative membrane potential must be zeroed by positive clamp voltages ( $\sim +65$  mV in (E)) to reach the  $E_K$  of about 0 mV. **(F)** Normalized macroscopic on-cell conductance (calculated by linear regression for the voltage range shown by red lines in (E)) under control (left), 1-EBIO (middle) and 1-EBIO/TRAM-34 (right) treatment conditions. Data are means ( $\pm$  SE;  $n = 4$ ) in (E) and individual values in (F).

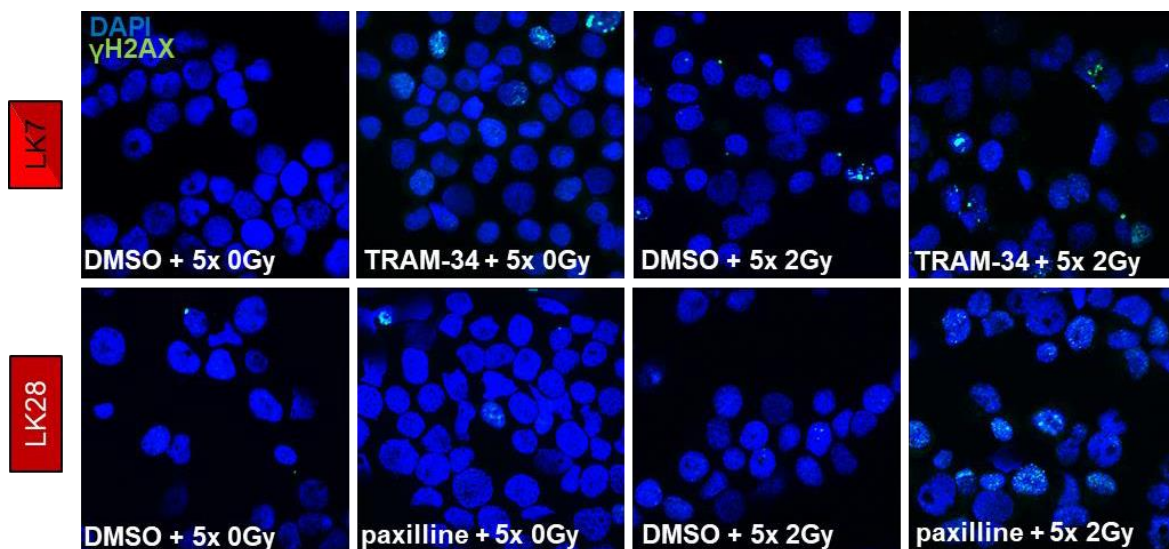


**Suppl. Fig. S4.** LK28 pGSCs functionally express  $BK_{Ca}$   $K^+$  channels in the plasma membrane as analyzed by patch clamp on-cell recording. **(A)** Current tracings recorded in on-cell mode as outlined in **(B)** from a spheroid-grown LK28 pGSC at 0 mV (1<sup>st</sup>-3<sup>rd</sup> tracing)

and +100 mV (4<sup>th</sup>-5<sup>th</sup> tracings) holding potential. Currents were obtained in the absence (1<sup>st</sup>, 3<sup>rd</sup>; and 4<sup>th</sup> tracings) and presence (2<sup>nd</sup> and 5<sup>th</sup> tracing) of the BK<sub>Ca</sub> K<sup>+</sup> channel blocker paxilline (5  $\mu$ M). (C) BK<sub>Ca</sub>-generated unitary current transitions recorded at different holding potentials (recording conditions as in (B)). (D-E) Dependence of the BK<sub>Ca</sub> K<sup>+</sup> channel amplitude and open probability on holding potential. Individual data from two cells (open circles and closed triangles) are shown.

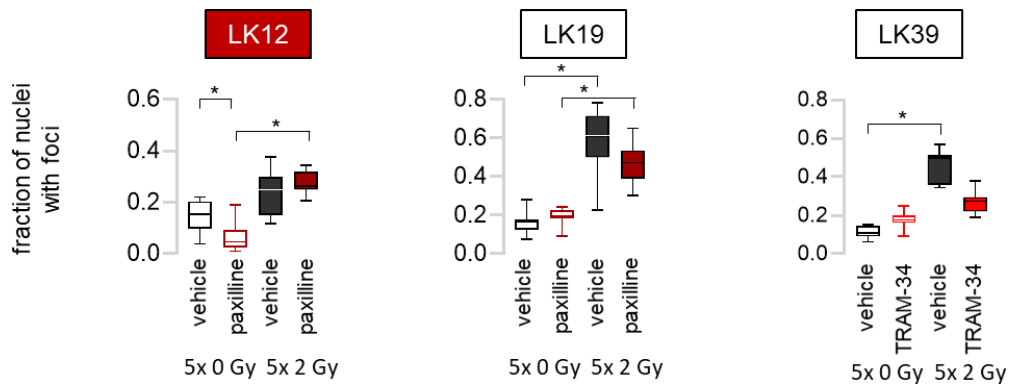


**Suppl. Fig. S5.** LK28 pGSCs exhibit a high fractional BK<sub>Ca</sub> K<sup>+</sup> conductance in the plasma membrane as determined by patch clamp whole-cell recording. **(A)** Light micrograph depicting a LK28 pGSC at the surface of a sphere during recording of BK<sub>Ca</sub> whole-cell currents (left), ionic composition and BK<sub>Ca</sub> channel inhibitor used for recording (middle), and pulse protocol applied (right). **(B)** Whole-cell current tracings recorded as outlined in (A) from a LK28 pGSC before (left), during (middle), and after (wash-out, right) bath application of paxilline (5 μM). **(C)** Dependence of mean (± SE, n = 7) whole cell current densities on clamp voltage. Currents were recorded as in (A, B) before (open circles) and during bath application of paxilline (5 μM, closed triangles). **(D)** Whole-cell conductance density of LK28 in the absence (open circles) and presence (closed triangles) of paxilline. Given are individual values of 7 cells calculated from the data in (C) by linear regression for the voltage range indicated by red line in (C). \* indicates p ≤ 0.05 (Welch-corrected t-test).

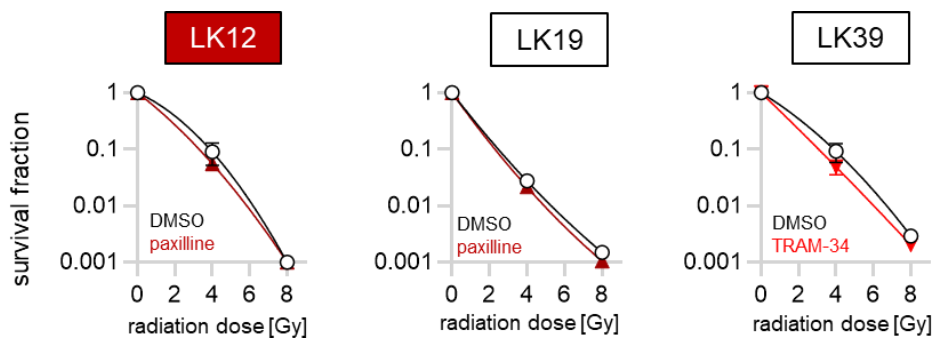


**Suppl. Fig. S6.** Nuclear γH2AX foci as surrogate marker of DNA double strand breaks (DSBs). Representative immunofluorescence micrographs from LK7 (top) and LK28 (bottom) pGSCs probed against γH2AX (green). Nuclei were counterstained with DAPI (blue). Cells had been fixed 24 h after treatment on 5 consecutive days with IK<sub>Ca</sub> blocker TRAM-34 (LK7) and BK<sub>Ca</sub> inhibitor paxilline (LK28) (0 or 5 μM, each) concomitant to fractionated irradiation (5x 0 or 5x 2 Gy) as indicated.



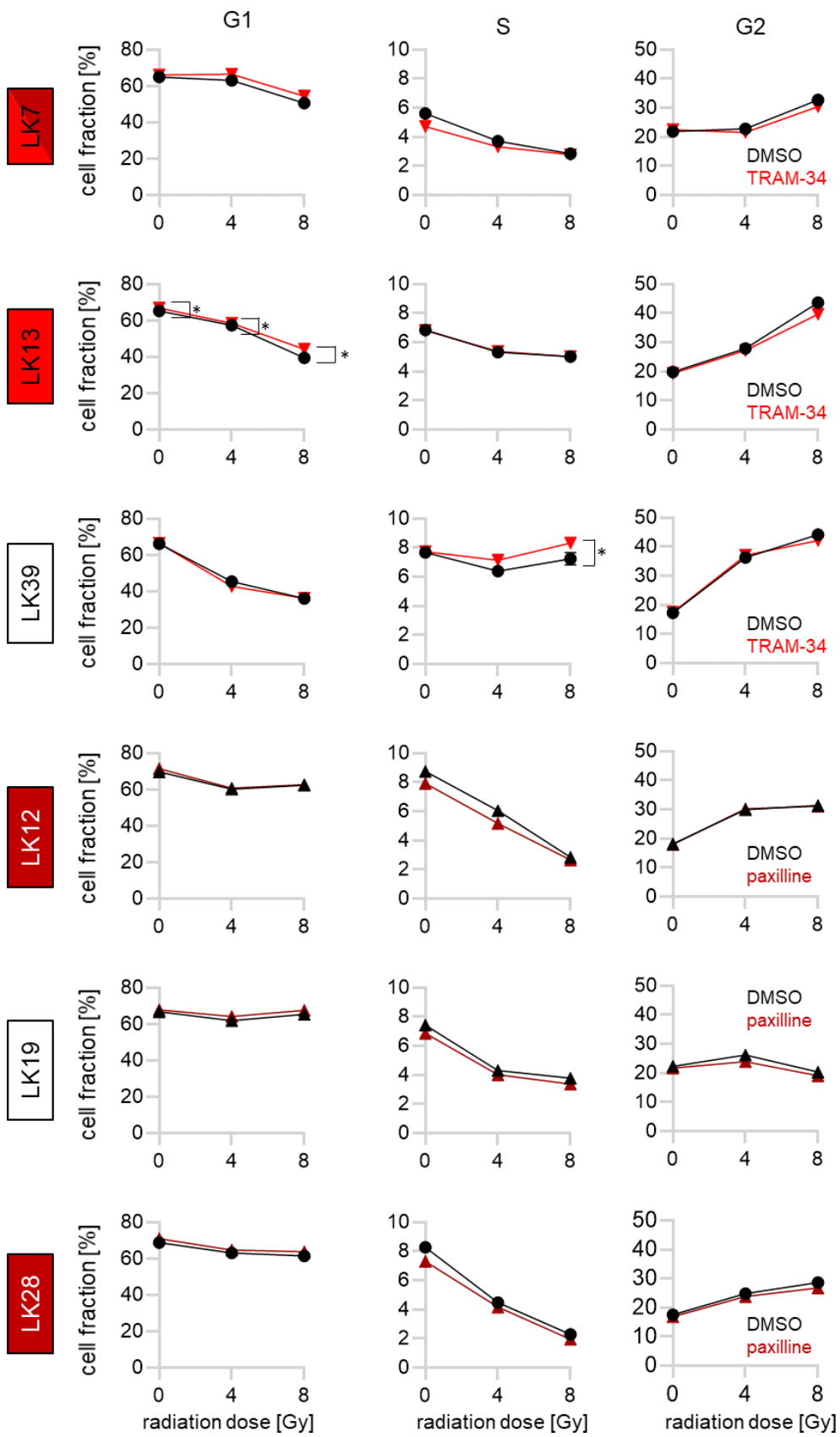


**Suppl. Fig. S7.**  $K_{Ca}$  channel targeting seems not to increase residual DSBs in LK12, LK19, or LK39 pGSCs. Fraction of nuclei with residual nuclear  $\gamma$ H2AX foci 24 h after treatment of LK12 (left), LK19 (middle) and LK39 (right) pGSCs on 5 consecutive days with  $K^+$  channel blockers TRAM-34 or Paxilline (0 or 5  $\mu$ M, each) concomitant to fractionated irradiation (5x 0 or 5x 2 Gy) as indicated. \* indicates  $p \leq 0.05$  (Welch ANOVA and Dunnett's T3 multiple comparison or non-parametric Kruskal-Wallis and Dunn's T3 multiple comparison test where appropriate).

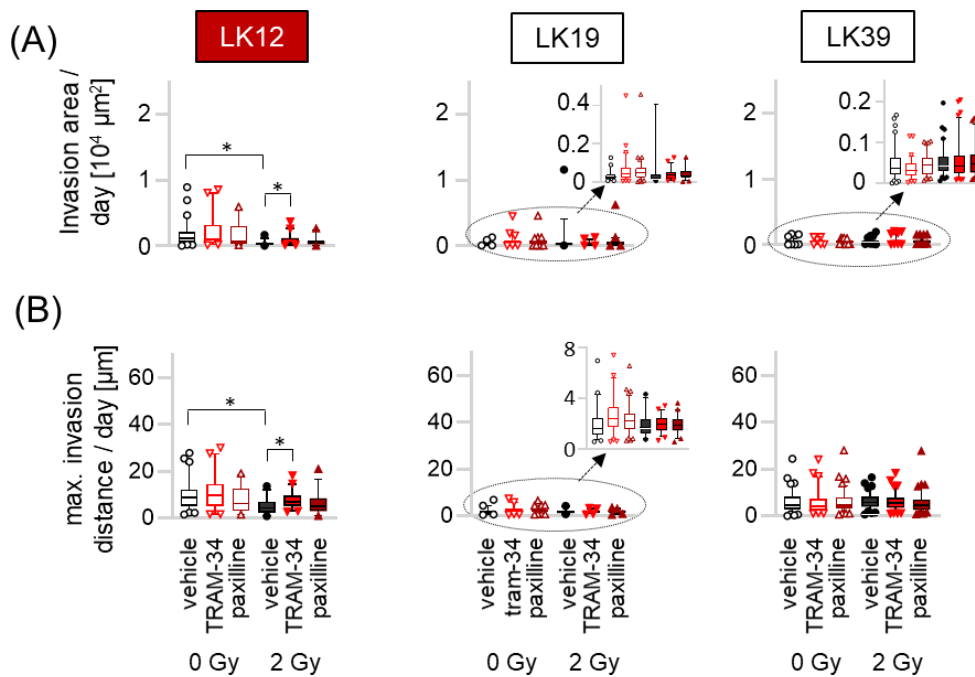


**Suppl. Fig. S8.** Influence of  $IK_{Ca}$  or  $BK_{Ca}$  inhibition on clonogenic survival of pGSC cultures. Mean ( $\pm$  SE,  $n = 3-5$ ) survival fractions (SF) as determined by pre-plating limited dilution assay of irradiated (single dose ( $D$ ) of 0, 4, or 8 Gy) LK12 (left), LK19 (middle), and LK39 (right) pGSCs pre-, co- and post-treated with paxilline (LK12 and LK19) or TRAM-34 (LK39) (0 or 5  $\mu$ M, each). Data were fitted according to the linear-quadratic model with the following equation  $SF = e^{-(\alpha \cdot D + \beta \cdot D^2)}$ .



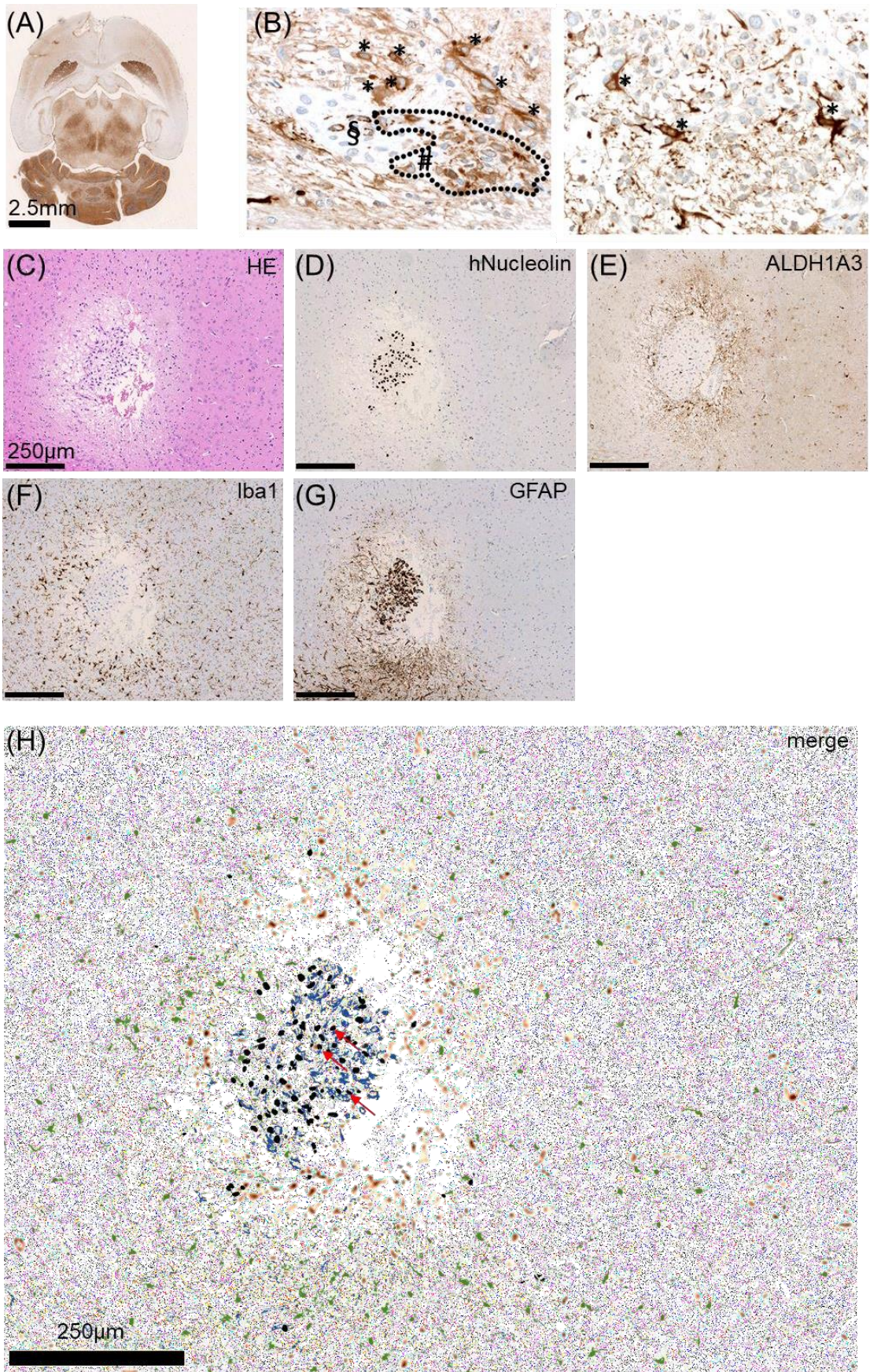


**Suppl. Fig. S9.** IK<sub>Ca</sub> or BK<sub>Ca</sub> targeting elicits only marginal effects on cell cycle distribution in irradiated pGSCs. Mean percentage ( $\pm$  SE; n = 9-12) of LK7, LK13, LK39, LK12, LK19, and LK28 pGSCs residing in G<sub>1</sub> (left), S (middle), and G<sub>2</sub> (right) phase of cell cycle 48 h after irradiation with 0, 4 or 8 Gy and concomitant pre- (1 h), co-, and post- (48 h) treatment with TRAM-34 (LK7, LK13, and LK39) or paxilline (LK12, LK19, and LK28) (0 or 5  $\mu$ M, each). DNA of permeabilized cells was stained with propidium iodide according to the Nicoletti protocol<sup>1</sup> and cell cycle distribution recorded by flow cytometry. \* indicates  $p \leq 0.05$  as assessed by two-tailed (Welch-corrected) t-test or non-parametric Mann-Whitney-U t-test, where appropriate.



**Suppl. Fig. S10.** Neither BK<sub>Ca</sub> nor IK<sub>Ca</sub> targeting inhibits cell invasion in pGSC cultures LK12 (left), LK19 (middle), and LK39 (right). **(A, B)** Evasion of GSCs from fibrin-embedded spheres. The increase in infiltrated sphere-surrounding area per day (A) and the maximal invasion distance/day (B) were analyzed on days 0, 7, 14, and 24 after radiation (0 or 2 Gy) and co- and post treatment with TRAM-34 or Paxilline (0 or 5  $\mu$ M, each). Pooled data are given as box plots with median and 5-95% whiskers (n = 30-90 spheres). \* indicates  $p \leq 0.05$ , as analyzed by non-parametric Kruskal-Wallis- with Dunn's multiple comparison test.





**Suppl. Fig. S11.** Histological analysis of orthotopically *xenografted* LK7 pGSCs. **(A)** Overview of a mouse brain (horizontal section) immunohistochemically probed against the mesenchymal stem cell marker protein ALDH1A3 demonstrating high ALDH1A3-immunoreactivity (brown) in hippocampal area, midbrain and cerebellum. **(B)** ALDH1A3-immunoreactive LK7 glioma area in higher magnification discloses ALDH1A3-positive cells with typical tumor cell appearance (#) but also ALDH1A3-positive glial shaped cells (\*) and blood vessels (§). **(C-G)** Light micrographs of the nuclei enriched LK7 glioma area in hemotoxylin eosin staining (C) and immunohistochemically probed in consecutive paraffine sections (5  $\mu$ m) against the marker hNucleolin used to identify human glioblastoma cells (D), the mesenchymal marker ALDH1A3 (E), the microglia/macrophage marker Iba1 (ionized calcium-binding adapter molecule-1, F), and the astrocytes marker GFAP (glial fibrillary acidic protein, G). Nuclei in (A-F) were counter-stained with hematoxylin (blue). The merged image (H) represents hNucleolin, ALDH1A3, Iba1, and GFAP immunoreactivity in black, orange, green, and blue colour, respectively. Coinduced hNucleolin and ALDH1A3 cells are indicated with red arrows.

## **Part B - Material and Methods**

*Meta-analysis of glioblastoma transcriptome and clinical databases.* To expose the dependence of the overall survival of (isocitrate dehydrogenase wildtype) glioblastoma patients, patient data were filtered for applied radiation therapy and stratified by the *KCCN4* (IK<sub>Ca</sub>) and *KCNMA1* (BK<sub>Ca</sub>) mRNA abundances of the glioblastoma resection specimens. For meta-analysis data of *The Chinese Glioma Genome Atlas (CGGA)*, *The Cancer Genome Atlas (TCGA)*, the *Ivy Glioblastoma Atlas Project (Ivy GAP)*, and the *Repository of Molecular Brain Neoplasia Data (REMBRANDT)* were pooled.



*Tübingen cohort of glioblastoma patients.* Overall survival of the Tübingen cohort was stratified by the *KCCN4* (IK<sub>Ca</sub>) and *KCNMA1* (BK<sub>Ca</sub>) mRNA abundances of the pGSC cultures. Clinical and neuropathological data as retrieved by chart review has been reported previously <sup>2, 3</sup>.

*Patient derived glioblastoma stem cell (PGSC) cultures.* Glioblastoma resectates were minced mechanically and enzymatically isolated cells grown in pGSC-selecting/inducing complete human NeuroCult NS-A Proliferation Medium including 20 ng/ml rhEGF, 10 ng/ml rhFGF and 0.0002% heparin (STEMCELL Technologies, Cologne, Germany) as described previously <sup>2, 4</sup>.

*Irradiation of cell cultures and K<sub>Ca</sub> K<sup>+</sup> channel targeting.* Single dose and fractionated ionizing radiation (6 MV photons) was applied to the pGSC cultures by a linear accelerator (LINAC SL15, Philips, Einthoven, The Netherlands). TRAM-34 (1-[(2-Chlorophenyl)diphenylmethyl]-1H-pyrazole) was synthesized in house by P.K. as described recently <sup>5</sup> and used as a specific inhibitor of IK<sub>Ca</sub> channels. IK<sub>Ca</sub> channels were activated with 1-EBIO (1-ethyl-2-benzimidazolinone) and BK<sub>Ca</sub> channels blocked by paxilline (both Sigma Aldrich, Taufkirchen, Germany)

*RNA Isolation and reverse-transcriptase polymerase chain reaction (RT-PCR).* RNA was isolated from pGSCs (~10<sup>6</sup> cells) by using NucleoSpin RNA Isolation Kit (Macherey-Nagel, Düren, Germany) following the manufacturer's instructions. The concentration of the eluted RNA was measured by NanoDrop ND-100 spectrometer (PEQLAB Biotechnologies GmbH, Erlangen, Germany) and samples were adjusted to 3 ng/μl in RNase-free water. To determine mRNA abundances of *KCNN4*, *KCNMA1*, *ALDH1A3*, *CXCR4*, *Sox2*, *Notch1*, *Oct4*, *MSI1*, *nestin*, *FABP7*, as well as of the housekeepers glyceraldehyde-3-phosphate dehydrogenase (*GAPDH*), β-actin (*ACTB*) and pyruvate dehydrogenase-β (*PDHB*) in a 20 ng RNA sample, fragments specific for *KCNN4* (IK<sub>Ca</sub>, QT00003780, QuantiTect Primer Assay, QIAGEN, Venlo, Netherlands), *KCNMA1* (QT00024157), *ALDH1A3* (QT00077588), *CXCR4* (QT00223188), *Sox2* (QT00237601), *Notch1* (QT01005109), *Oct4* (QT00210840), *MSI1*

(QT00025389), nestin (QT00235781), FABP7 (QT00007322), as well as for the housekeepers GAPDH (QT01192646), ACTB (QT00095431) and PDHB (QT00031227) were amplified by SYBR Green-based real-time PCR (1Step RT qPCR Green ROX L Kit, highQu, Kraichtal, Germany) in a LightCycler480 (Roche, Mannheim, Germany). Crossing point ( $C_p$ ) values and melt curves were analyzed by LightCycler-480 software and abundances of the individual mRNAs ( $A$ ) were normalized to the geometric mean of the three housekeeper mRNAs.

*Calculation of the molecular mesenchymal-to-proneural mRNA signature.* For every mRNA of a pGSC, the  $\log_{10}$  values ( $L$ ) of the housekeeper-normalized mRNA abundance ( $L = \log_{10}A$ ) was further normalized ( $N$ ) to the corresponding minimal ( $L_{\min}$ ) and maximal ( $L_{\max}$ ) values among all pGSCs by the use of the following equation:  $N = (L - L_{\min}) / (L_{\max} - L_{\min}) + 1$ . The molecular signature was then deduced by the geometric mean of  $N_{KCNN4}$ ,  $N_{KCNMA1}$ ,  $N_{ALDH1A3}$ ,  $N_{CXCR4}$ , and  $N_{Oct4}$ , divided by the geometric mean of  $N_{Nestin}$ ,  $N_{Sox2}$ ,  $N_{MSI1}$ ,  $N_{FABP7}$ , and  $N_{Notch1}$  according to <sup>2</sup>

*Patch-clamp recording.* Macroscopic on-cell (cell-attached) currents were recorded from LK13 and LK28 pGSCs as described recently <sup>2</sup>. In addition, whole-cell currents were obtained from LK28 pGSCs as detailed previously <sup>6</sup>. In brief, currents were recorded (10 kHz sampling rate) and 3 kHz low-pass-filtered by an EPC-9 amplifier (Heka, Lambrecht, Germany) using Pulse software (Heka) and an ITC-16 Interface (Instrutech, Port Washington, NY, USA). Borosilicate glass pipettes (~5 M $\Omega$  pipette resistance; GC150 TF-10, Clark Medical Instruments, Pangbourne, UK) manufactured by a microprocessor-driven DMZ puller (Zeitz, Augsburg, Germany) were used in combination with a STM electrical micromanipulator (Lang, Gießen, Germany). Cells were continuously superfused at 37°C with NaCl solution (in mM: 125 NaCl, 32 N-2-hydroxyethylpiperazine-N-2-ethanesulfonic acid (HEPES), 5 KCl, 5 D-glucose, 1 MgCl<sub>2</sub>, 1 CaCl<sub>2</sub>, titrated with NaOH to pH 7.4) additionally containing the BK<sub>Ca</sub> K<sup>+</sup> channel inhibitor paxilline (0 or 5  $\mu$ M), the IK<sub>Ca</sub> K<sup>+</sup> channel opener 1-

EBIO (0 or 200  $\mu\text{M}$ ) and/or the  $\text{IK}_{\text{Ca}}$   $\text{K}^+$  channel inhibitor TRAM-34 (0 or 1  $\mu\text{M}$ ). The pipette solution contained in on-cell mode (in mM) 130 KCl, 32 HEPES, 5 D-glucose, 1  $\text{MgCl}_2$ , 1  $\text{CaCl}_2$ , titrated with KOH to pH 7.4 and in whole-cell mode (in mM) 140 K-D-gluconate, 5 HEPES, 5  $\text{MgCl}_2$ , 1  $\text{K}_2$ -EGTA, 1  $\text{K}_2$ -ATP, titrated with KOH to pH 7.2.

Currents were elicited by 41 voltage square pulses (700 ms each) from 0 mV (on-cell) or -70 mV (whole-cell) holding potential to voltages between -75 mV and +75 mV (on-cell) or -100 mV and +100 mV (whole-cell) delivered in 5 mV increments. Clamp voltages refer to the cytosolic face of the plasma membrane and were not corrected (on-cell) or corrected offline by -10.6 mV for the applying liquid junction potential. For analysis, macroscopic on-cell and whole-cell currents were averaged between 100 and 700 ms of each voltage sweep. Inward currents are defined as influx of cations into the cells (or efflux of anions out of the cell), depicted as downward deflections of the current tracings, and defined as negative currents in the current voltage relationships. Macroscopic on-cell conductance and whole-cell conductance were calculated for the inward and outward currents between -25 mV and +75 mV and between 0 and +50 mV clamp voltage, respectively. Single channel properties (current amplitude, single channel conductance, and open probability) of  $\text{BK}_{\text{Ca}}$  were assessed by analyzing unitary current transitions in long-term on-cell recordings at various holding potentials.

*Immunofluorescence staining of residual  $\gamma\text{H2AX}$  foci as surrogate marker of un-repaired DNA double strand breaks (DSBs).* After seeding accutase-detached/singularized pGSCs in 6-well plates ( $6 \times 10^5$  cells/well in complete NSC medium), plates were treated 23 h post-plating with TRAM-34 (0 or 5  $\mu\text{M}$  in DMSO for LK7, LK13, LK39) or paxilline (0 or 5  $\mu\text{M}$  in DMSO for LK12, LK19, LK19) one hour prior to the first irradiation fraction (0 or 2 Gy). Irradiation was repeated every 24 h for further 4 days resulting in a fractionated irradiation dose of 5x 0 or 5x 2 Gy, respectively. 24h after the last radiation fraction, cells were detached (LK7) or singularized from spheres with accutase treatment and resuspended in

complete NSC medium (125  $\mu$ l) for cytospin centrifugation. Cells spun down on slides were fixed with formalin (4% in PBS, 15 min), washed 3x with phosphate-buffered solution (PBS) and permeabilized with Triton-X100 (0.1% in PBS, 3x 5 min) before probing against  $\gamma$ H2AX with anti- $\gamma$ H2AX-antibody (clone JBW301, 1:1000 in blocking reagent, EMD Millipore) using the Alexa Fluor™ 488 Tyramid SuperBoost™ Kit (B40912, ThermoFisher Scientific) according to the protocol supplied by the manufacturer.

*Clonogenic survival of irradiated cells.* Accutase-detached/singularized pGSC cells were sequentially 1:2 diluted in 96-well plates resulting in 12 cell dilutions (1024 to 0.5 cells in 100  $\mu$ l complete human NeuroCult NS-A Proliferation Medium). 24 hours after dilution, cells were irradiated with  $D = 0, 4$  or  $8$  Gy. IK<sub>Ca</sub> inhibitor TRAM-34 or BK<sub>Ca</sub> inhibitor paxilline (0 or 5  $\mu$ M in DMSO, each) were applied one hour prior to irradiation and post-incubated for 28 days. On day 14, medium (100  $\mu$ l) including inhibitor (0 or 5  $\mu$ M, each) was added to every well to prevent dry-out of the cultures. Four weeks after irradiation, the minimal cell number required to restore the culture (LK7, adherent growth) or for sphere formation (LK12, LK13, LK19, LK28, LK39) was determined. The reciprocal value of this minimal number defined the plating efficiency (PE). To calculate the survival fractions (SF), the PEs were normalized to the mean values of the corresponding mock-irradiated DMSO or inhibitor control PE<sub>0Gy</sub> according to the following equation:

$$SF_{0-8 \text{ Gy}} = PE_{0-8 \text{ Gy}}/PE_{0 \text{ Gy}}$$

The survival fractions (SF) thus obtained were plotted against the radiation dose ( $D$ ) and fitted according to the linear quadratic model with the following equation derived from the linear quadratic model:

$$SF = e^{-(\alpha \cdot D + \beta \cdot D^2)}$$

with  $\alpha, \beta$ : cell type-specific parameters.

*Cell cycle analysis.* pGSCs were irradiated 24 h post plating ( $6 \times 10^5$  cells/well in complete NSC medium) with 0, 4, or 8 Gy. From one hour prior to irradiation until 48 h post-irradiation,



cells were co-treated with TRAM-34 (LK7, LK13, LK39) or paxilline (LK12, LK19, LK19) (0 or 5  $\mu$ M in DMSO, each). 48 h after irradiation, cells were harvested, washed 1x in PBS, detached/singularized with accutase and incubated with Nicoletti reagent <sup>1</sup> (30 min at room temperature in the dark). Cellular DNA amount was defined by the propidium iodide fluorescence intensity as determined by flow cytometry (FACSscalibur with CellQuest software, BD, Franklin Lakes, NJ) at 488/10 nm excitation and 585/42 nm emission. For analysis of cell cycle distribution with the use of FCS Express-3 software (De Novo Software, Pasadena, CA, USA), the cell number/propidium iodide fluorescence histogram was plotted and percentage of cells residing in G<sub>1</sub>, G<sub>2</sub> and S phase of cell cycle was analyzed by integrating the respective peaks (G<sub>1</sub>, G<sub>2</sub>) and inter-peak (S) areas as defined by markers.

*Fibrin gel invasion.* Invasion assays were performed as described previously (Ganser, K et al. "Patient-individual phenotypes of glioblastoma stem cells are conserved in culture and associate with radioresistance, brain infiltration and patient prognosis." *International journal of cancer* vol. 150,10 (2022): 1722-1733). In brief, in 96-well plates fibrinogen (3 mg/ml, Millipore, Darmstadt, Germany) containing TRAM-34 or paxilline, (5  $\mu$ M final concentration, each) and thrombin (4 U/ml, Sigma Aldrich) solution (both in complete NeuroCult NS-A Proliferation Medium) were mixed 1+1 to cast a 2 mm thick layer of fibrin gel at the well bottom. After polymerization, pGSC spheres re-suspended in medium containing fibrinogen (3 mg/ml) and TRAM-34 or paxilline were placed onto the fibrin layers, before adding the same volumes of thrombin (4 U/ml)-containing medium. After polymerization and sphere embedding, the fibrin gels were overlaid with complete NeuroCult NS-A Proliferation Medium containing TRAM-34 or paxilline (all layers with final inhibitor concentrations of 0 or 5  $\mu$ M, each) to prevent drying-out of the gels during long-term incubation. Spheres were imaged directly after seeding (day 0) and after 7, 14 and 24 days and two dimension (2D)-projected surfaced area of sphere and surrounding invasion zone as well as the maximal invasion distance from the sphere circumference were recorded by a Celigo Imaging Cytometer

(Nexocelom Bioscience, Lawrence, Massachusetts, USA) and quantified by ImageJ software (open source).

*Orthotopic mouse models of patient-derived glioblastoma stem cells.* Stereotactic *xenotransplantation* of pGSCs was adapted from a protocol described previously <sup>6</sup>. In particular, the skullcap of 8-12 week old immunocompromised male and female NSG (NOD/SCID/IL2R $\gamma$ <sup>null</sup>, NOD.Cg-Prkdc<sup>scid</sup>Il2rg<sup>tm1Wjl</sup>/SzJ) mice was punctured 2.0 mm laterally of the bregma by the use of a dental driller and 10<sup>6</sup> pGSCs in 2  $\mu$ l PBS were injected stereotactically in 2.5 mm depth from the dura surface into the right striatum.

For the monitoring of tumor engraftment and growth, T2-weighted MRI sequences (TE = 12.9 ms, TR = 2500 ms, Matrix 256 x 256, FOV 30 x 30 mm<sup>2</sup>) were performed periodically on a 7 Tesla MRI ClinScan (Bruker BioSpin GmbH, Rheinstetten, Germany in the Werner Siemens Imaging Center Tübingen) equipped with a mouse whole brain volume coil (Paravision Version 6.0.1, Bruker BioSpin GmbH). In these T2-weighted MR images, tumors and surrounding edemas were defined as hyperintense area. As soon as tumors were visible (1 to 5 months after *xenografting*) the mice were stratified to the 4 treatment arms (see Fig. 3A of the main manuscript).

For volume analysis of LK7 *xenografts*, hyperintense brain lesions were contoured semi automatically with 3D slicer software (free open source) in consecutive MR image slices and volumes calculated. LK7 *xenografts* were imaged before (approximately day -20 and day 0) and after (approximately day +20, +40, +60) start of treatment on five consecutive days (days 1-5) with fractionated tumor irradiation (5x 0 or 5x 2 Gy) and concomitant IK<sub>Ca</sub> targeting (5x 0 or 5x 120 mg TRAM-34 /kg B.W. intraperitoneally, 6 h prior to the radiation fractions).

*Fractionated tumor irradiation, K<sub>Ca</sub> channel targeting and mouse survival.* Tumors were irradiated as described previously <sup>6</sup>. In brief, isoflurane-anaesthetized mice were immobilized

under a 6 MV linear accelerator (LINAC SL15 Philips) and the tumor-bearing half of the right hemispheres was irradiated (6 MV photons) on 5 consecutive days with a daily fraction of 0 or 4 Gy for histological analysis or 0 and 2 Gy for the survival study of LK7 -xenotransplanted mice (for long term mouse survival, we had to decrease radiation dose to 5x 2 Gy since DNA repair of NodScid gamma (NSG) is impaired due to the scid loss-of-function mutation of the Prkdc gene that encodes the catalytic subunit of a DNA-PK). On the days of irradiation, the IK<sub>Ca</sub> inhibitor TRAM-34 (0 or 120 mg/kg BW i.p. in Miglyol) was administered in LK7 and LK13 pGSC-carrying mice) and the BK<sub>Ca</sub> inhibitor paxilline (0 or 8 mg/kg BW i.p. in 9+1 DMSO/0.9% NaCl solution) was injected in LK28-carrying mice) 6 h prior to every irradiation fraction. Paxilline treated mice received an additional dose (0 or 8 mg/kg BW i.p.) 6 h after every irradiation fraction according to <sup>7</sup> and <sup>6</sup>, respectively. Mice were sacrificed 24 h after the last radiation fraction for histological tumor analysis. Survival of the LK7 pGSC xenografted mice was defined by the time when the mouse health scoring attained the prospectively defined termination criteria comprising severe loss of body weight, occurrence of neurological symptoms, pain as analyzed by grimace scoring, altered social behavior and overall appearance, or a combination of these parameters (treatment scheme in Fig. 3A of the main manuscript).

*Immunohistochemistry (IHC) of mouse brain sections.* Brains were resected and fixed in formalin (4% in PBS), embedded in paraffin, and sectioned (5 µm thick) by a microtome (Eprelia™ HM 430, Fisher Scientific, Sindelfingen, Germany). Sections were dewaxed (3x 5 min in xylol), hydrated in a ethanol/PBS dilution series and stained with hematoxylin/eosin according to <sup>8</sup>. Immunohistochemistry was performed by the mouse pathology facility of the University of Tübingen using an automated immunostainer (Ventana Medical Systems, Inc., Oro Valley, AZ, U.S.A.) according to the protocol supplied by the manufacturer. Sections were stained with the antibodies anti-Iba1 (1:2000, clone ERP16588, Abcam), anti hNucleolin (1:100, clone 4E2, Enzo Life Science, ADI-KAM-CP100-E), anti-ALDH1A3 (1:1000, PA5-29188, Thermo Fisher) or anti-γH2AX (1: 1000, ab11174, abcam). Appropriate positive and

negative controls were used to confirm the adequacy of the staining. All samples were scanned with the Nanozoomer (Hamamatsu) and processed with the programs Case Viewer (3DHISTECH, Budapest, Hungary) and Photoshop CS6 (Adobe Inc., San José, CA).

*Tumor brain invasion in vivo.* Number of isolated, invasive cells was quantified by outlining the tumor bulk in hematoxylin/eosin stained sections and superimposing this outline on the consecutive paraffine section immunohistochemically probed against hNucleolin. Brain infiltrating hNucleolin<sup>+</sup> glioblastoma cells that have evaded from the tumor bulk were counted separately for the rostral, occipital, medial and lateral evasion direction and related to the tumor bulk area using Nanozoomer Digital Pathology software (NDP, Hamamatsu, Japan). Likewise, to analyze brain invasion velocities, the maximal distance (again analyzed separately for rostral, occipital, medial and lateral direction) of brain-infiltrating hNucleolin<sup>+</sup> glioblastoma cells from the boundary of the tumor bulk was measured by NDP software and related to the tumor bulk area. The latter was used as an estimate of invasion time according to the following argumentation: Although imageable in MRI, histological tumor bulk volumes under control conditions (5x 0 Gy, vehicle) differed considerably within and between batches of pGSC *xenografts*. We assumed that large and small tumors resulted from early and late engraftment, respectively, and that farthest distant tumor cells should have evaded at an early time point of tumor bulk formation. Consequently, tumor bulk size as a rough surrogate of invasion time was deduced.

*Immunofluorescence staining of pGSC cultures and mouse xenografts.* pGSCs were detached/singularized with accutase (Sigma Aldrich, Taufkirchen, Germany) and stucked on object slides by cytopspin centrifugation (200 rpm for 2 min) before fixation (4% formalin in PBS for 15 min). Epitopes of slide-fixed pGSC cultures and of dewaxed and rehydrated brain slices (see above) were retrieved by microwave (600 W for 30 min) in citrate buffer (0.1 M citric acid monohydrate/ 0. 1M tri-sodium citrate dehydrate). After cooling-down on ice, immunofluorescenc staining was performed by Alexa Fluor™ 488 Tyramid SuperBoost kit

(B40912, goat anti mouse, Thermo fisher) for staining with anti-human nucleolin antibody (clone 4E2, 1:100, Enzo Life Science, ADI-KAM-CP100-E) and Alexa Fluor™ 594 Tyramid SuperBoost kit (B40925; goat anti rabbit, Thermo fisher) for staining with anti-ALDH1A3 antibody (1:1000, PA5-29188, Thermo Fisher) following the protocol for multiplex staining as provided by the manufacturer.

*Statistics.* Normal distribution was tested by Kolmogorov-Smirnov test, equal variances by F-test. Two sample groups were compared by two-tailed (Welch-corrected) t-test or non-parametric Mann-Whitney-U t-test, differences between more than two groups were estimated by ANOVA (Bonferroni or Šídák's multiple comparisons test), Welch-corrected ANOVA (Dunnett's T3 multiple comparison test) or non-parametric Kruskal-Wallis test (Dunn's multiple comparison test), where appropriate. Kaplan-Meier survival curves were compared by log-rank test. Error probabilities of  $p \leq 0.05$  were assumed to indicate statistical significant difference. Statistical tests were performed with Microsoft Excel (version 2019) and GraphPad Prism (version 8.4.0).

### **Part C – References**

1. Riccardi C, Nicoletti I. Analysis of apoptosis by propidium iodide staining and flow cytometry. *Nat Protoc* 2006;**1**: 1458-61.
2. Ganser K, Eckert F, Riedel A, Stransky N, Paulsen F, Noell S, Krueger M, Schittenhelm J, Beck-Wodl S, Zips D, Ruth P, Huber SM, et al. Patient-individual phenotypes of glioblastoma stem cells are conserved in culture and associate with radioresistance, brain infiltration and patient prognosis. *Int J Cancer* 2022;**150**: 1722-33.
3. Eckert F, Ganser K, Bender B, Schittenhelm J, Skardelly M, Behling F, Tabatabai G, Stransky N, Hoffmann E, Zips D, Huber SM, Paulsen F. Potential of pre-operative MRI features in glioblastoma to predict for molecular stem cell subtype and patient overall survival. *Radiother Oncol* 2023: 109865.
4. Klumpp L, Sezgin EC, Skardelly M, Eckert F, Huber SM. K(Ca)3.1 Channels and Glioblastoma: In Vitro Studies. *Current Neuropharmacology* 2018;**16**: 627-35.
5. Stransky N, Ganser K, Quintanilla-Fend L, Gonzalez Menendez I, Naumann U, Eckert F, P. K, Huber SM, Ruth P. TRAM-34 inhibits irradiation-induced hyperinvasion of glioma

cells and prolongs survival in the SMA-560 VM/Dk mouse model without impairing immune cell infiltration. (*unpublished observations*) 2023.

6. Edalat L, Stegen B, Klumpp L, Haehl E, Schilbach K, Lukowski R, Kuhnle M, Bernhardt G, Buschauer A, Zips D, Ruth P, Huber SM. BK K<sup>+</sup> channel blockade inhibits radiation-induced migration/brain infiltration of glioblastoma cells. *Oncotarget* 2016;**7**: 14259-78.
7. Stegen B, Butz L, Klumpp L, Zips D, Dittmann K, Ruth P, Huber SM. Ca<sup>2+</sup>-Activated IK K<sup>+</sup> Channel Blockade Radiosensitizes Glioblastoma Cells. *Mol Cancer Res* 2015;**13**: 1283-95.
8. Feldman AT, Wolfe D. Tissue processing and hematoxylin and eosin staining. *Methods Mol Biol* 2014;**1180**: 31-43.